KU Leuven

Biomedical Sciences Group

Faculty of Medicine

Department of Microbiology,
Immunology and Transplantation

NEW THERAPEUTIC APPROACHES AGAINST EMERGING FLAVIVIRUSES

Fikatas Antonios

Supervisor:	Prof. Dr. Dominique Schols
Co-supervisor:	Prof. Dr. Christophe Pannecouque
Chair examining committee:	Prof. Dr. Tassos Economou
Chair public defense:	Prof. Dr. Dirk Daelemans
Jury members	Prof. Dr. Piet Maes
	Prof. Dr. Paul Proost
	Prof. Dr. Kevin Arien
	Prof. Dr. Jan Munch

Dissertation presented in partial fulfilment of the requirements for
the degree of Doctor in Biomedical Sciences

October 2021

Table of Contents

List of abbreviations

AB	Apoptotic bodies
AC	Alternative current
ADE	Antibody-dependent enhancement
A549	Lung adenocarcinoma cells
AF4	Asymmetrical flow field-flow fractionation
ALS	Amyotrophic lateral sclerosis
ANKLE2	Ankyrin Repeat and LEM Domain Containing 2
APC	Antigen-presenting cells
APP	Amyloid precursor protein
Arf	ADP-ribosylation factor
BBB	Blood-brain barrier
BHK	Baby hamster kidney cells
BSA	Bovine serum albumin
C	Capsid
CC_{50}	50% cytotoxic concentration
CCL2	C-C motif chemokine ligand 2
CD4	Cluster of differentiation 4
CD8	Cluster of differentiation 8
CDE	Clathrin-dependent endocytosis
CE	Cholesteryl ester
Cer	Ceramide
CME	Cavolae-mediated endocytosis
CNS	Central nervous system
CPE	Cytopathogenic effect
CQ	Chloroquine

DAA	Direct-acting antivirals
DC	Dendritic cells
DCER	Dihydro ceramide
DC-SIGN	dendritic cell-specific intercellular adhesion molecule-3- grabbing non-integrin
DENV	Dengue virus
DG	Diacylglycerol
DHF	Dengue hemorrhagic fever
DMEM	Dulbecco's modified Eagle medium
DMSO	Dimethyl sulfoxide
DS	Dextran sulfate
DSS	Dengue shock syndrome
E	Envelope protein
EBM	EndoGrow Basal Medium
EC_{50}	50% Effective concentration
ECIS	Electric cell-substrate impedance
EGCG	Epigallocatechin gallate
EGM	Endothelial cell Growth Medium
EMC	Endoplasmic reticulum protein complex
ESCRT	Endosomal sorting complex required for transport
EVs	Extracellular vesicles
FBS	Fetal bovine serum
FDA	Food & drug administration
FGF	Fibroblast growth factor
GAG	Glycosaminoglycans
GBS	Guillain-Barré syndrome
GM-CSF	Granulocyte-macrophage colony-stimulating factor

GPI	Glycosylphosphatidylinositol
HIV	Human Immunodeficiency virus
HSV	Herpes virus
HCV	Hepatitis C virus
HUVEC	Human umbilical vein endothelial cells
Huh	Human hepatocytes
HSP90	Heat shock protein 90
HSC70	Heat shock cognate 70
HDA	Host-directed antivirals
HDL	High-density lipoprotein
HexCer	Hexosylceramides
HLA	Human leucocyte antigen
ICAM-1	Intercellular Adhesion Molecule 1
IEVs	ZIKV-infected EVs
IFITM3	Interferon-induced transmembrane protein 3
IFN	Interferon
IL	Interleukin
ISGs	Interferon-stimulated genes
Jeg3	Human placenta choriocarcinoma cells
LacCer	Lactosylceramide
LGTV	Langat virus
LC-ESI/MS/MS	Liquid Chromatography Electrospray Ionization Tandem Mass Spectrometry
LDL	Low density lipoprotein
LO	Large oncosomes
LPC	Lysophosphatidylcholine
LPE	Lysophosphatidylethanolamine

LPG	Lysophosphatidylglycerol
LPI	Lysophosphatidinositol
LPS	Lysophosphatidylserine
MAPK	Mitogen-activated protein kinase
MCP-1	Monocyte chemoattractant protein-1
MDDC	Monocyte-derived dendritic cells
MEM	Modified Eagle medium
MFT	Multifrequency mode
MHC	Major histocompatibility complex
MOG	Oligodendrocyte glycoprotein
MOI	Multiplicity of infection
MSC	Mesenchymal stem cells
MTS	3-(4,5-dimethylthiazol-2-yl)-5-(3-carboxymethoxyphenyl)-2-(4-sulfophenyl)-2 H-tetrazolium
MV	Microvesicles
MVB	Multivesicular bodies
NIEVs	Non-infected EVs
NK	Natural killer cells
NO	Nitric oxide
NS	Non-structural proteins
nSMase	Neutral sphingomyelinase
NTA	Nanoparticle tracking analysis
PAF1C	Polymerase-associated factor 1 complex
PC	Phosphatidylcholine
PDK	Primary dog kidney cells
PE	Phosphatidylethanolamine

PEG	Polyethylene glycol
PFA	Paraformaldehyde
PG	Phosphatidylglycerol
PI	Phosphatidylinositol
PI3K	Phosphoinositide 3-kinases
PLP	Proteolipid
PrM	Pre-membrane
PS	Phosphatidylserine
pTMD	Predicted transmembrane domain
RA	Rheumatoid arthritis
RANTES	Regulated upon Activation, Normal T Cell Expressed and Presumably Secreted chemokine
RIPA	Radio Immuno Precipitation Assay
ROS	Reactive oxygen species
RPMI	Roswell Park Memorial Institute medium
RVG	Rabies viral glycoprotein
SAR	Structure-activity relationship studies
SARS-CoV-2	Severe acute respiratory syndrome coronavirus 2
SDS	Sodium dodecyl sulfate
SEC	Size-exclusion chromatography
SISPA	Sequence Independent Single Primer Amplification
SM	Sphingomyelin
SMPD3	Sphingomyelin Phosphodiesterase 3
SNARE	SNAP receptor
SPR	Surface Plasmon Resonance
STAT2	Signal Transducer and Activator of Transcription 2
TBEV	Tick-borne encephalitis virus

TBS-T	Tris-Buffered Saline-Tween20
TEER	Transepithelial electrical resistance
TEM	Transmission electron microscopy
TF	Tissue factor
TG	Triglyceride
TGF	Transforming growth factor
TGN	Trans-Golgi network
TIM	T cell immunoglobulin and mucin domain-containing protein
TNF	Tumor necrosis factor
UC	Ultracentrifugation
UTRs	Untranslated regions
U87-MG	Uppsala 87 malignant glioma
VEGF	Vascular epidermal growth factor
Vero	African green monkey kidney cells
VLDL	Very low density lipoprotein
VLP	Virus-like particles
WHO	World Health Organization
WNV	West-Nile virus
YFV	Yellow fever virus
ZIKV	Zika virus
ZO-1	Zonula occluden-1
7DMA	7-Deaza-2′-C-Methyladenosine

Summary

Flaviviruses are single-stranded, positive sense RNA viruses that belong to the *Flaviviridae* family. Two of the most important human pathogens of this genus are dengue (DENV) and Zika virus (ZIKV). These flavivirus members are transmitted through different routes: (i) bites of infected female-mosquitoes (*Aedes aegypti* and *Aedes albopictus*), (ii) blood transfusion, (iii) sexual contact or (iv) mother- to-fetus (vertical transmission). Most of the infections caused by these viruses are asymptomatic or result in mild manifestations, including low-grade fever, joint pain and nausea. However, in extreme cases, DENV can lead to a severe and potentially life-threating dengue hemorrhagic fever/dengue shock syndrome, which is characterized by increased vascular permeability and plasma leakage. On the other hand, ZIKV has been associated with severe neurological manifestations, such as encephalitis, meningitis, microcephaly (infants) and the autoimmune disease Guillain-Barré syndrome (adults). Despite the extensive scientific efforts, no antivirals or vaccines are commercially available, demonstrating the urgent need for novel antiviral compounds. Therefore, the first aim of this thesis was to identify and characterize the mechanism of action of molecules with good potency against both DENV and ZIKV.

In **Chapter 3**, we identified a new class of antiviral molecules (tryptophan trimers and tetramers) with good activity *in vitro* (in the low micromolar range) against both viruses. These compounds belong to the large family of polyanions, which have been described in the literature as important entry inhibitors against several classes of viruses. Here, we show that this class of molecules inhibits viral infection by interfering with viral attachment processes. Surface plasmon resonance (SPR) experiments demonstrated that two of the selected compounds interact with the domain III of DENV virus envelope glycoprotein in a dose-dependent manner, thus preventing virus attachment to the host membrane. In collaboration with Prof. San-Félix (Instituto de Química Médica, Madrid, Spain) we also evaluated the antiviral activity of 13 structurally different derivatives in order to identify better the chemical groups, which are important for the potency of the molecules.

The second class of antiviral molecules studied in this thesis are the indole (ervantamine-silicine) alkaloids (**Chapter 4**). These molecules demonstrate good antiviral activity against DENV and ZIKV, with minimal cellular toxicity levels. Time-of-drug addition and subgenomic replicon assays showed that

these compounds suppress viral infection during the RNA replication/assembly stage. Additional studies have shown that molecules of this class demonstrate a cell- dependent inhibition profile, thus suggesting the involvement of cellular factors in the antiviral activity. Finally, selection of compound-resistant ZIKV strains and metagenomics sequencing analysis revealed mutants that harbor a single non-synonymous amino acid mutation at the non-structural NS4B protein, which plays an important role in the viral replication complex. However, further studies are needed to unravel the exact target of these indole alkaloid derivatives.

In the second topic of this PhD thesis (**Chapter 5**), we investigated one of the mechanisms that ZIKV uses to pass through the blood- brain barrier system (BBB) and to enter into the central nervous system (CNS). It is known that viruses exploit many cellular pathways during their infection cycle, in order to create an environment suitable for their replication. Recently, the role of extracellular vesicles (EVs) has been described as intracellular communicators in pathophysiological conditions. EVs are membrane-enclosed vesicles, which are secreted in response to extracellular stimuli. Several studies have shown that different viruses (e.g. HIV, HCV, influenza) recruit the exosomal pathway for their budding and egress. Here, we demonstrate that inoculation of hcMEC/D3 endothelial cells (*in vitro* cell model that resembles the BBB) with a ZIKV strain from the Asian lineage, resulted in the production and secretion of small EVs (<200 nm). To successfully isolate our vesicles from the supernatant of virus-infected cells (IEVs), we performed a differential centrifugation step, followed by (ultra)filtration and iodixanol-based gradient ultracentrifugation. Characterization of IEVs was achieved by conventional methods, including nanoparticle tracking analysis, electron microscopy and western blot. By applying several i*n vitro* assays, we observed that IEVs can incorporate viral elements (such as RNA, envelope glycoprotein and the non-structural NS1 protein) and further transfer their content to susceptible cell types of the CNS. Additionally, we explored the potential mechanism of both IEVs and ZIKV to pass through the BBB, by using a real-time, label-free impedance-based biosensor. Finally, for the first time in our knowledge, we conducted a comprehensive lipidomics analysis in both EV fractions and cells to identify lipid classes/species that are highly enriched into the vesicles, giving us new insights into EV biogenesis and signaling. Moreover, we compared the lipidomic profile of IEVs with the vesicles derived from non- infected cells and showed that specific lipid species (e.g. Cer (18:0/18:3))

is significantly upregulated (relative abundance) in the infected condition. These findings highlight the importance of studying lipid molecules as potential biomarkers during viral infection.

In summary, this thesis contributes to the characterization of two classes of novel inhibitors (targeting both viral and cellular factors) against DENV and ZIKV, as well as our effort to unravel how EVs could be used by ZIKV in order to pass through the BBB, transfer viral components and deliver them to other brain-associated cell types.

Samenvatting

Flavivirussen zijn positief enkelstrengige RNA-virussen die behoren tot de Flaviviridae-familie. Twee van de belangrijkste menselijke ziekteverwekkers zijn het denguevirus (DENV) en het Zika-virus (ZIKV). Deze flavivirussen worden langs verschillende wegen overgedragen: (i) de beet van virus-geïnfecteerde vrouwtjesmuggen (*Aedes aegypti* en *Aedes albopictus*), (ii) bloedtransfusie, (iii) seksueel contact en (iv) van moeder op foetus (verticale transmissie). Hoewel de meeste infecties die door deze virussen worden veroorzaakt asymptomatisch verlopen, zijn ze soms verantwoordelijk voor milde verschijnselen waaronder lichte koorts, gewrichtspijn en misselijkheid. In extreme gevallen kan DENV leiden tot een ernstige en mogelijk levensbedreigende dengue hemorragische koorts/dengueshock syndroom, die gekenmerkt wordt door een verhoogde vasculaire permeabiliteit en plasmalekkage. Anderzijds is ZIKV in verband gebracht met ernstige neurologische verschijnselen, zoals encefalitis, meningitis, microcefalie (zuigelingen) en de auto-immuunziekte Guillain-Barré-syndroom (volwassenen). Ondanks het uitgebreide wetenschappelijk onderzoek zijn er geen antivirale middelen of vaccins beschikbaar zodat er dringend behoefte is aan nieuwe moleculen. De eerste doelstelling van dit proefschrift is daarom het identificeren en karakteriseren van het werkingsmechanisme van moleculen met een goede antivirale werking tegen zowel DENV als ZIKV.

In hoofdstuk 3 hebben we een nieuwe klasse van antivirale moleculen geïdentificeerd (tryptofaantrimeren en -tetrameren) met een goede *in vitro* activiteit (in het laag micromolaire gebied) tegen beide virussen. Deze verbindingen behoren tot de familie van polyanionen, die in de literatuur beschreven worden als belangrijke inhibitoren van het binnendringen van verschillende virussen in de doelwitcellen. We toonden aan dat deze klasse van moleculen virusinfectie remt door te interfereren met virale bindingsprocessen. Oppervlakteplasmonresonantie (SPR)-experimenten tonen aan dat twee van de geselecteerde verbindingen op een dosis-afhankelijke manier interageren met het domein III van het DENV virusenvelopglycoproteïne, waardoor virusbinding aan het gastheermembraan wordt verhinderd. In samenwerking met Prof. San-Félix (Instituut voor Medische Chemie, Madrid, Spanje) hebben we ook de antivirale activiteit van 13 structureel verschillende derivaten geëvalueerd,

om beter de chemische groepen te identificeren die belangrijk zijn voor de krachtige antivirale werking van deze moleculen.

De tweede klasse van antivirale moleculen die in dit proefschrift werden bestudeerd zijn de indool (ervantamine-silicine)-alkaloïden (Hoofdstuk 4). Deze moleculen vertonen een goede antivirale activiteit tegen DENV en ZIKV, met een minimale cytotoxiciteit. Tijdsafhankelijke toevoeging van product en subgenomische replicontesten toonden aan dat onze moleculen de virale infectie onderdrukken tijdens de RNA replicatie/assemblage-fase. Aanvullende studies hebben aangetoond dat moleculen van deze klasse een celafhankelijk remmingsprofiel vertonen, wat de betrokkenheid van cellulaire factoren bij de antivirale activiteit suggereert. Metagenomische sequentie-analyse van ZIKV-stammen die resistent zijn voor deze moleculen wezen op één enkele niet- synonieme aminozuurmutatie in het niet-structurele NS4B- eiwit. Dit eiwit speelt een belangrijke rol in het virale replicatiecomplex. Verdere studies zijn echter nog nodig om het precieze doelwit van deze indoolalkaloïde derivaten te ontrafelen.

In het tweede onderwerp van dit proefschrift (Hoofdstuk 5), onderzochten we één van de mechanismen die ZIKV mogelijks gebruikt om de bloed-hersenbarrière (BBB) te penetreren en het centrale zenuwstelsel (CZS) binnen te dringen. Het is bekend dat virussen tijdens hun infectie gebruik maken van vele cellulaire wegen om een omgeving te creëren die geschikt is voor hun replicatie. Recent werd de rol van extracellulaire vesikels (EVs) beschreven als intracellulaire boodschappers in pathofysiologische omstandigheden. EVs zijn membraan-omhulde blaasjes, die worden afgescheiden als reactie op extracellulaire stimuli. Verschillende studies hebben aangetoond dat virussen zoals HIV, HCV en influenza de exosomale route recruteren voor hun vrijstelling uit de gastheercel. Hier toonden we aan dat inoculatie van hcMEC/D3 endotheelcellen (*in vitro* celmodel dat lijkt op de BBB) met een ZIKV- stam van de Aziatische lijn resulteerde in de productie en secretie van kleine EVs (<200 nm). Om deze blaasjes (IEVs) voldoende te isoleren uit het supernatant van de virus-geïnfecteerde cellen, voerden we een differentiële centrifugatiestap uit, gevolgd door (ultra)filtratie en iodixanol-gebaseerde gradiëntultracentrifugatie. IEVs werden gekarakteriseerd met conventionele methoden zoals nanopartikeltracking, elektronenmicroscopie en western blot analyse. Aan de hand van verschillende *in vitro* testen stelden we vast dat virale elementen van IEVs (zoals RNA, envelopeiwitten en het niet-structurele NS1-eiwit) kunnen worden opgenomen en overgedragen naar

celtypes van het CZS. Met een real-time, labelvrije impedantiebiosensor onderzochten we het mechanisme waarmee zowel IEVs als ZIKV de BBB kunnen penetreren. Tenslotte hebben we een uitgebreide lipidomicsanalyse uitgevoerd in zowel cellen als hun EVs om lipidenklassen/soorten te identificeren die sterk verrijkt zijn in vesikels, wat ons nieuwe inzichten geeft in EV biogenese en signalering. Bovendien hebben we het lipidomicsprofiel van IEVs vergeleken met de vesikels van niet-geïnfecteerde cellen en kunnen aantonen dat specifieke lipiden (bijv. Cer (18:0/18:3)) aangerijkt worden tijdens infectie. Deze bevindingen benadrukken het belang van het bestuderen van lipidenmoleculen als potentiële biomerkers tijdens virale infectie.

Samenvattend draagt dit proefschrift bij tot de karakterisering van nieuwe remmers tegen DENV en ZIKV (gericht tegen zowel virale als cellulaire factoren), alsook tot het ontrafelen van een mogelijk mechanisme waarbij EVs gebruikt worden door ZIKV om de BBB te penetreren, virale componenten over te dragen en af te leveren aan andere hersen-geassocieerde celtypes.

Chapter 1: General Introduction

1.1 Flaviviruses

Flaviviridae is a huge family of viruses composed of four distinct genera (*Figure 1.1*). Among these, flaviviruses (small enveloped viruses) constitute the genus, where a number of important human pathogens resides. Dengue virus (DENV), Zika virus (ZIKV), West Nile virus (WNV), yellow fever virus (YFV), tick-borne encephalitis virus (TBEV) are some of these members that are mainly transmitted through arthropod vectors (1).

1.1.1 Flavivirus structure

Flaviviruses share a common virion structure with a diameter of approximately 50 nm. They consist of a positive sense single- stranded RNA genome of 11 kb. This genome encodes for a polyprotein, flanked by 5' and 3' UTRs, that is processed by viral and host proteases to produce 10 different proteins, three structural (capsid: C, envelope: E, premembrane: prM) and seven non- structural (NS) proteins (NS1, NS2A, NS2B, NS3, NS4A, NS4B, NS5) (*Figure 1.2*). Structural proteins play a vital role in RNA protection, formation of viral particles, attachment to cellular receptors and entry/fusion. On the other hand, NS proteins are involved in viral replication, assembly, maturation as well as immune evasion from host responses (2).

Particularly, the C protein is responsible for genomic material encapsidation and interaction with viral RNA within mature virions (3). The E protein has an important function in cellular tropism and viral infection. It is composed of 3 main domains, EDI-EDIII. Specifically, EDI is located at the N-terminal side of the protein and is involved in its stabilization and virus production. EDII is essential for membrane fusion, while EDIII (C-terminal side) is critical for receptor recognition and constitutes the target of neutralizing antibodies (4). It has been proposed that changes in the structure of E protein may not only affect the binding process between cellular receptors and viral proteins, but they can also influence the affinity of antibodies to this protein. Finally, prM forms and protects viral envelope glycoprotein during assembly process (5).

Regarding NS proteins, NS1 is highly conserved and glycosylated with a multifunctional role in viral RNA replication (intracellular) and immune evasion (secreted) (6). NS2B is associated with the membrane endoplasmic reticulum and considered as a co-factor of NS3 protein. NS3 has a N-terminal protease and a C-terminal RNA helicase domain that mediates virus replication and assembly (7). NS4B has been described to suppress IFN- α/IFN- β responses and it constitutes a major protein in the formation of

viral replication complex (located in the endoplasmic reticulum) (8). Finally, NS5 constitutes the largest and one of the most conserved regions in the genome. Its dual role (methyltransferase: N-terminal, RNA- dependent RNA polymerase: C-terminal) is associated with RNA replication and evasion from host immune responses (9). The function of membrane-associated proteins NS2A and NS4A is less well characterized. However, several reports have shown their function in the induction of host membrane rearrangement, formation of viral replication complex and virion assembly (10)(11).
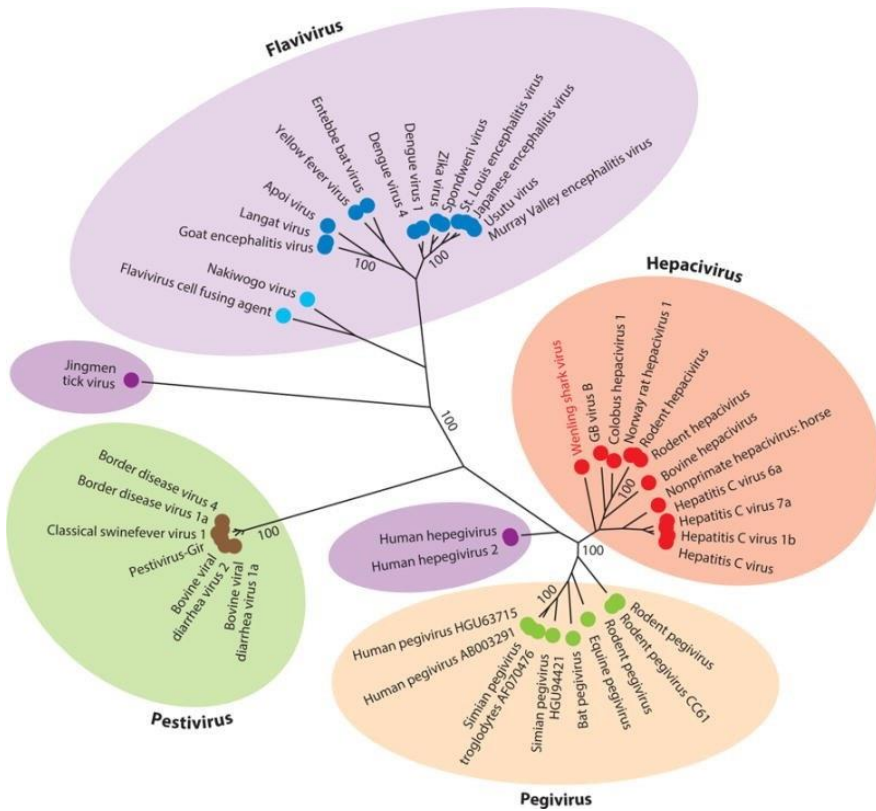
Figure 1.1: Phylogenetic analysis of NS3 gene of several members of all four genera of *Flaviviridae* family: Hepaci-, Pesti-, Pegi- and Flaviviruses (12)
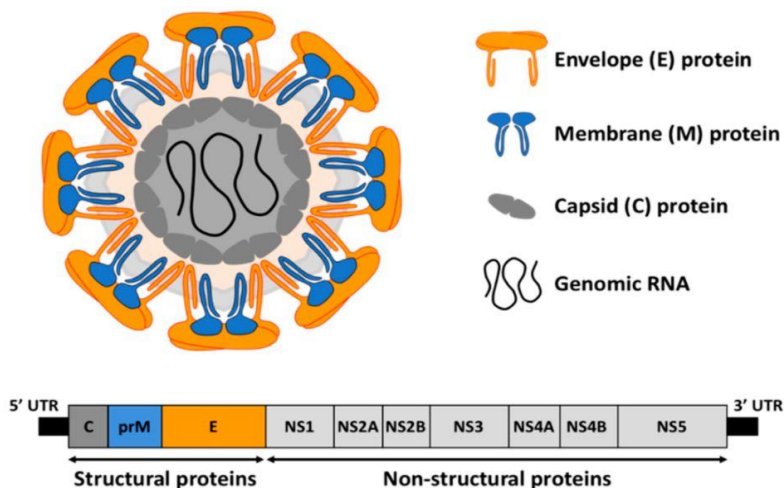
Figure 1.2: **Organization of Flavivirus genome.** _Upper_: Schematic presentation of a mature virion. The three main structural proteins are indicated in different colors: Envelope (yellow), (Pre)-membrane (blue), Capsid (grey), enclosing the genomic RNA. _Below_: RNA is translated as a single polyprotein and further processed by viral and host enzymes into 3 structural (C, prM, E) (colored) and 7 non-structural proteins (NS1, NS2A, NS2B, NS3, NS4A, NS4B, NS5) (light grey) (13).

1.2 Flavivirus replication cycle

The flavivirus replication cycle starts with a virion that enters into the cell through binding of virus envelope glycoprotein (E) with cellular receptors. Several entry receptors have been described in the literature, including glycosaminoglycans (GAGs), $\alpha_v\beta_3$ integrins, tyrosine kinase receptor AXL and immune receptor DC- SIGN. The interactions between the viral E glycoprotein and the receptors concentrate the viral particles on the cell surface. Subsequently, the formed virus-receptor complex is transferred towards a coated pit (clathrin) and membrane invagination is closed by dynamin-mediated scission. Following receptor-mediated endocytosis, the virus is taken up into endosomes, where a low-pH environment induces a series of alterations in the conformation of E- protein, leading to fusion between viral and endosomal membrane and subsequent release of the nucleocapsid into the cytoplasm. The initial steps in fusion process involve the disruption of E-

protein rafts through protonation of histidine residues and insertion of E-protein fusion loops into the outer membrane. Regarding the uncoating procedure, the mechanisms by which the viral genome is released from the nucleocapsid are largely unknown. However, it has been shown that an ubiquitination step of the capsid protein is required for that process. Once the positive-sense RNA genome is found in the cytoplasm, it is further transported to the endoplasmic reticulum (ER), where translation takes place to produce viral proteins. Polyprotein synthesis is initiated through the recognition of 5'-cap structure of mRNA by eIF4 factors. Then, the polyprotein is co- and post-translationally cleaved by a number of cellular (furin) and viral proteases (NS3-NS2B complex) to generate three structural and seven non-structural proteins, as described in the section *1.1.1*. The positive-sense RNA genome serves as a template for the production of new viral RNA copies, through the initial synthesis of a negative- sense RNA. This process is catalyzed by the activity of RNA- dependent RNA polymerase. Next, virus replication occurs within ER membranes (replication complex), where NS3 and NS5 play a crucial role in its formation. More specifically, viral RNA, NS proteins, as well as host factors (e.g. atlastins and reticulon) have been implicated in the formation of ER invaginations, the so-called vesicle packets (VP). These VPs are tightly connected to the cytoplasm via pores, though which other factors can enter.

Newly synthesized viral RNAs exit through the pore of VPs and can either be translated to viral proteins or function as templates for negative-sense RNA synthesis or selectively packaged into viral particles. The later stages of the flaviviral life cycle include the assembly of components into virion particles, the maturation of these into infectious particles, and finally their release to the extracellular space. Virus assembly occurs at the ER where viral genomes assemble with C, prM, and E proteins and bud into the ER lumen. During that process, several NS proteins, including NS2A, NS3 and NS5 are also involved. The immature viral particles are then transported via the secretory pathway to the Golgi apparatus and the *trans*-Golgi network (TGN), where acidic pH leads to conformational changes in the prM/E complex. These changes make prM accessible to cleavage by the cellular furin protease (maturation), producing the M and the pr peptide, which remains bound to the E-protein, until the mature viral particles are released from the cell to the extracellular space via exocytosis (14) (*Figure 1.3*).
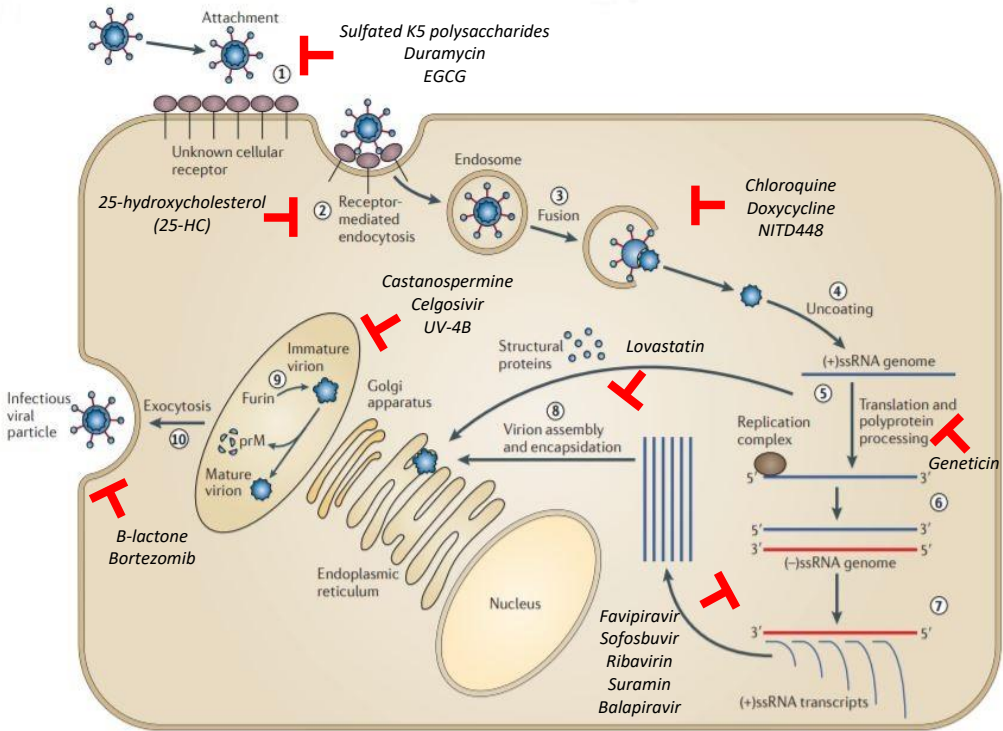
Figure 1.3: **Overview of flavivirus replication cycle.** (1) Viral particles attach to the cell surface and enter through receptor-mediated endocytosis into the cells (2). Then, virions are fused with the endosomal membrane (3) and viral RNA is released into the cytoplasm (4), where it is translated into a single polyprotein. Host and viral enzymes cut the polyprotein into 10 different proteins with a distinct role: three structural and seven non-structural (NS) proteins (5). NS are responsible for the replication of the viral genome into the endoplasmic reticulum complex (6, 7). Virus assembly occurs on the sites of endoplasmic reticulum membranes, where newly synthesized RNA and structural proteins bud out together (8). These immature viral particles are transported from the Golgi apparatus to the trans-Golgi network (TGN), where maturation takes place via furin-mediated cleavage of prM protein (9). Finally, infectious particles are released into the extracellular space through the secretory pathway (10) (15). A list of existing antiviral molecules, targeting different steps of virus lifecycle is also demonstrated.

In this PhD thesis, we focus on two closely related flaviviruses, DENV and ZIKV, which have a detrimental impact not only on people's lives, but also on the human society and the global economy.

1.3 Epidemiology and transmission

Multiple factors have advanced DENV and ZIKV as international public health concern. Particularly, these two viruses are mainly transmitted through species of *Aedes* mosquitoes (*Aedes albopictus* and *Aedes aegypti*). This can be accelerated due to a number of contributing factors, including climate change, travelling as well as increased growth of the population (16) (*Figure 1.4*).

1.3.1 Dengue virus

The first dengue-like symptoms were reported in the late 18th century in Spain, where the Queen Maria Luisa mentioned that she might suffer from an infection with comparable clinical manifestations. However, DENV was first isolated in 1943 in Japan during World War II (WWII). In that period, DENV fiercely spread through different regions and especially Southeast Asia and Pacific Islands. Following a number of epidemics in the late of 1960's, recent outbreaks took place in Latin America, Southeast Asia, as well as in Europe (17). Specifically, in 2012, Europe stated that a number of people, travelling back from Portugal (Madeira), tested positive for the virus. In addition, isolated cases were reported in France and Spain (2018), while the Philippines (2019) declared DENV as national epidemic, after an outbreak of dengue fever that costed the lives of hundreds of people (18).

As previously mentioned, DENV is spread to humans by the bite of female mosquitoes (*Aedes*). However, two distinct transmission cycles have been described: the sylvatic and the human (19). In the first one, virus transmission involves non-human primates and forest- dwelling mosquitoes in wild rural areas in West Africa and Southeast Asia. Regarding the human cycle, DENV transmission starts when a mosquito (vector) acquires its blood meal by an infected person. Then, the virus will arrive to the midgut epithelium, where it will replicate and further spread to other tissues, including the salivary glands. Once the virus is sufficiently replicated in this organ, the vector is capable to transmit DENV, via saliva, to new hosts (humans) through the next blood feeding.

1.3.2 Zika virus

ZIKV was isolated four years later, in 1947, from a rhesus macaque in the Zika forest, Uganda. The first findings that the virus is capable of infecting humans were reported in 1954, where neutralizing antibodies against ZIKV were detected in a young girl in Nigeria (20). Since then, no extensive outbreaks have occurred. However, several reports have demonstrated that the virus was circulating across different continents (20) (21). In 2007, the first large outbreak was confirmed on the Yap Islands, followed by two more recent epidemics in French Polynesia (2013) and Brazil (2015), where ZIKV infection led to severe manifestations and forced the World Health Organization (WHO) to declare the virus as Public Health Emergence of International Concern in 2016. Finally, some isolated cases were also stated in Europe (2015-2019), originating from travelers that came back from Asia and Latin America (22). Besides mosquito- mediated transmission of the virus, ZIKV can also spread to humans by sexual contact, blood transfusion or vertically from mother-to-child (23). These additional mechanisms of viral spread create severe health concerns and make treatment strategies more complicated.

Figure 1.4: **Global distribution of DENV and ZIKV.** Both viruses can circulate together in many regions across the world, including Central and South America, Southeast Asia as well as countries in Central Africa (24)

1.4 Clinical manifestations

1.4.1 Dengue virus

An estimated number of approximately 400 million people has been reported to combat an infection with dengue virus each year. From this number, almost 100 million develop clinical symptoms, of which 20,000 people are getting seriously ill and die (25). Four closely related, but antigenically distinct serotypes (DENV1, DENV2, DENV3, DENV4) co-circulate and are responsible

for these infections (26). Although the majority of them are asymptomatic, the clinical spectrum ranges from a mild febrile-like illness (headaches, joint pains, vomiting, nausea, aches) to a more severe dengue disease, which is characterized by increased vascular permeability and plasma leakage, that leads to bleeding, shock syndrome and eventually death (27). The severity of the disease is determined by a number of factors, including the viral strain, level of immune responses as well as host genetics.

1.4.2 Zika virus

As reported for DENV, ZIKV infection proceeds asymptomatically in most cases. Typical (mild) symptoms in ZIKV-infected patients involve fever, myalgia, rash, eye pain and conjunctivitis. Most of these infections are self-limited and last approximately one week. However, severe neurological manifestations have also been described in the literature. More specifically, ZIKV strains of the Asian lineage have been correlated with myelitis, encephalitis, the autoimmune disease Guillain-Barré syndrome (GBS, in adults) and microcephaly (in infants)(28).

1.5 Cellular tropism and pathogenesis

Both DENV and ZIKV have a wide range of cellular tropism. Enlightening the molecular mechanisms that lead to infection of different cell types and tissues might provide the "key points" to develop antiviral strategies against these viruses.

1.5.1 Dengue virus

As previously mentioned, DENV is mainly transmitted to humans through mosquito saliva. Once the virus enters into the host bloodstream, it firstly infects keratinocytes and the immature Langerhans cells (epidermal dendritic cells), followed by dendritic cells, macrophages and monocytes (29). In addition, it has been described that DENV is replicated in epithelial/endothelial cells, as well as in the liver and spleen both *in vitro* and *in vivo* (30) (31). Several studies have also confirmed the presence of the virus in other tissues/organs, including brain, lungs, kidney, bone marrow and heart, supporting a broad range of infection (32) (33). Despite our knowledge on the target cells that the virus infects, little is known on DENV pathogenesis and the factors that contribute to that. According to the literature, it has been

suggested that a combination of different parameters contributes to DENV susceptibility and subsequently to the severe dengue disease. Particularly, age, nutritional status and several viral/host proteins have been involved in the complexity of DENV pathogenesis.

NS1 is the only secreted protein, found in the blood of DENV patients. A high concentration of the protein has been associated with the development of dengue hemorrhagic fever (DHF) and shock syndrome (DSS) (34). DHF is characterized by an extensive plasma leakage (fluid leaks from blood vessels to the surrounding tissues), which might result in the DSS. In addition, NS1 has been shown to bind on endothelial cells and subsequently triggers vascular permeability and damage of the endothelium. This phenomenon is highly correlated with the secretion of elevated numbers of cytokines/chemokines (known as "cytokine storm"). Notably, plasma levels of IL-1β, IL-2, IL-6, IL-8, IL-10, tumor necrosis factor (TNF)-α, transforming growth factor (TGF)-β and IFN-α have been found to be upregulated in DENV- infected patients, especially in those experiencing DSS (35).

Furthermore, NS5 interacts with the PAF1C, a chromatin-associated complex that is essential for transcriptional elongation. Binding of these two proteins results in inhibition of interferon stimulated genes (ISGs) expression, which subsequently leads to abolishment of IFN-mediated antiviral responses (36). Moreover, NS5 has been reported to bind to the human signal transducer and activator of transcription 2 factor (STAT2), inducing its degradation (37). As indicated, NS proteins have emerged as a mechanism of innate immune evasion.

Additionally, several genetic factors have shown to be implicated in disease severity. Polymorphisms in a number of genes, such as TNF- α, TGF-β, vitamin D receptor and human leukocyte antigen (HLA) have been associated with virus susceptibility (38).

Finally, both *in vitro* and *in vivo* experiments have shown that the immune system is involved in dengue pathogenesis. Specifically, when a person is infected with one serotype, it will develop life-long immunity against this, but only partial protection against the others. As a result, individual infection with a different serotype will lead to a more severe disease (DHF/DSS), due to the antibody-dependent enhancement phenomenon (ADE). Heterotypic, non-neutralizing antibodies, which are produced from a primary infection, can bind to DENV viral particles during a secondary infection by another serotype.

However, this process will not lead to virus neutralization, but to a higher viral load and increased number of infected target cells (39).

Although extensive effort has been made to elucidate the main factors, contributing to DENV pathogenesis, there are still many challenges to account for. The lack of an appropriate animal model, the controversial role of NS1 protein, as well as the identification of all soluble factors necessary to induce endothelial destruction constitute hindrances in the full understanding of virus pathology.

1.5.2 Zika virus

ZIKV also exhibits a broad cellular tropism and persists in different body tissues and fluids. Viral replication has been demonstrated in keratinocytes, epidermal fibroblasts, dendritic cells, monocytes, macrophages, neural progenitor and placental cells (40)(41)(42). Besides these, ZIKV has been detected in the testicles, uterus, spleen, saliva, kidney and eye (43). Tropism of ZIKV can be correlated with the virus-specific clinical outcomes. High susceptibility of neural cells to ZIKV has been associated with the impaired development of fetal brain, which causes microcephaly and other neurological manifestations such as meningitis. Several articles have shown that ZIKV RNA can be isolated from the testicles, saliva and urine for at least 3 weeks after its clearance from the blood, suggesting its persistence in a number of tissues (44)(45). In addition, ZIKV infects endothelial cells and trophoblasts from placenta, and further crosses this tissue to reach into the brain of infants (46). Finally, persistence of ZIKV to the reproductive tract system (e.g. testicles, uterus, vagina) may contribute to vertical and sexual transmission of the virus (47). This mechanism is barely observed for other flavivirus members, indicating that ZIKV follows a distinct pattern of infection.

A number of host factors are known to mediate entry of ZIKV into cells, including DC-SIGN and several phosphatidylserine receptor proteins (e.g. TIM-1, TIM-4, AXL and Tyro3) (48). Among these, AXL (receptor tyrosine kinase) constitutes one of the most highly expressed proteins in the developing human cortex, glial cells, hippocampus and cerebellum (49). On the other hand, TIM-1 is the predominant entry factor expressed in human placental cells (46). Besides entry receptors, several factors have been implicated in ZIKV replication, such as atlastins. These endoplasmic-reticulum associated proteins constitute a group of GTPases with a crucial role in virus

replication. Moreover, members of atlastins have shown to interact with NS2A and NS2B-NS3 complex in virus replication sites (50).

As expected, most of the *in vitro* and *in vivo* studies focus on ZIKV- mediated neuropathogenesis. A virus-host specific interaction between NS4A and ANKLE2, a gene highly linked to hereditary microcephaly, has been described in the literature into humans and *Drosophila* (51) (52). Regarding GBS, the molecular mechanisms linked to this disease are poorly understood. However, researchers support that immune-related inflammation significantly contribute to this neurological disorder (53).

It is noteworthy to mention that due to a high degree of similarity at the amino acid sequence and the structure levels between ZIKV and DENV, antibodies produced after the infection by one virus, are able to cross-react with the other member, leading to a more severe disease (54). This particular phenomenon is commonly observed in regions where both viruses are endemic. Cross-reactivity between DENV and ZIKV composes one of the main obstacles in the antiviral treatment and vaccine development strategies.

Although *in vitro* and *in vivo* studies are performed to identify more cellular tissues/organs that can be permissive to DENV/ZIKV infection, and further explore their function in viral dissemination, the generation and use of animal models are of utmost importance to study virus pathogenesis. Finally, evaluation of efficacy of any antiviral molecules and/or vaccines should be performed *in vitro*, *ex vivo* and *in vivo*, in order to promote them as potential candidates for the treatment against these flaviviruses.

1.6 Treatment and prevention strategies

1.6.1 Mosquito control

As mentioned above, species of *Aedes* mosquitoes constitute the main vectors of DENV and ZIKV transmission. Specifically, *A. aegypti* (originating from Africa) is highly adapted to rural areas. On the other hand, *A. albopictus* (derived from Asia) has evolved to survive in colder regions, resulting in the efficient transmission of both viruses in areas where *A. aegypti* cannot (*Figure 1.5*). Several factors contribute to the global expansion of mosquitoes, including uncontrolled urbanization, increased international travel,

environmental changes and other socio-economic parameters (55). In addition, the viruses have been adapted to both vectors and hosts, in order to be sufficiently transmitted. Since no antivirals or vaccines are commercially available at the moment, effective vector control programs establish an advantageous approach to combat the infection by these two members. The major goal of this strategy is to either minimize the accumulation of vectors or reduce virus transmission to humans. This can be achieved through environmental management, as well as chemical and biological control (56). Management includes not only manipulation of the environment but also changes to human behavior. Particularly, recycling, cleaning or damage of containers (natural habitat of *Aedes* species mosquitoes in urban areas) can reduce the number of vectors. On the other hand, chemical control measurements involve the use of products, able to kill mosquitoes in the larval or adult stage. Larvicides and insecticides constitute examples of this class. Although these measures offer satisfactory results, development of resistance and human health issues compose inhibitory factors for their general use (57). In contrast to the chemical-based strategies, biological control is considered as an environmental-friendly approach to limit virus transmission. A typical example of this approach is the use of *Wolbachia* (58). This Gram-negative bacterium can be vertically transmitted and transferred to the eggs. This approach leads to the production and release of Wolbachia-infected female/male mosquitoes that give birth to viable but non-infectious offsprings, retaining their size population.
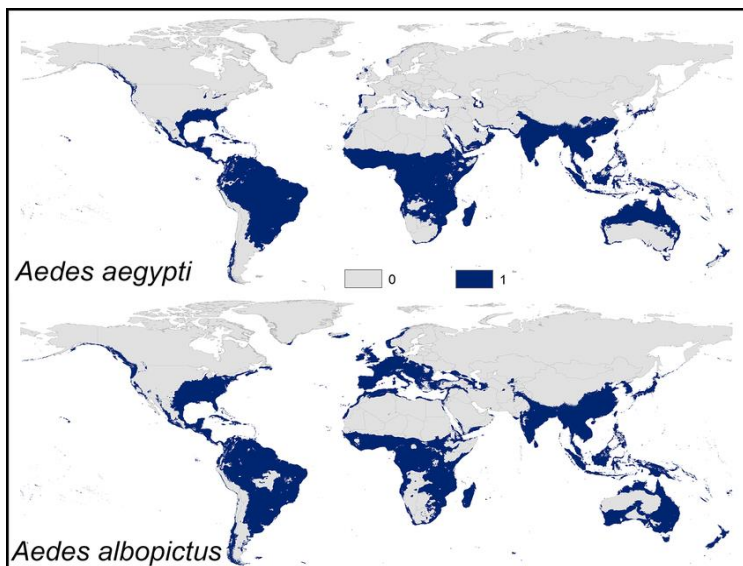
Figure 1.5: **Distribution of *Aedes aegypti* and *Aedes albopictus* across the world.** *Aedes aegypti*, the primary vector of DENV/ZIKV, circulates in South America, Africa and Southeast Asia (upper). On the other hand, *Aedes albopictus* can be found in the same regions, as well as Central and South Europe (bottom)(59).

1.6.2 Vaccines

Global spread of DENV and ZIKV has led to an enormous effort for vaccine development. To date, several vaccine platforms have been described in the literature, including virus-like particles (VLPs), live attenuated, inactivated, subunit and nucleic acid-based vaccines (DNA and RNA). During the process of vaccine construction, several goals have to be met, such as protective capacity, safety, induction of humoral (neutralizing antibodies) and cellular responses (T cell-mediated), as well as low-cost production. In the following section, we will describe the technologies (pros and cons) and the main challenges on DENV/ZIKV vaccine development.

1.6.2.1 DENV

Despite the fact that DENV has overwhelmed many regions across the world for more than 80 years, multiple difficulties have arisen on the development of a vaccine, able to efficiently protect against all DENV serotypes. These include: 1) Co-circulation of the four distinct serotypes, 2) lack of animal models that resemble human disease, 3) poor understanding of immune responses, following DENV infection.

31

1.6.2.1.1 Live attenuated vaccines

The only licensed vaccine candidate against DENV is a live-attenuated vaccine (Phase IV). Dengvaxia® (CYD-TDV) is a chimeric, recombinant, live attenuated tetravalent vaccine, developed by Sanofi Pasteur. The construct of this candidate is based on the backbone of the yellow fever virus strain 17D, which is modified to contain the genes of prM and E of each of the four DENV serotypes. CYD-TDV is used in approximately 20 countries since 2016, in a three-dose schedule (60). Despite its good safety and efficacy in individuals who were previously infected, an increased risk of hospitalizations (accompanied by high viral titers) has been described in people without prior exposure to the virus. In addition, variations in the efficacy of the vaccine have been demonstrated against the four serotypes.

Another live attenuated vaccine candidate is the TAK-003 (DENVax, developed by Takeda Pharmaceutical Company Ltd), which is constructed using recombinant DNA technology. DENVax is primarily based on the attenuation of a DENV2 strain (16681) in PDK cells (primary dog kidney). In addition, vaccine antigens were further developed by replacement of prM and E proteins of DENV1, DENV3 and DENV4 with those of the attenuated DENV2 strain. These formulations were found to be safe and able to elicit strong antibody and T-cellular responses against all four serotypes. TAK-003 is currently undergoing Phase III of clinical trials (61).

A third candidate (TDEV) is advanced to Phase II of clinical trials and composed of a tetravalent formulation, where 4 different strains (one from each serotype) were attenuated in PDK cells. Although, induction of neutralizing antibodies and a safety profile were observed, following a double-dose schedule, mild to moderate side effects were also recorded, including headache, pain and fatigue (62).

1.6.2.1.2 Inactivated vaccines

A purified inactivated vaccine candidate (DPIV) was developed by US Army Medical Research and is already in Phase I of clinical trials. DPIV is composed of formalin-treated (inactivated) viral particles of each of the four serotypes. Following a double-dose schedule, researchers have demonstrated a safety profile, along with a balanced immune response against all four serotypes. However, the levels of neutralizing antibodies have been shown to decrease over time (63).

There are major advantages linked to the use of inactivated vaccines as compared to the other platforms, and especially the live attenuated ones. More specifically, reversion to the wild-type strain could not occur. Furthermore, it is extremely difficult to produce antibodies against a potential dominant serotype that will subsequently lead to imbalanced immune responses. However, the main disadvantage is the lower immunogenicity, due to their inability to replicate within the host.

1.6.2.1.3 Nucleic acid-based vaccines

A tetravalent DNA vaccine (TVDV) was constructed by the US Army Medical Research. The formulations encode for the entire prM and E proteins of each of the four serotypes, cloned to a VR1012 plasmid vector. This monovalent DNA vaccine is being tested in Phase I of clinical trials, showing both high immunogenicity and protection (64).

1.6.2.1.4 Subunit vaccines

A monovalent vaccine formulation based on the ectodomains of the E-protein of each of the four serotypes (DEN-80) was developed and further cloned into expression plasmids. *Drosophila* Schneider-2 cells were used for the expression of prM/E and the recombinant antigens were further purified by immunoaffinity chromatography. This vaccine has shown to elicit strong neutralizing antibodies, with a good safety profile. In addition, the tetravalent version of this vaccine candidate (V180), has demonstrated even higher levels of neutralizing antibodies with a triple-dose schedule (65).

It is important to note that several DENV vaccine candidates, based on recombinant antigens (focused on E protein), have been developed so far. However, only V180 is advanced in Phase I of clinical trials until now.

1.6.2.1.5 Virus Like Particles (VLP)-based vaccines

This uprising technology is utilized in the development of new generation vaccines, as it provides improved safety, compared to live-attenuated candidates. Particularly, VLPs constitute structures that mimic viruses, but lack the viral genome. VLP-based vaccines induce strong T cell and neutralizing antibody responses, by displaying antigens on the surface of the particle. Some of DENV vaccine candidates, using this platform, miss viral prM protein, which is believed to play a vital role in the production of non-neutralizing antibodies that might lead to the development of the ADE phenomenon (66).

1.6.2.2 ZIKV

Concerning ZIKV, a number of different vaccine candidates have been developed. From these, nine have completed Phase I of clinical trials, while only one (DNA-based) is currently advanced to Phase II. In addition, more than 40 candidates are in preclinical development.

One of the major hurdles in ZIKV vaccine development is the establishment of protective efficacy and safety in a very special group, the pregnant women. As for DENV, similar vaccine platforms exist for ZIKV, including nucleic acid-based, viral vector-based, recombinant subunits, as well as live attenuated and inactivated viruses.

To date, the only candidate in the most advanced stage (Phase II) is a DNA-based vaccine (VRC- ZKADNA090-00-VP) that encodes the wild type prM and E proteins from the H/PF/2013 ZIKV strain. Findings from Phase I studies showed that administration of the vaccine presented mild side effects, but a protective amount of neutralizing antibodies had been developed (67). In addition, other promising vaccine platforms have drawn the attention, such as viral vector (adenovirus)-based candidates. High safety profile and ability of induction of both humoral- and cellular-mediated immune responses constitute the main factors to the development of these vaccines.

As indicated above, the majority of the existing vaccine platforms are based on the induction of neutralizing antibodies in order to provide protection to individuals. However, the key role of T-cell-mediated immune responses (mainly controlled by NS proteins) is not taken seriously into account, thus leading to "missing points", regarding their immunogenicity and protective capacity.

Despite the huge impact of flaviviruses on the economy and society, there are approved human vaccines against few of them (YFV, JEV, TBEV). Increased travelling in regions where both viruses circulate, as well as common transmission routes of DENV and ZIKV strongly highlight the importance of a prophylactic vaccine to prevent infection by these two viruses.

1.6.3 Antivirals

Difficulties in the development of efficacious vaccines against both DENV and ZIKV have turned researchers' attention to the development of antivirals. Even though no therapeutic antiviral drugs are available against any of these flaviviruses, a large number of compounds have been evaluated for their

activity. Particularly, repurposing studies have been introduced in order to screen FDA- approved drugs against DENV and ZIKV (68)(69). Since these molecules have already been tested for their safety profile, this strategy is less time-consuming and might provide good candidates against DENV/ZIKV infection. In addition, considerable efforts have been made by the scientific community to identify new antiviral molecules. These candidates should not only provide high efficiency and safety, but they have to be able to pass through physical barriers, such as placenta and BBB (in case of ZIKV).

Two distinct antiviral classes have been described so far: Direct-acting (DAAs) and host-directed (HDAs).

DAAs are compounds that directly interact with viral proteins (structural and NS) to exert antiviral functions. This interesting class of molecules offer a promising approach as they specifically target viral proteins, therefore presenting low cytotoxicity. Virus E protein, as well as NS5 and NS3 constitute the most attractive antiviral targets, as they play vital roles in the entry and replication processes. However, the major drawback of DAAs development is the high risk of resistance selection (70). On the other hand, HDAs can surpass the issue of resistance, thus increasing their efficacy. During the infection process, flaviviruses are able to recruit different cellular factors to establish a favorable environment. So, any host factor involved in each viral step of the flavivirus life cycle (e.g. entry, fusion, translation, replication, assembly) could be targeted by HDAs. However, targeting cellular factors/pathways could result in high cytotoxicity levels (71). Despite the large number of DAAs/HAAs identified in *in vitro* and *in vivo* assays for DENV (Table 1), ZIKV (Table 2) or even both of viruses (Table 3), only a few have proceeded towards clinical studies (discussed below) (72)(73).

Balapiravir (prodrug of the nucleoside analog 4'-azidocytidine) constitutes the only DAA, evaluated in clinical trials. This drug was firstly developed for the treatment against HCV, through its ability to interfere with the viral RNA replication stage (RdRp). Antiviral activity of balapiravir was also evaluated against DENV. Although promising *in vitro* results were obtained, no significant differences were observed in plasma viremia, decrease of fever as well as cytokine profile in DENV patients, who received the antiviral drug (compared to the placebo group), during Phase II of clinical trials (74).

Another example is chloroquine (CQ), a widely used anti- inflammatory drug, which showed antiviral activity against both DENV and ZIKV. CQ interferes

with the viral entry steps, and more specifically, the pH-dependent fusion between viral and host membranes (75). In addition, CQ showed to reduce virus production and inhibit cell death in ZIKV-infected human brain microvascular and neural stem cells, without cytotoxic effect. In contrast to ZIKV, CQ did not significantly reduce viremia (NS1 levels) in DENV-infected patients (76). Since CQ has already been approved (for the treatment against malaria and autoimmune diseases), it can be considered as a promising candidate against ZIKV infection. Furthermore, its safety profile (especially during pregnancy) has also been described (77).

Finally, celgosivir (6-O-butanoyl derivative of castanospermine) is an HDA prodrug that demonstrated good antiviral activity against DENV. Its function is based on the inhibition of endoplasmic-reticulum associated α-glucosidases, which are essential in the maturation of viral glycoproteins, thus preventing the virus assembly process. However, clinical studies with this compound resulted in no pronounced reduction of viremia and fever in DENV-infected patients (78).

Table 1: List of described anti-DENV compounds, evaluated in pre-clinical and clinical studies (72)

Compound	Target	Mechanism of action
Doxycycline	Envelope	Fusion inhibitor
Sulfated K5 polysaccharides	Envelope	Virus entry inhibitor
ST-148	Capsid	Capsid protein inhibitor
Balapiravir	NS5 (RdRp domain)	Viral RNA replication inhibitor
Retrocyclin	NS2B/NS3	Viral protease inhibitor
SDM25N	NS4B	IFN-signaling inhibitor
Duramycin	TIM1 receptor	Virus entry inhibitor
Celgosivir	ER-associated α-glucosidase	E/NS1 accumulation in ER
Castanospermine	ER-associated α-glucosidase	Folding interference of prM and E
Prednisolone	Anti-inflammatory activity	Viral replication inhibitor

Table 2: List of anti-ZIKV compounds, evaluated in pre-clinical and clinical studies (73)

Compound	Target	Mechanism of action
Favipiravir	NS5 (RdRp domain)	Viral RNA replication inhibitor
Sofosbuvir	NS5 (RdRp domain)	Viral RNA replication inhibitor
Sinefungin	NS5 (methyltransferase domain)	Viral RNA replication inhibitor
EGCG	Envelope phospholipids	Virucidal agent (possibly entry)
Temoporfin	NS2B/NS3	Viral protease inhibitor
Curcumin	NS2B/NS3	Viral protease inhibitor
PHA-6905097	Cyclin-dependent kinases	Viral RNA replication inhibitor
Memantine	Neurons	Neuronal cell death inhibitor
Emricasan	Caspase-3	Proteasome pathway inhibitor
Daptomycin	PG-rich late endosomal membranes	Viral entry inhibitor

Table 3: List of antiviral molecules, showing significant activity against both DENV and ZIKV (72) (73)

Compound	Target	Mechanism of action
7-deaza-2-CMA	NS5 (RdRp domain)	Viral RNA replication inhibitor
NITD008	NS5 (RdRp domain)	Viral RNA replication (Pyrimidine synthesis) inhibitor

Suramin	NS3	Protease inhibitor
7DMA	NS5 (RdRp domain)	Viral RNA replication inhibitor
Chloroquine	Interaction of virus/host membranes, furin-mediated maturation	pH-dependent fusion and maturation inhibitor
Lovastatin	Cholesterol synthesis	Viral RNA replication/assembly inhibitor
Bortezomib	Proteasome pathway	Viral egress inhibitor
Ribavirin	NS5 (RdRp domain)	Viral RNA replication (Purine synthesis) inhibitor
Cyclosporine	Interaction of cyclophilin A/NS5	Viral RNA replication/Protein folding inhibitor

Development of new antivirals, able to inhibit a large number of flaviviruses, is a challenging task. Several factors have to be taken into account, since members of the same virus family follow distinct pathways for their replication and infection. This is extremely important for molecules that target host factors. As observed from the Tables above (Table 1-3), a number of FDA-approved drugs present specificity for DENV, ZIKV or both viruses. This could be explained by the fact that closely related flaviviruses are able to interact with cellular components in a different way, thus affecting compounds' specificity (70).

Until now, treatment against DENV and ZIKV is based on relief of symptoms. Analgesics and antipyretics, such as acetaminophen, are applied to reduce the pain and fever in DENV/ZIKV-infected patients. Antiviral drug development should be cautiously performed to identify molecules with high antiviral activity against a number of flaviviruses, low cytotoxicity levels, high genetic barrier to resistance as well as effective distribution. To achieve this, screening of potential antiviral drugs should start in a number of different susceptible target cell lines (especially human cells) to evaluate their efficacy. In addition, three-dimensional organoids have been established to overlap the limitations of cell cultures, by providing a simplified version of organs (79). Finally, progression in animal models development (e.g. mice) is crucial to understand host- pathogen interactions. Evaluation of antiviral candidates into non-human primates will be a "key" in our effort to study DENV/ZIKV pathogenesis.

1.7 Extracellular vesicles and their role

Viruses manipulate several cellular pathways during entry, replication and egress processes. One of the most reported mechanisms that different viruses exploit to facilitate their infection, is the exosomal pathway, in which extracellular vesicles (EVs) establish the major "key players"(80). Despite the fact that EVs were first proposed as a waste disposal system, their role was revised in the early 1980's, where Pan and Johnstone successfully described the secretion of transferrin receptor from membrane-enclosed vesicles, released from sheep reticulocytes (81). This discovery constituted the starting point of EVs in the scientific community. During the last years, remarkable progress has been carried out on the significance of these tiny vesicles. Besides their ability to transfer any viral/host components to other susceptible cells, EVs can be recruited as drug delivery carriers, due to their safety profile (further discussed in Chapter 6). Compared to other systems, EVs can directly interact with the cellular membrane and internalize any drug molecule with increased efficacy. Moreover, their cellular-based origin allows them to reach into anatomical sites that are difficult to target (e.g. brain), without an extensive activation of immune responses. Based on that context, any efficient antiviral compound could be loaded (exogenously or endogenously) into cell-derived vesicles and further transported to various target organs/tissues in a highly specific manner. Using this approach, we are able to overcome potential issues that rise by the direct transfer of molecules, including poor biodistribution, off-target delivery and side effects.

1.7.1 Extracellular vesicle subpopulations

EVs are small vesicles (diameter ranging from nm to μm), composed of a lipid-bilayer membrane. Different cell types and body fluids have been shown to secrete EVs in response to stimuli. They are characterized by their capacity to incorporate and transfer proteins, lipids and nucleic acids to recipient cells, thus contributing as important intercellular communicators. The content of these secreted vesicles is largely dependent on the origin and the condition of the cells they originate from (82). In the literature, several cell lines have been described to produce and secrete heterogeneous EV populations, based on their size and biogenesis mechanisms. Particularly, five main EV populations have been proposed so far: apoptotic bodies (ABs), large oncosomes (LOs), microvesicles (MVs), exosomes and exomeres (*Figure 1.6*).

Apoptotic bodies have a size that ranges from 500 nm to 5 μm. They are released into the extracellular space (via membrane blebbing) during

apoptosis and have been found to contain remnants of apoptotic cells (e.g. organelles, nuclear fragments). In most cases, ABs are recognized and phagocytized by a number of different immune cells, including macrophages and dendritic cells, thus leading to their degradation. However, recent studies have demonstrated that ABs are involved in cancer progression and immunomodulation, through transfer of proteins and nucleic acid molecules (83). Although their function is still ambiguous, ABs seem to act as messengers, able to trigger biological responses.

On the other hand, LOs have been described as non-conventional EVs, with abnormal structure, that carry oncogenic-related molecules. These vesicles have approximately the same diameter as ABs (1-5 μm) and are exclusively secreted by cancer cells, through protrusions of the plasma membrane (84). Although the number of LO-related publications is limited, more researchers are making efforts to elucidate their vital role in the cancer field.

The smallest EV population that has been recently described is exomeres. Exomeres are small (< 50 nm) non-membranous nanoparticles, which are able to transfer functional cargo (e.g. receptors, lipids and nucleic acids) to recipient cells. Although isolation of these vesicles is quite challenging, since their size overlaps with the size of exosomes, development of new techniques (e.g. asymmetric flow field fractionation) allows the efficient separation of exomeres from other EVs (85). Studies are ongoing in order to decipher the functional role of this interesting class of EVs.

The two most studied EV populations are microvesicles and exosomes. MVs or ectosomes (100 nm – 1000 nm) are produced from the outward budding and fission of plasma membrane and are implicated in intercellular communication, through transport of active biomolecules (e.g. miRNAs, lipids). Specifically, the role of MVs has been described in apoptosis (86), inflammation and autophagy (87). In addition, several proteins have been identified as MV-specific markers, including integrins, tetraspanins and flotillins (88). As displayed in *Figure 1.6*, MVs and exosomes have comparable diameters. Furthermore, common markers have been reported (such as CD63, CD81 and ALIX) in both EV populations, making the isolation and discrimination of MVs from exosomes extremely difficult (89).

Finally, exosomes are formed within endosomal multivesicular bodies (MVBs) and typically have a diameter of 30-100 nm. Fusion of MVBs with the plasma membrane leads to their secretion into the extracellular space (90). However,

MVBs can also fuse with the lysosomes resulting in their degradation. The fate of MVBs depends on the content of the vesicles (91). As previously described, exosomes are highly enriched in tetraspanins (CD63, CD9, CD81), fusion proteins (GTPases, annexins), MVB-biogenesis related proteins (ALIX, TSG101) as well as lipids (e.g. cholesterol, phosphatidylserine, sphingomyelin) (92). The role of exosomes as regulators in cell-to-cell communication has been described in many pathophysiological conditions, including immune activation/evasion, heart function, neurological disorders and cancer progression and metastasis (further discussed below).
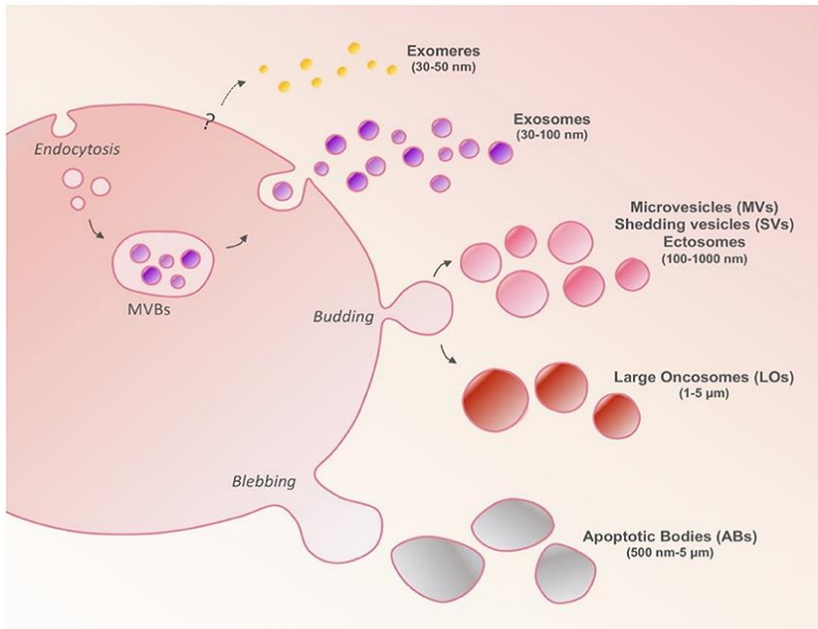
Figure 1.6: **Different populations of extracellular vesicles (EVs) are secreted by all cell types**. These EVs differ in size, composition and secretion mechanisms. Large oncosomes (LOs) are exclusively shed by cancer cells with a size range from 1 μm to 5 μm. Apoptotic bodies (ABs) are formed by the blebbing of plasma membrane during programmed cell death (500 nm-5 μm). Microvesicles (MVs) are derived from the outward budding and fission of plasma membrane and they have a smaller size range than ABs (100 nm-1000 nm). On the other hand, exosomes (50 nm-200 nm) are produced by the inward budding of cellular compartments (multivesicular bodies, MVBs) and secreted into extracellular space, followed by fusion with the plasma membrane. Finally, exomeres have a smaller size than exosomes (<50 nm) and found to be non-membranous particles with unknown biological functions (93).

1.7.2 Biogenesis mechanisms

Several mechanisms have been described to regulate cargo sorting and biogenesis of EV populations. In this part, we will review the basic molecules that contribute to the formation of exosomes and microvesicles. As mentioned in 1.1.7.1, the content of exosomes and microvesicles barely differs, possibly indicating that a number of host factors is needed for both EV populations. Particularly, the endosomal sorting complex required for transport (ESCRT) regulates cargo concentration (in MVBs), changes in membrane formation (initial step in EV formation) and membrane budding into the extracellular space (94). ESCRT proteins are associated with membranes and can be divided into two main complexes. ESCRT-0, - I and –II are implicated in cargo composition, membrane deformation and vesicle formation inside the endosomal membranes, while ESCRT-III is involved in vesicles release into MVBs (95). Most common ESCRT proteins found in EVs are ALIX and TSG101, which can co-merge and play a significant role in EV biogenesis (96). Role of ALIX has also been discussed in the formation of vesicles via the syntenin-syndecan complex (97), in which the adaptor syntenin is able to directly interact with ALIX, thus leading to intraluminal vesicle budding. Although the function of ESCRT complexes in EV biogenesis has been identified, different mechanisms (ESCT-independent) have also been characterized.

Tetraspanins are a family of transmembrane proteins with four domains (two extracellular loops and two short intracellular tails) that facilitate distinct roles in cell physiology, such as receptor signaling, fusion and protein trafficking (98). Extracellular loop domains interact with integrins, while cytoplasmic tails are linked to intracellular proteins, thus promoting cell signaling. In most EV studies, tetraspanins are used as markers to identify the presence of EVs in the preparations. For example, CD9, CD63 and CD81 are the most commonly used proteins.

Another ESCRT-independent mechanism that regulates budding of EV membranes involves the participation of lipids and lipid rafts. These macro- biomolecules can interact with a number of proteins (e.g. tetraspanins, cytoskeleton), thus playing a role in EV biogenesis. Moreover, lipids are important second messengers in signaling pathways, regulating membrane trafficking (99). Furthermore, lipid rafts (lipid micro domains) have been found to be important in cargo sorting within exosomes, as well as in MV biogenesis. In contrast to proteomic, few lipidomic studies have been

reported, showing that a set of lipids are enriched in EVs, derived from different biological sources. Specifically, cholesterol (EV formation) and sphingolipids (EV biogenesis) are highly abundant in the membranes of EVs. In addition, neutral sphingomyelinase enzyme has shown to participate in biogenesis of secreted vesicles, by hydrolyzing sphingomyelin to ceramide and phosphatidylcholine (PC). Ceramide is responsible to trigger the formation of MVBs, while PC is involved in membrane- mediated cell signaling (100). Since a limited number of studies is provided now, further work will be necessary to identify the key roles of specific lipid species/classes in EV biogenesis mechanisms.

Finally, ubiquitination serves as an important signal on cargo sorting during endocytosis and formation of MVBs (101). This particular modification of cargo proteins constitutes a crucial determinant for ESCRT-dependent sorting mechanism into the EV pathway and it has been described in the regulated release of neurodegenerative proteins, as well as in enveloped virus budding process (102)(103).

Contrary to MVs, exosome production and secretion requires fusion of MVBs with the plasma membrane. Several proteins have been associated with EV formation, fusion with plasma membrane and signaling processes. Major examples of these proteins are Ras, Rab, Rho, Arf and SNAREs. Particularly, Rab GTPases are involved in transport and fusion with the membrane, whereas Rho are associated with MV formation through reorganization of actin protein (104). On the other hand, SNAREs constitute crucial components of fusion process between vesicles and plasma membrane. Interaction of the SNARE complex with regulatory proteins (such as Munc18-1) results in efficient exocytosis (105). Finally, Arf GTPases interact with diverse proteins to regulate trafficking in the endocytic pathway. In addition, an important GTPase (Arf6) has been shown to interact with cytoskeleton proteins (e.g. myosin and actin), along with proteins of the ESCRT complex, in order to actively participate in EV biogenesis machinery (106). In conclusion, the diversity of biogenesis mechanisms described above suggests that multiple cellular pathways may influence the production and secretion of distinct EV populations with unique cargos and functions.

1.7.3 Uptake mechanisms

Following secretion of EVs into the extracellular space, vesicles can be taken up by recipient cells through different routes. Internalization of EVs is an

energy-dependent process, where proteins and lipid molecules are involved in. Below, we will discuss in more detail the main EV uptake mechanisms (*Figure 1.7*).

Most of the experimental procedures propose that EVs are mainly taken up via endocytosis. Clathrin-mediated endocytosis (CME) facilitates cellular internalization and recycling of molecules through progressive assembly of clathrin-coated vesicles. Clathrin is a scaffold protein composed of three heavy and three light chains. These vesicles incorporate a range of different proteins (such as actin and myosin), during the maturation process. Next, clathrin-coated vesicles bend the membrane, thus creating a vesicular bud that subsequently pinches off (107).

Besides CME, clathrin-independent endocytotic pathways also exist. One such mechanism is caveolin-dependent endocytosis (CDE). Caveolae are small cholesterol/sphingolipid-enriched invaginations of the plasma membrane that can be internalized into the cell. Caveolar invaginations bud from the plasma membrane in a dynamin-dependent mechanism to form caveolar vesicles. In addition, caveolin-1 seems to act as a regulator in this process, by stabilizing cavolae at the membrane (108).

Macropinocytosis is a type of endocytosis that involves the uptake of non- specific material. This process is facilitated by the inward folding of cell surface ruffles, which subsequently leads to fusion with the basal membrane and formation of macropinosomes (actin- dependent mechanism) (109). In addition, phagocytosis constitutes an internalization mechanism of opsonized material and is mediated by immune cells, such as macrophages. This receptor-based event involves the progressive formation of invaginations surrounding the material destined for internalization, with or without the participation of enveloping membrane extensions (as indicated in micropinocytosis). Opposed to macropinosomes, phagosomes can engulf specific material and larger particles. Finally, it has been established that phosphoinositide 3-kinases (PI3Ks) are crucial in enabling membrane insertion into forming phagosomes (109).

Lipid rafts are microdomains with altered phospholipid composition, found in the plasma membrane. They have multiple functions, as they affect membrane fluidity and are involved in protein trafficking. In addition, they are implicated in signaling processes. Components of lipid rafts are highly organized and more tightly packed than the surrounding lipid bilayer.

Flotillins (lipid raft EV markers) have been found to interact with glycosylphosphatidylinositol (GPI)-anchored proteins during the internalization stage. Besides their function in EV uptake, lipid rafts have been reported to contribute to viral particles uptake through interaction with glycoproteins (110).

Finally, a possible entry mechanism of EVs into cells is via direct fusion of EV membrane with the cell plasma membrane. During that process, both lipid bilayers are coming into close proximity, leading to the formation of a bud with fused outer leaflets. According to the literature, a number of different protein families have been participated in this mechanism, including SNAREs and Rab (111).
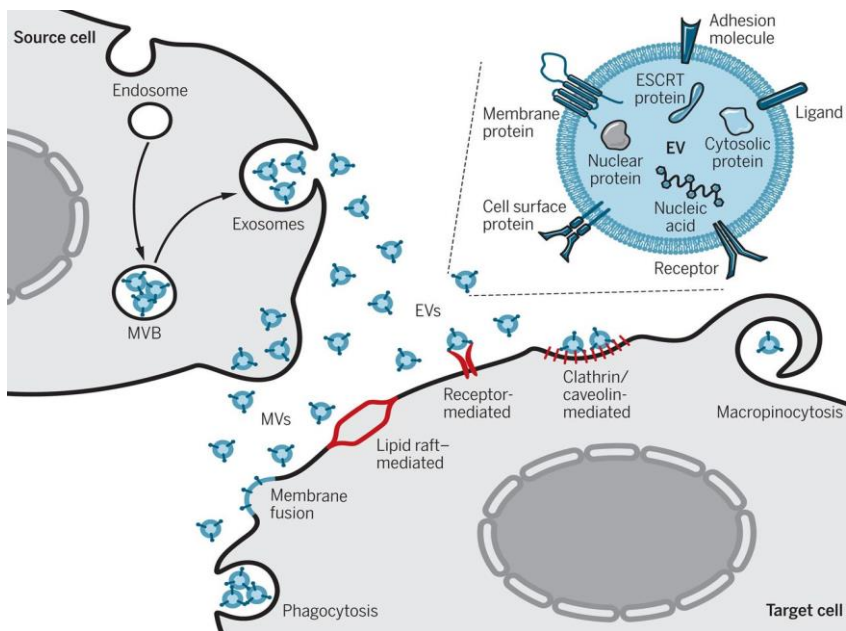
Figure 1.7: **Biogenesis, composition and uptake mechanisms of EVs.** Exosomes are formed into MVBs through the endocytic pathway and further secreted into the extracellular space, after fusion with the plasma membrane. EVs are composed of a lipid-bilayer membrane, which encloses proteins, lipids and nucleic acid molecules. Several EV uptake mechanisms have been described, including phagocytosis, membrane fusion, clathrin/cavolae- and receptor-mediated endocytosis, as well as micropinocytosis (112).

1.7.4 Role of extracellular vesicles in pathophysiological conditions

The role of EVs has been described in many normal but also in pathological conditions. In this section, we will provide some examples on how these secreted vesicles affect the function of target cells.

1.7.4.1 Immunomodulation

Antigen-presenting cells (APCs) and especially dendritic cells (DCs), have been shown to regulate specific immune responses to recipient cells. Particularly, EVs-derived from mature dendritic cells are able to modulate host responses, by presenting MHC type-I and –II peptides on their membranes, thus leading to direct binding on T-cell receptors. This process will result in activation of $CD4^+/CD8^+$ cellular responses (113). Besides antigens, APCs-derived EVs transfer other signaling material, including co-stimulatory proteins (e.g. CD80, CD86) and adhesion molecules. In addition, mast cell-derived EVs contain high levels of heat shock proteins HSP60 and HSC70 that promotes DC maturation (113). Moreover, macrophage-derived EVs can incorporate IL-1β and members of the TNF family (e.g. FasL, CD154). Subsequently, these EVs-carrying TNF family proteins are recognized by distinct immune cells, such as natural killer cells (NKs) and DCs (114). Finally, the immunomodulatory role of mesenchymal stem cells (MSCs) has been extensively reported in the literature, through their interaction with the immune cells. MSCs secrete a number of vesicles that incorporate chemokines, cytokines (e.g. TGF- β, IL-6, IL-10), as well as miRNAs to attract different types of T cells. These MSCs-derived EVs present therapeutic properties and can easily be administered for the treatment of inflammatory and autoimmune diseases (115) (116).

Regarding the latter, EVs also have a role in mediating autoimmune diseases. Particularly, EVs-derived from the serum of patients with rheumatoid arthritis (RA) present higher levels of proinflammatory cytokines (TNF-α, IL-6), chemokines (CCL2, CCL5), as well as adhesion molecules (ICAM-1, ICAM-2), as compared to the EVs from healthy donors (117).

1.7.4.2 Cancer and cardiovascular disorders

The role of EVs in cancer progression and metastasis has been extensively studied. A variety of cytokines, growth factors, adhesion molecules and extracellular matrix proteins are secreted by tumor cells via EVs, thus

mediating cell-to-cell communication within the tumor microenvironment. These vesicles act as vehicles to achieve interplay between normal and cancer cells, promoting angiogenesis, tumor formation and immune suppression. Specifically, Zhu *et al* showed that MSCs-derived EVs are able to trigger VEGF-mediated pathways in tumor cells through the activation of Erk 1/2 and MAPK kinases, thus resulting in increased angiogenesis (118). In addition, EVs derived from cancer cells have been demonstrated to activate signal transduction pathways involved in cancer progression. Beckler and colleagues identified the presence of mutated KRAS in EVs, released by colon cancer cells and showed that the mutated form of this GTPase can induce changes in the composition of the vesicles, leading to tumor progression in the recipient wild-type KRAS- expressing cells (119). Moreover, EVs contain several mRNA/miRNAs that affect cell phenotypes and facilitate the activation of proinflammatory responses. Besides these, EVs can contribute to tumor suppression by miRNA-mediated interference with therapeutic agents, leading to drug resistance (120). Finally, nasopharyngeal carcinoma-derived EVs are enriched in galectin-9, which constitutes a TIM-3 receptor ligand that promotes T-cell apoptosis (immunosuppressive role) (121). EV- mediated intracellular communication has also been discussed in cardiovascular diseases. Increased levels of miR-939 have been detected in serum-derived EVs from patients with myocardial ischaemia and injury. In addition, plasma-derived vesicles incorporate miR-21-3p, which is associated with aberrant enlargement of cardiac tissue (122).

1.7.4.3 Brain function and neurological disorders

EVs have been considered as a major way of intercellular communication in the normal physiology of the nervous system. Different reports demonstrated the release of EVs from different cell types such as astrocytes, microglia, endothelial cells and neurons (123). Secreted vesicles released by differentiated neurons are regulated by synaptic glutaminergic activity, possibly contributing to the normal synaptic physiology. Astrocyte- and neuron-derived EVs contain both VEGF and FGF factors that promote vascularization of developing brains (123). Oligodendrocyte-derived EVs are responsible for the cross-talk with the neuronal axons, through transfer of myelin proteins, such as proteolipid (PLP), basic 2'3'-cyclic nucleotide 3'-phosphohydrolase protein (CNP) and myelin oligodendrocyte glycoprotein (MOG) (124). Another important class of brain cells are microglia, which constitute the immune cells of the central nervous system (CNS) and are also

involved in tissue repair. Microglia-derived EVs not only support neuronal energy metabolism (through transfer of enzymes), but they also contain other specific proteins, including HSP90, galectin-3 and enolase to provide a crucial role in protein secretion (125). Finally, endothelial cells establish the main cell type that gives rise to the blood-brain barrier system (BBB). Vesicles secreted by these cells have the ability to cross through the BBB and deliver brain-specific proteins (potential biomarkers) into the blood system, thus contributing to a more detailed picture of brain-related diseases. Moreover, their ability to easily pass the BBB and further transfer a number of proteins (e.g. receptors), make EVs a great and promising tool for drug delivery.

Except for their physiological functions in the brain system, EVs might also play a vital role in neurodegenerative diseases, such Alzheimer, Parkinson, Prion diseases and ALS. Prion diseases are neurodegenerative disorders, composed of misfolded proteins in the CNS. Several groups have described the ability of EVs to incorporate and release prion proteins (protection from degradation) to susceptible cells (126). Parkinson's disease is characterized by the presence of lesions (Lewy bodies) that mainly contain aggregates of α-synuclein. Different mechanisms have been involved in the release of α-synuclein into EVs, including the autophagy-lysosome pathway as well as the overexpression of Rab11 GTPase (127). On the other hand, Alzheimer's disease is a late-onset disorder that results in progressive neurodegeneration and characterized by the accumulation of amyloid-β (Aβ) peptides (known as amyloid plaques), derived from proteolysis of the amyloid precursor protein (APP), in the brain of patients. APP protein along with proteolytic enzymes have been found in the neuroblastoma- and microglia-derived EVs, thus implicated in Aβ pathology. Until now, there is no specific mechanism involved in the extracellular release of APP protein (128). Finally, the potential function of EVs has been discussed in the development of ALS, a neurodegenerative disorder of the motor neurons, with no available treatment. Specifically, mutated forms of superoxide dismutase 1 are associated with the disease and are also found into secreted EVs (129).
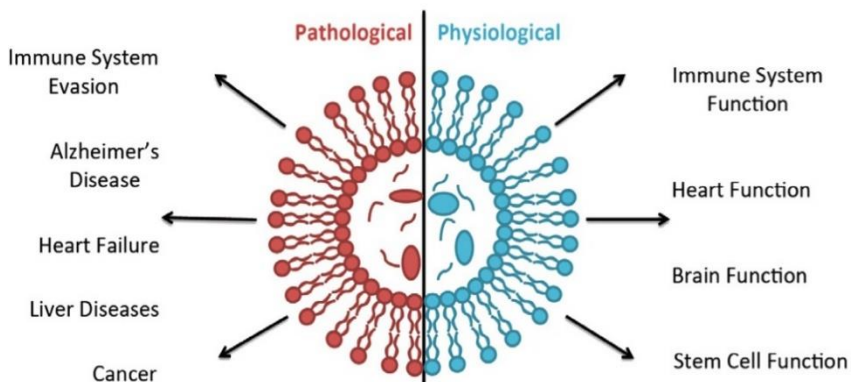
Figure 1.8: EVs act as intercellular messengers, facilitating the interaction between cells of the same or different type. Based on their content, EVs are essential in many pathophysiological conditions, including cancer, neuropathological manifestations and viral infections (130).

1.7.4 EV isolation techniques

A number of different EV isolation procedures have been characterized so far. However, the choice of the appropriate method is quite challenging, since no "gold standard" exists. The main factors that determine which isolation protocol is going to be followed depend on the cellular source (origin of EVs) and the downstream applications. The most standard technique is differential centrifugation, followed by ultracentrifugation (UC). This process involves a series of centrifugation steps to remove dead cells and cellular debris, accompanied by centrifugation at extremely high speeds (> 100,000 g forces) to collect EVs as a pellet. Although this procedure is straightforward, it requires time and large volumes of starting material. In addition, co-precipitation of non-vesicular contaminants constitute a restricting factor in EV analysis (131). In order to diminish contamination by non-EV associated proteins, a density gradient-based separation protocol can be applied. Two main types of gradients are mostly used to isolate vesicles, based on their densities: sucrose and iodixanol. Although the sucrose gradient sufficiently isolate EVs, it has been found highly toxic and it does not allow to discriminate vesicles from viruses (132). On the contrary, iodixanol-based gradients (Optiprep™) can overcome these limitations. Ultrafiltration provides an alternative isolation method, in which EVs can be distinguished from smaller material. However, non-vesicular content and lipoproteins can also remain in

the filter, thus providing low purity, as compared to the ultracentrifugation-based methods. In most studies, ultrafiltration requires extra steps of purification to achieve high EV purity (133). Size-based isolation methods have been increasingly used by scientific community. Particularly, size exclusion chromatography (SEC) separates small from large molecules, by trapping the first into the pores of a matrix, while allowing the latter to flow through. SEC is mostly applied to different body fluids (e.g. serum, urine) in order to remove any contaminants and lipoproteins, which are highly enriched and can co- localize with the EVs (134). Studies have shown that a combination of SEC, density gradient and ultracentrifugation allow the efficient separation of EVs from lipoproteins (e.g. HDL, LDL, VLDL). Although the yield of the vesicles is relatively low, a high purity and specificity are ensured. In addition, polymer-based precipitation methods, such as PEG and commercial isolation kits, have been applied for EV isolation. This particular isolation technique is quite fast and provides high recovery of vesicles, thus promoting them as potential clinical tools for biomarker discovery. Despite their "enriched" yield, the purity obtained with this method is poor, as compared to the aforementioned techniques, due to co-precipitation of non-vesicular-associated proteins that may affect conclusions on EV function (135). Furthermore, affinity-based capture methods have been described to offer extremely high EV purity and sensitivity, while maintaining the integrity of the vesicles. For example, several tetraspanins (e.g. CD63, CD9, CD81) are used to capture specific EV subpopulations with high specificity. The major disadvantage of this method is that antigen-captured EVs do not represent the whole heterogeneous population of vesicles, secreted by different cellular sources. Moreover, the beads or the antibodies used during the process may also interfere with the downstream analysis. Recently, Wan and colleagues developed a magnetic bead-based EV isolation method, using lipid-based nanoprobes (136). This technology enables a short-time enrichment of vesicles, with good efficiency, as compared to this observed in ultracentrifugation. Finally, novel technologies have been developed to provide higher EV scalability, purity and integrity, such as a asymmetric flow field-flow fractionation (AF4). AF4 is an elution-based procedure, able to separate particles from few nanometers to micrometers. This method allows size-based separation of sample components in an increasing order of molecular weight or hydrodynamic diameter, when a crossflow is applied across the channel. The advantages of this technique over conventional methods are reproducibility, great recovery of various biological species (such

as lipoproteins, ribosomal subunits and virus-like particles) and high speed (~1h). However, the expertise of the technology makes AF4 an unable approach to be used by its own. Coupling of this method with an electric field results in further separation of the particles, depending on additional physical characteristics (e.g. surface charge). High specificity can be also attained by the ability of AF4 to discriminate between exosomes and exomeres, providing an important tool for molecular diagnostics and therapeutics (137). To conclude, the large variety of isolation techniques provides researchers with the ability to use the appropriate method for their application and downstream analysis.

Table 4: Details on existing EV isolation methods

Isolation methods	Advantages	Disadvantages
Ultracentrifugation (UC)	-easy-to-follow protocol -widely used	-time consuming -large volumes required -low EV purity
Density gradient (ODG)	-small sample volume -high purity/specificity -efficient separation from viruses	-time consuming -low recovery -extra equipment required
Ultrafiltration	-relatively fast method -straightforward -low cost	-intermediate recovery and purity -usually extra steps required for EV isolation
Size exclusion chromatography (SEC)	-quite fast -high purity/specificity -better reproducibility than UC	-high protein contamination in blood samples (sample needs to be diluted) -low recovery
Precipitation kits (polymer-based)	-High recovery -fast and easy to follow	-Low purity due to contaminants -difficult to correlate EV-specific functions
Asymmetric flow field-flow fractionation (AF4)	-Fast -improved isolation efficiency/purity -small sample volume	-low recovery -complexity in the set-up process
Immunoaffinity	-high specificity/purity -extremely high sensitivity	-prior knowledge of EV/antibody characteristics -evaluation of marker-specific EV subpopulations

As mentioned in paragraph 1.7, several viruses exploit the EV cellular machinery pathway to promote replication, infection and spread to other cells/tissues. Apart from pathology, viruses also use EVs to modulate host antiviral immune responses (138) (*Table 5*). EVs produced by virus-infected cells are involved in intercellular communication between infected and uninfected cells. Unlike EVs-derived from cancer or immune cells, it is difficult to fully separate EVs and infectious (or defective) viral particles, due to similar physiochemical characteristics, such as the size, density and content. In addition, viruses and EVs follow similar pathways during their biogenesis (ESCRT complex), uptake (clathrin-mediated endocytosis) and budding (SNAREs). For example, enveloped viruses, such as retroviruses and flaviviruses, use the endocytic route to enter into susceptible cells and recruit the secretory pathway for their egress into the extracellular space (similar to EVs). Furthermore, EVs are able to incorporate viral proteins and genetic material, leading to the modulation of the recipient cells' function. On the other hand, several reports have described the ability of different viruses to hijack the ESCRT pathway (ALIX- HIV) and tetraspanins (CD81-HCV) during their infection (139)(140). Here, we present some examples to show how EVs exert different mechanisms that contribute to flavivirus pathogenesis. Particularly, EVs-derived from HCV-infected human hepatocytes contain HCV genomic RNA, along with the complex Ago2-HSP90-miR-122, thus facilitating viral replication and stability (141). In addition, EV-mediated transmission of arthropod-borne flaviviruses (Langlat virus, LGTV) from vectors to vertebrates (human) has been described. LGTV-infected tick cells release EVs, which transfer viral RNA, envelope and NS1 proteins to human skin keratinocytes. Moreover, LGTV infects murine brain-endothelial cells, leading to EV production. These vesicles transmit infectious RNA and proteins to the brain, resulting in increased neuropathogenesis (142). Regarding DENV, several reports have demonstrated the ability of EVs derived from infected cells to incorporate and deliver viral content to susceptible cells. Specifically, DENV-infected mosquito cells (C6/36) secrete a number of large/medium EVs, which contain the full-length viral genome and lead to infection of naïve mosquito and mammalian cells (143). This transmission is mediated through interaction of envelope glycoprotein with the tetraspanin Tsp29b (ortholog of human CD63). Moreover, EVs from DENV-infected macrophages have shown to activate endothelial cells, by the transfer of viral NS3 protein and different miRNAs. Activation of these cells by EVs induce changes in the endothelium physiology, through the production and secretion of chemokines/cytokines

(TNF-α, MCP-1, IL-10, RANTES) (144). The inhibitory role of EVs has been demonstrated by the identification of interferon-inducible transmembrane proteins 3 (IFITM3) into EVs-derived from DENV infected cells (145). IFITM3 is a potent antiviral effector that suppresses the entry of a broad range of enveloped viruses and its presence promotes an antiviral effect into uninfected cells. Finally, DENV can activate platelets via pattern recognition receptor CLEC2 (C-type lectin) to release EVs. These vesicles further stimulate the expression of CLEC5A and TLR2 on neutrophils and macrophages, thereby inducing neutrophil extracellular trap (NET) formation and release of proinflammatory cytokines. Increased NET formation is strongly associated with the severity of DENV disease (146).

Infection of brain-related cells (cortical neurons) with ZIKV modulates the expression of neutral Sphingomyelinase (nSMase)-2/SMPD3, thus inducing production and secretion of EVs. Transmission of viral-associated proteins and nucleic acids through these vesicles might result in neurological disorders, such as microcephaly in the developing embryonic brains. Furthermore, it has been shown that semen- and saliva-derived EVs prevent ZIKV attachment to the target cells, inhibiting virus infection. However, these type of EVs do not present any antiviral activity against SARS-CoV2, proposing that both body fluids secrete a large number of EVs that specifically interfere with a number of different viruses (147) (148). To conclude, understanding the interplay between viruses and EVs might help to develop mechanisms in order to respond better to public health threats caused by these pathogens.

Table 5: Examples of EV-mediated mechanisms in viral pathogenesis (138)

Virus (*family*)	Mechanism of pathogenesis	Effect	Outcome
Herpes simplex 1 (*Herpesviridae*)	HSV-1 mRNA/miRNA transport through EVs	Enhancement	Facilitation of virus transmission to host cells
Epstein-Barr (*Herpesviridae*)	EVs-carrying LMP1 inhibit IFN-γ production and T-cell activation	Enhancement	Evasion of host immune responses
Epstein-Barr (*Herpesviridae*)	EVs-carrying MHC-II (from infected B-lymphocytes) are recognized by CD4$^+$ T-cells	Inhibition	Activation of host immune responses
Ebola (*Filoviridae*)	EVs-bound VP40 interact with cyclin D1	Enhancement	Dysregulation of cell cycle, leading to reduced viability of target cells

Respiratory syncytial (*Paramyxoviridae*)	Modulation of EV miRNA/piRNA content	Enhancement	Increased virus infectivity and transmission
Influenza A (*Orthomyxoviridae*)	Modulation of EV miRNA content	Enhancement	Alterations in cellular pathways, promotion of viral persistence
Influenza A (*Orthomyxoviridae*)	Incorporation of EV markers (e.g. CD9, CD81)	Enhancement	Formation of virion structure
Hepatitis B (*Hepadnaviridae*)	EVs-containing HBx induce expression of viral proteins	Enhancement	Facilitation of oncogenic activities
Hepatitis B (*Hepadnaviridae*)	HBV-infected EVs contain vRNA, which induce natural killer group 2D expression	Inhibition	Activation of natural killer cells
SARS-CoV-2 (*Coronaviridae*)	EVs-containing ACE2 enzyme restrict Spike-dependent infection	Inhibition	Inhibition of viral susceptibility of new host cells
Human Immunodeficiency (*Retroviridae*)	Transport of EVs-carrying co-receptor CCR5 to naïve neighboring cells	Enhancement	Facilitation of viral infection and spread
Human Immunodeficiency (*Retroviridae*)	Delivery of antiviral components (e.g. cytidine deaminase APOBEC3G) to target cells	Inhibition	Inhibition of HIV replication, through interference with reverse transcriptase
Human Immunodeficiency (*Retroviridae*)	EVs-carrying Nef protein triggers CD4$^+$ T cells apoptosis	Enhancement	Evasion from host immune responses and induction of viral transmission
Hepatitis C (*Flaviviridae*)	HCV-infected EVs contain full-length vRNA and proteins	Enhancement	Establishment of viral infection, promotion of viral spread
Langat (*Flaviviridae*)	Tick-cell-derived EVs incorporate vRNA, E and NS1 proteins	Enhancement	Increased viral transmission to humans
Dengue (*Flaviviridae*)	DENV-infected EVs (derived from C6/36 cells) carry viral particles	Enhancement	Facilitation of viral propagation
Dengue (*Flaviviridae*)	DC-derived EVs contain mRNA/miRNA, related to immune responses	Inhibition	Production of inflammatory responses to restrict virus infection
Dengue (*Flaviviridae*)	Macrophage-derived EVs transport NS3 protein, thus activating endothelial cells	Enhancement	Establishment of proinflammatory responses
Zika (*Flaviviridae*)	Macrophage-derived EVs induce the secretion of proinflammatory cytokines in placenta	Enhancement	Promotion of inflammation
Zika (*Flaviviridae*)	EV-mediated transport of vRNA and E protein to susceptible cells	Enhancement	Facilitation of virus transmission and spread
Zika (*Flaviviridae*)	EVs-containing interferon-induced factor (IFITM3) suppress viral replication in fetus brain	Inhibition	Restriction of viral spread and transmission

References

1. Mayer S V, Tesh RB, Vasilakis N. The emergence of arthropod-borne viral diseases: A global prospective on dengue, chikungunya and zika fevers. Acta Trop. 2017. 166:155-163

2. Fernandez-Garcia MD, Mazzon M, Jacobs M, Amara A. Pathogenesis of Flavivirus Infections: Using and Abusing the Host Cell. Cell Host Microbe [Internet]. 2009;5(4):318–28.

3. Sotcheff S, Routh A. Understanding flavivirus capsid protein functions: The tip of the iceberg. Pathogens. 2020;9(1).

4. Zhang X, Jia R, Shen H, Wang M, Yin Z, Cheng A. Structures and functions of the envelope glycoprotein in flavivirus infections. Viruses. 2017;9(11):1–14.

5. Op De Beeck A, Molenkamp R, Caron M, Ben Younes A, Bredenbeek P, Dubuisson J. Role of the Transmembrane Domains of prM and E Proteins in the Formation of Yellow Fever Virus Envelope. J Virol. 2003;77(2):813–20.

6. Rastogi M, Sharma N, Singh SK. Flavivirus NS1: A multifaceted enigmatic viral protein. Virol J [Internet]. 2016;13(1):1–10.

7. Luo D, Vasudevan SG, Lescar J. The flavivirus NS2B-NS3 protease-helicase as a target for antiviral drug development. Antiviral Res. 2015;118(September 2005):148–58.

8. Lee CM, Xie X, Zou J, Li S-H, Lee MYQ, Dong H, et al. Determinants of Dengue Virus NS4A Protein Oligomerization. J Virol. 2015;89(12):6171–83.

9. Best SM. The Many Faces of the Flavivirus NS5 Protein in Antagonism of Type I Interferon Signaling. J Virol. 2017;91(3):1–14.

10. Xie X, Gayen S, Kang C, Yuan Z, Shi P-Y. Membrane Topology and Function of Dengue Virus NS2A Protein. J Virol. 2013;87(8):4609–22.

11. Miller S, Kastner S, Krijnse-Locker J, Bühler S, Bartenschlager R. The non-structural protein 4A of dengue virus is an integral membrane protein inducing membrane alterations in a 2K-regulated manner. J Biol Chem. 2007;282(12):8873–82.

12.   Hartlage AS, Cullen JM, Kapoor A. The strange, expanding world of animal Hepaciviruses. Annu Rev Virol. 2016. 3(1):53-75

13.   Ávila-Pérez G, Nogales A, Martín V, Almazán F, Martínez-Sobrido L. Reverse genetic approaches for the generation of recombinant Zika virus. Viruses. 2018;10(11).

14.   Diosa-Toro M, Prasanth KR, Bradrick SS, Garcia Blanco MA. Role of RNA-binding proteins during the late stages of Flavivirus replication cycle. Virol J. 2020;17(1):1–14.

15.   Suthar MS, Diamond MS, Gale M. West Nile virus infection and immunity. Nat Rev Microbiol. 2013;11(2):115–28.

16.   Mackenzie JS, Gubler DJ, Petersen LR. Emerging flaviviruses: The spread and resurgence of japanese encephalitis, west nile and dengue viruses. Nat Med. 2004;10(12S):S98–109.

17.   Weaver SC, Reisen WK. Present and future arboviral threats. Vol. 85, Antiviral Research. 2010. 328–345 p.

18.   Dyer O. Dengue: Philippines declares national epidemic as cases surge across South East Asia. BMJ [Internet]. 2019;366(August):l5098.

19.   Vasilakis N, Holmes EC, Fokam EB, Faye O, Diallo M, Sall AA, et al. Evolutionary Processes among Sylvatic Dengue Type 2 Viruses. J Virol. 2007;81(17):9591–5.

20.   Gubler DJ, Vasilakis N, Musso D. History and Emergence of Zika Virus. J Infect Dis. 2017;216(Suppl 10):S860–7.

21.   Kuno G. Zika virus. Mol Detect Hum Viral Pathog. 2016;29(3):313–20.

22.   Spiteri G, Sudre B, Septfons A, Beauté J. Surveillance of zika virus infection in the EU/EEA, june 2015 to january 2017. Eurosurveillance. 2017;22(41):1–7.

23.   Gregory CJ, Oduyebo T, Brault AC, Brooks JT, Chung KW, Hills S, et al. Modes of Transmission of Zika Virus. J Infect Dis. 2017;216(Suppl 10):S875–83.

24.   Pre-existing immunity to dengue virus shapes Zika-specific T cell response. La Jolla Institute for Allergy and Immunology

25.   Bhatt S, Gething PW, Brady OJ, Messina JP, Farlow AW, Moyes CL, et

al. The global distribution and burden of dengue. Nature [Internet]. 2013;496(7446):504–7.

26. Racherla RG, Pamireddy ML, Mohan A, Mudhigeti N, Mahalakshmi PA, Nallapireddy U, et al. Co-circulation of four dengue serotypes at South Eastern Andhra Pradesh, India: A prospective study. Indian J Med Microbiol [Internet]. 2018;36(2):236–40.

27. Martina BEE, Koraka P, Osterhaus ADME. Dengue virus pathogenesis: An integrated view. Clin Microbiol Rev. 2009;22(4):564–81.

28. Méndez N, Oviedo-Pastrana M, Mattar S, Caicedo-Castro I, Arrieta G. Zika virus disease, microcephaly and Guillain-Barré syndrome in Colombia: Epidemiological situation during 21 months of the Zika virus outbreak, 2015-2017. Arch Public Heal. 2017;75(1):1–11.

29. Begum F, Das S, Mukherjee D, Mal S, Ray U. Insight into the tropism of dengue virus in humans. Viruses. 2019;11(12).

30. Póvoa TF, Alves AMB, Oliveira CAB, Nuovo GJ, Chagas VLA, Paes M V. The pathology of severe dengue in multiple organs of human fatal cases: Histopathology, ultrastructure and virus replication. PLoS One. 2014;9(4).

31. Basílio-de-Oliveira CA, Aguiar GR, Baldanza MS, Barth OM, Eyer-Silva WA, Paes M V. Pathologic study of a fatal case of dengue-3 virus infection in Rio de Janeiro, Brazil. Brazilian J Infect Dis. 2005;9(4):341–7.

32. Salgado DM, Eltit JM, Mansfield K, Panqueba C, Castro D, Vega MR, et al. Heart and skeletal muscle are targets of dengue virus infection. Pediatr Infect Dis J. 2010;29(3):238–42.

33. Noisakran S, Onlamoon N, Hsiao HM, Clark KB, Villinger F, Ansari AA, et al. Infection of bone marrow cells by dengue virus in vivo. Exp Hematol. 2012;40(3):250–9.

34. Libraty DH, Young PR, Pickering D, Endy TP, Kalayanarooj S, Green S, et al. High circulating levels of the dengue virus nonstructural protein NS1 early in dengue illness correlate with the development of dengue hemorrhagic fever. J Infect Dis. 2002;186(8):1165–8.

35. Raj Kumar Patro A, Mohanty S, Prusty BK, Singh DK, Gaikwad S, Saswat

T, et al. Cytokine signature associated with disease severity in dengue. Viruses. 2019;11(1):1–12.

36.   Petit MJ, Kenaston MW, Nagainis AA, Shah PS. Nuclear dengue virus NS5 antagonizes expression of PAF1- dependent immune response genes Author summary. 2021;

37.   Ashour J, Laurent-Rolle M, Shi P-Y, García-Sastre A. NS5 of Dengue Virus Mediates STAT2 Binding and Degradation. J Virol. 2009;83(11):5408–18.

38.   Perez AB, Sierra B, Garcia G, Aguirre E, Babel N, Alvarez M, et al. Tumor necrosis factor-alpha, transforming growth factor-β1, and interleukin-10 gene polymorphisms: Implication in protection or susceptibility to dengue hemorrhagic fever. Hum Immunol. 2010;71(11):1135–40.

39.   Shukla R, Ramasamy V, Shanmugam RK, Ahuja R, Khanna N. Antibody-Dependent Enhancement: A Challenge for Developing a Safe Dengue Vaccine. Front Cell Infect Microbiol. 2020;10(October):1–12.

39.   Rosenberg AZ, Weiying Y, Hill DA, Reyes CA, Schwartz DA. Placental pathology of zika virus: Viral infection of the placenta induces villous stromal macrophage (Hofbauer Cell) proliferation and hyperplasia. Arch Pathol Lab Med. 2017;141(1):43–8.

40.   Ngono AE, Shresta S. Immune response to dengue and Zika. Annu Rev Immunol. 2018;36:279-308.

41.   Placental Pathology of Zika virus: Viral infection of the placenta induces villous stromal macrophage (Hofbauer cell) proliferation and hyperplasia. Arch Pathol Lab Med. 2017:141(1):43-48

42.   Tang H, Hammack C, Ogden SC, Wen Z, Qian X et al. Zika Virus Infects Human Cortical Neural Progenitors and Attenuates their Growth. Cell Stem Cell. 2016. 18(5):587–90.

43.   Shaily S, Upadhya A. Zika virus: Molecular responses and tissue tropism in the mammalian host. Rev Med Virol. 2019;29(4):1–16.

44.   Osuna CE, Lim SY, Deleage C, Griffin BD, Stein D et al. Zika viral dynamics and shedding in rhesus and cynomolgus macaques. Nat Med. 2016. 22(12):1448-1455

45. Miner JJ, Diamond MS. Zika virus pathogenesis and tissue tropism. Cell Host Microbe. 2017. 21(2):134-142

46. Tabata T, Petitt M, Puerta-Guardo H, Michlmayr D, Wang C et al. Zika virus targets different primary human placental cells suggesting two routes for vertical transmission. Cell Host Microbe. 2016. 20(2):155-166

47. Musso D, Roche C, Robin E, Nhan T, Teissier A, Cao-Lormeau VM. Potential sexual transmission of Zika virus. Emerg Infect Dis. 2015. 21(2):359-61

48. Hamel R, Dejarnac O, Wichit S, Ekchariyawat P, Neyret A, Luplertlop N, et al. Biology of Zika Virus Infection in Human Skin Cells. J Virol. 2015;89(17):8880–96.

49. Meertens L, Labeau A, Dejarnac O, Cipriani S, Sinigaglia L, Bonnet-Madin L, et al. Axl Mediates ZIKA Virus Entry in Human Glial Cells and Modulates Innate Immune Responses. Cell Rep. 2017;18(2):324–33.

50. Monel B, Rajah MM, Hafirassou ML, Ahmed SS, Burlaud-Gallard J et al. Atlastin endoplasmic reticulum-shaping proteins facilitate Zika virus replication. J Virol. 2019.93:e01047-19

51. Shaheen R, Maddirevula S, Ewida N, Alsahli S, Abdel-Salam GMH, Zaki MS et al. Genomic and phenotypic delineation of congenital microcephaly. Genet Med. 2019. 21(3):545-552

52. Yamamoto S, Jaiswal M, Charng WL, Gambin T, Karaca E, Mirzaa G et al. A drosophila genetic resource of mutants to study mechanisms underlying human genetic diseases. Cell. 2014. 159(1):200-214

53. Muñoz LS, Parra B, Pardo CA, Neuroviruses Emerging in the Americas Study. Neurological implications of Zika virus infection in adults. J Infect Dis. 2017. 216(suppl_10):S897-S905

54. Dejnirattisai W, Supasa P, Wongwiwat W, Rouvinski A, Barba-Spaeth G, Duangchinda T, et al. Dengue virus sero-cross-reactivity drives antibody-dependent enhancement of infection with zika virus. Nat Immunol. 2016;17(9):1102–8.

55. Kraemer MUG, Reiner RC, Brady OJ, Messina JP, Gilbert M, Pigott DM, et al. Past and future spread of the arbovirus vectors Aedes aegypti

and Aedes albopictus. Nat Microbiol. 2019;4(5):854–63. Available from: http://dx.doi.org/10.1038/s41564-019-0376-y

56. Shaw WR, Catteruccia F. Vector biology meets disease control:using basic research to fight vector-borne diseases. Nat Microbiol. 2019. 4(1):20-34

57. Moyes CL, Vontas J, Martins AJ, Ng LC, Koou SY, Dusfour I, et al. Contemporary status of insecticide resistance in the major aedes vectors of arboviruses infecting humans (PLoS Negl Trop Dis). PLoS Negl Trop Dis. 2021;15(1):1–2.

58. Yen PS, Failloux AB. A review: Wolbachia-based population replacement for mosquito control shares common points with genetically modified control approaches. Pathogens. 2020;9(5):1–14.

59. Kamal M, Kenawy MA, Rady MH, Khaled AS, Samy AM. Mapping the global potential distributions of two arboviral vectors Aedes aegypti and Ae. Albopictus under changing climate. PLoS One. 2018;13(12).

60. Agarwal R, Wahid MH, Yausep OE, Angel SH, Lokeswara AW. The Immunogenicity and Safety of CYD-Tetravalent Dengue Vaccine (CYD-TDV) in Children and Adolescents: A Systematic Review. Acta Med Indones. 2017;49(1):24–33.

61. Halstead S. Recent advances in understanding dengue [version 1; peer review: 2 approved]. F1000Research. 2019;8:1–12.

62. Watanaveeradej V, Simasathien S, Nisalak A, Endy TP, Jarman RG, Innis BL, et al. Safety and immunogenicity of a tetravalent live-attenuated dengue vaccine in flavivirus-naive infants. Am J Trop Med Hyg. 2011;85(2):341–51.

63. Modjarrad K, Lin L, George SL, Stephenson KE, Eckels KH, De La Barrera RA, et al. Preliminary aggregate safety and immunogenicity results from three trials of a purified inactivated Zika virus vaccine candidate: phase 1, randomised, double-blind, placebo-controlled clinical trials. Lancet. 2018;391(10120):563–71.

64. Danko JR, Beckett CG, Porter KR. Development of dengue DNA vaccines. Vaccine. 2011;29(42):7261–6.

65. Araujo SC, Pereira LR, Alves RPS, Andreata-Santos R, Kanno AI,

Ferreira LCS, et al. Anti-flavivirus vaccines: Review of the present situation and perspectives of subunit vaccines produced in escherichia coli. Vaccines. 2020;8(3):1–30.

66. Zhang N, Li C, Jiang S, Du L. Recent advances in the development of virus-like particle-based flavivirus vaccines. Vaccines. 2020;8(3):1–20.

67. Dowd KA, Ko SY, Morabito KM, Yang ES, Pelc RS, DeMaso CR, et al. Rapid development of a DNA vaccine for Zika virus. Science. 2016;354(6309):237–40.

68. Barrows NJ, Campos RK, Powell S, Prasanth KR, Schott-lerner G, Soto-acosta R, et al. A screen of FDA-approved drugs for inhibitors of ZIka virus infection. Cell Host Microbe. 2016;20(2):259–70.

69. Amemiya T, Gromiha MM, Horimoto K, Fukui K. Drug repositioning for dengue haemorrhagic fever by integrating multiple omics analyses. Sci Rep. 2019;9(1):1–13.

70. Boldescu V, Behnam MAM, Vasilakis N, Klein CD. Broad-spectrum agents for flaviviral infections: Dengue, Zika and beyond. Nat Rev Drug Discov. 2017;16(8):565–86.

71. Kaufmann SHE, Dorhoi A, Hotchkiss RS, Bartenschlager R. Host-directed therapies for bacterial and viral infections. Nat Rev Drug Discov. 2018;17(1):35–56.

72. Troost B, Smit JM. Recent advances in antiviral drug development towards dengue virus. Curr Opin Virol. 2020;43(Table 1):9–21.

73. Baz M, Boivin G. Antiviral agents in development for zika virus infections. Pharmaceuticals. 2019;12(3).

74. Nguyen NM, Tran CNB, Phung LK, Duong KTH, Huynh HLA, Farrar J, et al. A randomized, double-blind placebo controlled trial of balapiravir, a polymerase inhibitor, in Adult dengue patients. J Infect Dis. 2013;207(9):1442–50.

75. Al-Bari MAA. Targeting endosomal acidification by chloroquine analogs as a promising strategy for the treatment of emerging viral diseases. Pharmacol Res Perspect. 2017;5(1):1–13.

76. Low JGH, Ooi EE, Vasudevan SG. Current status of dengue therapeutics research and development. J Infect Dis. 2017;215(Suppl

2):S96–102.

77.   Mcgready R, Thwai KL, Cho T, Samuel, Looareesuwan S, White NJ, et al. The effects of quinine and chloroquine antimalarial treatments in the first trimester of pregnancy. Trans R Soc Trop Med Hyg. 2002;96(2):180–4.

78.   Low JG, Sung C, Wijaya L, Wei Y, Rathore APS, Watanabe S, et al. Efficacy and safety of celgosivir in patients with dengue fever (CELADEN): A phase 1b, randomised, double-blind, placebo-controlled, proof-of-concept trial. Lancet Infect Dis [Internet]. 2014;14(8):706–15.

79.   Sridhar A, Simmini S, Ribeiro CMS, Tapparel C, Evers MM, Pajkrt D, et al. A Perspective on Organoids for Virology Research. Viruses. 2020;12(11):1–10.

80.   Urbanelli L, Buratta S, Tancini B, Sagini K, Delo F, Porcellati S, et al. The role of extracellular vesicles in viral infection and transmission. Vaccines. 2019;7(3):1–20.

81.   Johnstone RM, Adam M, Hammond JR, Orr L, Turbide C. Vesicle formation during reticulocyte maturation. Association of plasma membrane activities with released vesicles (exosomes). J Biol Chem. 1987;262(19):9412–20.

82.   Yáñez-Mó M, Siljander PRM, Andreu Z, Zavec AB, Borràs FE, Buzas EI, et al. Biological properties of extracellular vesicles and their physiological functions. J Extracell Vesicles. 2015;4(2015):1–60.

83.   Xu X, Lai Y, Hua ZC. Apoptosis and apoptotic body: Disease message and therapeutic target potentials. Biosci Rep. 2019;39(1):1–17.

84.   Editor D, Meehan B. ._Oncosomes - large and small_ what are they, where they came from_ _ Meehan _ Journal of Extracellular Vesicles.pdf. 2016;1:4–5.

85.   Zhang Q, Higginbotham JN, Jeppesen DK, Yang YP, Li W, McKinley ET, et al. Transfer of Functional Cargo in Exomeres. Cell Rep. 2019;27(3):940-954.e6.

86.   Guo Y, Tan J, Miao Y, Sun Z, Zhang Q. Effects of microvesicles on cell apoptosis under hypoxia. Oxid Med Cell Longev. 2019;2019.

87. Dini L, Tacconi S, Carata E, Tata AM, Vergallo C, Panzarini E. Microvesicles and exosomes in metabolic diseases and inflammation. Cytokine Growth Factor Rev. 2020;51(January):27–39.

88. Crescitelli R, Lässer C, Szabó TG, Kittel A, Eldh M, Dianzani I, et al. Distinct RNA profiles in subpopulations of extracellular vesicles: Apoptotic bodies, microvesicles and exosomes. J Extracell Vesicles. 2013;2(1):1–10.

89. NICOLAS RH, GOODWIN GH. Overview of Extracellular Vesicles, Their Origin, Composition, Purpose, and Methods for Exosome Isolation and Analysis. Cells. 2019;41–68.

90. Raposo G, Stoorvogel W. Extracellular vesicles: Exosomes, microvesicles, and friends. J Cell Biol. 2013;200(4):373–83.

91. Grant BD, Donaldson JG. Pathways and mechanisms of endocytic recycling. Nat Rev Mol Cell Biol. 2009. 10(9):597-608

92. Théry C, Witwer KW, Aikawa E, Alcaraz MJ, Anderson JD, Andriantsitohaina R, et al. Minimal information for studies of extracellular vesicles 2018 (MISEV2018): a position statement of the International Society for Extracellular Vesicles and update of the MISEV2014 guidelines. J Extracell Vesicles. 2018;7(1).

93. Marostica G, Gelibter S, Gironi M, Nigro A, Furlan R. Extracellular Vesicles in Neuroinflammation. Front Cell Dev Biol. 2021;8(January):1–13.

94. Colombo M, Moita C, Van Niel G, Kowal J, Vigneron J, Benaroch P, et al. Analysis of ESCRT functions in exosome biogenesis, composition and secretion highlights the heterogeneity of extracellular vesicles. J Cell Sci. 2013;126(24):5553–65.

95. Rev C, Mol B. The ESCRT machinery: From the plasma membrane to endosomes and back again. Crit Rev Biochem Mol Biol. 2014;49(3):242–61.

96. Morita E, Sandrin V, Chung HY, Morham SG, Gygi SP, Rodesch CK, et al. Human ESCRT and ALIX proteins interact with proteins of the midbody and function in cytokinesis. EMBO J. 2007;26(19):4215–27.

97. Baietti MF, Zhang Z, Mortier E, Melchior A, Degeest G, Geeraerts A, et

al. Syndecan-syntenin-ALIX regulates the biogenesis of exosomes. Nat Cell Biol. 2012;14(7):677–85.

98. Termini CM, Gillette JM. Tetraspanins function as regulators of cellular signaling. Front Cell Dev Biol. 2017;5(APR):1–14.

99. Trajkovic K. Ceramide triggers budding of exosome vesicles into multivesicular endosomes. Science. 2008;320(5873):179.

100. Aktepe TE, Mackenzie JM. Shaping the flavivirus replication complex: It is curvaceous! Cell Microbiol. 2018;20(8):1–10.

101. Raiborg C, Stenmark H. The ESCRT machinery in endosomal sorting of ubiquitylated membrane proteins. Nature. 2009;458(7237):445–52.

102. Howitt J, Hill AF. Exosomes in the pathology of neurodegenerative diseases. J Biol Chem. 2016;291(52):26589–97.

103. Schorey JS, Cheng Y, Singh PP, Smith VL. Exosomes and other extracellular vesicles in host–pathogen interactions. EMBO Rep. 2015;16(1):24–43.

104. Blanc L, Vidal M. New insights into the function of Rab GTPases in the context of exosomal secretion. Small GTPases. 2018;9(1–2):95–106.

105. Han J, Pluhackova K, Böckmann RA. The multifaceted role of SNARE proteins in membrane fusion. Front Physiol. 2017;8(JAN).

106. Muralidharan-Chari V, Clancy J, Plou C, Romao M, Chavrier P, Raposo G et al. ARF6-regulated shedding of tumor cell-derived plasma membrane microvesicles. Curr Biol. 2009. 19(22):1875-85

107. Kaksonen M, Roux A. Mechanisms of clathrin-mediated endocytosis. Nat Rev Mol Cell Biol. 2018;19(5):313–26.

108. Nabi IR, Le PU. Caveolae/raft-dependent endocytosis. J Cell Biol. 2003;161(4):673–7.

109. Mulcahy LA, Pink RC, Carter DRF. Routes and mechanisms of extracellular vesicle uptake. J Extracell Vesicles. 2014;3(1):1–14.

110. Teissier É, Pécheur EI. Lipids as modulators of membrane fusion mediated by viral fusion proteins. Eur Biophys J. 2007;36(8):887–99.

111. Jahn R, Sudhof T. Membrane fusion and exocytosis. Annu Rev

Biochem. 1999;777–810.

112. Wiklander OPB, Brennan M, Lötvall J, Breakefield XO, Andaloussi SEL. Advances in therapeutic applications of extracellular vesicles. Sci Transl Med. 2019;11(492):1–16.

113. Martins S de T, Kuczera D, Lötvall J, Bordignon J, Alves LR. Characterization of dendritic cell-derived extracellular vesicles during dengue virus infection. Front Microbiol. 2018;9(AUG):1–19.

114. Mittal S, Gupta P, Chaluvally-Raghavan P, Pradeep S. Emerging role of extracellular vesicles in immune regulation and cancer progression. Cancers (Basel). 2020;12(12):1–16.

115. Song N, Scholtemeijer M, Shah K. Mesenchymal Stem Cell Immunomodulation: Mechanisms and Therapeutic Potential. Trends Pharmacol Sci. 2020;41(9):653–64.

116. Timaner M, Tsai KK, Shaked Y. The multifaceted role of mesenchymal stem cells in cancer. Semin Cancer Biol. 2020;60:225–37.

117. Schioppo T, Ubiali T, Ingegnoli F, Bollati V, Caporali R. The role of extracellular vesicles in rheumatoid arthritis: a systematic review. Clin Rheumatol. 2021;

118. Zhu W, Huang L, Li Y, Zhang X, Gu J, Yan Y, et al. Exosomes derived from human bone marrow mesenchymal stem cells promote tumor growth in vivo. Cancer Lett. 2012;315(1):28–37.

119. Beckler MD, Higginbotham JN, Franklin JL, Ham AJ, Halvey PJ, Imasuen IE, et al. Proteomic analysis of exosomes from mutant KRAS colon cancer cells identifies intercellular transfer of mutant KRAS. Mol Cell Proteomics. 2013;12(2):343–55.

120. Mills J, Capece M, Cocucci E, Tessari A, Palmieri D. Cancer-derived extracellular vesicle-associated microRNAs in intercellular communication: One cell's trash is another cell's treasure. Int J Mol Sci. 2019;20(24).

121. Klibi J, Niki T, Riedel A, Pioche-Durieu C, Souquere S, Rubinstein E, et al. Blood diffusion and Th1-suppressive effects of galectin-9-containing exosomes released by Epstein-Barr virus-infected nasopharyngeal carcinoma cells. Blood. 2009;113(9):1957–66.

122. Fu S, Zhang Y, Li Y, Luo L, Zhao Y, Yao Y. Extracellular vesicles in cardiovascular diseases. Cell Death Discov. 2020;6(1).

123. Schiera G, Di Liegro CM, Di Liegro I. Extracellular Membrane Vesicles as Vehicles for Brain Cell-to-Cell Interactions in Physiological as well as Pathological Conditions. Biomed Res Int. 2015. 152926

124. Frühbeis C, Fröhlich D, Kuo WP, Amphornrat J, Thilemann S, Saab AS, et al. Neurotransmitter-Triggered Transfer of Exosomes Mediates Oligodendrocyte-Neuron Communication. PLoS Biol. 2013;11(7):e1001604.

125. Drago F, Lombardi M, Prada I, Gabrielli M, Joshi P, Cojoc D, et al. ATP modifies the proteome of extracellular vesicles released by microglia and influences their action on astrocytes. Front Pharmacol. 2017;8(DEC):1–14.

126. Fevrier B, Vilette D, Archer F, Loew D, Faigle W, Vidal M, et al. Cells release prions in association with exosomes. Proc Natl Acad Sci U S A. 2004;101(26):9683–8.

127. Grazia Spillantini M, Anthony Crowther R, Jakes R, Cairns NJ, Lantos PL, Goedert M. Filamentous α-synuclein inclusions link multiple system atrophy with Parkinson's disease and dementia with Lewy bodies. Neurosci Lett. 1998;251(3):205–8.

128. Rajendran L, Honsho M, Zahn TR, Keller P, Geiger KD, Verkade P, et al. Alzheimer's disease β-amyloid peptides are released in association with exosomes. Proc Natl Acad Sci U S A. 2006;103(30):11172–7.

129. Grad LI, Pokrishevsky E, Silverman JM, Cashman NR. Exosome-dependent and independent mechanisms are involved in prion-like transmission of propagated Cu/Zn superoxide dismutase misfolding. Prion. 2014;8(5):331–5.

130. Isola A, Chen S. Exosomes: The Messengers of Health and Disease. Curr Neuropharmacol. 2016;15(1):157–65.

131. Baranyai T, Herczeg K, Onódi Z, Voszka I, Módos K, Marton N, et al. Isolation of exosomes from blood plasma: Qualitative and quantitative comparison of ultracentrifugation and size exclusion chromatography methods. PLoS One. 2015;10(12):1–13.

132. Cantin R, Diou J, Bélanger D, Tremblay AM, Gilbert C. Discrimination between exosomes and HIV-1: Purification of both vesicles from cell-free supernatants. J Immunol Methods. 2008;338(1–2):21–30.

133. Oeyen E, Van Mol K, Baggerman G, Willems H, Boonen K, Rolfo C, et al. Ultrafiltration and size exclusion chromatography combined with asymmetrical-flow field-flow fractionation for the isolation and characterisation of extracellular vesicles from urine. J Extracell Vesicles. 2018;7(1):1490143.

134. Bancu I, Oliveira-tercero A, Menezes-neto A, Hernando A, Portillo D, Lauzurica-valdemoros R, et al. Size-exclusion chromatography-based enrichment of extracellular vesicles from urine samples. J Extracell Vesicles. 2015;4:27369.

135. Konoshenko MY, Lekchnov EA, Vlassov A V., Laktionov PP. Isolation of Extracellular Vesicles: General Methodologies and Latest Trends. Biomed Res Int. 2018. 2018:8545347

136. Wan Y, Cheng G, Liu X, Hao SJ, Nisic M, Zhu CD et al. Rapid magnetic isolation of extracellular vesicles via lipid-based nanoprobes. Nat Biomed Eng. 2017. 1:0058

137. Zhang H, Lyden D. Assymetric-flow field-flow fractionation technology for exomere and small extracellular vesicle separation and characterization. Nat Protoc. 2019. 14(4):1027-1053

138. Caobi A, Nair M, Raymond AD. Extracellular vesicles in the pathogenesis of viral infections in humans. Viruses. 2020;12(10):1200.

139. Barroso-González J, García-Expósito L, Puigdomènech I, de Armas-Rillo L, Machado JD, Blanco J, et al. Viral infection: Moving through complex and dynamic cell-membrane structures. Commun Integr Biol. 2011;4(4):398–408.

140. Dreux M, Garaigorta U, Boyd B, Décembre E, Chung J, Whitten-Bauer C, et al. Short-range exosomal transfer of viral RNA from infected cells to plasmacytoid dendritic cells triggers innate immunity. Cell Host Microbe. 2012;12(4):558–70.

141. Bukong TN, Momen-Heravi F, Kodys K, Bala S, Szabo G. Exosomes from Hepatitis C Infected Patients Transmit HCV Infection and Contain

Replication Competent Viral RNA in Complex with Ago2-miR122-HSP90. PLoS Pathog. 2014;10(10).

142. Zhou W, Woodson M, Neupane B, Bai F, Sherman MB, Choi KH, et al. Exosomes serve as novel modes of tick-borne flavivirus transmission from arthropod to human cells and facilitates dissemination of viral RNA and proteins to the vertebrate neuronal cells. PLoS Pathogens. 2018. 14(1):e1006764.

143. Vora A, Zhou W, Londono-Renteria B, Woodson M, Sherman MB, Colpitts TM, et al. Arthropod EVs mediate dengue virus transmission through interaction with a tetraspanin domain containing glycoprotein Tsp29Fb. Proc Natl Acad Sci U S A. 2018;115(28):E6604–13.

144. Velandia-Romero ML, Caldern-Pelaez MA, Balbas-Tepedino A, Alejandro Marquez-Ortiz R, Madroñero LJ, Prieto AB, et al. Extracellular vesicles of U937 macrophage cell line infected with DENV-2 induce activation in endothelial cells EA.hy926. PLoS One. 2020;15(1):1–25.

145. Zhu X, He Z, Yuan J, Wen W, Huang X, Hu Y, et al. IFITM3-containing exosome as a novel mediator for anti-viral response in dengue virus infection. Cell Microbiol. 2015;17(1):105–18.

146. Sung PS, Huang TF, Hsieh SL. Extracellular vesicles from CLEC2-activated platelets enhance dengue virus-induced lethality via CLEC5A/TLR2. Nat Commun. 2019;10(1):1–13.

147. Conzelmann C, Groß R, Zou M, Krüger F, Görgens A, Gustafsson MO, et al. Salivary extracellular vesicles inhibit Zika virus but not SARS-CoV-2 infection. J Extracell Vesicles. 2020;9(1):1808281.

148. Müller JA, Harms M, Krüger F, Groß R, Joas S, Hayn M, et al. Semen inhibits Zika virus infection of cells and tissues from the anogenital region. Nat Commun. 2018;9(1):2207.

Chapter 2: Research Objectives

Flaviviruses are responsible for significant morbidity and mortality worldwide. Two of the most common pathogens of this genus are dengue (DENV) and Zika (ZIKV) virus, which have a serious impact on health systems and economy. Despite the great effort made by the scientific community, no antivirals have been approved for any of these viruses. These agents can target either a cellular factor or a viral protein, in order to inhibit virus replication and infection.

In the first part of this PhD work, we tested a number of different molecules, from the European COST action program, for their potential activity against DENV and ZIKV. We first evaluated their potency and cytotoxicity in several susceptible cell lines, such as lung adenocarcinoma, placenta choriocarcinoma and hepatocytes. From the initial screening, we identified two distinct classes of compounds (polyanionic dendrimers and indole alkaloids) that present good antiviral activity (in the low micromolar range) against both viruses, with minimal cytotoxicity levels. Using several *in vitro* assays, including time-of-drug-addition studies, subgenomic replicon, virus inactivation assays as well as surface plasmon resonance technology and selection/sequencing of virus-resistant mutants, we thoroughly determined their mechanism of action, thus proposing them as potential antivirals for further evaluation studies. In addition, structure-activity relationship experiments were performed to identify the chemical groups that are crucial in the potency of the molecules (**Chapter 3 and 4**).

In the second part of the thesis, we focus on virus-host cellular interactions. Particularly, viruses are known to exploit several cellular patterns to enter, replicate and infect cellular tissues/organs. One of these mechanisms involves the recruitment of the exosomal pathway. During the last years, increased interest has grown on the role of extracellular vesicles (EVs) in many pathophysiological conditions. In **Chapter 5**, we investigated whether EVs derived from ZIKV-infected brain endothelial cells (IEVs) are able to incorporate and transfer viral material to susceptible cells of the blood-brain barrier (BBB) system. Several cellular assays (e.g. immunofluorescence staining, qRT-PCR and transwell studies) showed that IEVs can be recognized by naïve brain-related cells and transport viral components to them. Moreover, impedance-based biosensor experiments demonstrated that these vesicles are capable to pass through the BBB system via transcellular route, inducing temporal rearrangements in adherent proteins. Furthermore, we implemented an extensive lipidomics analysis on both cells and their secreted EVs to provide more information on potential sorting and biogenesis mechanisms. Finally, we compared the EV lipidomic profile between non-

infected and infected conditions, in order to identify potential "biomarkers" during ZIKV infection.

Chapter 3: Tryptophan trimers and tetramers inhibit dengue and Zika virus replication by interfering with viral attachment processes

3.1 Abstract

Here, we report a class of tryptophan trimers and tetramers that inhibit (at low micromolar range) dengue and Zika virus infection *in vitro*. These compounds (AL family) have three or four peripheral tryptophan moieties directly linked to a central scaffold through their amino groups, thus their carboxylic acid groups are free and exposed to the periphery. Structure activity relationship (SAR) studies demonstrated that the presence of extra phenyl rings with substituents other than COOH at the N1 or C2 positions of the indole side-chain is a requisite for the antiviral activity against both viruses. The molecules showed potent antiviral activity, with low cytotoxicity, when evaluated on different cell lines. Moreover, they were active against laboratory and clinical strains of all four serotypes of dengue virus as well as a selected group of Zika virus strains. Additional mechanistic studies performed with the two most potent compounds (AL439 and AL440) demonstrated an interaction with the viral envelope glycoprotein (domain III) of dengue 2 virus, thus preventing virus attachment to the host cell membrane. Since no antiviral agent is approved at the moment against these two flaviviruses, further pharmacokinetic studies with these molecules are needed for their development as future therapeutic/prophylactic drugs.

3.2 Introduction

The *Flaviviridae* is a large family of viruses comprising four distinct genera, *Hepaci-*, *Pegi-*, *Pesti-* and *Flaviviruses* (1). The *Flavivirus* genus contains many important human pathogens, such as dengue virus (DENV) and Zika virus (ZIKV). These members are mainly transmitted by two mosquito species (*Aedes aegypti* and *Aedes albopictus*) and constitute a significant cause of morbidity and mortality worldwide (2–4). Socioeconomical events, such as population growth, uncontrolled urbanization as well as increased international air traffic constitute main factors for the emergence of both DENV and ZIKV worldwide (5). Moreover, the lack or reduction of appropriate vector control programs in some geographical areas arise the possibility of their establishment, which might result in future outbreaks (6). The most recent example was in Philippines in 2019, where an outbreak of dengue fever led to hundreds of deaths and it was declared as a national epidemic. Despite

the long-term efforts to restrict the spread and infection by these viruses, no antivirals are commercially available at this moment. In addition, new flaviviruses may appear in the near future, making even more urgent the need for the development of novel compounds (7,8).

DENV is the most prevalent arbovirus, infecting approximately 400 million people per year, of which almost 100 million develop clinical symptoms (9). There are four antigenically distinct serotypes (DENV 1-4), which cause both a mild febrile-like illness (dengue fever) and severe dengue, characterized by increased vascular permeability and plasma leakage, which may result in a shock syndrome and eventually death (10,11).

The closely related ZIKV was first discovered in 1947 in Uganda, but was neglected until 2007 after its re-appearance during an outbreak on Micronesian Yap Islands (12). In addition, two large outbreaks in French Polynesia (2013), Brazil and other Central/South American countries (2015- 2016) led the World Health Organization (WHO) to declare ZIKV as Public Health Emergency of International Concern in 2016 (13,14). During that period, almost 40,000 symptomatic cases were reported in the Americas (15). In general, ZIKV causes mild symptoms, like fever, headache and joint pain. However, the virus has gained increased interest during the last years, because of its correlation with severe neurological manifestations in newborns (microcephaly) and in adults (Guillain-Barré syndrome) (16,17). Moreover, several studies have confirmed that ZIKV is not only transmitted to humans by virus-infected mosquitoes, but also through blood transfusion, sexual contact and vertically, lowering the viral barrier (18–20).

Over the past few years, great effort is carried out in vaccine and antiviral research against these two viruses. Particularly, numerous vaccine platforms have been developed including recombinant viral proteins, whole inactivated virus, live-attenuated virus as well as DNA subunits. Among them, the live attenuated tetravalent vaccine (Dengvaxia®) was licensed against DENV in approximately 20 countries in 2016. Although the vaccine boosts a strong immune response in individuals with a prior history of DENV infection, the risk of severe dengue is significantly increased in those who have not experienced an infection before, resulting in high numbers of hospitalizations (21,22). Although the underlying cause of this phenomenon is not yet identified, different reports state that the vaccine may act as silent/primary infection, producing insufficient neutralizing antibody levels. Subsequently, a secondary

infection leads to more severe disease symptoms due to antibody-dependent enhancement (ADE) (23). Despite the promising outcomes in vaccine development, important limitations need to be considered, as one of the main hurdles regarding their efficacy and safety, is the antibody cross- reactivity between ZIKV and DENV (24,25).

In addition, a large number of Food and Drug Administration (FDA)- approved drugs has been re-evaluated against both viruses, targeting different viral and host proteins (26,27). However, none of these drugs is approved at the moment. Therefore, there is an imperative need for the development of novel antivirals, in order to prevent/treat infection by these emerging flaviviruses. Among them, entry inhibitors are particularly attractive, due to their ability to block *de novo* cell infection, averting the uptake of the virus by uninfected cells (28). In the huge family of those inhibitors, polyanionic molecules represent one of the major classes, exerting antiviral activity against several viruses, such as HIV and HSV (29–31). However, in some cases, their mechanism of action remains unclear.

In this study, we screened a library of chemically divergent compounds (approximately 500 molecules) for their activity against DENV and ZIKV infection. Among them, a novel series of tryptophan (Trp) trimers and tetramers (belonging to the AL class, which is developed in our group, Figure 1) was identified as potent inhibitors against both flaviviruses in the low micromolar range. Structure- activity relationship studies helped us to determine the structural requirements for their selective antiviral activity. These molecules were found to be active in non-human primate and human cell lines. Further mechanism of action studies revealed that these compounds inhibit viral replication during the early stages, by interacting with the domain III of the envelope protein of DENV. This domain plays a pivotal role in the attachment and entry of the virus into target cells via its interaction with specific host receptors (32,33).

3.3 Results

3.3.1 Synthesis and Structure-activity relationship (SAR) studies

The synthesis of trimers: AL352, AL438, AL439, AL440, AL467 and AL455 (Figure 1) has been recently published (34). To complete the structure-activity relationship studies some novel compounds have been synthesized: trimers AL544, AL545, AL437, AL484, tetramer AL531 and monomers AL441, AL442 (Figure 1). These molecules were prepared using the synthetic strategies described in the Supplemental Material. As seen from Figure 3.1, all the tripodal N1 substituted derivatives possess a common 4-(2-carboxyethyl)-4-nitroheptanedioic acid central core. On the other hand, the tetrapodal derivative AL531 has a pentaerythritol central core. In order to evaluate the antiviral activity of these analogues, the prototype strains of DENV2 (NGC) and ZIKV (MR766) were tested in African green monkey kidney cells (Vero). Cytotoxicity assessment was performed in parallel. As shown in Table 3.1, modifications on the structure of AL analogues lead to significant differences in their antiviral activity. In particular, the unsubstituted trimer AL352 did not show any antiviral activity up to 100 µM. Besides, the N1-methyl trimer AL544 also proved inactive at sub-toxic concentration. However, the N1-benzyl trimers AL440 and AL439, bearing extra benzyl and 4-fluorobenzyl rings respectively, at the N1 position of the indole side-chain of Trp, showed remarkable antiviral activity against DENV2 (EC$_{50}$: 3.5 and 3.6 µM, respectively) and ZIKV (EC$_{50}$: 3.3 and 5.8 µM, respectively). On the contrary, trimer AL438, substituted at N1 with a 4-carboxybenzyl moiety, was not found to be active against these viruses. Displacement of the substituted phenyl ring at the C2 position of the indole side-chain led to the trimers AL467 (4- CF$_3$- phenyl at C2) and AL545 (3-CF$_3$-phenyl rings at C2), which showed activity against both, DENV and ZIKV, at low micromolar range. On the contrary, AL455 with a 4-carboxyphenyl moiety at C2, showed no activity. Moreover, the trimer AL437 with a phenylsulfenyl moiety at the C2 position presented no activity, while trimer AL484 with a 4-nitrophenylsulfenyl moiety at C2 was active against both DENV and ZIKV. This result confirms that substituted phenyl rings with non-carboxylated groups at C2 position of the indole ring are beneficial for antiviral activity. In addition, the 4- carboxybenzyl group at N1 position present in monomer AL441 abolished the antiviral activity, while the substituted with a 4- fluorobenzyl group monomer AL442 was active. On the other hand, AL442 was less potent than

the trimer AL439 and tetramer AL531, despite the fact that these three analogues are substituted with the same group at the N1 position (4-fluorobenzyl). Although the tetramer AL531 showed a remarkable antiviral activity against DENV2 and ZIKV (EC$_{50}$: 4.0 and 1.9 μM, respectively), its marked cellular cytotoxicity made it a less attractive candidate for further evaluation. These findings suggest that multivalence can play an important role in the improved antiviral activity.

In order to gain more information on the mechanism of action of this series of molecules, compounds AL439 and AL440, with the best selectivity indexes (cellular cytotoxicity/antiviral activity) and minimum cytotoxicity were selected for further studies.
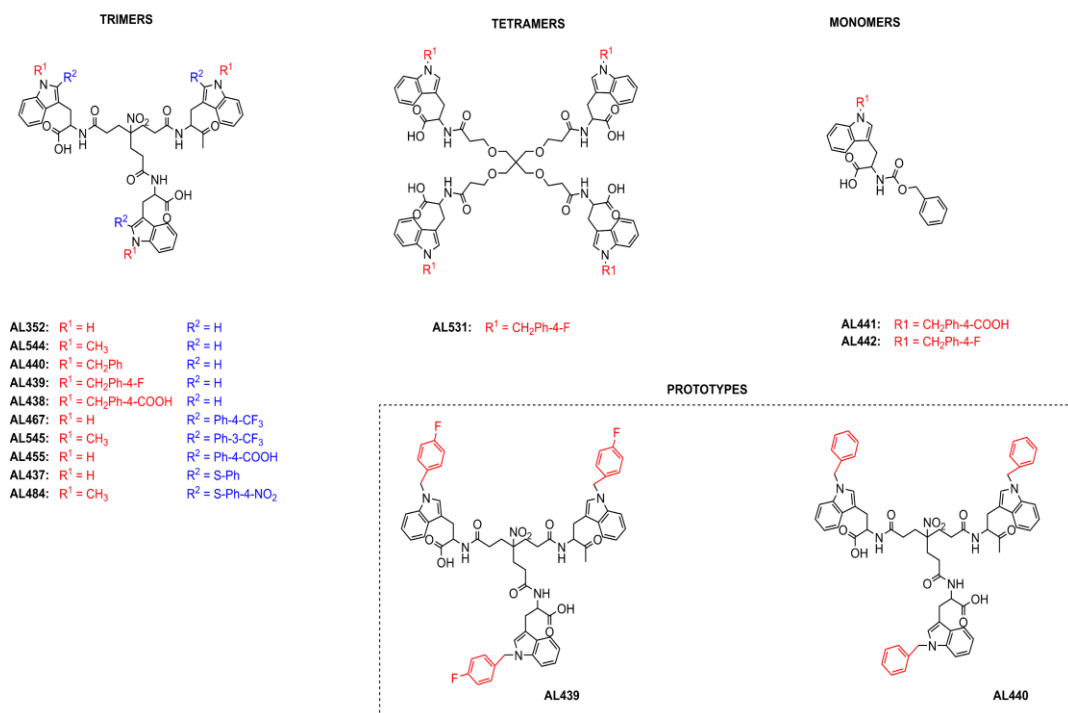

TRIMERS

AL352: R^1 = H   R^2 = H
AL544: R^1 = CH$_3$ R^2 = H
AL440: R^1 = CH$_2$Ph   R^2 = H
AL439: R^1 = CH$_2$Ph-4-F   R^2 = H
AL438: R^1 = CH$_2$Ph-4-COOH   R^2 = H
AL467: R^1 = H   R^2 = Ph-4-CF$_3$
AL545: R^1 = CH$_3$ R^2 = Ph-3-CF$_3$
AL455: R^1 = H   R^2 = Ph-4-COOH
AL437: R^1 = H   R^2 = S-Ph
AL484: R^1 = CH$_3$ R^2 = S-Ph-4-NO$_2$

TETRAMERS

AL531: R^1 = CH$_2$Ph-4-F

MONOMERS

AL441: R1 = CH$_2$Ph-4-COOH
AL442: R1 = CH$_2$Ph-4-F

PROTOTYPES

AL439   AL440

Figure 3.1: Structure of the tested analogues

Table 3.1: Cytotoxicity and antiviral activity of a series of AL compounds against DENV2 and ZIKV prototype strains in Vero cells.

Compound	Mol wt (Da)	[a]CC$_{50}$ (µM)	[b]EC$_{50}$ (µM) (DENV2)	EC$_{50}$ (µM) (ZIKV)	[c]SI$_{DENV2}$	SI$_{ZIKV}$
AL352	835.9	>100	>100	>100	>1	>1
AL544	877.9	>100	>100	>100	>1	>1
AL440	1106.2	98 ± 3	3.5 ± 2.9	3.3 ± 1.4	28	29.7
AL439	1160.2	80 ± 30	3.6 ± 1.1	5.8 ± 1.1	22.2	13.8
AL438	1238.3	>100	>100	>100	>1	>1
AL467	1268.1	>100	8.0 ± 1.4	10.5 ± 5.0	>12.5	>9.5
AL545	1310.2	43 ± 8	0.7 ± 0.3	1.3 ± 0.5	61.4	33
AL455	1196.2	>100	>100	>100	>1	>1
AL437	1160.3	83.5 ± 6.5	>100	>100	0.8	0.8
AL484	1337.4	>100	3.6 ± 0.4	15.6 ± 13.6	27.7	6.4
AL531	1601.7	42.5 ± 1.3	4.0 ± 1.6	1.9 ± 0.1	10.6	22.4
AL441	472.5	>100	>100	>100	>1	>1

| AL442 | 446.5 | 45.6 ± 5 | 10.8 ± 4.3 | 6.9 ± 2.2 | 4.2 | 6.6 |

[a]CC_{50}:Concentration required to reduce cell viability by 50%.

[b]EC_{50}: Effective concentration of each compound, able to inhibit viral replication by 50%. The laboratory-adapted strains DENV2 NGC and ZIKV MR766 were used.

[c]Selectivity index (CC_{50}/EC_{50}) for each molecule is also included

3.3.2 Cytotoxicity and antiviral activity of AL439 and AL440 against DENV and ZIKV infection in different cell lines

Table 3.2 shows the cellular cytotoxicity of each molecule, evaluated in different cell lines. Particularly, AL439 and AL440 showed higher cytotoxic levels in placenta choriocarcinoma (Jeg3, CC_{50}: 35 μM to 45 μM) and human umbilical vein endothelial cells (HUVEC, CC_{50}: 42.4 μM to 43.7 μM), compared to the other human cells. In addition, AL439 was marginally toxic in green monkey (Vero) and baby hamster (BHK) kidney cells (80 μM and 88 μM, respectively). Next, the inhibitory effects of AL439 and AL440 against the prototype strains of DENV2 (Table 3.3) and ZIKV (Table 3.4) were evaluated in several susceptible cell lines. Although these derivatives were active against both flaviviruses, minor differences were observed among the selected cell lines. More specifically, AL439 and AL440 demonstrated insignificantly higher activity in human hepatocarcinoma (Huh, EC_{50}: 0.6 μM to 1.4 μM), choriocarcinoma (Jeg3, EC_{50}: 0.3 μM to 0.9 μM) and lung adenocarcinoma cells (A549, EC_{50}: 0.8 μM to 2.7 μM) than in hamster (BHK, EC_{50}: 1.0 μM to 4.0 μM) and green monkey kidney cells (Vero, EC_{50}: 3.3 μM to 5.8 μM) against both viral strains. Furthermore, the activity of AL439 and AL440 in HUVEC cells (EC_{50}: 2.1 μM to 5.5 μM) was quite comparable to those observed in non-human cells (Vero and BHK). Finally, Table 3.5 exhibits the antiviral activity of both AL derivatives in monocyte-derived dendritic cells (MDDCs). This cell line represents one of the primary target cell types during a flavivirus infection. Notably, both molecules were active against the prototype strains of DENV2 (EC_{50}: 3.6 μM to 7.6 μM) and ZIKV (EC_{50}: 1.5 μM to 3.9 μM), with no cytotoxic effects at the highest tested concentration (CC_{50} > 50 μM).

Table 3.2: Cellular cytotoxicity of AL439 and AL440 in different cell lines

	Vero	BHK	Huh	Jeg3	A549	HUVEC
Compound	CC_{50} (μM)					
AL439	80 ± 30	88 ± 17	>100	35 ± 10	>100	42.4 ± 1.7
AL440	98 ± 3	>100	>100	45 ± 5	>100	43.7 ± 5.1

Data represent AVG ± SD values of at least three independent experiments.

Table 3.3: Antiviral activity of AL439 and AL440 against DENV2 prototype strain in different cell lines

DENV2 NGC strain						
	Vero	BHK	Huh	Jeg3	A549	HUVEC
Compound	EC_{50} (μM)					
AL439	3.6 ± 1.1	1.4 ± 0.1	1.2 ± 0.1	0.5 ± 0.1	0.8 ± 0.1	3.3 ± 0.8
AL440	3.5 ± 2.9	3.8 ± 1.8	1.1 ± 0.1	0.9 ± 0.2	1.0 ± 0.1	4.8 ± 1.6

Data represent AVG ± SD values of at least three independent experiments.

Table 3.4: Antiviral activity of AL439 and AL440 against ZIKV prototype strain in different cell lines

ZIKV MR766 strain						
	Vero	**BHK**	**Huh**	**Jeg3**	**A549**	**HUVEC**
Compound	EC_{50} *(µM)*					
AL439	5.8 ± 1.1	4.0 ± 0.1	0.6 ± 0.2	0.6 ± 0.1	2.7 ± 0.6	2.1 ± 0.7
AL440	3.3 ± 1.4	1.0 ± 0.3	1.4 ± 0.3	0.3 ± 0.1	2.2 ± 0.2	5.1 ± 2.2

Data represent AVG ± SD values of at least three independent experiments.

Table 3.5: Anti-DENV, anti-ZIKV activities and cytotoxicity of AL439 and AL440 in MDDC.

		DENV2 NGC		ZIKV MR766	
Compound	CC_{50}^{a}*(µM)*	EC_{50}^{a} *(µM)*	*SI*	EC_{50} *(µM)*	*SI*
AL439	>50	7.6 ± 0.8	> 6.5	1.5 ± 0.2	> 33
AL440	>50	3.6 ± 0.8	> 13.9	3.9 ± 0.6	> 12.8

[a]All values were calculated as AVG ± SD from four different donors.

3.3.3 Evaluation of antiviral activity against ZIKV by immunofluorescence staining

We further assessed the antiviral activity of AL440 against the prototype ZIKV MR766 strain using immunofluorescence staining for viral envelope glycoprotein. As shown in Figure 3.2, incubation of Vero cells with 20 µM

(Figure 3.2C) and 10 μM of AL440 (Figure 3.2D) led to inhibition of virus infection. However, treatment of cells with less than 2 μM of AL440 (Figure 3.2E, 3.2F) was not able to hamper the infection. Negative (DMSO-treated cells in the absence of AL440, Figure 3.2A) and positive controls (virus-infected cells in the absence of AL440, Figure 3.2B) were also included.
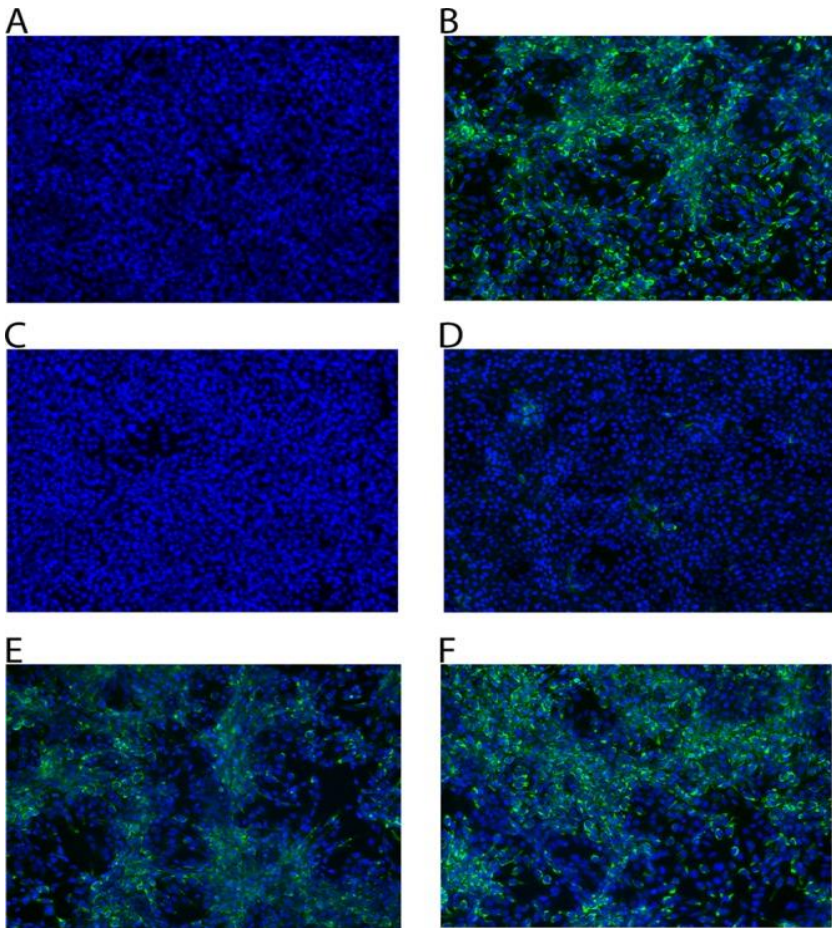

Figure 3.2: **Detection of ZIKV infection using immunofluorescence staining for envelope glycoprotein in the absence and presence of AL440.** Exposure of Vero cells to the prototype ZIKV MR766 strain (MOI 0.2) along with AL440 at different concentrations. Fluorescence images were acquired 72h post infection. (A) Cell control, (B) Virus control, (C) 20 μM, (D) 10 μM, (E) 2 μM, (F) 0.4 μM

3.3.4 Antiviral activity of AL439 and AL440 against different DENV and ZIKV laboratory and clinical strains

In order to assess the broad-spectrum activity, AL439 and AL440 were tested against a panel of different laboratory and clinical strains of DENV and ZIKV in Vero cells. Tables 3.6 and 3.7 summarize the results of these experiments. In general, comparable antiviral activity was noticed against the laboratory-adapted and the clinical strains of DENV for both compounds. However, an improvement in antiviral activity was observed for AL439 against the DENV4 clinical strain (EC$_{50}$: 1.2 ± 0.1 μM), as compared to the one against the DENV4 Dak laboratory strain (EC$_{50}$: 7.3 ± 2.8 μM) (Table 3.6).

Regarding their activity against ZIKV, no differences were observed between the laboratory strain (MR766) and the clinical isolates (PRVAVC59 and FLR) in the presence of AL439. On the contrary, the activity of AL440 was slightly higher against ZIKV FLR strain (EC$_{50}$: 0.7 ± 0.2 μM), as compared to MR766 (EC$_{50}$: 3.3 ± 1.4 μM) and PRVAVC59 (EC$_{50}$: 4.0 ± 0.7 μM) (Table 3.7).

Table 3.6: Antiviral activity of AL439 and AL440 against several DENV laboratory and clinical strains in Vero cells

	Laboratory				Clinical			
	DENV1 Djibouti	DENV2 NGC	DENV3 H87	DENV4 Dak	DENV1	DENV2	DENV3	DENV4
Compound	*EC$_{50}$ (μM)*							
AL439	1.7 ± 0.4	3.6 ± 1.1	3.9 ± 3.0	7.3 ± 2.8	1.5 ± 0.2	2.4 ± 0.9	1.1 ± 0.1	1.2 ± 0.1
AL440	2.5 ± 0.8	3.5 ± 2.9	5.1 ± 4.5	5.7 ± 1.1	2.1 ± 0.3	2.5 ± 0.7	5.5 ± 2.5	4.4 ± 0.2

Table 3.7: Antiviral activity of AL439 and AL440 against several ZIKV laboratory and clinical strains in Vero cells

	Laboratory	Clinical	
	ZIKV MR766	ZIKV PRVAVC59	ZIKV FLR
Compound	EC_{50} *(μM)*		
AL439	5.8 ± 1.1	5.2 ± 0.6	4.5 ± 1.0
AL440	3.3 ± 1.4	4.0 ± 0.7	0.7 ± 0.2

3.3.5 AL compounds inhibit DENV infection during the early stages

To pinpoint at which stage of viral replicative cycle AL439 and AL440 act, a time-of-drug addition assay was performed. As shown in Figure 3.3 (panel A), pretreatment of cells with 10 μM of AL compounds for 2 h before the virus addition (time point 0) resulted in a complete inhibition of viral infection. A similar inhibition profile was observed when the compounds and the virus were added at the same time to the cells. On the other hand, viral infection was only inhibited by approximately 25%, when AL439 and AL440 were added 2h p.i. Addition of compounds at later time points did not longer affect viral infection. Results obtained using dextran sulfate (DS, entry inhibitor) and 7-Deaza-2'-*C*-Methyladenosine (7DMA, viral polymerase inhibitor) are also represented in Figure 3.3. Specifically, DS showed a suppression of viral infection during the early stages (- 2h, 0h p.i.), while 7DMA was able to limit the infection even at 12h p.i. Based on these data, it is suggested that AL439 and AL440 interfere with the early stages of viral infection.

To further confirm these findings, a subgenomic replicon assay was carried out. In particular, different concentrations of AL439 and AL440 were added into BHK/DENV cells. Based on the data shown in Figure 3.3 (panel B), we observed that neither compound inhibited the replication (no change in luciferase activity), indicating a possible interaction with the structural proteins of the virus. However, we noticed that treatment of cells with 100 μM of molecules led to a decrease in luciferase activity. This observation

can be explained by the increased cellular toxicity. A comparable result was obtained for the reference entry inhibitor (DS). On the other hand, 7DMA presented a strong inhibition of viral replication (approximately 100% luciferase reduction was observed at 20 µM).

In addition, we examined the effect of AL439 and AL440 on DENV attachment. Specifically, we incubated Vero cells in the presence of several concentrations of AL molecules along with DENV2 strain for 2h at $4°C$, allowing viral attachment to the cells. Then, cells were washed and incubated with medium for an additional 72h. Interestingly, we observed that virus infection can be effectively inhibited even if the compounds were removed 2h p.i. (EC_{50}:3.6± 0.04 µM and 3.8± 0.1 µM for AL439 and AL440, respectively). These findings are quite comparable with our observations from the initial screening and indicate that our compounds interfere with the attachment of the virus to the cells, corroborating the results that we obtained from the aforementioned assays.
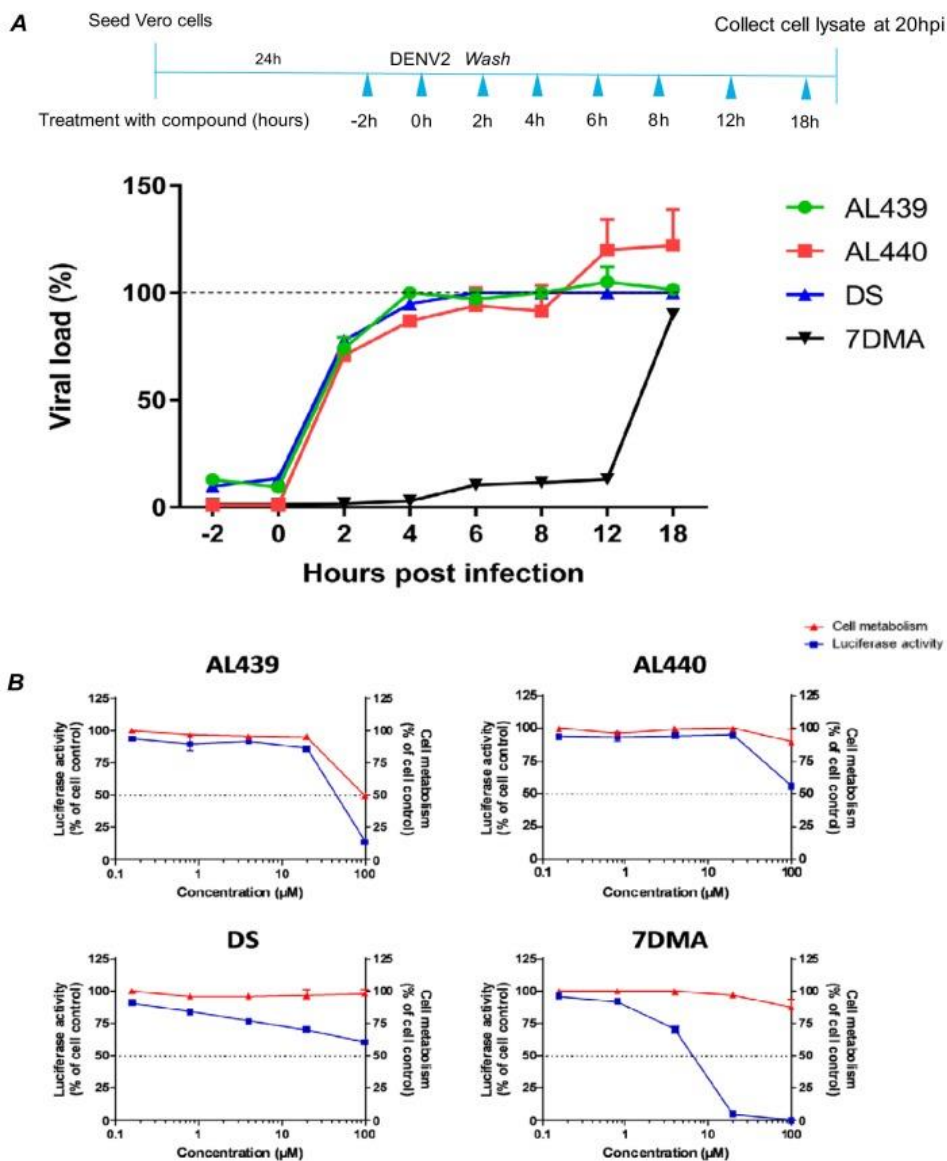
Figure 3.3: **AL compounds inhibit the infection during the early stages without any effect on the replication complex.** *Panel A*: Schematic representation of time-of-drug addition assay (upper). Pretreatment of cells with the compounds during the first hours (-2h, 0h) inhibits DENV infection. No inhibition was noticed after addition of the molecules at later time points (2h -18h). Both AL analogues (green-red) show a similar profile with the established entry inhibitor DS (blue). On the other hand, viral polymerase inhibitor 7DMA (black) is able to suppress the infection even at later stages (12h p.i.). Dashed line represents virus control (below). *Panel B*: Stably

transfected BHK cells with a DENV subgenomic replicon were incubated with serial dilutions of AL molecules (0.8-100 μM). A decrease in the luciferase activity was only observed for the replication inhibitor 7DMA, but not for AL439, AL440 and DS (blue). Incubation of AL439 and AL440 at the highest concentration led to the reduction of cellular metabolism (red). All data are the average of two independent experiments.

3.3.6 AL compounds interact with DENV viral particles in a direct way

To find out whether AL440 directly interacts with the virus, an ultrafiltration assay was performed. Specifically, the viral stock was incubated with AL440 at different concentrations (50 μM, 10 μM and 2 μM) for 1h. The samples were then passed through a concentrator filter unit (10 kDa cut-off) to remove any unbound material (due to smaller size) and the retained fraction on the filter was evaluated in a plaque assay for inhibition of viral infectivity. As shown in Figure 3.4A, cells were completely infected after their treatment with 2 μM of AL440. On the other hand, incubation of cells with 10 μM AL440 resulted in a reduction in the number of viral plaques. Finally, presence of AL440 at the highest concentration (50 μM) protected the cells from viral infection (less than 10 viral plaques were observed). As expected, incubation with epigallocatechin gallate (EGCG, 0.1 mg/ml, positive control) demonstrated a decrease in the number of viral plaques. Furthermore, these findings were confirmed by the virus inactivation assay. More specifically, viral particles were allowed to incubate with 10 μM of AL440 and the sample was subsequently diluted to suboptimal concentrations (condition where the compound is no longer active, while viral particles are still present and infectious, unless they are inactivated by the molecule) before infecting the cells. As shown in Figure 3.4B, the presence of AL440 led to protection of the cells. On the other hand, absence of AL440 (virus control) resulted in a complete destruction of the cell monolayer. The above data clearly showed that AL440 had a direct impact on free viral particles as such.
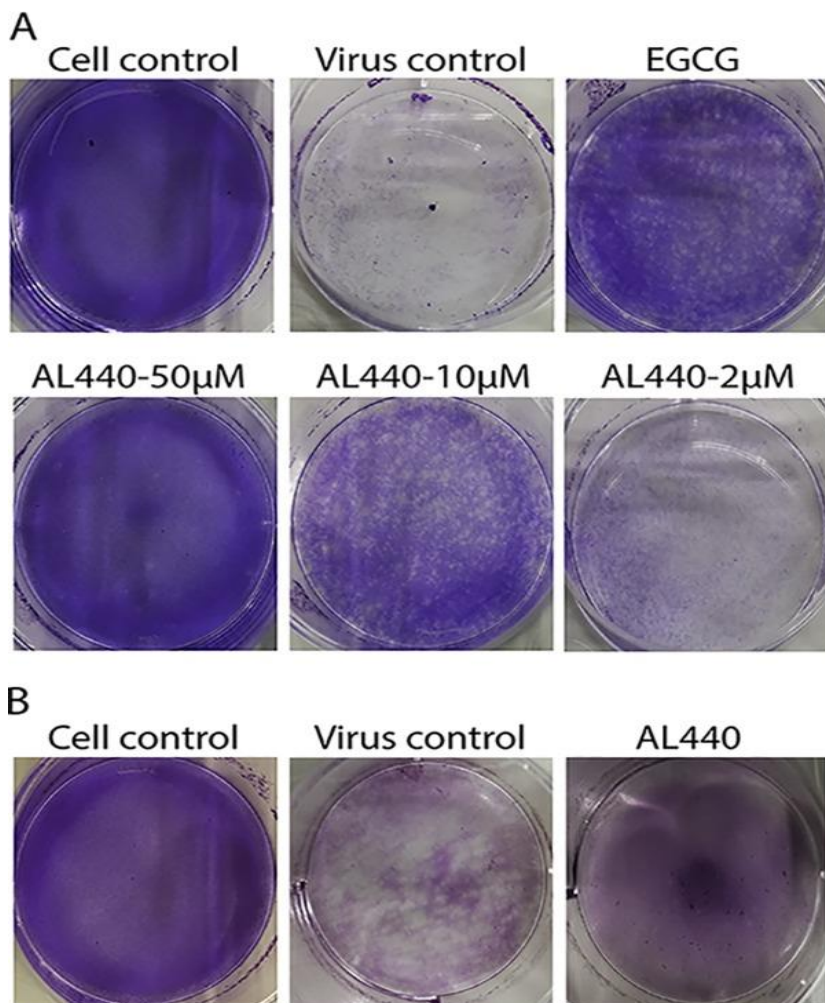
Figure 3.4: **AL compounds interact with the viral particles.** *(A) Ultrafiltration*: EGCG (0.1 mg/ml) and different concentrations of AL440 were mixed with DENV2 stock and further passed through a filter unit. Incubation of each sample (retained at the filter) on BHK cells showed that increasing concentrations of the compound reduce the number of viral plaques, as compared to virus control. *(B) Virus Inactivation*: DENV2 stock treated with 10 μM of AL440 was subsequently diluted 100 times and the mixture was used to infect BHK cells. The diluted sample demonstrated a strong inhibition of viral infection, as compared to virus control (no treatment with AL440).

3.3.7 AL compounds inhibit DENV infection by interacting with the domain III of the virus envelope protein

To investigate the potential binding of AL439 and AL440 to envelope glycoprotein (E) of DENV, a surface plasmon resonance (SPR) analysis was implemented. As shown in Figure 3.5, AL compounds were able to bind to E protein (Domain III) in a dose-dependent manner. More specifically, the binding capacity (association phase corresponding to response units) of AL440 was slightly stronger, as compared to this of AL439 (Figure 3.5A, 3.5B). However, both molecules presented a similar binding profile, with an association phase from 0 to 125 sec, followed by an immediate dissociation phase, where the compounds leave from the target protein. In addition, DS (positive control) showed a strong interaction with the E protein of DENV. In contrast, the negative control AL438 (a compound from our series displaying no antiviral activity against DENV, Table 3.1) showed no interaction with the E protein (Figure 3.5C, 3.5D). Comparison between AL molecules and DS revealed distinct differences, as the binding efficiency of DS to E protein was more pronounced (approximately 2X stronger) and its full dissociation from the target appeared at later time points, as compared to AL439 and AL440 (Figure 3.4A-C).
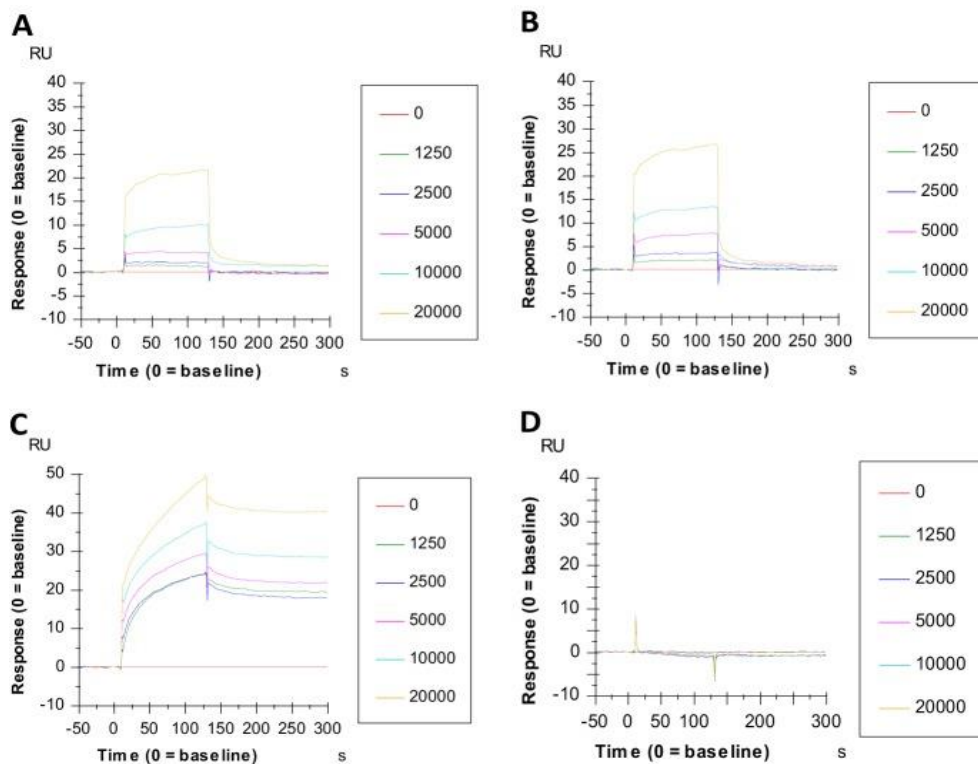
Figure 3.5: **Surface Plasmon Resonance technology shows the interaction of AL compounds with the Domain III of DENV Envelope protein**. Sensograms show the binding signal between the envelope protein of DENV (Domain III) and the AL compounds. Two-fold serial dilutions of (A) AL439 and (B) AL440 were added to the chip (concentration of each analogue showed in nM range). The binding capacity is measured from 0s to 125s, followed by the quick dissociation phase. The binding profiles of (C) DS and (D) AL438 are also depicted. The y axis indicates the resonance signal in resonance units (RU), whereas x axis the time of experiment (sec).

3.4 Discussion

In this study, a library of several classes of molecules was tested against DENV and ZIKV in order to evaluate their activity. Among these, a new generation of Trp trimers and tetramers was identified to have a broad-spectrum activity against several laboratory and clinical strains of both flaviviruses.

To define the structural requirements, which are crucial for the antiviral activity of the molecules, SAR studies were performed. Most modifications took place at N1 and C2 position of the indole side- chain of tryptophan and clearly showed the importance of extra phenyl rings bearing substituents different from -COOH at these positions for the antiviral activity. However, no substituent leads to loss of antiviral activity. Introduction of –COOH on the indole side chain results in an increase not only of the size of molecule, but also of the density (charge distribution), leading to the conclusion that different parameters might have an effect on the potency of molecules. We also showed that the increasing number of Trp residues on the central scaffold of molecules slightly increases their inhibitory activity, as indicated from the comparison of AL439 (three groups) and AL442 (one group), concluding that there is a certain degree of multivalence that contributes to the enhancement of antiviral activity. Regarding the tetramer derivative, elevated cytotoxic levels could be explained by its physiochemical properties and more specifically the increased lipophilicity that determines parameters, such as absorption and cytotoxicity of a molecule (35,36). To ascertain the mode of action of this series of molecules, the most potent compounds (AL439 and AL440) were chosen for further analysis.

Screening studies showed that AL439 and AL440 are active against several laboratory and clinical strains of both flaviviruses. However, slight differences in antiviral activity against these strains can be explained by several conformational changes on the target protein (37). In addition, we noticed that these molecules are active in all tested cell lines (EC_{50}: 0.5-7.6 µM and EC_{50}: 0.3-5.8 µM, for DENV2 and ZIKV, respectively); however, they also presented different cytotoxic profiles. More specifically, AL439 and AL440 displayed higher cytotoxic levels in HUVEC and Jeg3 cells (CC_{50} <50 µM), as compared to the other cell lines. A reason for this observation is that the molecules follow a distinct pattern for their activity, and possibly, they are able to influence several metabolic processes, affecting cell's viability (38).

Time-of-drug addition and subgenomic replicon experiments showed that these analogues act during the early stages of viral replication, possibly on the entry process. To further determine which step of virus entry is targeted, an attachment assay was performed. In this experiment, inhibition of viral infection was observed even after the removal of compounds 2h p.i. We confirmed these data by SPR, where both analogues displayed an interaction with the domain III of E glycoprotein (located at C-terminus). This particular

domain participates in cell-receptor recognition and contains antigenic epitopes that interact with potent neutralizing antibodies (39–42). Blocking this part of the protein has an unfavorable impact on viral entry into host cells (43). Interestingly, we observed a difference at the binding capacity between the DS and AL analogues with E protein. We hypothesize that the binding site on viral E glycoprotein has positively charged residues to form interactions with the negative charges of the Trp residues and the extra phenyl rings on the N1 or C2 indole side chains, in a weaker manner (faster dissociation rate), as compared to the DS-E interaction (44). Unfortunately, we were not able to determine the apparent K_D values for the binding of AL439 and AL440 to domain III of the viral E glycoprotein. This could be due to self-aggregation problems that give a prominent and constant signal, which results in non-saturation of the whole complex (45). In addition, the fact that the dissociation phase of our molecules is too fast (Figure 3.5A, 3.5B) can be explained not only by the nature of the analogues (typical SPR profile of small molecules) but also due to the presence of additional binding site(s) on other parts of the envelope protein.

Furthermore, several AL derivatives included in this study were also evaluated against HIV-1 (strain NL4.3) replication. Interestingly, we observed that AL439 and AL440 were not active at concentrations up to 40 μM, while AL437 and AL455 (not active against DENV and ZIKV) showed activity in the low micromolar range (EC_{50}:10 μM and 2.4 μM, respectively). These findings clearly suggest that the activity of AL439 and AL440 is specific against DENV and ZIKV.

In the literature, there are several reports on the role of polyanions as entry inhibitors, especially against HIV infections (46,47). One of the main advantages of this interesting class over small molecule drugs, is their ability to bind on the target in a multivalent way, considering them as promising antiviral candidates (48). Comparison between our molecules and the established entry inhibitor DS (control in this study) revealed numerous advantages, as AL439 and AL440 have a precise structure, well-defined composition and a moderate molecular size. These properties provide higher diffusion rate of these compounds, as compared to the sulfated polysaccharide DS (49). In addition, the sulfated groups (-OSO_3H) present on DS, can be exposed to changes in the human microenvironment, which lead to the loss of its activity (50). However, some problems associated with polyanionic substances should also be noted, as poor absorption,

anticoagulant properties and reduced *in vivo* efficacy have been considered as major drawbacks for their use as antiviral agents (51). Based on the synthetic accessibility of our molecules and the aforementioned reasons, defined molecular structure, relatively moderate molecular weight and the presence of COOH instead of OSO_3H can increase the therapeutic properties of these compounds that might be broader than those of DS.

To summarize, a novel class of Trp trimers and tetramers has been synthesized and evaluated for its antiviral activity against two emerging flaviviruses, DENV and ZIKV. These compounds are active in the low micromolar range against several strains in different susceptible cell lines. The mechanism of action was also determined, suggesting their role as entry inhibitors through the interaction with the DENV E-protein. Finally, taking into account the high degree of conservation in nucleotide/amino acid sequences among different flaviviruses, assessment of antiviral activity of these compounds should be performed against other members of this family, such as yellow fever and Japanese encephalitis virus to figure out their efficacy and qualify them as potential antiviral agents with broad- spectrum activity.

3.5 Materials and Methods

3.5.1 Cell lines and viruses

African green monkey kidney cells (Vero, ATCC) and human lung epithelial adenocarcinoma cells (A549, ATCC) were grown in Minimum Essential Medium Eagle (1X MEM-Rega3, Gibco, Belgium) supplemented with 8% fetal bovine serum (FBS, HyClone, US), 1 mM sodium bicarbonate (Gibco), 2 mM L- glutamine (Gibco) and 1X non-essential amino acids (100X, Gibco). Baby hamster kidney cells (BHK, kindly provided by Prof. M. Diamond, Washington University, USA) and hepatocarcinoma cells (Huh) were grown in Dulbecco's Modified Eagle Medium (1X DMEM, Gibco) supplemented with 10% FBS, 1 mM sodium pyruvate (Gibco), 0.01 M HEPES (Gibco) and 1X non-essential amino acids. Placenta choriocarcinoma cells (Jeg3, ATCC) were grown in 10% FBS, 1 mM sodium pyruvate and 1X non-essential amino acids. Finally, low-passage human umbilical vein endothelial cells (HUVEC, Lonza) were grown in endothelial cell growth basal medium 2 (EBM- 2, Lonza),

supplemented with EGM-™2 SingleQuots kit (Lonza). All cell lines were maintained at 37°C in a humidified 5% CO_2 incubator.

Several laboratory and clinical strains of DENV and ZIKV were used in this study. DENV serotypes 1-4 clinical isolates were obtained by Prof. Kevin Ariën from the Institute of Tropical Medicine (ITM, Antwerp, Belgium). All samples for routine diagnostics from patients presenting at the ITM polyclinic are stored after completion of the routine tests. The ITM has the policy that sample leftovers of patients presenting at the ITM polyclinic can be used for research unless the patients explicitly state their objection. The Institutional Review Board of ITM approved the policy of this presumed consent as long as patients' identity is not disclosed to third parties. DENV was isolated from stored serum samples from previously diagnosed acute dengue infections. Laboratory-adapted DENV serotype 1 Djibouti strain D1/H/IMTSSA/98/606 (GenBank accession number AF298808.1) (52), DENV serotype 3 H87 prototype strain (M93130.1) (53) and DENV serotype 4 Dak strain HD 34 460 (MF004387.1, unpublished data available) were kindly provided by Prof. X. de Lamballerie (Université de la Méditerranée, Marseille, France). Laboratory-adapted DENV serotype 2 New Guinea-C strain (NGC, M29095.1) (54) was a kind gift from Dr. V. Deubel (formerly at Institute Pasteur, Paris, France). Finally, the prototype ZIKV strain MR766 (MK105975.1, ATCC) and two clinical strains PRVAVC59 (MH916806, ATCC) and FLR (KX087102.2, ATCC) were also tested. All viral strains were propagated in C6/36 mosquito cells from *Aedes albopictus* (ATCC). The viruses present in the supernatant of these cells were collected 5-6 days post infection (p.i.) and stored at - 80 ^{0}C. Titration of the virus was performed by plaque assay using BHK cells. More specifically, serial ten-fold dilutions of each viral strain were inoculated for 2 h at 37°C on BHK cells ($8*10^5$ cells/well), grown in 6- well plates (Corning, USA). Cells were washed twice with infection medium (DMEM 2% FBS) and incubated with an overlay containing 2% Avicel (IMCD Benelux) and DMEM with 2% FBS at 1:1 ratio for 30 min at room temperature. The cells were incubated for 5 days at 37°C, then washed with cold PBS, fixed with 70% ethanol and finally stained with 0.1% crystal violet. The viral titer was calculated by counting the number of plaques and expressed as plaque forming units per milliliter (PFU/ml).

3.5.2 Cell viability and antiviral activity

All tested compounds were dissolved in dimethyl sulfoxide (DMSO). A final concentration of DMSO was maintained at 0.01% in order to evaluate its potential effect in all performed cellular assays.

The viability of cells in the presence of the compounds was assessed by the MTS method (3- (4,5-dimethylthiazol-2-yl)-5-(3-carboxymethoxyphenyl)-2-(4-sulfophenyl)-2*H*-tetrazolium, Promega, Leiden, The Netherlands). More specifically, every cell line was seeded at 10^4 cells/well in a 96-well plate (Corning, USA). After 24h, cells were incubated with 5-fold serial dilutions of each compound (range from 0.8 μM to 100 μM) for 72h. Then, medium was replaced by 50 μl of 0.2% MTS in PBS and incubated for 3-4 h at 37°C. The CC_{50} values (compound concentration, reducing the number of cells by 50%) were determined by measuring the optical density at 490 nm (SpectraMax Plus 384, Molecular Devices).

For the antiviral testing, cells were seeded at 10^4 cells/well (100 μl of infection medium) in 96- well plates. After an overnight incubation, compounds were added in 5-fold serial dilutions, as previously described. Cells were infected at different multiplicity of infection (MOI 1 for DENV and MOI 0.2 for ZIKV). After 2h, cells were washed in order to remove unbound viral particles and further incubated with new medium in the presence of the compounds. Supernatant was collected 72h p.i. and the virus yield was measured by Cells Direct One-step qRT-PCR kit (Thermo Fisher), according to manufacturer's instructions. RT-PCR was performed using the ABI 7500 Fast Real-Time PCR System (Applied Biosystems, NJ, USA) and all the data were analyzed with the ABI PRISM 7000 software (v2.0.5., Applied Biosystems). The primer and probe sequences used for qRT- PCR were 5'- GGA TAG ACC AGA GAT CCT GCT GT-3' (DENV 1-4 forward), 5'- CAT TCC ATT TTC TGG GGT TC-3' (DENV 1-3 reverse), 5'- CAA TCC ATC TTG CGG CGC TC-3' (DENV 4 reverse), 5'- FAM-CAG CAT CAT TCC AGG CAC AG-MGB-3' (DENV 1-3 probe), 5'-FAM-CAA CAT CAA TCC AGG CAC AG-MGB-3' (DENV 4 probe), 5'- TGA CTC CCC TCG TAG ACT G-3' (ZIKV forward), 5'- CAC CTT AGT CAC CTT CCT CTC T-3' (ZIKV reverse) and 5'- 6- FAM/AGA TCC CAC/ZEN/AAA TCC CCT CTT CCC/3IABkFQ-3' (ZIKV probe). Finally, the amplification conditions were indicated below: 50°C for 15 min, 95°C for 2 min, followed by 45 cycles of 95°C for 15 sec and 60°C for 1 min. The infection efficiency was calculated using a curve of serial dilutions

of standard samples for each virus. All data were analyzed in GraphPad Prism 7 software.

3.5.3 Antiviral activity in monocyte dendritic-derived cells (MDDC)

Peripheral blood mononuclear cells (PBMCs), obtained from four different healthy donors (provided from Rode Kruis Vlaanderen, Leuven), were resuspended in Roswell Park Memorial Institute medium (RPMI 1640), supplemented with 10% FBS and 2 mM L- glutamine. The next day, cells were stimulated with 50 ng/ml of GM-CSF and 25 ng/ml of IL-4 and seeded in a 6- well plate ($1.5*10^6$ cells/well) for 5 days at 37°C, in order to obtain MDDCs. The cells were seeded at $3*10^4$ cells/well in 24-well plates (Corning, USA) and incubated with the compounds in 5-fold serial dilutions for 30 min. Then, DENV-2 NGC or ZIKV MR766 were added to the cells. After 2h, MDDCs were centrifuged and washed two times with fresh medium. Finally, cells were incubated in infection medium (RPMI 2% FBS) for 48h, collected and then subjected for One-step qRT-PCR analysis.

3.5.4 Immunofluorescence assay

Vero cells (10^4 cells/well) were seeded in a black 96-well plate (Falcon, Germany). After 24h, cells were infected with ZIKV MR766 strain at MOI 0.2 in the presence of AL440 (20 µM-10 µM -2 µM-0.4 µM) at 37°C for 2h. Cells were washed twice with PBS to remove the unbound viral particles and incubated at 37°C with infection medium for 72h. Next, cells were fixed for 5 min with 2% paraformaldehyde (PFA, Sigma Aldrich, USA) at room temperature and permeabilized with 0.1% TritonX-100 (Sigma-Aldrich, USA) for 10 more minutes. In addition, 1% Bovine Serum Albumin (BSA, Cell Signaling Technology, The Netherlands) diluted in PBS was used to block the fixed cells for 1h. After two washing steps, cells were incubated with the primary 4G2 pan-flavivirus antibody (Merck Millipore, Belgium) overnight at 4°C. Goat anti-mouse IgG Alexa Fluor 488 (Invitrogen) was used as a secondary antibody. The nucleus was stained with DAPI (Invitrogen). Fluorescence microscopy was performed on a Zeiss Axiovert 200M inverted microscope (Germany) using 10X EGFP objective.

3.5.5 Time-of-drug addition assay

Vero cells (10^4 cells/well) were seeded in a 96-well plate and infected with DENV-2 NGC strain at MOI 1 for 2h. Cells were washed and treated with an active concentration of each compound (3-fold higher than EC_{50} values) at different time points pre- (2h) and post- infection (0, 2, 4, 6, 8, 12 and 18h). After 20h (time point corresponding to one complete viral replication cycle), cells were collected and the viral RNA levels were measured by real time RT- PCR. In addition, dextran sulfate with average molecular weight 8000 Da (DS) and 7- Deaza-2'-C-Methyladenosine (7DMA) were included as reference compounds. DS is a negatively charged inhibitor of the entry/fusion process, while 7DMA is a nucleosidic viral polymerase inhibitor. Both compounds were added at 10 µM final concentration.

3.5.6 Subgenomic replicon assay

To evaluate whether the compounds interact with the non-structural proteins (NS) or the replication complex (indirectly), BHK cells stably transfected with a DENV subgenomic replicon (BHK/DENV, obtained from Prof. M. Diamond) were used. The replicon system encodes all NS proteins, as well as a *Firefly* luciferase expression cassette instead of prM and E proteins of DENV2 viral strain. Briefly, BHK/DENV ($6*10^3$ cells/well) were seeded in DMEM 2% FBS supplemented with 3 µg/ml puromycin for antibiotic selection (Sigma-Aldrich, USA), in a white-bottom 96-well plate (Nunclon™ Delta Surface, ThermoFischer Scientific). The next day, serial dilutions of AL439 and AL440 were added to the cells. After 3 days, supernatant was removed, cells were washed with PBS, the Renilla-Glo™ Luciferase Assay Reagent (ThermoFischer Scientific) was added to each well and the plate was incubated for 15 min. Finally, luminescence was measured at 490 nm (Tecan Spark 10M Multimode Microplate Reader, BioExpress). DS and 7DMA were included as control compounds, while cytotoxicity of the AL compounds in BHK/DENV cells was performed in parallel, using the MTS method as described above.

3.5.7 Viral attachment assay

Vero cells were exposed to DENV2 NGC (MOI 1) in the presence of different concentrations of compounds (40 µM 20 µM, 10 µM, 5 µM and 2.5 µM) for 2h at 4°C (condition that allows virus attachment, but no internalization). Cells were washed twice with infection medium to remove non-specific material

and incubated at 37°C (facilitates virus entry/fusion) without the compounds for 72h. Supernatant was collected and virus yield was measured by One-step real-time RT- PCR.

3.5.8 Ultrafiltration and virus inactivation assay

Direct interactions between AL440 and DENV2 NGC strain were evaluated using two different methodologies.

First, in the ultrafiltration assay, viral stock (10^4 PFUs) was incubated with different concentrations of AL440 (2 µM, 10 µM and 50 µM) at 37°C for 1h. Each sample was further passed through a 10 kDa cut-off concentrator filter unit (Vivaspin^R 500, Vivaproducts), followed by three centrifugation steps, in order to allow non-binding, free compound (< 10 kDa) to infiltrate. The fraction retained by the filter (virus-compound complex) was added into BHK cells for a plaque assay. Epigallocatechin gallate (EGCG, 0.1 mg/ml) was used as a positive control to assess the specificity of the assay, as it has been shown that interacts with the viral particles. Viral stock was also incubated in the absence of the compounds (virus control) and treated the same way. Finally, an equal volume of normal medium was added to control plates. The presence/number of plaques was evaluated per each condition and compared with the virus control.

Second, during the virus inactivation assay, aliquots of DENV2 stock (10^4 PFUs) were incubated with a concentration of AL440 (10 µM), able to inhibit viral infection at 37°C for 1h. Sample was next diluted 100 times with fresh medium to reach a concentration of the compound below the EC_{50} values and used to infect susceptible Vero cells. Virus infectivity was further assessed by the plaque reduction assay (titration), using BHK cells. Virus and cell controls were also included.

3.5.9 Surface Plasmon Resonance technology (SPR)

To study interactions of the compounds with the envelope protein of DENV, SPR analysis was performed on a Biacore T200 instrument (GE Healthcare, Uppsala, Sweden). Briefly, the domain III of recombinant envelope protein (GenWay Biotech Inc., San Diego, USA) of DENV2 was immobilized on a CM5 sensor chip in 10 mM sodium acetate buffer, pH 5, using a standard amine coupling chemistry, resulting in a chip density of 250 RU. A reference flow cell was used to evaluate non-specific binding to the chip. AL439 and AL440 were

diluted in PBS supplemented with 0.005% surfactant P20 and 5% DMSO (pH 7.4) to obtain different concentrations between 1.25 μM and 20 μM (in 2- fold dilution steps). AL438 was included as negative control in this study. Samples were injected for 2 min at a flow rate of 30 μl/min and the dissociation was followed for 4 min. Several buffer blanks were used for double referencing. The chip was finally regenerated with 1 M NaCl in 10 mM NaOH followed by 10 mM glycine-HCl pH 1.5. All responses were adjusted for DMSO effects using a solvent correction procedure.

"Data availability"

Accession numbers for each viral strain are provided below (GenBank):

AF298808.1 (DENV serotype 1 Djibouti D1/H/IMTSSA/98/606 strain), M29095.1 (DENV serotype 2 NGC strain), M93130.1 (DENV serotype 3 H87 strain), MF004387.1 (DENV serotype 4 Dak strain), MK105975.1 (ZIKV MR766 strain), MH916806.1 (ZIKV PRVAVC59 strain) and KX087102.2 (ZIKV FLR strain).

3.6 Supplemental Material

3.6.1. Synthetic Schemes

First, the corresponding sulfenylating agent, phenylsulfenyl chloride (PS-Cl) or *p*-nitro-benzenesulfenyl chloride (*p*NPS-Cl) were obtained following reported procedures (55) (56). Reaction of these sulfenyl halides, with the methyl protected tryptophan trimer 1 (57) in dry THF/acetic acid afforded the C2-sulfenyltryptophan intermediates 2 and 3 in 83 and 88 yield respectively (Scheme 1). Reaction of intermediate 3 with methyl iodide, in the presence of cesium carbonate (Cs$_2$CO$_3$) at 80 ºC, followed by deprotection (LiOH/H$_2$O) of intermediate 4 afforded the N1 methyl Trp derivative AL-484 in 90% yield (Scheme 1). In addition, the N1 unsubstituted Trp derivative AL437 was prepared in 90% yield by deprotection (LiOH/H$_2$O) of the sulfenyl intermediate 2 (Scheme 1).
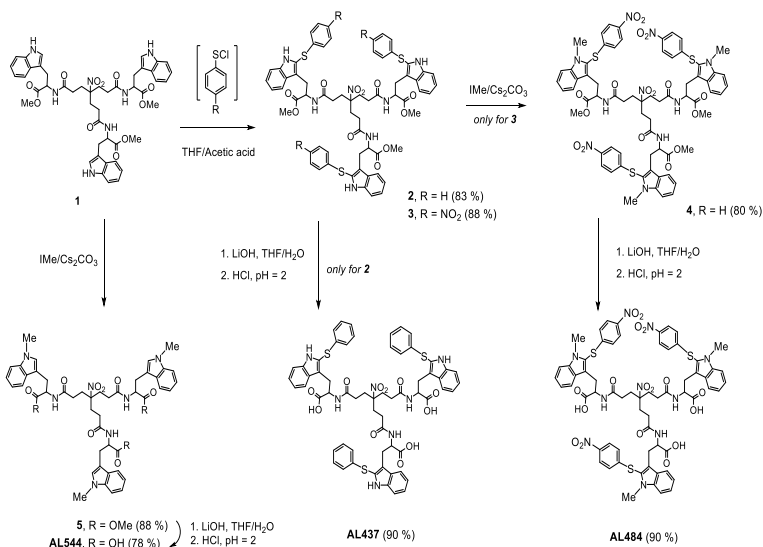
Scheme 1. Synthesis of the 2-sulfenyltryptophan AL437, AL484 and Nα methyl tryptophan AL-544 trimers

In addition, reaction of trimer 1 with methyl iodide in the presence of cesium carbonate (Cs_2CO_3) at 80 ºC, followed by subsequent deprotection ($LiOH/H_2O$) of intermediate 5 afforded compound AL- 544 in 78% yield (Scheme 1).

Next, reaction of tetramer 6 (57) with *p*-fluoro benzyl bromide, in the presence of Cs_2CO_3 at 80 ºC, followed by subsequent deprotection ($LiOH/H_2O$) of intermediate 7 afforded tetramer AL-531 in 80% yield (Scheme 2).
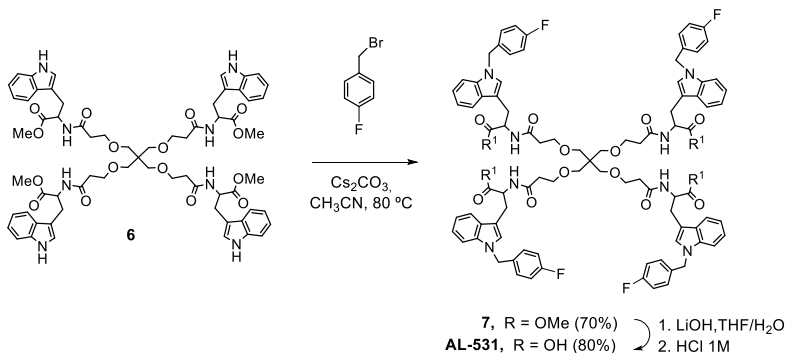
Scheme 2. Synthesis of the N1-benzyl tryptophan tetramer AL531

The synthesis of the N1 substituted monopodal derivatives AL441 and AL442 started with the commercially available scaffold 8 (Scheme 3). Reaction of 8 with the corresponding benzyl iodide, in the presence of cesium carbonate (Cs$_2$CO$_3$) at 80 ºC, followed by subsequent deprotection (LiOH/H$_2$O) of intermediates 9 and 10 afforded compounds AL-441 and AL-442 in 71 and 80 % yield respectively (Scheme 3).

8

9, R = COOMe (62 %)
10, R = F (70 %)

AL-441, R = COOH (71 %)
AL-442, R = F (80 %)
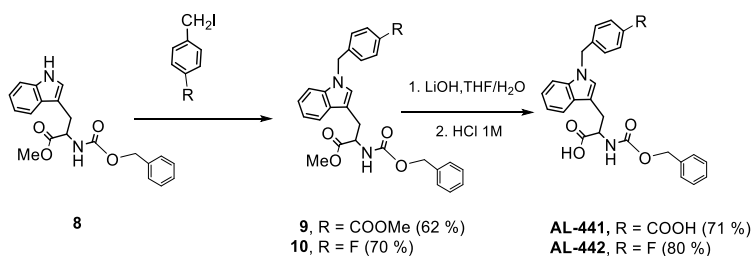
Scheme 3. Synthesis of the N1-benzyl tryptophan monomers AL441 and AL442

3.7 References

1.   Simmonds P, Becher P, Bukh J, Gould EA, Meyers G, Monath T, et al. Ictv Consortium. ICTV virus taxonomy profile: Flaviviridae. J Gen Virol. 2017;98:2–3.

2.   Suwanmanee S, Luplertlop N. Dengue and Zika viruses: lessons learned from the similarities between these Aedes mosquito-vectored arboviruses. J Microbiol. 2017;55:81–9.

3.   Dissanayake HA, Seneviratne SL. Liver involvement in dengue viral infections. Rev Med Virol. 2018;28:1–11.

4.   Weaver SC, Costa F, Garcia-Blanco MA, Ko AI, Ribeiro GS, Saade G, et al. Zika virus: History, emergence, biology, and prospects for control. Antiviral Res. 2016;130:69-80.

5.   Paixão ES, Teixeira MG, Rodrigues LC. Zika, chikungunya and dengue: The causes and threats of new and reemerging arboviral diseases. BMJ Glob Heal. 2018;3:1–6.

6.   Gubler DJ. Epidemic dengue. 2002;10:100–3.

7.   Gould E, Pettersson J, Higgs S, Charrel R, de Lamballerie X. Emerging arboviruses: Why today? One Heal. 2017;4:1–13.

8.   Dallmeier K, Neyts J. Zika and Other Emerging Viruses: Aiming at the Right Target. Cell Host Microbe. 2016;20:420–2.

9.   Raekiansyah M, Mori M, Nonaka K, Agoh M, Shiomi K, Matsumoto A, et al. Identification of novel antiviral of fungus-derived brefeldin A against dengue viruses. Trop Med Health. 2017;45:1–7.

10.   Yung CF, Lee KS, Thein TL, Tan LK, Gan VC, Wong JGX, et al. Dengue serotype-specific differences in clinical manifestation, laboratory parameters and risk of severe disease in adults, Singapore. Am J Trop Med Hyg. 2015;92:999–1005.

11.   Vervaeke P, Vermeire K, Liekens S. Endothelial dysfunction in dengue virus pathology. Rev Med Virol. 2015;25:50-67

12.   Wikan N, Smith DR. Zika virus: History of a newly emerging arbovirus. Lancet Infect Dis. 2016;16:e119–e26.

13. Chan JFW, Choi GKY, Yip CCY, Cheng VCC, Yuen KY. Zika fever and congenital Zika syndrome: An unexpected emerging arboviral disease. J Infect. 2016;72:507–24.

14. Roos RP. 2016. Zika virus-A public health emergency of international concern. JAMA Neurol 73:1395–6.

15. Lozier M, Adams L, Febo MF, Torres-Aponte J, Bello-Pagan M, Ryff KR, et al. Incidence of Zika virus disease by age and sex - Puerto Rico, November 1, 2015-October 20, 2016. Morb Mortal Wkly Rep. 2016;65:1219–23.

16. Ming G li, Song H, Tang H. Racing to Uncover the Link between Zika Virus and Microcephaly. Cell Stem Cell. 2017;20:749–53.

17. Pinto-Díaz CA, Rodríguez Y, Monsalve DM, Acosta-Ampudia Y, Molano González N, Anaya JM, et al. Autoimmunity in Guillain Barré syndrome associated with Zika virus infection and beyond. Autoimmun Rev. 2017;16:327–34.

18. Magnus MM, Espósito DLA, Costa VA da, Melo PS de, Costa-Lima C, Fonseca BAL da, et al. Risk of Zika virus transmission by blood donations in Brazil. Hematol Transfus Cell Ther. 2018;40:250–4.

19. Hastings AK, Fikrig E. Zika virus and sexual transmission: A new route of transmission for mosquito-borne flaviviruses. Yale J Biol Med. 2017;90:325–30.

20. Cao B, Diamond MS, Mysorekar IU. Maternal-fetal transmission of zika virus: Routes and signals for infection. J Interf Cytokine Res. 2017;37:287–94.

21. Aguiar M, Stollenwerk N, Halstead SB. The Impact of the Newly Licensed Dengue Vaccine in Endemic Countries. PLoS Negl Trop Dis. 2016;10:1–23.

22. Halstead SB. Safety issues from a Phase 3 clinical trial of a live-attenuated chimeric yellow fever tetravalent dengue vaccine. Hum Vaccines Immunother. 2018;14:2158–62.

23. Martínez-Vega RA, Carrasquila G, Luna E, Ramos-Castañeda J. ADE and dengue vaccination. Vaccine. 2017;35:3910–2.

24. Diamond MS, Ledgerwood JE, Pierson TC. Zika Virus Vaccine Development: Progress in the Face of New Challenges. Annu Rev Med. 2019;70:121–35.

25. Blackman MA, Kim IJ, Lin JS, Thomas SJ. Challenges of Vaccine Development for Zika Virus. Viral Immunol. 2018;31:117–23.

26. Low JGH, Ooi EE, Vasudevan SG. Current status of dengue therapeutics research and development. J Infect Dis. 2017;215(Suppl 2):S96–102.

27. Saiz JC, Martín-Acebes MA. The race to find antivirals for zika virus. Antimicrob Agents Chemother. 2017;61:1–9.

28. Zhou Y, Simmons G. Development of novel entry inhibitors targeting emerging viruses. Expert Rev Anti Infect Ther. 2012;10:1129–38.

29. Witvrouw M, De Clercq E. Sulfated polysaccharides extracted from sea algae as potential antiviral drugs. Gen Pharmacol. 1997;29:497–511.

30. Vacas-Córdoba E, Maly M, De la mata FJ, Gómez R, Pion M, Muñoz-Fernández MÁ. Antiviral mechanism of polyanionic carbosilane dendrimers against HIV-I. Int J Nanomedicine. 2016;11:1281–94.

31. Witvrouw M, Fikkert V, Pluymers W, Matthews B, Mardel K, Schols D, et al. Polyanionic (i.e., polysulfonate) dendrimers can inhibit the replication of human immunodeficiency virus by interfering with both virus adsorption and later steps (reverse transcriptase/integrase) in the virus replicative cycle. Mol Pharmacol. 2000;58:1100–8.

32. Alhoot MA, Rathinam AK, Wang SM, Manikam R, Sekaran SD. Inhibition of dengue virus entry into target cells using synthetic antiviral peptides. Int J Med Sci. 2013;10:719–29.

33. Watterson D, Kobe B, Young PR. Residues in domain III of the dengue virus envelope glycoprotein involved in cell-surface glycosaminoglycan binding. J Gen Virol. 2012;93:72–82.

34. Martínez-Gualda B, Sun L, Martí-Marí O, Noppen S, Abdelnabi R, Bator CM, et al. A scaffold simplification strategy leads to a novel generation of dual human immunodeficiency virus and enterovirus

A71 entry inhibitors. J Med Chem. 2019; doi:10.1021/acs.jmedchem.9b01737

35. Gao Y, Gesenberg C, Zheng W. Oral Formulations for preclinical studies: Principle, design, and development considerations. Developing Solid Oral Dosage Forms: Pharmaceutical Theory and Practice: Second Edition. 2017;Elsevier Inc 455–495 p.

36. Arnott JA, Planey SL. The influence of lipophilicity in drug discovery and design. Expert Opin Drug Discov. 2012;7:863–75.

37. Witvrouw M, Weigold H, Pannecouque C, Schols D, De Clercq E, Holan G. Potent anti-HIV (type 1 and type 2) activity of polyoxometalates: Structure-activity relationship and mechanism of action. J Med Chem. 2000;43:778–83.

38. Olsen DB, Eldrup AB, Bartholomew L, Bhat B, Bosserman MR, Ceccacci A, et al. A 7-deaza-adenosine analog is a potent and selective inhibitor of hepatitis C virus replication with excellent pharmacokinetic properties. Antimicrob Agents Chemother. 2004;48:3944–53.

39. Zhang X, Jia R, Shen H, Wang M, Yin Z, Cheng A. Structures and functions of the envelope glycoprotein in flavivirus infections. Viruses. 2017;9:1–14.

40. Marzinek JK, Lakshminarayanan R, Goh E, Huber RG, Panzade S, Verma C, et al. Characterizing the Conformational Landscape of Flavivirus Fusion Peptides via Simulation and Experiment. Sci Rep. 2016;6:1–15.

41. Wu KP, Wu CW, Tsao YP, Kuo TW, Lou YC, Lin CW, et al. Structural basis of a flavivirus recognized by its neutralizing antibody: Solution structure of the domain III of the Japanese encephalitis virus envelope protein. J Biol Chem. 2003;278:46007–13.

42. Chávez JH, Silva JR, Amarilla AA, Moraes Figueiredo LT. Domain III peptides from flavivirus envelope protein are useful antigens for serologic diagnosis and targets for immunization. Biologicals. 2010;38:613–8.

43. Modis Y, Ogata S, Clements D, Harrison SC. Variable surface epitopes

in the crystal structure of dengue virus type 3 envelope glycoprotein. J Virol. 2005;79:1223–123.

44. Martínez-Gualda B, Sun L, Martí-Marí O, Mirabelli C, Delang L, Neyts J, et al. Modifications in the branched arms of a class of dual inhibitors of HIV and EV71 replication expand their antiviral spectrum. Antiviral Res. 2019;168:210–4.

45. Giannetti AM, Koch BD, Browner MF. Surface plasmon resonance based assay for the detection and characterization of promiscuous inhibitors. J Med Chem. 2008;51:574–80.

46. Lüscher-Mattli M. Polyanions - A lost chance in the fight against HIV and other virus diseases? Antivir Chem Chemother. 2000;11:249–59.

47. Leydet A, Jeantet-Segonds C, Bouchitté C, Moullet C, Boyer B, Roque JP, et al. Polyanion inhibitors of human immunodeficiency virus and other viruses. 6. Micelle-like anti-HIV polyanionic compounds based on a carbohydrate core. J Med Chem. 1997;40:350–6

48. MacIel D, Guerrero-Beltrán C, Ceña-Diez R, Tomás H, Muñoz-Fernández MÁ, Rodrigues J. New anionic poly(alkylideneamine) dendrimers as microbicide agents against HIV-1 infection. Nanoscale. 2019;11:9679–90.

49. Keeney M, Jiang XY, Yamane M, Lee M, Goodman S, Yang F. Nanocoating for biomolecule delivery using layer-by-layer self-assembly. J Mater Chem B. 2015;3:8757–70.

50. Balzarini J, Van Damme L. Microbicide drug candidates to prevent HIV infection. Lancet. 2007;369:787–97.

51. Pirrone V, Wigdahl B, Krebs FC. The rise and fall of polyanionic inhibitors of the human immunodeficiency virus type 1. Antiviral Res. 2011;90:168–82.

52. Tolou HJG, Couissinier-Paris P, Durand JP, Mercier V, de Pina JJ, de Micco P, et al. Data from "Evidence for recombination in natural populations of dengue virus type 1 based on the analysis of complete genome sequences". J Gen Virol. 2001;82:1283–90.

53. Osatomi K, Sumiyoshi H. Complete nucleotide sequence of dengue

type 3 virus genome RNA. Virology. 1990;176:643–7.

54.   Irie K, Mohan PM, Sasaguri Y, Putnak R, Padmanabhan R. Sequence analysis of cloned dengue virus type 2 genome (New Guinea-C strain). Gene. 1989;75:197–211.

55.   Mueller WH, Butter PE. Factors influencing the nature of the episulfonium ion in sulfenyl chloride addition to terminal olefins. J Am Chem Soc. 1968;90:2075-2081.

56.   Raban M., Jones FB Jr. Stereochemistry at trivalent nitrogen. XI. Effect of polar substituents on the barrier to rotation about the sulfenyl sulfur-nitrogen bond in N-alkyl-N-arenesulfonylarenesulfenamides. J Am Chem Soc. 1971;93:2692- 2699.

57.   Martínez-Gualda B, Sun L, Martí-Marí O, Noppen, S, Abdelnabi R., Bator   C.M., et al. Med. Chem. 2019; PubMed ID: 3180904, DOI: 10.1021/acs.jmedchem.9b01737.

Chapter 4: A novel series of indole alkaloid derivatives inhibit dengue and Zika virus infection by interference with the viral replication complex

4.1 Abstract

Here, we identified a novel class of compounds, which demonstrated good antiviral activity against dengue and Zika virus infection. These derivatives constitute intermediates in the synthesis of indole (ervatamine-silicine) alkaloids and share a tetracyclic structure with an indole and a piperidine fused to a seven-membered carbocyclic ring. Structure-activity relationship studies indicated the importance of the substituent at the C-6 position and especially the presence of a benzylester for the activity and cytotoxicity of the molecules. In addition, the stereochemistry at the C-7 and C-8 positions, as well as the presence of the oxazolidine ring influenced the potency of the compounds. Mechanism of action studies with two analogues of this family (compounds **22** and *trans*-**14**) showed that this class of molecules suppressed viral infection during the later stages of the replication cycle (RNA replication/assembly). Moreover, a cell-dependent antiviral profile of the compounds against several Zika strains was observed, thus possibly implying the involvement of cellular factor(s) in the activity of the molecules. Sequencing of compounds-resistant Zika mutants revealed a single non- synonymous amino acid mutation (aspartic acid to histidine) at the beginning of the predicted transmembrane domain 1 of NS4B protein, which plays a vital role in the formation of the viral replication complex. To conclude, our study provides detailed information on a new class of NS4B- associated inhibitors and strengthens the importance of identifying host-viral interactions in order to tackle flavivirus infections.

4.2 Introduction

Flaviviruses (belonging to the *Flaviviridae* family*)* are small enveloped viruses with a positive sense single-stranded RNA. Their genome is approximately 11 kilobases in size and encodes for a single polyprotein, which is post-translationally processed by several viral and host enzymes into three structural (capsid, envelope and pre- membrane) and seven non-structural proteins (NS1, NS2A, NS2B, NS3, NS4A, NS4B and NS5) (1). Two of the most important human pathogens in this family are dengue (DENV) and Zika virus (ZIKV) that are mainly spread through *Aedes* mosquitoes in many regions across the world (such as Americas, Africa, Southeast Asia and Pacific Islands)

(2), (3). Additionally, more transmission routes have been reported such as sexual contact and from mother-to-child (4), (5).

DENV, a prevailing arbovirus, is found in tropical and sub-tropical areas and it is responsible for more than 300 million infections per year (6). In most cases, the virus can cause flu-like illness symptoms, such as headache and fever. However, in extreme conditions, DENV has been associated with severe dengue disease, which might lead to shock syndrome and death (7), (8). There are four antigenically different, but closely related serotypes (DENV1, DENV2, DENV3 and DENV4), which co-circulate with other flavivirus members, including ZIKV (9).

ZIKV was first isolated from rhesus macaques in the 1950's and it was responsible for three main outbreaks: in Southeast Asia (Yap Islands, 2007), Pacific Islands (French Polynesia, 2013) and South America (Brazil, 2015). During that period, ZIKV was considered as Public Health Emergence of International Concern by the World Health Organization (WHO) (10). Although the virus generally causes asymptomatic infections, it has been correlated with neurological disorders including microcephaly and the autoimmune disease Guillain-Barré syndrome (11), (12).

Currently, an approved vaccine against DENV (Dengvaxia®) has been shown to efficiently enhance immune responses in people who were previously infected by the virus. However, important limitations have been raised due to its efficacy and side effects in those with no signs of previous viral infection (13), (14). On the other hand, no ZIKV vaccines are available at the moment. As previously mentioned, the fact that ZIKV infection mostly occurred in areas where DENV is endemic makes vaccine development even more complex due to serological cross-reactivity between the two viruses (15).

Therefore, development of an effective treatment against both flaviviruses is of utmost importance. During the last years, the research community has made serious efforts to identify potent antiviral molecules against both DENV and ZIKV. These compounds can either target viral proteins (direct-acting) or cellular factors (host- acting) to tackle the infection. Screening assays with a number of Food and Drug Administration-repurposing drugs have revealed analogues targeting several viral proteins (e.g. sofosbuvir against NS5, castanospermine against envelope protein) (16), (17). Despite the promising outcomes, important limitations have to be considered for their use since occurrence of mutations in the viral genome is common, possibly leading to

the generation of resistant strains, which might evade the compounds' pressure. On the other hand, host-factor targeted molecules are able to address the problem of a low genetic barrier to resistance (18). Particularly, several compounds targeting cellular factors have shown to present antiviral activity against DENV and ZIKV, including chloroquine, bortezomib and lovastatin. However, these molecules do not display a significant improvement in patient symptoms when evaluated in clinical trials (19), (20). Taking all the above into consideration, it is evident that development and characterization of novel molecules will be crucial in the fight against these two emerging flaviviruses.

In the present study, we identified and characterized a novel class of indole derivatives, having in common an oxazolopiperidone moiety, with pronounced antiviral activity (in the low micromolar range) against DENV and ZIKV. Following a number of *in vitro* antiviral assays, we showed that our compounds possibly interfere with the viral RNA replication and assembly processes. Moreover, selection and sequencing analysis of compounds-resistant virus mutants revealed a single non-synonymous amino acid mutation, located right at the beginning of predicted transmembrane domain 1 (pTMD1) of ZIKV NS4B protein. This motif possesses a dual role, as it is involved in the formation of the viral replication complex system and antagonizes interferon (IFN)-host responses (21). Finally, a cell-dependent inhibition profile indicated the possible involvement of cellular factors on the activity of the molecules.

4.3 Results

4.3.1 Cellular cytotoxicity and antiviral activity of indole alkaloid derivatives against DENV and ZIKV replication in several susceptible host cell lines

The synthesis of this series of molecules is described in the Supplemental material. As shown in Figure 4.1, all analogues are synthetic intermediates of ervatamine-silicine indole alkaloids. To evaluate the antiviral activity of the compounds, African green monkey kidney cells (Vero) were infected with DENV2 NGC and ZIKV MR766 prototype strains in the presence of these molecules. Cellular cytotoxicity was assessed in parallel. Based on the results

from Table 4.1, we could divide the compounds into three distinct groups based on their antiviral activity and cytotoxic profile. More specifically, *(a)* compounds **22**, **20**, *trans*-**14** and *cis*-**12** presented good activity against DENV2 (EC$_{50}$: 0.3-5.9 µM), but no or limited (36.2 ± 6.5 µM) inhibition against ZIKV. On the other hand, *(b)* compounds *trans*-**13**, *cis*-**13**, *cis*-**11**, lacking the benzyloxy substituent at C-6 (Figure 4.1, red circle) were active against both DENV (1.1-10.9 µM) and ZIKV (3.3-7.2 µM), but showed more pronounced cytotoxicity (CC$_{50}$: < 40 µM) in our evaluation. Finally, *(c) cis*-**10** and *trans*-**10** derivatives displayed good antiviral activity against both viruses (EC$_{50}$: 0.4-2.7 µM and 0.2-12 µM for DENV and ZIKV, respectively) with no associated cytotoxicity. Similar results were observed for **24**, an analogue without the sulphonamide group in the indole nitrogen moiety (Figure 4.1, blue circle). In addition, analogue **21**, which lacks the oxazolidine ring (Figure 4.1, green circle), was less active against DENV (37.1 ± 6.0 µM), as compared to the other molecules. Furthermore, molecules **15a** and **15b** (de-ethyl analogues of *cis*- **12** and *trans*-**14,** respectively), bearing a methylester at C-6 (instead of a larger benzylester group) (Figure 4.1, yellow circle), showed more pronounced cytotoxicity and decreased antiviral activity against DENV, as compared to their analogues. Moreover, stereochemistry at the C-7 position seemed to affect the cytotoxicity levels between **15a** (CC$_{50}$ >100 µM) and **15b** (CC$_{50}$: 41.8 ± 9.8 µM) (Figure 4.1, blue arrows). Finally, *cis*-**10** and *cis*-**12** displayed C-7/C-8-*cis* and C-8/C-8a-*trans* relative configurations (Figure 4.1, orange arrows), although with opposite absolute stereochemistry, which seemed to be beneficial for the antiviral activity.
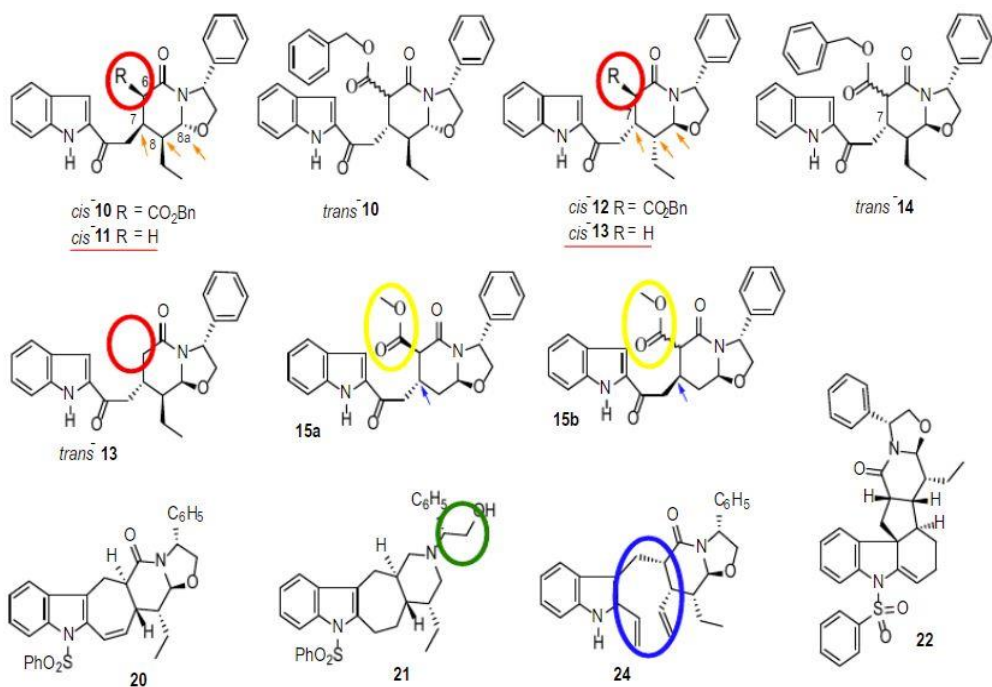
Figure 4.1: Structure of indole alkaloid derivatives. Chemical groups and sites, crucial for the enhancement of antiviral activity, are marked in circles and arrows.

Table 4.1: Antiviral activity, cellular cytotoxicity and selectivity index of a novel series of compounds in Vero cells

Compound	EC_{50} $(\mu M)^a$ (DENV2 NGC)	EC_{50} (μM) (ZIKV MR766)	CC_{50} $(\mu M)^b$	SI $_{DENV2}{}^c$	SI $_{ZIKV}$
15a	19.4 ± 7.5	40 ± 3.8	41.8 ± 9.8	2.1	1
15b	18.6 ± 3.5	12.1 ± 1.7	>100	5.4	8.3
20	5.9 ± 3.9	>100	>100	>17	>1
21	37.1 ± 6.0	4.0 ± 2.0	>100	>2.7	>25
22	2.8 ± 2.8	>100	>100	>35.7	>1
24	0.4 ± 0.2	0.2 ± 0.1	80 ± 35	200	400
Cis-**10**	1.0 ± 0.2	0.8 ± 0.1	>100	>100	>125
Trans-**10**	2.7 ± 0.9	12 ± 3.8	>100	>37	>8.3
Cis-**11**	10.9 ± 1.7	7.2 ± 1.4	27.7 ± 9.4	2.5	3.8
Cis-**12**	0.3 ± 0.1	36.2 ± 6.5	>100	>333	>2.7
Cis-**13**	1.1 ± 0.2	3.3 ± 0.5	5.8 ± 0.1	5.3	1.8
Trans-**13**	4.0 ± 2.8	6.5 ± 0.2	9.2	2.3	1.4
Trans-**14**	2.8 ± 1.9	>100	>100	>35.7	>1

[a]EC_{50}: Effective concentration of the compound, able to inhibit viral replication by 50%, as assessed by qRT-PCR of supernatants at 72h pi

[b]CC_{50}: Concentration of the compound required to reduce cell viability by 50%, as assessed by MTS analysis of cell lysates at 72h pi

[c]SI: Selectivity index (CC_{50}/EC_{50})

To obtain more knowledge on this class of indole derivatives, two analogues (**22** and *trans*-**14**) were chosen for further analysis. This choice was made based on their good selectivity index and the absence of solubility issues that could hamper the experiments. Table 4.2 shows the antiviral activity and cellular cytotoxicity of compounds **22** and *trans*-**14** against the prototype DENV2 NGC strain, evaluated in different cells. These molecules showed no cellular cytotoxicity in all evaluated cells lines (CC_{50} >100). Both analogues

inhibited viral replication in the low micromolar range; However, a slightly different antiviral profile was observed in the five susceptible cell lines. Specifically, **22** and *trans*-**14** were more potent in baby hamster kidney (BHK, EC_{50}: 0.08 to 0.15 µM), placenta choriocarcinoma (Jeg3, EC_{50}: 0.3 to 1.0 µM), lung epithelial adenocarcinoma (A549, EC_{50}: 0.03 to 0.04 µM) and hepatocarcinoma cells (Huh, EC_{50}: 0.1 to 0.4 µM), as compared in Vero (EC_{50}: 2.8 µM) cells.

Table 4.2: Antiviral activity and cellular toxicity profiles of **22** and *trans*-**14** against DENV2 NGC laboratory strain, evaluated in five different susceptible cell lines

	Vero		BHK		Huh		Jeg3		A549	
Compound	EC_{50}	CC_{50}	EC_{50}	CC_{50}	EC_{50}	CC_{50}	EC_{50}	CC_{50}	EC_{50}	CC_{50}
22	2.8 ± 2.8		0.15 ± 0.08		0.4 ± 0.1		1.0 ± 0.4		0.03 ± 0.02	
		>		>		>		>		>
Trans-**14**	2.8 ± 1.9	100	0.08 ± 0.04	100	0.1 ± 0.1	100	0.3 ± 0.1	100	0.04 ± 0.02	100

Data represent AVG ± SD values of at least three independent experiments.

Data indicating EC_{50}, CC_{50} and SI values for the compounds in Vero cells are reused from Table 4.1

To determine their broad-spectrum activity, compounds **22** and *trans*-**14** were tested against a number of different laboratory and clinical strains of DENV in Vero cells. As shown in Table 4.3, both molecules presented slightly stronger activity against the clinical isolates (EC_{50}: 0.6 to 1.9 µM), as compared to the laboratory strains (EC_{50}: 2.2 to 6.0 µM). Moreover, we also assessed their antiviral activity against three ZIKV strains (the laboratory strain MR766 and the clinical PRVAVC59 and FLR isolates) in several susceptible cells (Table 4.4). Surprisingly, neither molecule was found to be active against any of the tested viral strains in Vero cells (EC_{50}: >100 µM). Subsequently, **22** and *trans*-**14** compounds were evaluated in human-related cell lines (Huh, Jeg3 and A549) against all ZIKV strains. Remarkably, both compounds were active in the low micromolar range against the tested ZIKV strains in Jeg3 (EC_{50}: 0.2 to 1.2 µM) and A549 (EC_{50}: 0.1 to 0.6 µM), but not in Huh (EC_{50}: >100 µM) cells, strongly indicating a possible cell type-dependent antiviral profile.

Table 4.3: Antiviral activity of **22** and *trans*-**14** against several DENV laboratory and clinical strains in Vero cells

	Laboratory strains				Clinical strains			
	DENV1 Djibouti	DENV2 NGC	DENV3 H87	DENV4 Dak	DENV1	DENV2	DENV3	DENV4
Compound	EC_{50} (µM)							
22	2.2 ± 0.4	2.8 ± 2.8	3.2 ± 0.5	2.7 ± 1.1	0.6 ± 0.1	0.6 ± 0.4	0.8 ± 0.5	0.8 ± 0.6
Trans-**14**	6.0 ± 5.7	2.8 ± 1.9	3.2 ± 1.0	2.9 ± 1.3	1.1 ± 0.2	1.3 ± 0.3	0.8 ± 0.4	1.9 ± 1.7

Data represent AVG ± SD values of at least three independent experiments.

Data indicating EC_{50} values against the DENV2 NGC laboratory strain are reused from Table 4.1

Table 4.4: Antiviral activity of **22** and *trans*-**14** against several ZIKV laboratory and clinical strains evaluated in four different susceptible cell lines

	Vero			*Huh*			*Jeg3*			*A549*		
	MR	*PR*	*FLR*	*MR*	*PR*	*FLR*	*MR*	*PR*	*FLR*	*MR*	*PR*	*FLR*
Compound	EC_{50} (µM)											
22	>100			>100			0.2±0.1	0.2±0.1	0.9±0.6	0.1±0.1	0.2±0.1	0.1±0.1
Trans-**14**							0.2±0.1	0.7±0.3	1.2±1.0	0.2±0.1	0.6±0.4	0.2±0.1

Data represent AVG ± SD values of at least three independent experiments.

Data indicating EC_{50} values against the ZIKV MR766 strain in Vero cells are reused from Table 4.1

Based on our findings shown in Table 4.4, we also assessed the activity of compound **22** against the prototype ZIKV MR766 strain using immunofluorescence staining for the presence of viral envelope protein. Particularly, two cell lines were used (A549 and Vero), as striking differences in antiviral activity levels were observed. As shown in Figure 4.2, incubation of A549 cells with high concentrations (10 µM and 50 µM) of **22** (Figure 4.2E, 4.2F - left panel) led to full inhibition of viral infection, whereas lower concentrations (0.4 µM and 2 µM) of the compound (Figure 4.2C, 4.2D – left

panel) resulted in decreased levels of viral infection. On the contrary, treatment of Vero cells with the compound was not able to block virus replication, even at the highest tested concentration of 50 μM (Figure 4.2C-4.2F – right panel). In both experiments, negative (non-infected, dimethyl sulfoxide (DMSO)-treated cells without **22**, Figure 4.2A) and positive controls (virus-infected cells without **22**, Figure 4.2B) were included.
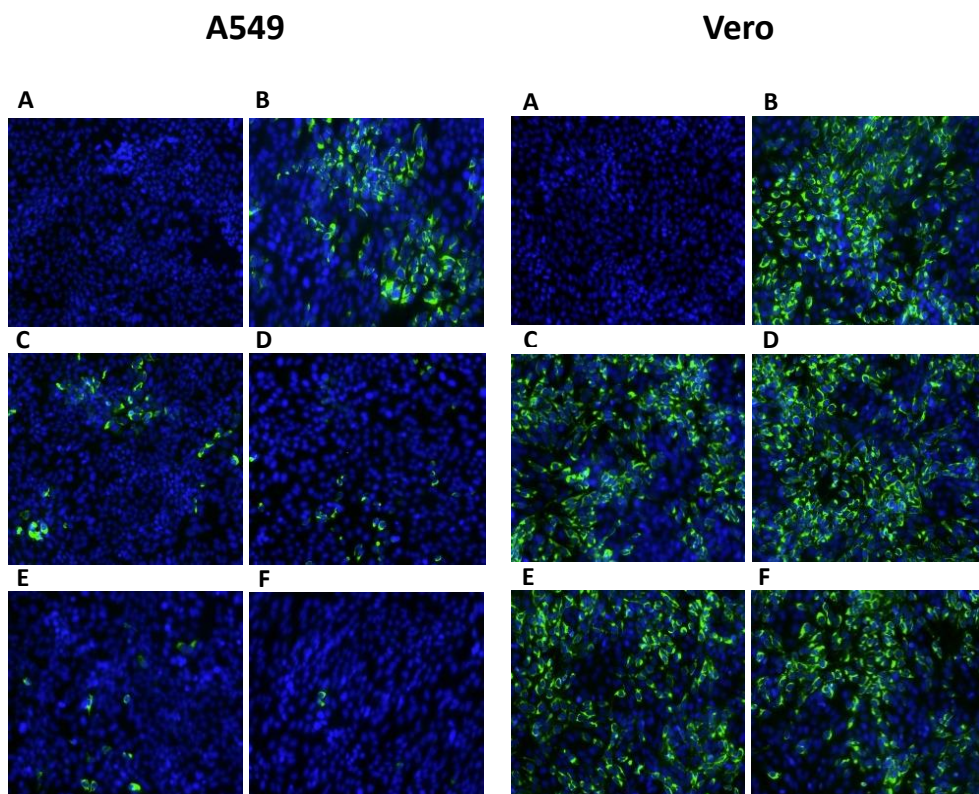
A549   **Vero**

Figure 4.2: **Detection of ZIKV envelope protein in the presence of 22 using immunofluorescence staining in A549 and Vero cells**. Both A549 and Vero cells were exposed to the ZIKV MR766 strain at an MOI of 0.2 and incubated with several concentrations of compound **22**. Fluorescence images were acquired 72h post infection. (A) Cell control, (B) Virus control, (C) 0.4 μM of **22**, (D) 2 μM of **22**, (E) 10 μM of **22**, (F) 50 μM of **22**

4.3.2 Compounds 22 and *trans*-14 interfere with DENV RNA replication/assembly

To gain more insight into the mechanism of action of compounds **22** and *trans*-**14**, time-of-drug addition and subgenomic replicon assays were performed. In the first set of assays, we treated Vero cells with **22** and *trans*- **14** at a concentration of 9 µM (approximately 3-fold EC_{50} values) at different time points pre- and post-infection (Figure 4.3A). T_{0h} corresponds to the time point where cells were exposed to the virus. As shown in Figure 4.3A, both analogues were able to inhibit virus replication at later stages (between 8h ($p^{****}<0.0001$) and 12h ($p^{**}= 0.005$)). At 12h post infection (pi), an increase of viral load was observed. To assess these findings, established inhibitors like dextran sulfate (DS, 8000 Da average molecular weight) and 7- Deaza-2'-C-Methyladenosine (7DMA) were included in the study. Specifically, DS (entry inhibitor) inhibited viral infection only during the early stages (-2h, 0h) ($p^{***}= 0.0002$). On the other hand, the nucleoside analogue 7DMA (replication inhibitor) presented a similar profile to our molecules, by suppressing viral replication even 12h pi ($p^{**}= 0.0012$). To consolidate these results, we proceeded with the subgenomic replicon assay. Specifically, serial dilutions of **22** and *trans*-**14** (100 µM, 20 µM, 4 µM, 0.8 µM) were added into BHK/DENV cells. As observed in Figure 4.3B, incubation of cells with both compounds led to a decrease in luciferase activity (blue), which corresponded to inhibition of viral replication and a possible interaction with the non-structural proteins (statistical analysis is provided in the Supplemental Material. Data for 7DMA were similar to these obtained with our molecules. In parallel, no cytotoxic effects were noticed at all tested concentrations (red).
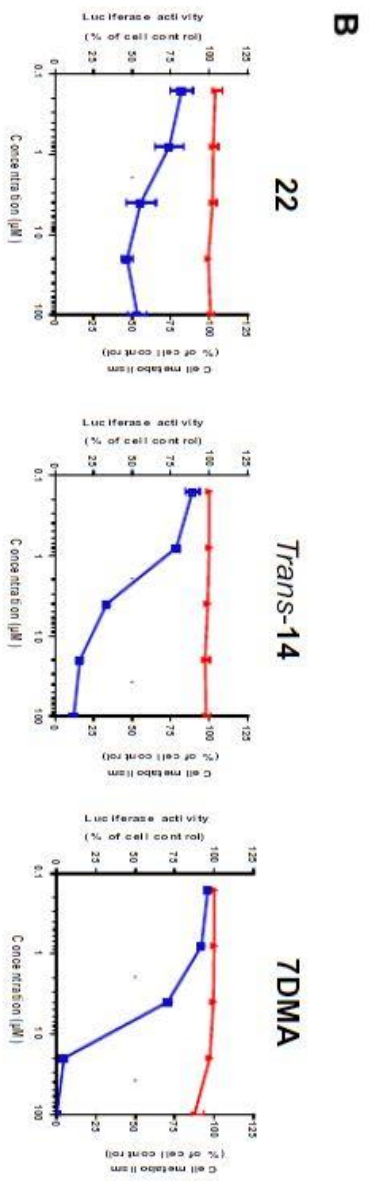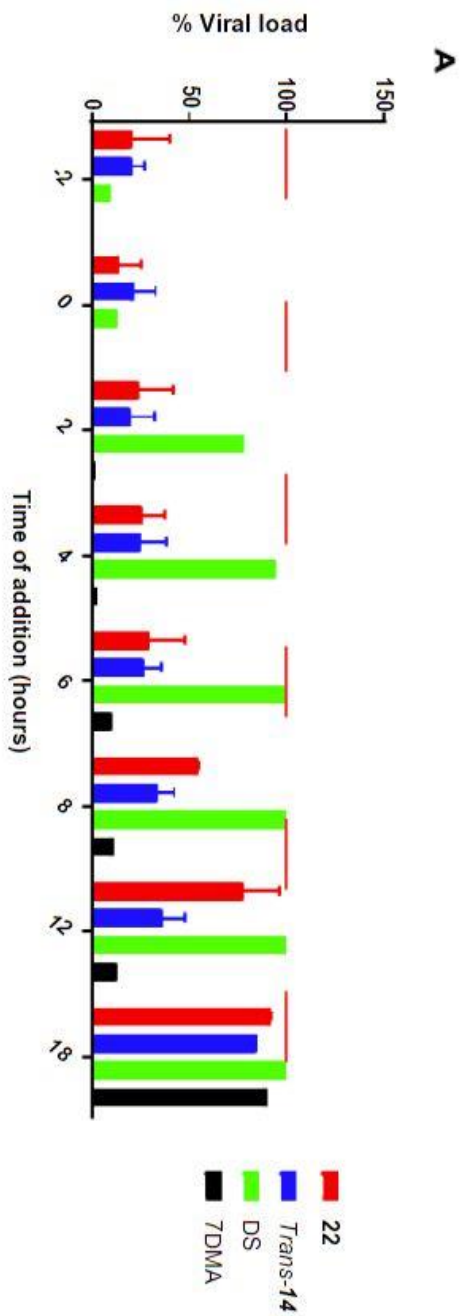
Figure 4.3: **Compounds interfere with the viral RNA replication/assembly.** (A) Treatment of Vero cells with 9 µM of **22** (red) and *trans*-**14** (blue) shows an inhibition of DENV infection even at later stages (8h-12h pi), as assessed by qRT-PCR of cell lysates 20h pi. Viral polymerase inhibitor 7-Deaza-2'-C-Methyladenosine (7DMA) (black) presents a similar profile, as it suppresses the infection at 12h pi. On the other hand, the entry inhibitor dextran sulfate (DS) (green) inhibits virus replication only at the early stages (-2h – 0h). Dashed red line represents virus control. (B) Compounds **22** and *trans*-**14** were incubated into BHK/DENV cells at different concentrations. A decrease in the luciferase activity was observed for both compounds, as well as the viral inhibitor 7DMA (blue), as assessed by luminescence. These results indicate an interaction with the non-structural proteins or the replication complex. Incubation of **22** and *trans*-**14** shows no cellular cytotoxicity at the tested concentrations (red). All data are the average of two independent experiments.

4.3.3 Compounds do not interact with intact viral particles

Next, we investigated whether these compounds are able to directly target viral particles. Specifically, two *in vitro* assays were performed, ultrafiltration and virus inactivation. In the first assay, DENV2 stock was incubated with **22** (50 µM, 10 µM, 2 µM) for 1h, followed by filtration to remove the unbound compound. In case the compound does not strongly interact with the viral particles, it appears in the flow through ($3.5*10^2$ PFU/ml, $p^{***} = 0.0002$). A plaque assay was used to further evaluate the presence of viable virus in the fraction retained on the filter. As shown in Figure 4.4A, inoculation of BHK cells treated with different concentrations of compound **22** resulted in the formation of viral plaques, thus implying no suppression of viral infection (2 µM **22**: $1.3*10^3$ PFU/ml, p = 0.57, 10 µM **22**: $5*10^2$ PFU/ml, p= 0.051, 50 µM **22**: $2.5*10^2$ PFU/ml, $p^* = 0.007$). On the other hand, incubation of BHK with epigallocatechin gallate (EGCG, 1 mg/ml, positive control) showed a complete inhibition of viral infection ($p^{****} < 0.0001$). Virus control was also included to evaluate the significance of our results ($5.5*10^2$ PFU/ml) (Supplemental Material). Moreover, we confirmed these findings by the virus inactivation assay where viral stock was incubated with 10 µM of **22**, followed by dilution of the sample to reach a non-active (suboptimal) concentration of the compound. As indicated in Figure 4.4B, compound **22** did not inhibit the viral infection process ($2.5*10^4$ PFU/ml, p = 0.56). Comparable results were also observed for virus control ($3.5*10^4$ PFU/ml), suggesting that **22** did not interact with the intact viral particles.
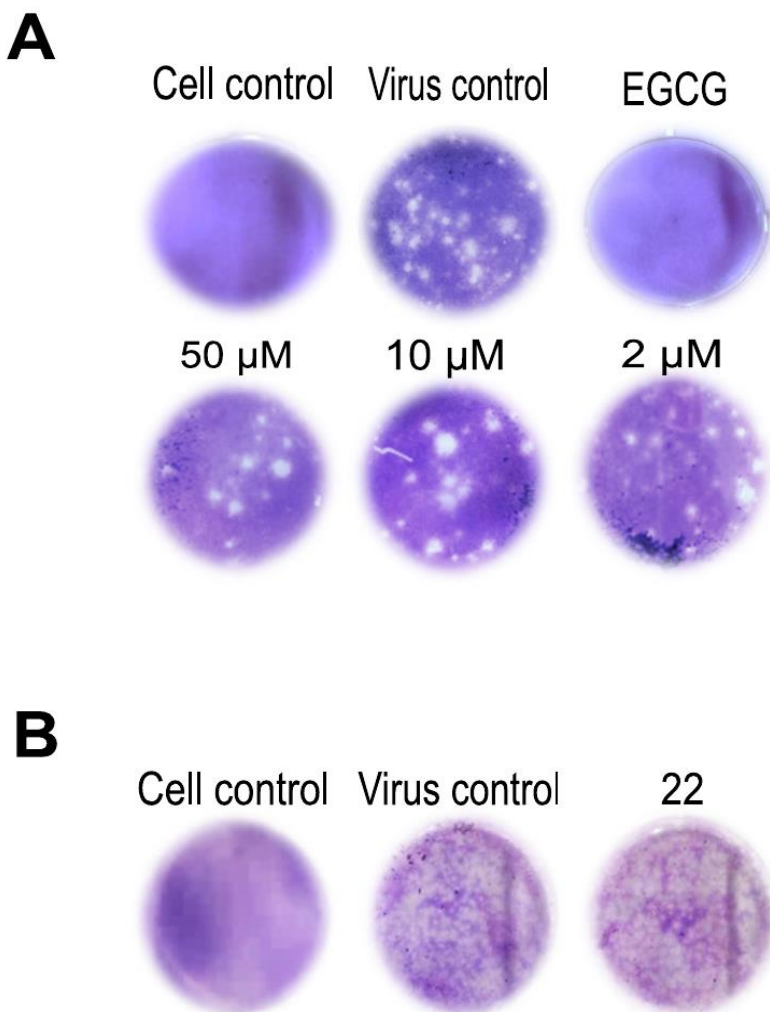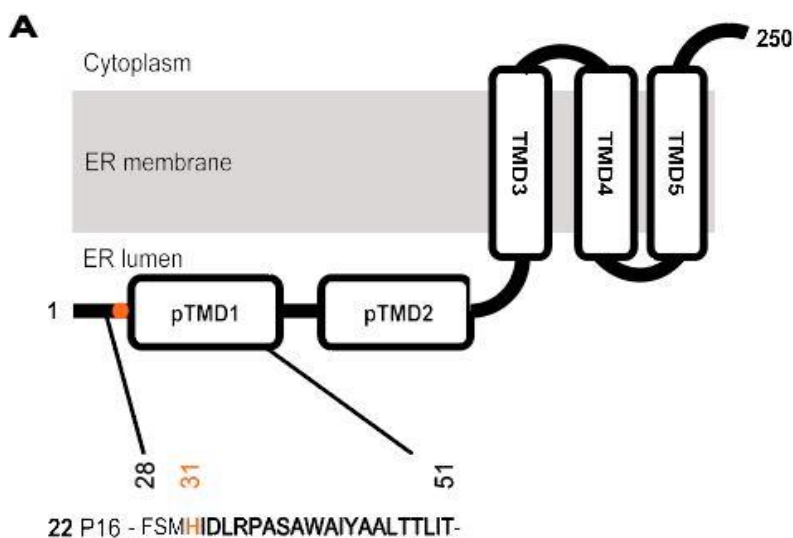
Figure 4.4: Compounds do not interact with the intact viral particles. (A) 50 µM, 10 µM and 2 µM of **22**, as well as the positive control epigallocatechin gallate (EGCG) (1 mg/ml) were mixed with DENV2 stock and passed through a filter. Incubation of **22**- treated samples on BHK cells resulted in no inhibition of viral infection in each tested condition (formation of viral plaques). Inoculation of cells with EGCG-treated sample demonstrated full inhibition of viral infection. (B) 10 µM of **22** were mixed with DENV2 viral stock and further diluted (100-fold) to infect BHK cells. No suppression of viral infection was noticed in the compound-treated sample, as assessed by the plaque assay. Both positive (virus-infected cells) and negative (non-infected, DMSO-treated cells) controls were included in the assays.

4.3.4 Sequence analysis of compounds-resistant viral mutants and cross-resistance assay

To identify the potential target protein, we proceeded with the selection of resistant viruses by sub-cultivating ZIKV MR766 strain in the presence of increasing concentrations of **22** and *trans*-**14** in A549 cells. Two passages (P1 and P16) were selected for a whole genome sequencing using the MinION technology (accession numbers are provided in the "Data availability" part). Comparative analysis across the ZIKV genomes at P16 revealed a single substitution at nucleotide position 6984 (from *G* to *C*), which corresponded to a non-synonymous amino acid change from aspartic acid (*D*) to histidine (*H*) for both **22** and *trans*- 14 viral mutants (Figure 4.5A). This mutation is located at amino acid position 31 of the NS4B protein. Based on the topology of DENV2 and Japanese encephalitis virus (JEV) NS4B (22), (23) that position is located at the beginning of one of its predicted transmembrane domains, the pTMD1.

To verify that these indole alkaloids target the same protein, we evaluated the antiviral activity of the selected compounds **20**, **22, 24,** *trans*-**14**, *cis*-**10** and *trans*-**10** against the wild type ZIKV MR766, *trans*-**14**- and **22**-resistant virus mutants (Figure 4.5B). Although all derivatives presented high inhibitory activity against the wild type ZIKV MR766 strain (EC$_{50}$: 0.1-4.2 µM), a complete loss of activity against the **22**-resistant mutant (EC$_{50}$ > 100 µM) was observed. However, assessment of activity against the *trans*-**14** resistant strain revealed differences among the molecules. Interestingly, we observed that only *cis*-**10** (EC$_{50}$: 1.4±0.5 µM) and *trans*- **10** (EC$_{50}$: 2.4±1.8 µM) analogues retained their inhibitory activity, with EC$_{50}$ values quite comparable to those observed for the wild type strain (Figure 4.5B, yellow). DS was used as a reference compound in this assay, since it suppresses viral infection with a completely different mode of action.

A

Cytoplasm

ER membrane

ER lumen

1

28 31

pTMD1 pTMD2

TMD3 TMD4 TMD5

250

51

22 P16 - FSMHIDLRPASAWAIYAALTTLIT-

Trans-14 P16 - FSM HIDLRPASAWAIYAALTTLIT-

Virus P16 - FSM DIDLRPASAWAIYAALTTLIT-

B

Compound	Wild type virus $EC_{50\,(\mu M)}$	22-Res virus $EC_{50\,(\mu M)}$ (fold-shift)	Trans-14-R virus $EC_{50\,(\mu M)}$ (fold-shift)
20	0.3 ± 0.2	>100 (>333)	>100 (>333)
22	0.1 ± 0.05	>100 (>1000)	>100 (>1000)
24	0.4 ± 0.1	>100 (>250)	>100 (>250)
Cis-10	0.3 ± 0.1	>100 (>333)	1.4 ± 0.5 (4.6)
Trans-10	4.2 ± 0.8	>100 (>24)	2.4 ± 1.8 (0.6)
Trans-14	0.2 ± 0.1	>100 (>500)	>100 (>500)
DS	0.1 ± 0.03	0.13 ± 0.02 (1.3)	0.13 ± 0.01 (1.3)

Figure 4.5: **Sequence analysis of the viruses used in the cross-resistance assay.** (A) NS4B membrane topology and alignment of amino acid sequences at the N-terminal site of the protein in **22**- and *trans*- **14** resistant virus mutants as compared to virus control. An aspartic acid to histidine (*D31H*) non-synonymous mutation is located at pTMD1 domain and marked in orange. Passage 16 (P16) of each virus strain was used in the assay. (B) Antiviral activity of several derivatives against the viruses used above (wild- type ZIKV MR766 strain, **22**- and *trans*-**14** resistant virus mutants) was evaluated by qRT- PCR in the supernatant of A549 cells at 72h pi. Fold shifts in EC_{50} values are also indicated into parentheses, while major findings on the activity of some analogues against the *trans*-**14** resistant mutant and wild-type virus were noted in yellow.

4.3.5 Compounds 22 and *trans*-14 constitute specific inhibitors of DENV and ZIKV

In order to address the specificity of our molecules, we evaluated the antiviral activity of compounds **22** and *trans*-**14** against viruses of different families. Particularly, HIV-1 (NL4.3), HIV-2 (ROD), influenza A (H1N1 and H3N2), influenza B as well as human coronavirus (229E) were tested. Interestingly, the tested derivatives were devoid of any antiviral activity against these viruses (data not shown), indicating that our molecules are highly selective against DENV and ZIKV.

4.4 Discussion

Despite our growing interest to curb the public health threat from both DENV and ZIKV, there are no approved antiviral drugs available at the moment (24). In the present study, we screened a number of molecules from a library of chemically diverse compounds for their activity against both DENV and ZIKV. A novel class of indole alkaloids was found to be active in the low micromolar range against the prototype DENV2 NGC strain in several virus-susceptible cell lines. Interestingly, striking differences in antiviral activity against the prototype ZIKV MR766 strain were observed among the tested cell lines, suggesting a possible cell-dependent inhibition profile.

To map the essential modifications required in the structure of this class for the antiviral activity against DENV and ZIKV, SAR studies were performed. Particularly, we demonstrate the importance of the substituent and its size at

the C-6 position for both activity and cytotoxicity of the molecules. In addition, the presence of an oxazolidine ring seems to be crucial for the potency of the compounds. Finally, stereochemistry at the C-7 and C-8 positions has an impact on the inhibitory activity and cellular cytotoxicity of the analogues (Figure 4.1 and Table 4.1).

To gain more insight into the antiviral activity and mechanism of action of these indole alkaloid derivatives, the analogues **22** and *trans*-**14** were selected for further analysis, based on their selectivity index and absence of solubility issues even at the highest concentrations. As previously mentioned, these molecules presented broad-spectrum activity against all DENV serotypes, with slightly higher potency against the clinical isolates (EC_{50}: 0.6- 1.9 μM), as compared to the laboratory strains (EC_{50}: 2.2-6.0 μM). Interestingly, a cell-dependent antiviral profile was noticed against ZIKV strains, since **22** and *trans*-**14** were able to inhibit infection in human A549 (EC_{50}: 0.1-0.6 μM) and Jeg3 (EC_{50}: 0.2-1.2 μM) but not in human Huh and monkey Vero cells (EC_{50}> 100 μM). We speculate that even though ZIKV and DENV belong to the same virus family and share high sequence similarity, they present differences in the pathways they follow to infect human- and non-human derived cells (25). Our findings further highlight the importance of cell line selection in the development and evaluation of new antiviral compounds, strengthening the idea that antiviral screening assays should not be restricted to a single type of susceptible cells (26).

Additionally, time-of-drug addition and subgenomic replicon assays revealed that our compounds act during viral RNA replication/assembly. Despite the fact that **22** and *trans*-**14** belong to the same family of molecules, sharing some common features, such as the oxazolopiperidone moiety, minor differences were noticed in their antiviral profile. This divergence can be explained either by the fact that these analogues target a different protein or a different site on the same viral protein. To address this question, compound-resistance selection experiments were performed in A549 cells. The choice of this cell line was based on the following three criteria: (a) high ZIKV replication kinetics, (b) clear visible cytopathogenic effect and (c) no cytotoxicity or solubility issues at higher tested concentrations of the molecules (27). Whole genome sequencing and comparative analysis between compounds-resistant virus mutants and the wild type virus indicated a single non-synonymous amino acid change at position 31 of NS4B in both **22**- and *trans*-**14** resistant viral strains. This substitution led to replacement

of the negatively charged aspartic acid with the partially protonated histidine. Notably, we further demonstrated that our compounds do not interact with the intact viral particles (Figure 4.4), thus possibly suggesting the involvement of cellular factor(s), associated with the NS4B protein. NS4B is an integral endoplasmic reticulum membrane protein, which consists of five domains (pTMD1, pTMD2, TMD3, TMD4 and TMD5) (Figure 4.5A) (28). This non-structural protein plays a vital role in viral RNA replication by interacting with the endoplasmic reticulum membrane protein complex (EMC), in which a large number of host proteins reside (29) (23). Our single point mutation (*D31H*) is located right at the beginning of pTMD1 domain (ER lumen), which has also been implicated in IFN-antagonism host responses (30). The fact that compounds **22** and *trans*-**14** do not exhibit anti-ZIKV activity in Vero cells, an IFN-I defective cell line (31), could suggest a possible interference of our molecules within the interferon pathway. However, a similar antiviral profile was observed in IFN-competent Huh cells (32), indicating that compounds **22** and *trans*-**14** are associated with a different function of NS4B. Given that the topology of NS4B of the closely related dengue virus, as well as the discrimination of its different domains (pTMDs and TMDs) have been described by Miller *et al*, we can use this proposed model to specify the topology of the single mutation in the compound-resistant strains (Figure 4.5A) (28). Several reports have shown that position 31 of NS4B protein is not only characterized by a high degree of conservancy among ZIKV strains (33), but also between different flaviviruses, such as DENV and yellow fever virus (23), proposing it as a potential vulnerable point for these members.

In addition, a phenotypic resistance assessment was performed in order to examine whether several derivatives of this family are cross-resistant to the viral mutants that we developed (Figure 4.5B)**.** Surprisingly, we indicated that only two analogues, *cis*-**10** and *trans*- **10**, have shown to be active against the *trans*-**14** resistant mutant, whereas no activity was noticed against **22**- resistant mutant for all the tested molecules. These findings were quite interesting, since no qualitative differences on the amino acid level were observed between the **22**- and *trans*-**14**-resistant mutants. In order to obtain more information, we implemented variant calling by using wild type ZIKV MR766 (passage 16) as a reference. Notably, the frequency of variants at nucleotide position 6984 slightly differed between the two resistant mutants, thus highly reflecting differences on their population/sample (Supplemental

Material). Based on these elements, we hypothesize that the varying rate of occurrence of these mutations could possibly explain the deviations on the inhibitory activity of some analogues against these two mutants. However, this speculation needs further investigation. Undoubtedly, the fact that *cis*-**10** and *trans*-**10** maintain their inhibitory activity against the *trans*-**14** resistant mutant can qualify them as more promising analogues for future studies

The molecules presented in this study constitute intermediates in the enantioselective synthesis of silicine alkaloids, having a distinct stereochemistry. The large family of indole alkaloids has been found to possess extremely broad pharmacological activities and thus can be used for treatment of viral infections. Numerous studies have reported the antiviral activity of several indole alkaloid derivatives against a number of viruses, such as HIV (34), influenza (35) and DENV (36).

To summarize, we have developed and determined the antiviral activity profile of a new series of indole alkaloid derivatives against DENV and ZIKV. These molecules presented promising antiviral activity against all DENV serotypes in a number of susceptible host cell lines. On the other hand, a cell-dependent inhibitory activity was observed against ZIKV strains, while no activity was noticed against a number of other viruses, including HIV, influenza and coronavirus, thus considering them as specific inhibitors against these two flaviviruses. Mode of action studies and whole genome sequencing analysis suggested a possible involvement of host factor(s), associated with the pTMD1 domain of ZIKV NS4B, a protein with a crucial role in the viral replication complex. To address this, further studies are ongoing in order to elucidate the exact molecular mechanism of these compounds. To the best of our knowledge, we describe for the first time a novel class of indole alkaloid derivatives targeting indirectly the multifunctional ZIKV NS4B protein and more specifically the pTMD1 domain, thus opening new horizons in virus-host interactions' network. In-depth analysis and identification of cellular factors able to interact with these viral proteins might be of utmost importance to unravel new mechanisms that flaviviruses use during their replication cycle. Finally, evaluation of antiviral activity of these compounds needs to be performed against other members of flaviviruses to potentially promote them as pan-flavivirus inhibitors.

4.5 Materials and methods

4.5.1 Cells and viruses

Different cell lines were used to evaluate the antiviral activity and cellular cytotoxicity of the tested molecules. Hepatocarcinoma (Huh, ATCC) and baby hamster kidney cells (BHK, kindly provided by Prof. M. Diamond, Washington University, USA) were grown in Dulbecco's Modified Eagle Medium (1X DMEM, Gibco) supplemented with 10% fetal bovine serum (FBS, HyClone, US), 1 mM sodium pyruvate (Gibco), 0.01 M HEPES (Gibco) and 1X non-essential amino acids. Placenta choriocarcinoma cells (Jeg-3, ATCC) were grown in 10% FBS, 1 mM sodium pyruvate and 1X non-essential amino acids. Finally, lung epithelial adenocarcinoma cells (A549, ATCC) and African green monkey kidney cells (Vero, ATCC) were grown in Minimum Essential Medium Eagle (1X MEM-Rega3, Gibco, Belgium) supplemented with 8% FBS, 1 mM sodium bicarbonate (Gibco), 2 mM L-glutamine (Gibco) and 1X non-essential amino acids (100X, Gibco). Vero cells were used for the initial screening and lead identification of our "hits". All cell lines were maintained at 37°C in a humidified 5% CO_2 incubator.

In addition, a number of laboratory and clinical strains of both DENV and ZIKV were used in this study. Details about the strains, propagation and titration of viral stocks were previously described (37).

4.5.2 Evaluation of antiviral activity and cellular viability

MTS method (3-(4,5-dimethylthiazol-2-yl)-5-(3-carboxymethoxyphenyl)-2-(4- sulfophenyl)-2*H*-tetrazolium, Promega, Leiden, The Netherlands) was used to assess cell viability in the presence of our molecules. Each cell line was seeded at 10^4 cells/well in a 96-well plate (Corning, USA). After 24h, cells were incubated with serial dilutions (5-fold) of each compound (100 μM – 20 μM – 4 μM – 0.8 μM) for 72h. Medium was replaced by 0.2% MTS, diluted in PBS and incubated for additional 3 h at 37°C. The CC_{50} values (compound's concentration, able to reduce cell's viability by 50%) were determined by measuring the optical density at 490 nm (SpectraMax Plus 384, Molecular Devices).

Regarding the antiviral assay, all cell lines were seeded at the same density as previously described. Briefly, 5-fold serial dilutions of compounds were added in the presence of each viral strain at a multiplicity of infection (MOI) of 1 for

DENV and of 0.2 for ZIKV. Cells were washed 2h pi and further incubated with fresh medium, containing the appropriate concentration of compounds. Supernatant was collected at 72h pi and the virus yield was determined by the Cells Direct One-step qRT-PCR kit (Thermo Fisher), according to the manufacturer's instructions. Primers, probes, as well as qRT-PCR conditions and analysis of the results are reported in our former manuscript (37). All compounds were dissolved in dimethyl sulfoxide (DMSO). The final concentration of DMSO in all tested conditions was 0.01%.

4.5.3 Immunofluorescence assay

Vero and A549 cells (10^4 cells/well) were seeded in black 96-well plates (Falcon, Germany). The next day, cells were infected with the prototype ZIKV strain (MR766) at an MOI of 0.2 in the presence of serial dilutions of **22** (50 µM-10 µM-2 µM-0.4 µM) at 37°C for 2h. Cells were washed with PBS and incubated with cell culture infection medium for 72h. Later, they were fixed with 2% aqueous paraformaldehyde (PFA, Sigma Aldrich, USA) at room temperature and permeabilized with 0.1% TritonX-100 (Sigma-Aldrich, USA). 1% Bovine Serum Albumin (BSA, Cell Signaling Technology, The Netherlands) diluted in PBS was used to block the fixed cells for 1h. Cells were further incubated with the primary 4G2 pan-flavivirus antibody (Merck Millipore, Belgium) overnight at 4°C. Goat anti-mouse IgG Alexa Fluor 488 (Invitrogen) was used as a secondary antibody while the nucleus was stained with DAPI (Invitrogen). Fluorescence microscopy was performed on a Zeiss Axiovert 200M inverted microscope (Germany) using 10X EGFP objective.

4.5.4 Time-of-drug addition assay

To define at which stage of viral replication our compounds are active, Vero cells (10^4 cells/well) were infected with DENV2 NGC strain at an MOI of 1 for 2h. Then, cells were washed twice with PBS and treated with an active concentration of each molecule (3-fold higher than the corresponding EC_{50} values) at different time points pre- and post-infection (-2, 0, 2, 4, 6, 8, 12 and 18h). Cell lysates were collected 20h pi and the viral RNA levels were measured by qRT- PCR. Two reference compounds were used in this assay at 10 µM. Dextran sulfate 8000 Da (DS), an established entry/fusion inhibitor and 7- Deaza-2'-C-Methyladenosine (7DMA), a viral polymerase inhibitor**.**

4.5.5 Subgenomic replicon assay

To assess any interaction with the non-structural proteins (NS) or the replication complex, a subgenomic replicon assay was performed. Briefly, BHK cells stably transfected with DENV2 replicon (encodes the *Firefly* luciferase expression cassette instead of prM and E proteins, as well as NS proteins) were seeded in DMEM 2% FBS supplemented with 3 µg/ml puromycin (Sigma-Aldrich, USA) in a white-bottom 96-well plate (Nunclon™ Delta Surface, Thermo Fisher Scientific). Serial dilutions of **22** and *trans*-**14** were added to the cells (100 µM - 20 µM – 4 µM – 0.8 µM - 0.16 µM) for 72h. Cells were further washed twice, the Renilla-Glo™ Luciferase Assay Reagent (Thermo Fisher Scientific) was added to each well and the luminescence was measured at 490 nm (Tecan Spark 10M Multimode Microplate Reader, BioExpress). 7DMA was also included as control, while cytotoxicity of the molecules was determined in parallel, using the MTS method.

4.5.6 Ultrafiltration and virus inactivation assay

To evaluate whether **22** can directly interact with DENV2 NGC strain, ultrafiltration and virus inactivation assays were performed. In the first assay, viral stock (10^4 PFUs) was incubated with compound **22** at different concentrations (50 µM, 10 µM and 2 µM) for 1h and subsequently passed through a 10 kDa cut-off concentrator filter unit (Vivaspin^R 500, Vivaproducts) to allow non-binding compound to permeate. The fraction, still present on the filter, was added to BHK cells for a plaque assay to evaluate its infectivity/inhibition. Epigallocatechin gallate (EGCG, 1 mg/ml) was used as a positive control to evaluate the assay's specificity.

In the virus inactivation assay, viral stock was incubated with 10 µM **22** for 1h. Sample was diluted 100-fold to obtain a concentration of the compound inferior to the EC_{50} values and used to infect Vero cells. Virus infectivity/inhibition was assessed by plaque reduction assay. Finally, positive (viral stock without the selection pressure of any compound) and negative controls (DMSO-treated cells) were also included.

4.5.7 *In vitro* selection of compound-resistant ZIKV mutants

Compounds-resistant viral strains were obtained through subsequent passaging of the prototype ZIKV MR766 strain in the presence of increasing concentrations of **22** or *trans*-**14**. For the selection procedure, A549

(10^5 cells/24-well) were used. More specifically, we started by incubating A549 cells with ZIKV MR766 strain in the presence of **22** or *trans*-**14** at 0.1 μM and 0.2 μM, respectively. Three days post infection, CPE was observed and the supernatant/condition (200 μl) was used to infect fresh susceptible cells, by maintaining the same concentration of the compounds. When CPE was noticed for the second time, we increased the concentration of each molecule. In total, sixteen passages (P1-P16) were obtained for each compound (2 μM final concentration). In order to exclude any spontaneous mutations that can naturally occur, A549 cells were inoculated with ZIKV MR766 strain in the absence of our molecules (virus control). Approximately 500 μl of each passage/condition were kept at -80°C for sequencing analysis.

4.5.8 RNA purification and metagenomic library preparation

Two passages (P1 and P16) were sequenced using a metagenomic protocol. To prepare for sequencing, total RNA was extracted from 140 μl of the supernatant of six different samples (3 conditions per passage) using the QIAmp Viral RNA kit (QIAGEN). Carrier RNA was replaced by linear polyacrylamide and an intermediate on-column DNase treatment was performed using the RNase-Free DNase Set (QIAGEN) to remove any residual DNA fragments. Samples were eluted twice in RNase free water (QIAGEN) with 60 μl and 40 μl, respectively. RNA was further subjected to random reverse transcription and amplification using the Sequence Independent Single Primer Amplification (SISPA) approach, as detailed in (38).

4.5.9 MinION nanopore sequencing and data analysis

MinION sequencing libraries were generated from 200 ng of cDNA for each sample using the Ligation Sequencing Kit 1D (SQK-LSK109) and the Native Barcoding Expansion 1-12 kit (EXPNBD104) (Oxford Nanopore Technologies). Libraries were loaded onto a FLO-MIN106 flow cell and ran for 48 h with live basecalling enabled using the high-accuracy basecalling.

Raw reads were demultiplexed using qcat v1.1.0 (https://github.com/nanoporetech/qcat) and SISPA primers from both the 5' and 3' ends were trimmed using seqtk v1.3 (https://github.com/lh3/seqtk). Minimap2 v2.17 (https://github.com/lh3/minimap2) was utilized to map the reads against the prototype ZIKV MR766 strain (GenBank accession number: MK105975) and the resulting alignments were visually assessed with Tablet v1.19.09.03 (39). To calculate coverage depth and compute sequencing

statistics, Samtools v1.7 (40) and SeqKit v0.12.1 (41) were employed. Majority consensus was called at a minimum depth of 20x and 60% support fraction, with any base location not fulfilling the depth and support fraction assigned an N IUPAC ambiguity code. Finally, multiple sequence alignments were generated on both nucleotide and amino acid levels with Aliview (42).

4.5.10 Cross-resistance assay

To identify whether different analogues of this family (Table 4.1) share the same target protein, a cross-resistance assay was performed. Briefly, A549 (10^4 cells/well) were incubated with **22**, **20**, **24**, *trans-**14***, *cis-**10***, and *trans-**10*** at 5-fold serial dilutions (100 μM-0.8 μM) and subsequently exposed to the wild type ZIKV MR766, the **22**- or the *trans-**14*** resistant viral strains (passage 16). Supernatant was collected 72h pi and vRNA levels were measured by qRT-PCR analysis. DS was included as a reference compound in this assay.

4.5.11 Statistical analysis

One-way ANOVA, followed by correction post-test (Bonferroni) was used to evaluate significant differences for Figure panels 3A, 3B and 4A. Unpaired t- test was performed for Figure panel 4B. Significance was calculated based on p values (ns: $p > 0.05$, *: $p < 0.05$, **: $p < 0.005$, ***: $p < 0.0005$, ****: $p < 0.0001$

Data availability

Accession numbers for each viral strain used in this study are provided below (GenBank):

AF298808.1 (DENV serotype 1 *Djibouti D1/H/IMTSSA/98/606* strain) (43), M29095.1 (DENV serotype 2 *NGC* strain) (44), M93130.1 (DENV serotype 3 *H87* strain) (45), MF004387.1 (DENV serotype 4 *Dak* strain, unpublished), MK105975.1 (ZIKV *MR766* strain), MH916806.1 (ZIKV *PRVAVC59* strain) and KX087102.2 (ZIKV *FLR* strain).

ZIKV genomic sequences generated in this study are deposited in GenBank under the following accession numbers:

MW143017 (**22**-*resistant mutant passage 1*), MW143018 (*trans-**14**-resistant mutant passage 1*), MW143019 (*wild type virus passage 1*), MW143020

(**22**- *resistant mutant passage 16*), MW143021 (*trans*- **14**-*resistant mutant passage 16*), MW143022 (*wild type virus passage 16*).

## 4.6 Supplemental Material

4.6.1. Synthesis of compounds

Compounds subjected to antiviral activity assays were prepared in the context of our studies in the total synthesis of Corynantean-type indole alkaloids of the ervatamine-silicine group (46), (47), (48), which are characterized by a rearranged skeleton lacking the characteristic tryptamine moiety present in most monoterpenoid indole alkaloids. Ervatamine-silicine-type alkaloids (49), (50) share a tetracyclic structure with an indole and a piperidine fused to a seven-membered carbocyclic ring, but they differ in the relative stereochemistry of C-16 and C-20 stereocenters (there are also C-20 *E*-ethylidene derivatives), the oxidation level at C-6, and the presence or absence of a C-16 methoxycarbonyl group. However, because of their common biogenetic origin from secologanin, the configuration of the C-15 stereocenter is usually *S*.
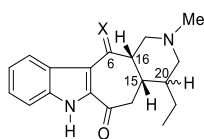
Silicine   X = H, H; 20-β-H
20-Episilicine X = H, H; 20-α-H
6-Oxosilicine X = O; 20-β-H
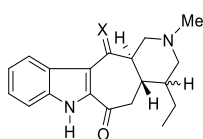
16-Episilicine   X = H, H; 20-β-H
16,20-Episilicine   X = H, H; 20-α-H
6-Oxo-16-Episilicine X = O; 20-β-H
6-Oxo-16,20-Episilicine X = O; 20-α-H
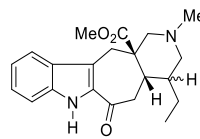
20-Epiervatamine X = H, H;
20-β-H
Ervatamine   X = H, H;
20-α-H

Representative alkaloids of the ervatamine-silicine group.

Chiral oxazolopiperidone lactams, easily available in a single step by cyclocondensation of δ-oxo-acid derivatives with (*R*)- or (*S*)- phenylglycinol, bear a strategically versatile functionalized piperidine ring embedded in a conformationally rigid bicyclic system allowing the stereoselective introduction of substituents in most positions of the aza-heterocycle. In previous work, we have established a versatile methodology for the preparation of a variety of enantiopure nitrogen heterocycles with a high degree of stereoselectivity and a predictable absolute configuration as a result of extensive studies on the scope and limitations of this procedure. The

potential of this approach has been demonstrated in our research group with the synthesis of a variety of natural products, among them indole alkaloids of the ervatamine-silicine group.

Scheme 1. Synthetic strategies.
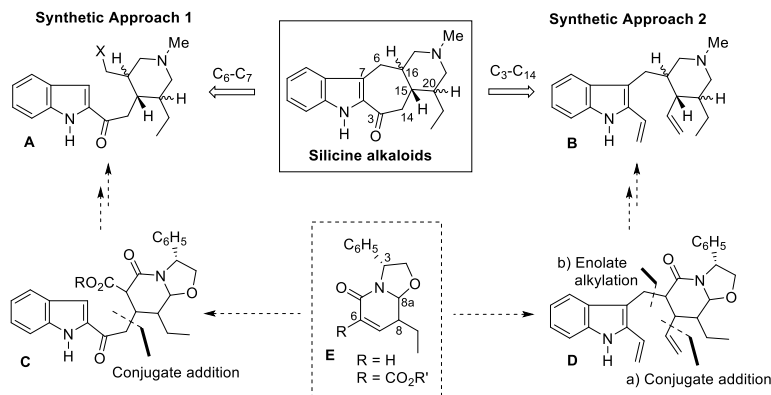
Two strategies were devised for the construction of the tetracyclic system of silicine alkaloids from a piperidine precursor bearing substituents at the C-3, C-4, and C-5 positions (Scheme 1, A and B). In both cases the seven-membered carbocyclic ring was constructed at the last stages of the synthesis, either by intramolecular alkylation (or acylation) of the indole 3-position (Synthetic Approach 1, C_6-C_7 bond formed) from type-A precursors or by ring-closing metathesis (Synthetic Approach 2, C_3-C_{14} bond formed) from intermediates B. As can be observed in Scheme 1, the three stereogenic centers of silicine alkaloids, at C-15, C-16, and C-20, were embedded in the piperidine moiety. Unsaturated ethyl-substituted (*R*)-phenylglycinol-derived lactams of type E enabled the stereoselective introduction of substituents at the 4-position of the piperidine ring by conjugate addition reactions, and at the 3-position in a good degree of stereoselectivity by enolate alkylation, giving access to a broad variety of enantiopure 3,4,5-trisubstituted piperidines. Therefore, synthetic intermediates of type C may be accessible by conjugate addition reactions of the enolate of 2-acylindole to unsaturated lactams E whereas intermediates of type D can be prepared from E by conjugate addition of a vinyl residue and a subsequent alkylation to introduce a 2-vinyl-3-indolylmethyl fragment.

The required unsaturated lactams 6-8, which differ in the configuration of the stereocenters at the C-8 and/or C-8a positions, were prepared from the

134

corresponding (*R*)-phenylglycinol-derived bicyclic lactams (1-3), as previously reported. Unsaturated lactams 5 and 9, prepared from 1 and 4, respectively, were also included in our studies to analyze the influence of the benzyloxycarbonyl and the ethyl substituents in the bioactivity of the resulting conjugate addition products (Scheme 2).
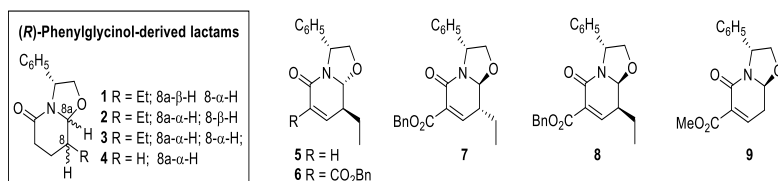
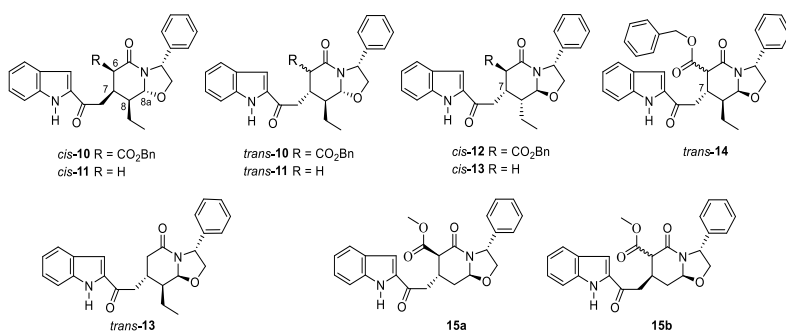**Scheme 2**. Unsaturated (*R*)-phenylglycinol bicyclic lactams

Conjugate addition reactions of 2-acetylindole enolates to unsaturated lactams was carried out using an excess of 2- acetylindole (5 equivalents) using LDA as a base in THF (Scheme 3).
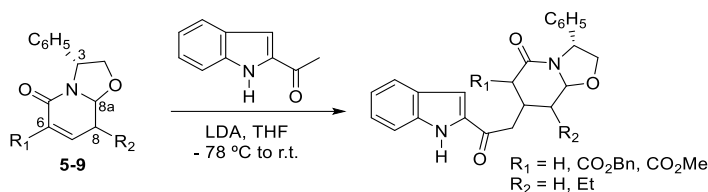
Scheme 3. Conjugate addition reactions of 2-acetylindole enolate to unsaturated lactams.

Following the above general procedure, compounds *cis*-10 and *trans*- 10 were isolated in 90% yield from unsaturated lactam 6 in a 77:23 ratio, respectively (Scheme 4). A similar result was observed when lactam 7 was subjected to the above conditions, affording *cis*- 12 and its C-7 epimer (*trans*-12) in a 77:23 ratio and 62% overall yield. Compound *trans*-14 was obtained from the H-8/H-8a *cis* unsaturated lactam 8, along with its C-7 isomer (*cis*-14), in 86% overall yield and a 84:16 ratio. Oxazolopiperidones *cis*-10, *trans*-10, *cis*-12, and *trans*-14 were selected to analyze the influence of the relative configuration of the stereocenters at the oxazolopiperidone C-6, C-7, C-8, and C-8a positions in the viral activity. Conjugate addition of 2-acetylindole enolate to the non-activated unsaturated lactam 5 resulted in a mixture of products *cis*-11 and *trans*-11 in good chemical yield (73%) but lower stereoselectivity (42:58), whereas lactam 9, lacking the ethyl substituent,

afforded a mixture of 15a and 15b (70:30) in 50% yield. Conjugate addition adducts *trans*-10, *trans*- 14, and 15b, with a H-7/H-8a *cis* relative configuration, were isolated as epimeric mixtures at the isomerizable stereocenter of the C-6 position. Finally, compounds *cis*-13 and *trans*-13 were obtained by isomerization of the C-8 and/or the C-8a stereocenters of *trans*- 11 under acidic conditions. Derivatives *cis*-11, *cis*-13, and *trans*-13, lacking the benzyloxycarbonyl substituent at C-6, were prepared to analyze the influence of this substituent in the bioactivity, whereas 15a and 15b can be considered deethyl analogues of *cis*-12 and *trans*-14 bearing a methoxycarbonyl instead of a benzyloxycarbonyl group.

cis-10 R = CO$_2$Bn
cis-11 R = H

trans-10 R = CO$_2$Bn
trans-11 R = H

cis-12 R = CO$_2$Bn
cis-13 R = H

trans-14

trans-13

15a

15b

Scheme 4. Synthetic adducts resulting from conjugate addition reactions.

The moderate stereoselectivity observed in the above conjugate addition reactions prompted us to explore an alternative approach for the synthesis of silicine alkaloids in which the closure of the seven-membered carbocyclic ring is performed by ring-closing metathesis from an appropriate diene (Scheme 1). The overall sequence for the synthesis of (-)-16-episilicine is outlined in Scheme 5. Conjugate addition of the non-stabilized nucleophile vinylmagnesium bromide to the unsaturated lactam 16 took place in very high facial selectivity, leading to compound 17 (mixture of C-6 epimers). Preparation of the required diene 19a was carried out by alkylation of the sodium enolate of 17 with indolylmethyl bromide 18, followed by Wittig methylenation and removal of the *tert*-butoxycarbonyl group under acidic conditions. Compound 19a was isolated in good overall yield (43%, three steps from 17) along with minor amounts of the C-6 epimer 19b. The crucial ring-closing metathesis of 19a was performed using the second-generation Grubbs catalyst under refluxing toluene to give the expected compound 20 in 87% yield. Catalytic hydrogenation of the double bond of 20 followed by treatment with LiAlH$_4$ - AlCl$_3$, which provoked the reduction of the lactam

carbonyl and the reductive opening of the oxazolidine ring, gave tetracycle 21. Conventional synthetic transformations from 21, including the removal of the benzenesulfonyl protecting group, debenzylation of the nitrogen in the presence of (Boc)$_2$O, chemoselective oxidation of the methylene next to the indole 2-position, and nitrogen methylation, furnished the alkaloid (-)-16-episilicine.
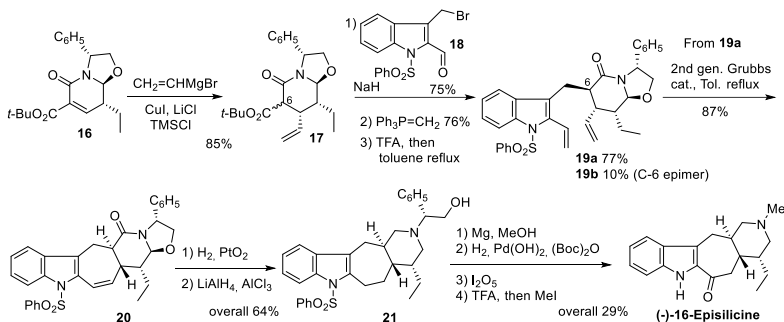
Scheme 5. Enantioselective total synthesis of (-)-16-episilicine.

Surprisingly, when compound 19b, the C-6 epimer of 19a, was subjected to the above ring-closing metathesis conditions, the main product observed was the Diels-Alder adduct 22 (50% yield), whereas the expected *cis*-fused pentacyclic compound 23 was formed in only 24% yield (Scheme 6). The different behavior of 19a and 19b under the thermal conditions used in the ring-closing metathesis reaction could have a conformational origin due to their opposite configuration at the 6-position of the rigid oxazolopiperidone system. Finally, removal of the benzenesulfonyl group of 19b with potassium fluoride afforded compound 24.
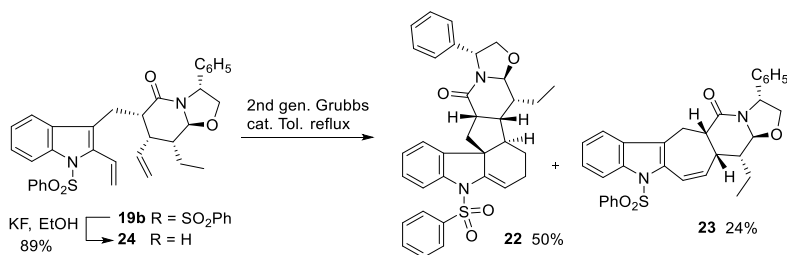
Scheme 6. RCM reaction from isomer 19b.

Compounds 20 and 21 shared the tetracyclic system present in (-)-16-episilicine. The pentacyclic derivative 20 constituted a conformationally

restricted analogue of 21 due to the lactam function and the presence of the oxazolidine ring. Product 22 displayed a unique complex structure and was also selected for biological assays.

4.6.2 Statistical analysis

One-way ANOVA, followed by Bonferroni correction test were performed to evaluate significant differences in Figure panels 3A, 3B and 4A. Unpaired t-test was performed in Figure panel 4B.

Significance was calculated based on p values:

Non-significant, $p > 0.05$; *, $p < 0.05$; **, $p < 0.005$; ***, $p < 0.0005$; ****, $p < 0.0001$

Particularly, for Fig 4.3A, we compared the percentage of detected viral load after the treatment of cells with the tested compounds (**22**, *Trans*-**14**, DS, 7DMA) with this observed for virus control (no treatment with compounds, red dashed line in the panel) at each time point, separately. As clearly shown, our molecules suppress viral replication 8h-12h post infection (as we proposed in the manuscript).

In addition, we provide the statistical differences on the replicon levels among the three compounds (luciferase values from different concentrations among the molecules), in order to compare their inhibitory activity profile (Fig 4.3B). As shown from the figure panel 3B, significant differences on the replicon levels were noticed, especially at highest concentrations (20 μM and 100 μM).
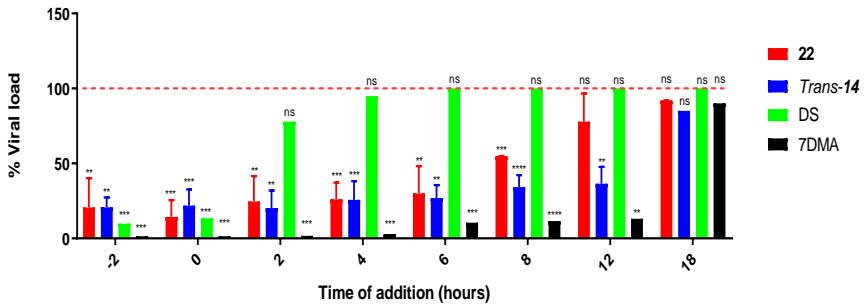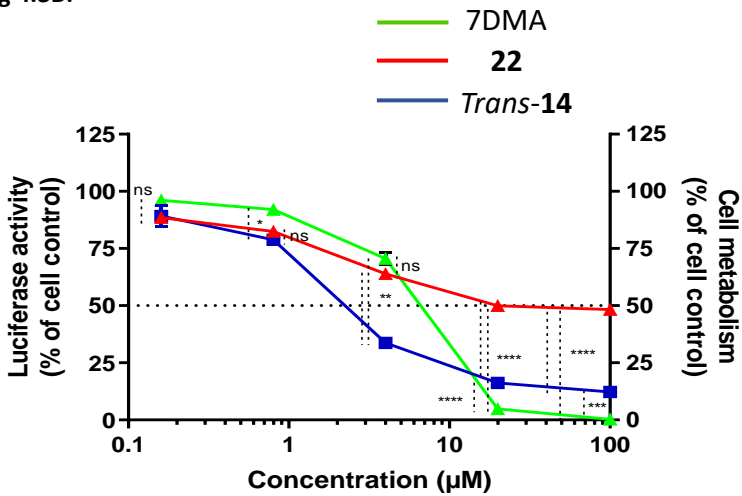
Fig 4.3A:

Fig 4.3B:

For Figure 4.4, one-way ANOVA (4.4A) and unpaired t-test (4.4B) were performed. In both panels, each condition was compared to the corresponding virus control for the statistical analysis.
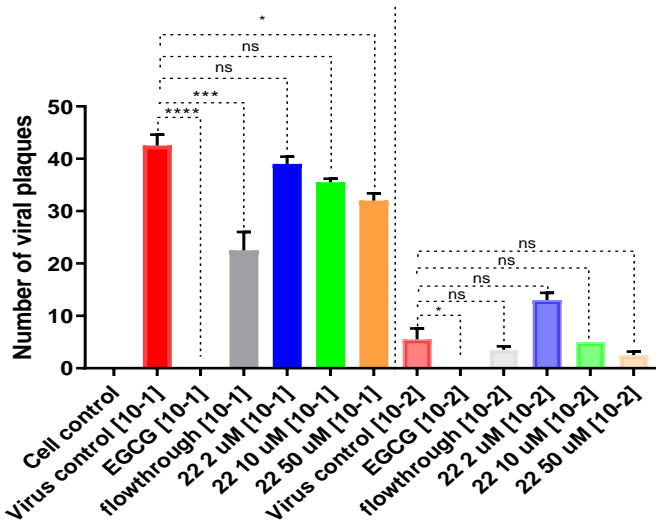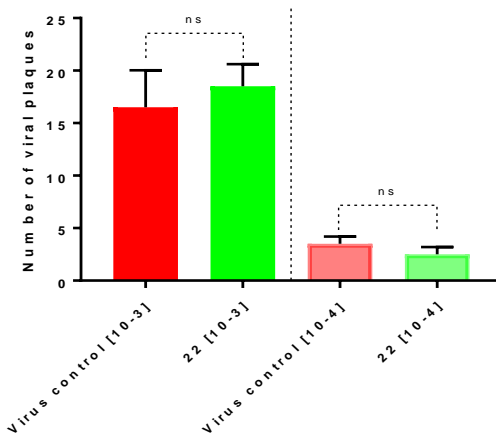
Fig4.4A:

Fig 4.4B:

4.6.3 Variant calling

In an attempt to extract more information on nucleotide differences between **22**-res and *trans*-**14**-res in passage 16, LoFreq* (51) was utilized against the indexed virus control consensus sequence, which was used as a reference.

Upon variant calling, only consensus level variants (frequency > 50%) were considered for our comparative mutation analysis (Figures A and B).
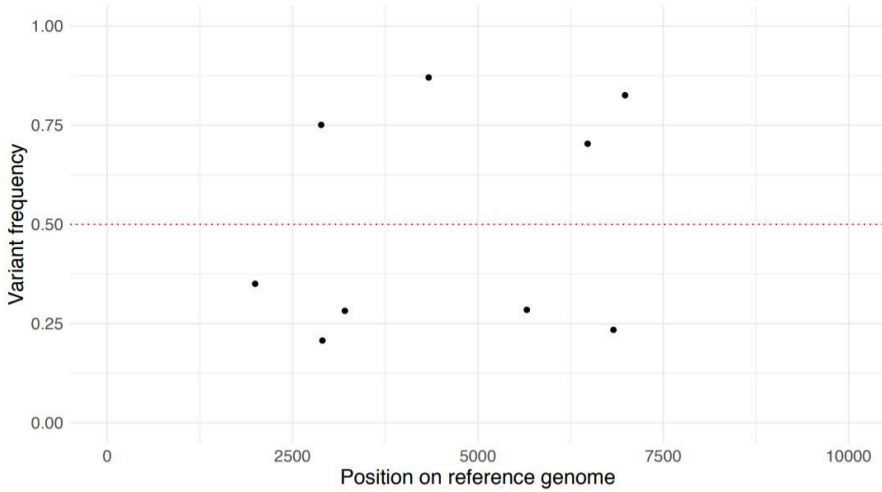

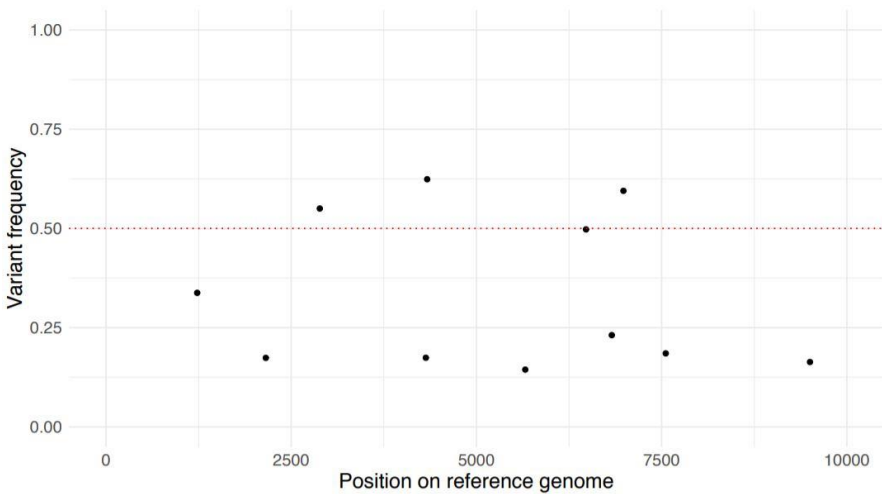**Figure A**: Variant frequencies of **22**-res compared to virus control (passage16)

Figure B: Variant frequencies of *trans*-**14**-res compared to virus control (passage 16)

In the figure, X-axis represents the position of the mutation across the virus control genome (passage 16), while Y-axis depicts the frequency at which each mutation is present in the sequencing data. A dashed red line indicates our threshold of 50% frequency.

We showed that there are no qualitative differences on the amino acid level between the two resistant mutants. After implementation of the variant calling workflow, we observe that the frequency of the variants (above 50%) at the indicated positions between both strains slightly differ. For example, at nucleotide position 6984, the mutation for **22**-resistant seems to be present in approximately 80% of the sequence reads, while the same mutation for *trans*-**14**-resistant is found in less than 60% of the reads. Differences on the frequencies at which each variant occurs, highly reflect differences on the population of the variants present within each sampled mutant strain.

4.7 References

1. Bollati M, Alvarez K, Assenberg R, Baronti C, Canard B, Cook S, et al. Structure and functionality in flavivirus NS-proteins: Perspectives for drug design. Antiviral Res. 2010;87:125–48.

2. Kazmi SS, Ali W, Bibi N, Nouroz F. A review on Zika virus ;outbreak, epidemiology, transmission and infection dynamics. J Biol Res. 2020;27:1–11.

3. Rezende HR, Romano CM, Claro IM, Caleiro GS, Sabino EC, Felix AC, et al. First report of Aedes albopictus infected by Dengue and Zika virus in a rural outbreak in Brazil. PLoS One. 2020;15:e0229847.

4. Ferdousi T, Cohnstaedt LW, McVey DS, Scoglio CM. Understanding the survival of Zika virus in a vector interconnected sexual contact network. Sci Rep. 2019;9:1–15.

5. Blohm GM, Lednicky JA, Márquez M, White SK, Loeb JC, Pacheco CA, et al. Evidence for Mother-to-Child Transmission of Zika Virus Through Breast Milk. Clin Infect Dis. 2018;66:1120–1.

6. Begum F, Das S, Mukherjee D, Mal S, Ray U. Insight into the tropism of dengue virus in humans. Viruses. 2019;11:1136.

7. Pang X, Zhang R, Cheng G. Progress towards understanding the pathogenesis of dengue hemorrhagic fever. Virol Sin. 2017;32:16–22.

8. Hottz ED, Oliveira MF, Nunes PCG, Nogueira RMR, Valls-de-Souza R, Da Poian AT, et al. Dengue induces platelet activation, mitochondrial dysfunction and cell death through mechanisms that involve DC-SIGN and caspases. J Thromb Haemost. 2013;11:951-62.

9. Borchering RK, Huang AT, Mier-y-Teran-Romero L, Rojas DP, Rodriguez-Barraquer I, Katzelnick LC, et al. Impacts of Zika emergence in Latin America on endemic dengue transmission. Nat Commun. 2019;10:5730.

10. Baud D, Gubler DJ, Schaub B, Lanteri MC, Musso D. An update on Zika virus infection. Lancet. 2017;390:2099–109.

11. Rather IA, Lone JB, Bajpai VK, Park YH. Zika virus infection during

pregnancy and congenital abnormalities. Front Microbiol. 2017;8:1–7.

12. Leung C. A lesson learnt from the emergence of Zika virus: What flaviviruses can trigger Guillain-Barré syndrome? J Med Virol. 2020; doi: 10.1002/jmv.25717.

13. Thomas SJ, Yoon IK. A review of Dengvaxia®: development to deployment. Hum Vaccines Immunother. 2019;15:2295–314.

14. Halstead SB. Dengvaxia sensitizes seronegatives to vaccine enhanced disease regardless of age. Vaccine. 2017;35:6355–8.

15. Ngono AE, Shresta S. Cross-reactive T Cell immunity to dengue and zika viruses: New insights into vaccine development. Front Immunol. 2019;10:1–9.

16. Sacramento CQ, De Melo GR, De Freitas CS, Rocha N, Hoelz LVB, Miranda M, et al. The clinically approved antiviral drug sofosbuvir inhibits Zika virus replication. Sci Rep. 2017;7:40920.

17. Whitby K, Pierson TC, Geiss B, Lane K, Engle M, Zhou Y, et al. Castanospermine, a Potent Inhibitor of Dengue Virus Infection In Vitro and In Vivo. J Virol. 2005;79:8698–706.

18. Plummer E, Buck MD, Sanchez M, Greenbaum JA, Turner J, Grewal R, et al. Dengue Virus Evolution under a Host-Targeted Antiviral. J Virol. 2015;9:5592–601.

19. Low JGH, Ooi EE, Vasudevan SG. Current status of dengue therapeutics research and development. J Infect Dis. 2017;215:S96–102.

20. Choy MM, Zhang SL, Costa V V., Tan HC, Horrevorts S, Ooi EE. Proteasome Inhibition Suppresses Dengue Virus Egress in Antibody Dependent Infection. PLoS Negl Trop Dis. 2015;9:e0004058.

21. Castillo Ramirez JA, Urcuqui-Inchima S. Dengue Virus Control of Type i IFN Responses: A History of Manipulation and Control. J Interf Cytokine Res. 2015;35:421–30.

22. Zou J, Xie X, Lee LT, Chandrasekaran R, Reynaud A, Yap L, et al. Dimerization of Flavivirus NS4B Protein. J Virol. 2014;88:3379–91.

23. Zmurko J, Neyts J, Dallmeier K. Flaviviral NS4b, chameleon and jack-in-the-box roles in viral replication and pathogenesis, and a molecular target for antiviral intervention. Rev Med Virol. 2015;25:205–23.

24. Barrows NJ, Campos RK, Liao K, Reddisiva K, Soto-acosta R, Yeh SC, et al. Biochemistry and molecular biology of flaviviruses. Chem Rev. 2018;118:4448–4482.

25. Brault JB, Khou C, Basset J, Coquand L, Fraisier V, Frenkiel MP, et al. Comparative analysis between flaviviruses reveals specific neural stem cell tropism for Zika virus in the mouse developing neocortex. EBioMedicine. 2016;10:71–6.

26. Franco EJ, Rodriquez JL, Pomeroy JJ, Hanrahan KC, Brown AN. The effectiveness of antiviral agents with broad-spectrum activity against chikungunya virus varies between host cell lines. Antivir Chem Chemother. 2018;doi: 10.1177/2040206618807580.

27. Himmelsbach K, Hildt E. Identification of various cell culture models for the study of Zika virus. World J Virol. 2018;7:10–20.

28. Miller S, Sparacio S, Bartenschlager R. Subcellular localization and membrane topology of the dengue virus type 2 non-structural protein 4B. J Biol Chem. 2006;281:8854-63

29. Mohd Ropidi MI, Khazali AS, Nor Rashid N, Yusof R. Endoplasmic reticulum: A focal point of Zika virus infection. J Biomed Sci. 2020;27:27.

30. Xie X, Zou J, Wang QY, Shi PY. Targeting dengue virus NS4B protein for drug discovery. Antiviral Res. 2015;118:39-45

31. Van Cleef KWR, Overheul GJ, Thomassen MC, Kaptein SJF, Davidson AD, Jacobs M, et al. Identification of a new dengue virus inhibitor that targets the viral NS4B protein and restricts genomic RNA replication. Antiviral Res. 2013;99:165–71.

32. Zhang T, Lin RT, Li Y, Douglas SD, Maxcey C, Ho C, et al. Hepatitis C virus inhibits intracellullar interferon alpha expression in human hepatic cell lines. Hepatology. 2005;42:819-27

33. Sironi M, Forni D, Clerici M, Cagliani R. Nonstructural proteins are

preferential positive selection targets in Zika virus and related flaviviruses. PLoS Negl Trop Dis. 2016;10:e0004978.

34. Jassim SAA, Naji MA. Novel antiviral agents: A medicinal plant perspective. J Appl Microbiol. 2003;95:412–27.

35. Moradi MT, Karimi A, Lorigooini Z. Alkaloids as the natural anti-influenza virus agents: a systematic review. Toxin Rev. 2018;37:11–8.

36. Hishiki T, Kato F, Tajima S, Toume K, Umezaki M, Takasaki T, et al. Hirsutine, an indole alkaloid of uncaria rhynchophylla, inhibits late step in dengue virus lifecycle. Front Microbiol. 2017;8:1674.

37. Fikatas A, Vervaeke P, Martínez-Guald B, Martí-Marí O, Noppen S, Meyen E, et al. Tryptophan trimers and tetramers inhibit dengue and Zika virus replication by interfering with viral attachment processes. Antimicrob Agents Chemother. 2020;64:e02130-19.

38. Kafetzopoulou LE, Efthymiadis K, Lewandowski K, Crook A, Carter D, Osborne J, et al. Assessment of metagenomic Nanopore and Illumina sequencing for recovering whole genome sequences of chikungunya and dengue viruses directly from clinical samples. Eurosurveillance. 2018;23:1800228.

39. Milne I, Stephen G, Bayer M, Cock PJA, Pritchard L, Cardle L, et al. Using tablet for visual exploration of second-generation sequencing data. Brief Bioinform. 2013;14:193–202.

40. Li H, Handsaker B, Wysoker A, Fennell T, Ruan J, Homer N, et al. 1000 Genome Project Data Processing Subgroup. The Sequence Alignment/Map format and SAMtools. Bioinformatics. 2009;25:2078–9.

41. Shen W, Le S, Li Y, Hu F. SeqKit: A cross-platform and ultrafast toolkit for FASTA/Q file manipulation. PLoS One. 2016;11:e0163962.

42. Larsson A. AliView: A fast and lightweight alignment viewer and editor for large datasets. Bioinformatics. 2014;30:3276–8.

43. Tolou HJG, Couissinier-Paris P, Durand JP, Mercier V, de Pina JJ, de Micco P, et al. Data from "Evidence for recombination in natural populations of dengue virus type 1 based on the analysis of complete

genome sequences". J Gen Virol. 2001;82:1283–90.

44.   Irie K, Mohan PM, Sasaguri Y, Putnak R, Padmanabhan R. Data from "Sequence analysis of cloned dengue virus type 2 genome (New Guinea-C strain)". Gene. 1989;75:197–211.

45.   Osatomi K, Sumiyoshi H. Data from "Complete nucleotide sequence of dengue type 3 virus genome RNA". Virology. 1990;176:643–7.

46.   Amat M, Checa B, Llor N, Molins E, Bosch J. Enantioselective total synthesis of the indole alkaloid 16-episilicine. Chem Commun (Camb). 2009;20:2935–7

47.   Amat M, Llor N, Checa B, Molins E, Bosch J. A synthetic approach to ervatamine-silicine alkaloids. Enantioselective total synthesis of (-)-16-episilicine. J Org Chem. 2010;75:178–89.

48.   Amat M, Checa B, Llor N, Pérez M, Bosch J. Conjugate addition of 2-acetylindole enolates to unsaturated oxazolopiperidone lactams: Enantioselective access to the tetracyclic ring system of ervitsine. European J Org Chem. 2011;5:898–907

49.   Romo D, Meyers AI. Chiral non-racemic bicyclic lactams. Vehicles for the construction of natural and unnatural products containing quaternary carbon centers. Tetrahedron. 1991;47:9503–69

50.   Escolano C, Amat M, Bosch J. Chiral oxazolopiperidone lactams: Versatile intermediates for the enantioselective synthesis of piperidine-containing natural products. Chem - A Eur J. 2006;12:8198–207

51.   Wilm A, Aw Kim PP, Bertrand D, Ting Yeo GH, Ong SH, Wong CH, Khor CC, Petric R, Hibberd ML, Nagarajan N. LoFreq: a sequence-quality aware, ultra-sensitive variant caller for uncovering cell-population heterogeneity from high-throughput sequencing datasets. Nucleic Acids Res. 2012;40:11189-201

Chapter 5: Deciphering the role of extracellular vesicles derived from ZIKV-infected hcMEC/D3 cells on the blood-brain barrier system

5.1 Abstract

To date, no vaccines or antivirals are available against Zika virus (ZIKV). In addition, the mechanisms underlying ZIKV-associated pathogenesis of the central nervous system (CNS) are largely unexplored. Getting more insight on the cellular pathways that ZIKV employs to facilitate infection of susceptible cells will be crucial for the establishment of an effective treatment strategy. In general, cells secrete a number of vesicles, known as extracellular vesicles (EVs), in response to viral infections. These EVs serve as intercellular communicators. In this work, we investigated the role of EVs derived from ZIKV-infected human brain microvascular endothelial cells on the blood-brain barrier (BBB) system. We demonstrated that ZIKV-infected EVs (IEVs) can incorporate viral components, including ZIKV RNA, NS1 and E-protein and further transfer them to different cell types of the CNS. Using label-free impedance-based biosensing, we observed that ZIKV and IEVs can temporally disturb the monolayer integrity of BBB-mimicking cells, possibly by inducing structural rearrangements of the adherent protein VE-cadherin. Finally, differences in the lipidomic profile between EVs and their parental cells possibly suggest a preferential sorting mechanism of specific lipid species into the vesicles. Overall, these data suggest that IEVs could be used as vehicles for ZIKV transmission via the BBB.

5.2 Introduction

Zika virus (ZIKV) is an emerging, single-stranded RNA virus of positive polarity that belongs to the large family of *Flaviviridae*. This flavivirus member is mainly transmitted to humans by two species of *Aedes* mosquitoes (*aegypti* and *albopictus*) (1). In addition, several studies have described that ZIKV can be transmitted via other routes as well, including sexual contact, blood transfusion and from mother to child (2) (3). ZIKV was first isolated in Uganda in 1947 but was initially neglected until more recent outbreaks emerged on the Yap Islands (2007), French Polynesia (2013) and Brazil (2015) (4), after which the World Health Organization (WHO) declared the virus a Public Health Emergency of International Concern in 2016 (5). As most infections caused by flavivirus members, ZIKV infection is usually asymptomatic with mild manifestations, such as headache, joint pain and low-grade fever.

However, several cases of ZIKV-associated neurological manifestations raised questions to the scientific community and encouraged them to study how this virus is able to reach the central nervous system (CNS) and causes abnormalities such as microcephaly and Guillain-Barré syndrome (6) (7) (8). Even though extensive efforts have been made to understand which factors lead to ZIKV-associated neuropathogenesis, our knowledge is still very limited. So far, no antivirals or vaccines are available to combat this virus.

In general, viruses infect and replicate into their hosts, by hijacking a number of cellular mechanisms. Several studies have reported that viruses can exploit the exosomal pathway in order to spread their infection and further modify the function of target cells (9) (10). This particular pathway controls the intercellular communication via membrane-enclosed vesicles, known as extracellular vesicles (EVs). EVs consist of three main types of vesicles, depending on their biogenesis mechanisms (11). Particularly, exosomes (50- 150 nm) follow the endocytic route and are formed in the late endosomes (multivesicular bodies, MVBs). Fusion of MVBs with the plasma membrane leads to their secretion into extracellular space. On the other hand, microvesicles (100-1000 nm) and apoptotic bodies (500 nm-2 μm) are directly released from the plasma membrane (12). Even though these distinct EV populations are secreted by all cell types, it is extremely challenging to properly discriminate them. For that reason, scientists suggest the use of small and medium/large extracellular vesicles (EVs) as nomenclature to describe EVs smaller and larger than 200 nm in size, respectively, according to the Minimal Information for Studies of Extracellular Vesicles (MISEV 2018) (13).

In order to study the role of EVs in viral infections, it is critical to be able to isolate pure vesicles. This is a challenging task, since viruses and EVs share multiple pathways and can be present at similar sites such as the plasma membrane and MVBs (14). Particularly, in the case of ZIKV, the virus enters into cells through the clathrin-dependent pathway (primary route of EV uptake from target cells) and follows exocytosis during its budding and egress (15). In addition, numerous studies have shown that several viruses are able to incorporate EV material into their interior content and vice versa, thus making discrimination more cumbersome (16) (17).

Throughout literature, several reports describe the ability of ZIKV to reach the CNS and infect susceptible cells including neurons (18), astrocytes (19) and

microglia (20). However, the mechanism by which ZIKV crosses the blood- brain barrier (BBB), a very tightly sealed structure, is largely unexplored. The BBB is mainly composed of brain microvascular endothelial cells surrounded by other cell types such as pericytes and microglia. It forms a dynamic and complex barrier that prevents microbes to pass from the peripheral circulation to the brain and CNS (21). The fact that the BBB is highly semipermeable to substances raises many questions on the capability of ZIKV to pass through this system without being recognized by the host immune responses.

In this study, we propose that EVs might serve as vectors to facilitate ZIKV transmission through the BBB. This hypothesis is based on the fact that EVs act as intercellular communicators by transferring proteins, lipids and nucleic acid molecules to recipient cells (22) (23). As such, we aimed to unravel the potential role of EVs from ZIKV-infected human brain microvascular endothelial cells in viral dissemination. First, EVs were successfully isolated from a well- studied *in vitro* model of the BBB (human brain microvascular endothelial cells, hcMEC/D3) by combining several isolation procedures, in order to minimize the possibility of viral contamination in our preparations. Next, we characterized the fractions by nanoparticle tracking analysis (NTA), transmission electron microscopy (TEM) and western blot. In addition, the functional role of non-infected (NIEVs) and ZIKV-infected EVs (IEVs) was determined by a series of *in vitro* cellular assays. Our results demonstrated that IEVs can incorporate and deliver viral components (ZIKV RNA as well as NS1 and E proteins) into susceptible cell lines. Real-time impedance measurements showed that ZIKV and IEVs induce temporal disturbances in the monolayer integrity of BBB-mimicking cells during the first minutes of inoculation, potentially by inducing a rearrangement of VE-cadherin, a protein with a unique role in BBB architecture. In addition, a comprehensive lipidomics analysis revealed a potential selective sorting mechanism of specific lipid classes into EVs. By comparing the lipidomic profile of cell lysates and EV preparations, we pinpointed the significance of these macro biomolecules on biogenesis and signaling processes. Finally, we identified differences in the relative abundance (%mol) of various lipid species between NIEVs and IEVs, thus advancing them as potential biomarkers during ZIKV infection. Here, we propose that ZIKV- infected EVs constitute an efficient mechanism of virus transmission to the BBB system, mainly through transient disruption of monolayer integrity.

5.3 Results

We used hcMEC/D3 cells, a stable and well-characterized model of human brain microvascular endothelial cells that maintains the BBB phenotype *in vitro*. HcMEC/D3 cell-derived EVs from infected and non-infected conditions were isolated using a well-established protocol described by Zhou W *et al* (24) with some slight modifications (Figure 5.1A). Particularly, differential centrifugation, followed by (ultra)filtration and density gradient separation were applied in order to acquire our EV preparations. In order to proceed with the characterization of our vesicles and the assessment of their functionality, we divided the EVs into six different fractions. The density of each fraction was determined by a control density gradient experiment using similar volumes of each iodixanol solution, as indicated in the Materials and Methods section. Cell viability was also assessed in parallel and measured at 95% throughout all experiments. Several conventional methods were performed to characterize our EV populations. Specifically, NTA analysis revealed that the presence of virus did not significantly change the size of infected EVs (IEVs), as compared to the control ones (NIEVs) (approximately 170 nm) (Figure 5.1B). In addition, the number of particles did not seem to significantly alter between the two conditions (approximately $1.5*10^8$ particles/ml). Furthermore, we examined the presence of EVs by TEM. As shown in Figure 5.1C, we were able to detect "cup-shaped" vesicles, smaller than 200 nm in both NIEVs (upper) and IEVs (bottom). Although we did not observe any viral particles in our EM images, derived from IEV preparations, we cannot exclude the possibility of their presence in these fractions. Finally, western blot analysis was used to evaluate the presence of specific EV markers (Figure 5.1D). Interestingly, differences in the presence of certain markers were observed not only between the NIEVs and IEVs, but also among the different fractions. Notably, the tetraspanin CD63 was detected in fractions 3, 4, 5 and 6 of both NIEVs and IEVs. However, there was a clear increase in CD63 levels in fractions 5 and 6, as compared to the amounts in fractions 3 and 4 of IEVs. Similar results were noticed for ALIX and TSG101, two proteins with a crucial role in EV biogenesis, in fractions 3, 5 and 6 between NIEVs and IEVs. However, an increase in expression levels for both markers was detected in fraction 4 of IEVs, as compared to this of NIEVs. To define the purity of our EVs, we evaluated whether calnexin and apolipoprotein A were present in the fractions. Calnexin is an endoplasmic reticulum protein that is often used as a negative marker in most EV studies. As expected, calnexin was only

detectable in cell lysates. On the other hand, apolipoprotein A is used to indicate the presence of high-density lipoproteins (HDL), since they can co- isolate with EVs due to their similar density. Interestingly, apolipoprotein A was mainly detected in the upper fractions (5 and 6) in both EV populations, whereas lower levels were noticed in fraction 4. Finally, we examined whether IEVs were able to incorporate any viral proteins into their content. In particular, ZIKV NS1 protein was solely detected in the upper fractions of IEVs. On the other hand, no NS1 was detected in any of the NIEV fractions nor in the cell control (lysate). These data suggest that our EVs are highly heterogeneous in size and composition and can incorporate viral components in their interior.

Since we observed that secreted NS1 protein was detectable in some IEV fractions, we examined whether these vesicles were able to transfer other viral material to naïve cells. Interestingly, viral envelope glycoprotein (E protein) was detected in cells exposed to several IEV fractions (Figure 5.2A). However, the amount of E protein was different among the tested fractions. EV-depleted supernatant (supernatant obtained during the second round of ultracentrifugation, during which EVs were acquired from the pellet) was used as negative control, while virus-infected cells provided the positive control. In addition, we determined whether ZIKV RNA could be detected in IEVs-infected cells, using quantitative real-time PCR (E-protein detection). As shown in Figure 5.2B, incubation of uninfected hcMEC/D3 cells with IEVs resulted in the detection of ZIKV RNA. In parallel, inoculation of cells with ZIKV PRVABC59 strain led to higher levels of viral RNA with a significant difference between ZIKV- and IEVs-infected cells. To rule out the possibility of RNA being present outside of our vesicles, we pretreated IEVs with RNase A (5 µg/ml) for 15 min, followed by their incubation in recipient hcMEC/D3 cells. As can be seen in Figure 5.2B, no significant differences were observed in the viral load between the RNase A-treated and non-treated IEVs. Since the BBB is a complex structure and it is not only composed of microvascular endothelial cells, we aimed to mimic this system *in vitro* using a transwell assay. In this experiment, U87-MG glioblastoma cells were seeded at the bottom chamber, while hcMEC/D3 were placed at the upper one. After achieving confluence, the hcMEC/D3 monolayer was exposed to IEVs. These vesicles were able to pass through the monolayer and further deliver viral RNA to U87-MG cells (Figure 5.2C). ZIKV virions were also added on hcMEC/D3 cells, as positive control in this assay.
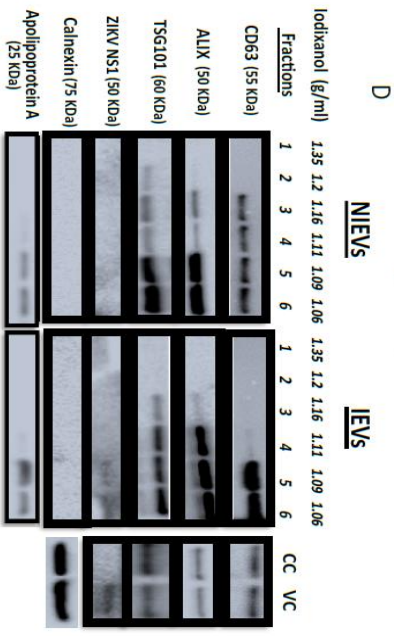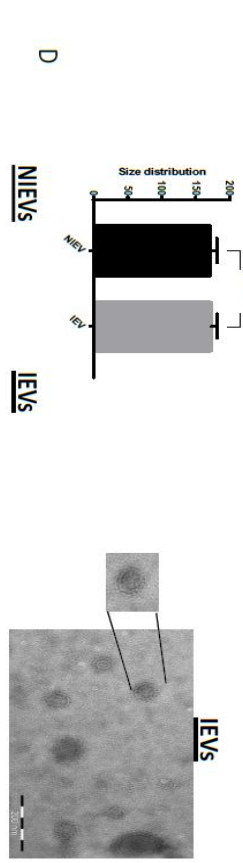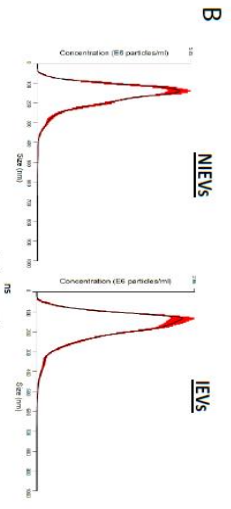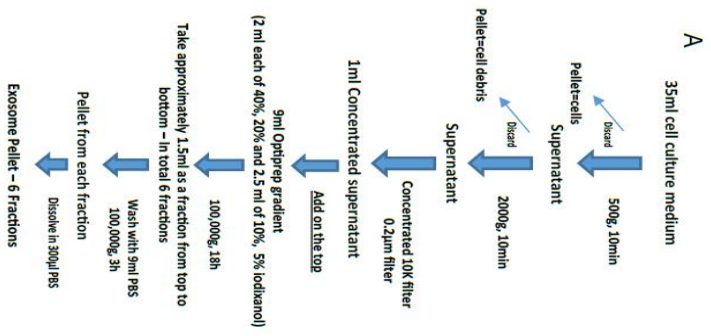
Figure 5.1: **Isolation and characterization of non-infected and ZIKV infected cell-derived EVs:** (A) Experimental workflow for EV isolation from human brain microvascular endothelial cells (hcMEC/D3). (B) Nanoparticle tracking analysis reveals no differences in size and number of particles between non-infected (NIEVs) and infected EVs (IEVs). (C) Electron microscopy shows the presence of membrane-enclosed vesicles smaller than 200 nm in both non-infected (upper) and infected (bottom) EV preparations. Scale bar graph: 200 nm (D) Western blot analysis demonstrates the presence of distinct profiles of several EV- and non-EV markers among fractions of both NIEVs and IEVs. 30 µl of each fraction (density is indicated in g/ml) were loaded into the SDS polyacrylamide gel. Lysates from non-infected (CC) and ZIKV-infected cells (VC) were also included.

Next, we evaluated the potential mechanisms that both virus and EVs use to pass through the BBB system, by applying a real-time electrical impedance assay. As shown in Figure 5.3, cellular changes were measured at different frequencies. Specifically, low frequencies (4,000 Hz, Resistance) give an assessment of cell-cell contacts (paracellular route), while higher frequencies (64,000 Hz, Capacitance) demonstrate how confluent the monolayer is (transcellular route) (25). After the addition of ZIKV and IEVs, we observed significant changes in capacitance, during the first 30 to 45 min of incubation, but not at later stages (2 days p.i.) (Figure 5.3A). More specifically, a subtle, non-significant decrease in resistance was observed after ZIKV/EVs addition, as compared to the mock-infected condition (cell control) ($p > 0.05$) (Figure 5.3B). Looking at high frequencies (64,000 Hz), ZIKV and IEVs (not NIEVs) significantly increased the capacitance value, suggesting that they induce temporary changes in the monolayer integrity (Figure 5.3B). These transient disturbances in the monolayer of the BBB model were further investigated by evaluating the expression levels of VE- cadherin, an adherent protein exclusively found in endothelial cells with a unique role in maintaining their barrier integrity.
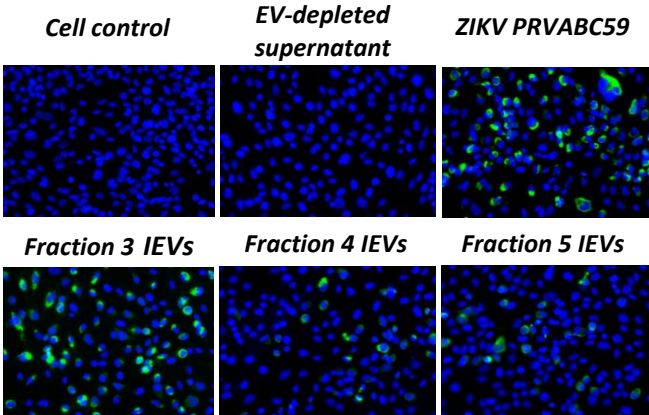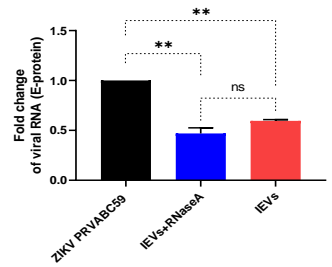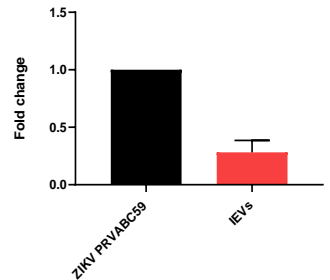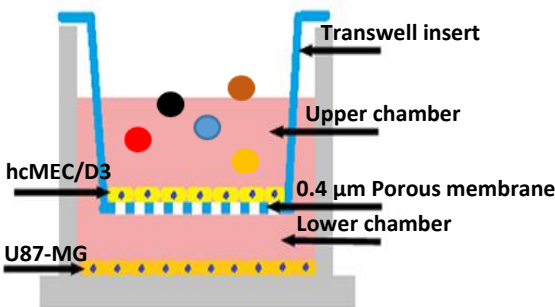
A

Cell control

EV-depleted supernatant

ZIKV PRVABC59

Fraction 3 IEVs

Fraction 4 IEVs

Fraction 5 IEVs

B

C

Transwell insert

Upper chamber

hcMEC/D3

0.4 μm Porous membrane

Lower chamber

U87-MG

Figure 5.2: **ZIKV infected cell-derived EVs (IEVs) are able to transfer viral material to naïve cells**: (A) Detection of ZIKV envelope protein (green) in hcMEC/D3 cells after their inoculation (72h) with different IEV fractions (20X objective). Positive (ZIKV-infected cells) and negative (EV-depleted supernatant) controls are also included. (B) Fold change in viral RNA levels (detection of E-protein) among ZIKV-infected (black), IEVs-pretreated with RNase A (blue) and IEVs-infected (red) hcMEC/D3 cells. Pretreatment of IEVs with RNase A shows no differences in viral RNA levels with untreated IEVs, indicating that most of the RNA resides inside the vesicles. (C) Representation of the Transwell assay setup to demonstrate that IEVs (colored spheres), isolated from hcMEC/D3 cells, can transfer viral RNA to glioblastoma cells (U87-MG, lower chamber) (6 days post-infection). ZIKV virions (virus stock) was also included in the assay.

Particularly, immunofluorescence staining and western blot analysis were performed at three different time points (30 min, 1h and 24h p.i.). As shown in Figure 5.4A (immunofluorescence), incubation of hcMEC/D3 cells with ZIKV and IEVs resulted in changes in the architecture of VE-cadherin at 30 min p.i. (indicated by white arrows). However, this observation is less pronounced, when the cells were inoculated with the NIEVs. These subtle modifications seem to be restored at later stages, except for ZIKV, where blunt changes were still observed at 1h p.i. TNF-α was also used as a positive control in this study, since it has been associated with the dysregulation of VE- cadherin. In addition, western blot analysis revealed that the expression levels of VE- cadherin did not significantly alter among different time points after the addition of ZIKV and EVs, as compared to cell control (Figure 5.4B).
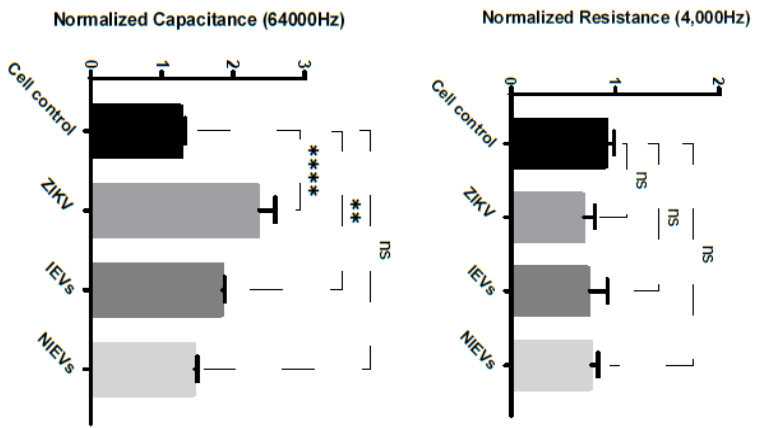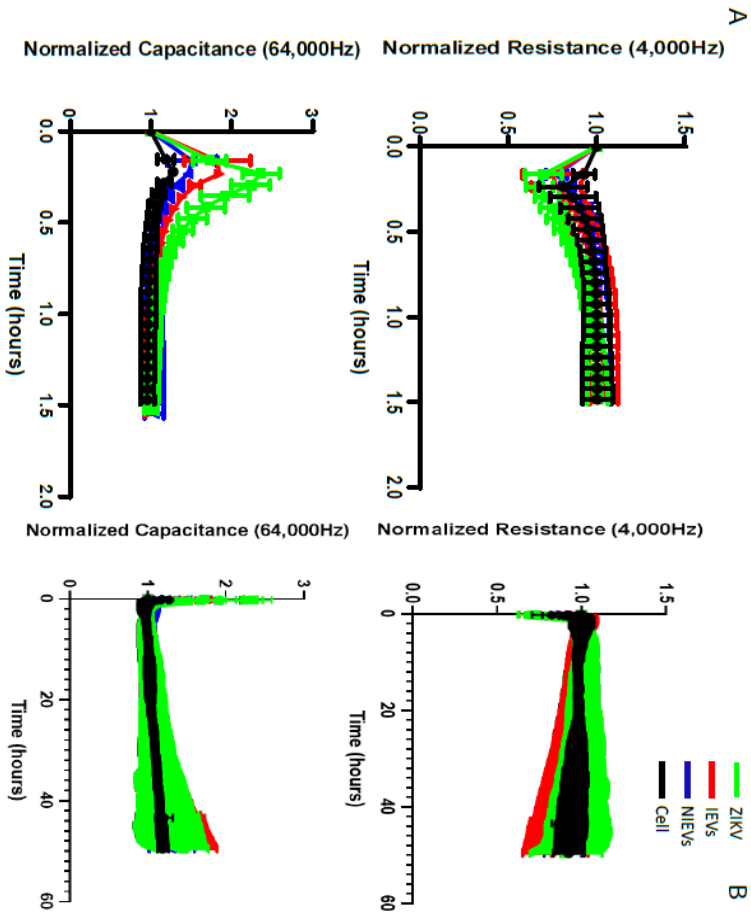
Normalized Capacitance (64,000Hz)   Normalized Resistance (4,000Hz)

Normalized Capacitance (64,000Hz)   Normalized Resistance (4,000Hz)

Normalized Capacitance (64000Hz)   Normalized Resistance (4,000Hz)

Figure 5.3: **Both ZIKV and IEVs induce temporal disturbances in the monolayer integrity of BBB during the first minutes**: (A) Normalized resistance (4,000 Hz, upper) and capacitance (64,000 Hz, bottom) values indicate that ZIKV (green) and IEVs (red) can induce temporal changes in monolayer integrity of hcMEC/D3 cells, which could potentially result in passing via transcellular route within the first 30 to 45 minutes (left panel). However, no further changes are observed during the later stages (2 days post-infection, right panel). (B) Maximal changes (as compared to cell control, black) in the permeability of BBB during the first minutes demonstrate that ZIKV and IEVs (not NIEVs) significantly alter capacitance (lower), but not resistance (upper) values. Normalization of the resistance/capacitance values was performed by dividing each data point by the value at the time point prior to sample addition. Data are acquired from 3 independent experiments.

As shown, IEVs can be used by ZIKV as vehicles to deliver their infectious content to recipient cells. Besides proteins and viral RNA, these vesicles have a high lipid content, which plays an essential role in EV biogenesis and signal transduction. As such, we aimed to characterize the lipidomic profile of hcMEC/D3 cells and EVs. As indicated by the western blot analysis (Figure 5.1), apoA was detectable in the upper fractions (5 and 6), but not in the middle (3, 4) and lower ones (1, 2). Hence, we divided our EVs into two different groups (upper and middle fractions) for analysis, based on the levels of apolipoprotein A, which possibly indicates the co-presence of HDL in our preparations. A total of approximately 2,000 lipid species, from 14 different lipid classes were identified by a well-established lipidomic analysis (SM, CE, Cer, LacCer, HexCer, PC, LPC, PE, LPE, PG, PI, PS, TG, DG). The data are shown as percentage of the total amount of lipid species per class (%mol) (Supplemental and Figure 5.5). The most abundant lipid species/class (~200) were illustrated as heatmaps in the Figure 5.5 as well as in Supplemental figure.

Consistent with other reports on lipid content of EVs (26), we observed that our vesicles are mainly enriched in cholesterol, SM and DG, as compared to most of the phospholipids and especially PC (data not shown). Focusing on each lipid class separately (colored boxes to group and compare the abundance of lipid species within each class), a number of lipid species were found to be largely present in both cells and EVs, indicating their preference in the sorting mechanism. Specifically, LPE (20:4), LPC (18:1), SM(18:1/16:0) and LacCer(18:1/16:0) were the most abundant lipid species of their class. On

the other hand, PE(18:1/18:1), LPC(18:1), PG(16:0/18:1), PI(18:0/20:3), PC(P- 18:0/18:1) and HexCer(18:1/16:0) levels were much higher in cells, as compared to those in EV preparations (Supplemental figure). Finally, all lipid species/class that were enriched in EVs were depicted in Figure 5.5. The most pronounced differences were noticed for Cer(18:1/14:0), DG(20:0/20:0) and PG(14:0/20:4), three lipids with a crucial role in the activation of signaling cascades and the maintenance of membrane curvature. Furthermore, it is noteworthy to mention the differences among the tested groups, as slight changes (in the percentage) were observed between the middle (absence of apoA) and upper (presence of apoA) fractions, indicating that lipoproteins can affect the way we interpret the results. Finally, Cer(18:0/18:3) was significantly increased in IEVs, as compared to the NIEVs (relative distribution), while four other lipid species, including sphingolipids (Cer and LacCer) and PS(18:0/18:1), also appeared slightly increased (non-significant) in the infected condition as compared to the non-infected one (Figure 5.5B). These findings suggest the importance of lipid molecules, as potential "signatures" during ZIKV infection.

A

Cell control

Virus control

NIEVs

IEVs

TNF-α

30 min   1 hour   24 hours

VE-cadherin
DAPI

B

30 min   1 hour   24 hours

IEV NIEV vc cc   IEV NIEV vc cc   IEV NIEV vc cc

Clathrin ————————————————— 190KDa
VE-cadherin ———————————————— 125KDa

Normalized expression

ns   ns   ns

cc 30 min, vc 30 min, NIEVs 30 min, IEVs 30 min, cc 1 hour, vc 1 hour, NIEVs 1 hour, IEVs 1 hour, cc 24 hours, vc 24 hours, NIEVs 24 hours, IEVs 24 hours
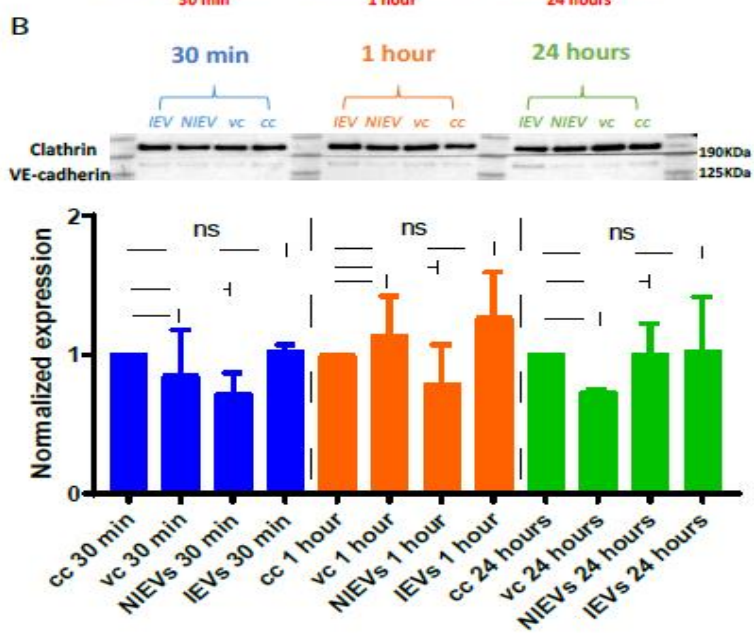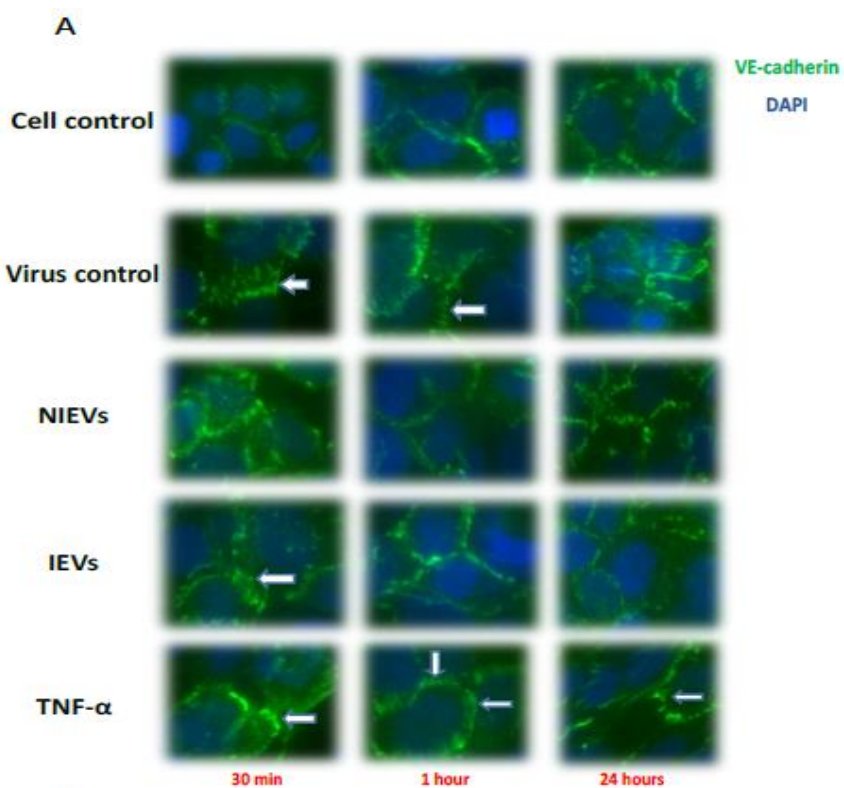
Figure 5.4: **ZIKV and IEVs induce structural rearrangements of VE-cadherin at the early time points**: (A) Alterations in the architecture of VE-cadherin (white arrows) are observed at 30 min in ZIKV-infected and IEV-treated hcMEC/D3 cells. These changes are restored at later time points, except for ZIKV-infected cells, where reorganization of VE-cadherin is still detectable at 1h post infection. TNF-α (100 ng/ml) is used as a positive control (40X objective). (B) Expression levels of VE-cadherin are not significantly changed in ZIKV- and EV-treated cells after 30 min, 1h and 24h. Clathrin is used as an internal loading control in the western blot analysis.
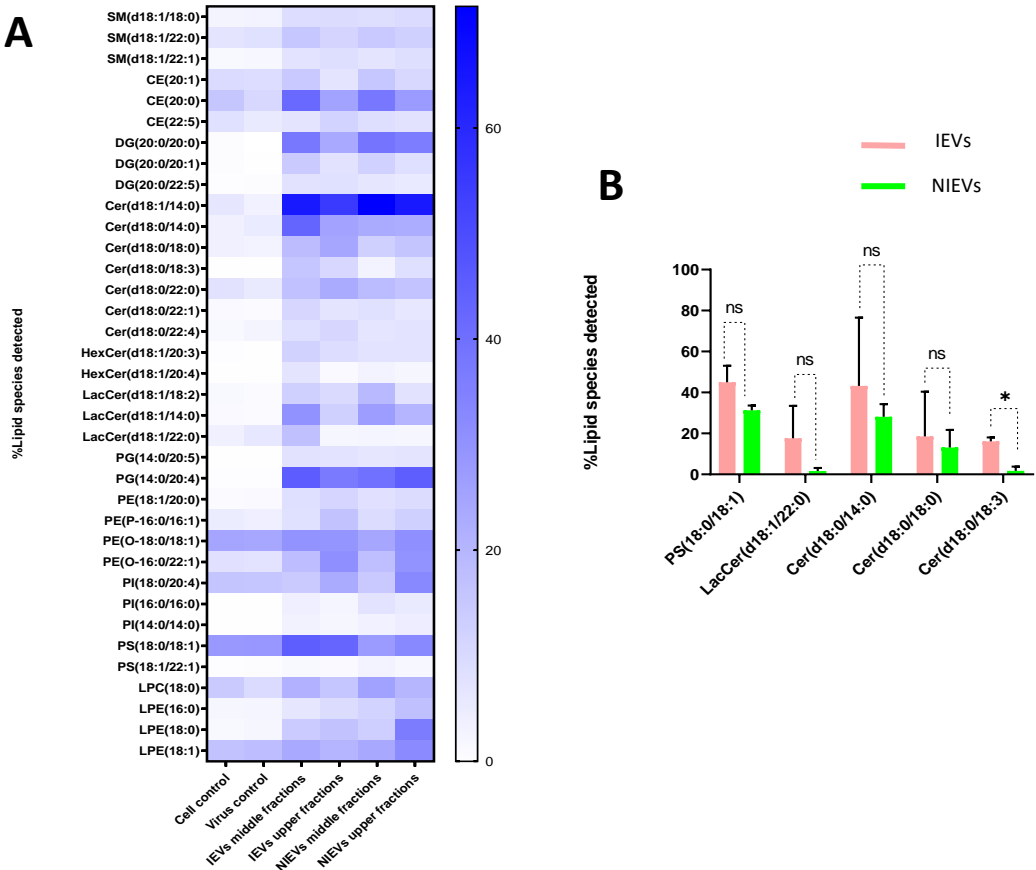

Figure 5.5: **Distinct differences in the lipidomic profile between cell lysates and EV preparations, as well as NIEVs and IEVs**: (A) Lipidomic heat map showing an increase (in percentage) of molecular lipid species per class into EV preparations, as compared to cell lysates. Each horizontal row represents a molecular lipid and each vertical

column represents a sample. Lipid abundance ratios are colored according to their percentage. (B) Five distinct lipid species have shown to be upregulated in infected condition (%mol), but only the levels of Cer(d18:0/18:3) are significantly changed in IEVs (pink), as compared to NIEVs (green) (p<0.05). SM: sphingomyelin, CE: cholesteryl ester, DG: diacylglycerol, Cer: ceramide, LacCer: lactosylceramide, HexCer: hexosylceramide, PG: phosphatidylglycerol, PE: phosphatidylethanolamine, PI: phosphatidylinositol, PS: glycerophosphoserine, LPC: lysophosphatidylcholine, LPE: lysophosphatidylethanolamine. Data shown are from 3 independent experiments (mean ± SD values).

Additionally, we looked at the degree of saturation (%mol) of the detected lipid classes, as it provides information on the structure and the functionality of these biomolecules. As shown in Figure 5.6, both EVs and cell lysates contain more saturated and monounsaturated fatty acids compared to di- and poly-unsaturated ones. Taking a closer look at the lipid classes found in the inner and outer leaflet, we found that SM, Cer, LacCer and HexCer (outer) contained more saturated and less monounsaturated fatty acids in both EVs and cell lysates. On the other hand, lipid classes found in the inner leaflet (PS, PE, PG) consisted of similar levels of saturated and monounsaturated fatty acids, while no diunsaturated lipids were detected in any of these lipid classes, except for HexCer and LacCer (~20%). Polyunsaturated fatty acids were not observed for SM, while higher levels were detected for HexCer. Moreover, it is interesting to point out that DG and Cer contain more saturated fatty acids in EVs than cell lysates. Finally, we observed a similar tendency in the degree of saturation for all tested lipid classes in both EVs and cell lysates. These notable differences in the degree of saturation can affect membrane dynamics and stability of EVs (26).
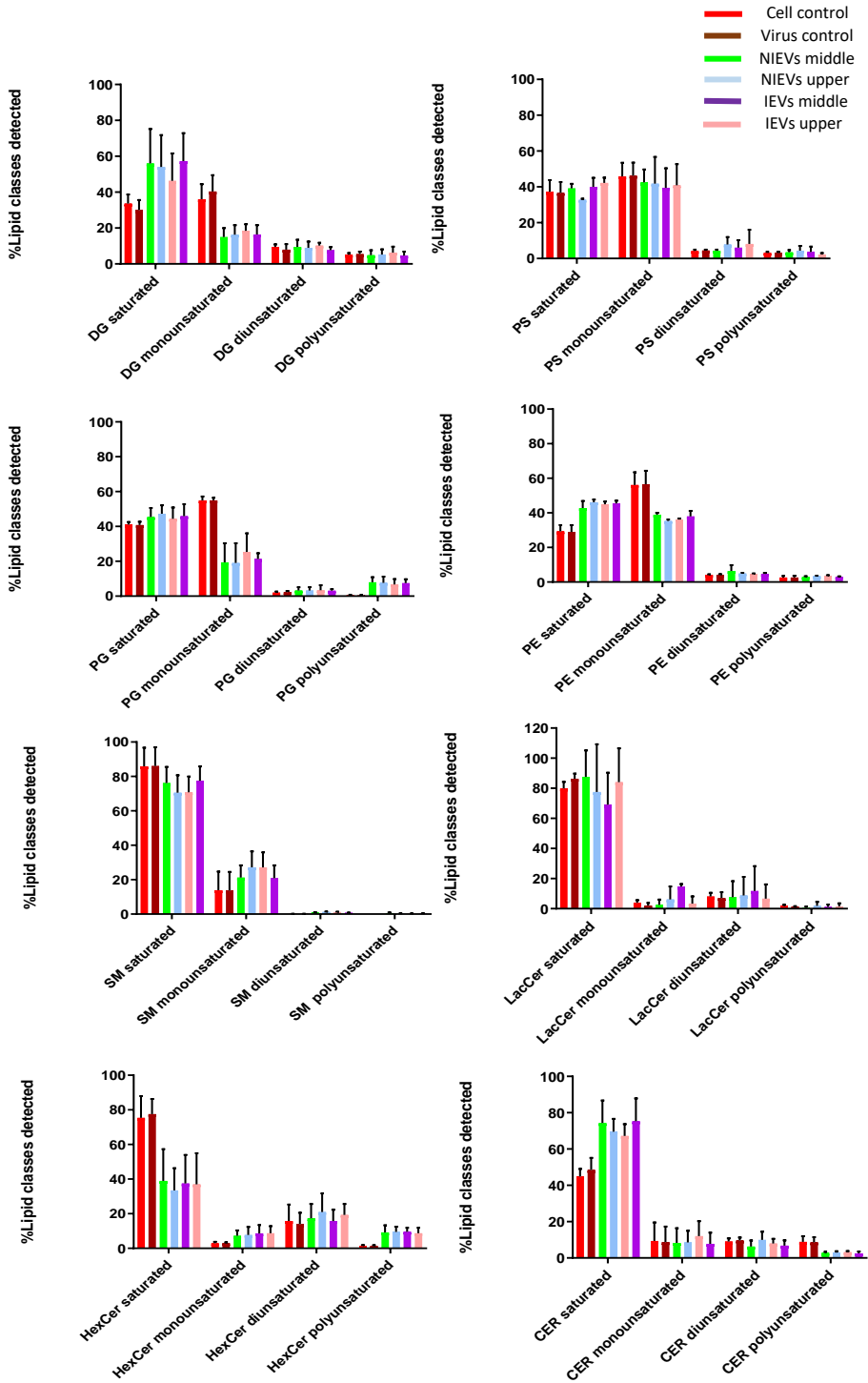
Figure 5.6: **Degree of saturation of lipids in EVs and cells.** Most of the detected lipid classes are saturated or monounsaturated, as compared to di- and poly-unsaturated ones in both EV preparations and cell lysates. Different color bars are depicted: Cell control (red), Virus control (brown), NIEVs middle fractions (green), NIEVs upper fractions (light blue), IEV middle fractions (purple), IEVs upper fractions (pink). DG: diacylglycerol, PS: glycerophosphoserine, PE: phosphatidylethanolamine, PG: phosphatidylglycerol, SM: sphingomyelin, LacCer: lactosylceramide, HexCer: hexosylceramide, Cer: ceramide. Data shown are from 3 independent experiments. The results are expressed as molar percentages (mol%).

5.4 Discussion

Although EVs have been initially described as a mechanism of discarding cellular waste (27), recent studies have demonstrated their crucial role in intercellular communication through active transport of proteins, lipids and nucleic acids to recipient cells (28). During viral infections, many viruses exploit the EV machinery to replicate, infect and evade host immune responses (29), (30). Despite the growing interest in this field, isolation of EVs is still considered a limiting factor, as there is no "gold standard". A number of different approaches have been used to isolate these vesicles, including size exclusion chromatography, ultracentrifugation, precipitation as well as microfluidics. Since EV biogenesis and viral replication/assembly share common pathways, it is extremely important to choose an isolation procedure in order to minimize the presence of viral particles in EV isolates (31). For that reason, we adopted a density gradient (iodixanol-based) ultracentrifugation protocol to purify our vesicles. This method provides an effective separation of EVs from viruses with comparable velocities. NTA showed that infection of hcMEC/D3 cells with ZIKV did not increase the size and the number of secreted vesicles, possibly indicating that viral particles are not present inside the EVs. This hypothesis was further confirmed by electron microscopy images, where no viral particles were detected in the IEVs. These findings are in agreement with another study by Vora *et al* (32), where no intact DENV particles (another flavivirus member) were detected in mosquito-cell derived EV fractions. This suggests that our isolation procedure offers good purity. Nevertheless, as previously mentioned, we cannot exclude the possibility that some viral particles might remain in the EV preparations, due to their high similarity and the lack of a universal isolation procedure that removes all viral contaminants. Detection of several EV markers in fractions 3, 4, 5 and 6 in both non-infected and infected conditions clearly indicates

that we have successfully isolated EVs. In addition, we noticed not only an increased shift in the expression levels of CD63, ALIX and TSG101, but also the detection of NS1 in fractions 5 and 6 of IEVs. These results could possibly suggest that upper (5 and 6) EV fractions might be used (more often) by the virus to transfer viral material and facilitate further infection. Finally, detection of apolipoprotein A at fractions 5 and 6 clearly indicates that lipoproteins can also co-isolate with EVs at upper fractions thereby possibly affecting the functional role of EV preparations (33).

Furthermore, the presence of both E-protein and viral RNA in our vesicles (even after their treatment with RNase A) suggest that both viral proteins and RNA are highly secured inside EVs via which they can potentially be transferred to recipient cells. This observation was well-supported by the transwell assay, where hcMEC/D3-cell derived IEVs could pass the initial layer of endothelial cells and deliver their viral content to glial cells, and most probably to other cell types of CNS as well.

Although the general molecular mechanisms by which several viruses, including ZIKV, are able to pass through the tight endothelial layer of BBB have been described (34), (35), the exact pathways still remain unknown. Most of these studies focus on permeability, by evaluating transepithelial electrical resistance (TEER) measurements using a voltmeter (36) or by labeling with fluorescein isothiocyanate-dextran (37). However, the main disadvantages of these two methods is the lack of TEER measurements for the detection of short permeability changes, as well as the inability of TEER to distinguish between resistance and capacitance at different currents (38). To surpass this limitation, a label-free impedance-based biosensor was applied. This technology allows a real-time measurement of endothelial permeability at multiple frequencies of alternating current (AC) flow and can discern changes in capacitance and resistance. At low AC frequency, current will mostly flow underneath cells and through the paracellular passage between the cells, while at high AC frequency most current will flow capacitively through the cell membranes (transcellular). Hence, changes in impedance at low frequency are more indicative for changes in barrier function while changes in capacitance at high frequency will be indicative for changes in cell monolayer integrity. Interestingly, changes in capacitance could be observed for ZIKV suggesting that there is a temporary loss in monolayer integrity. The same effect is also observed, but to a lesser extent for IEVs. However, it is extremely difficult to discern the actual mechanism

behind this observation, since both values can be affected. Our work provides additional insights to previous studies, leading to the following conclusions. First, inoculation of endothelial cells with ZIKV and IEVs leads to transient disturbances at the early time points, which are restored during the later stages. This illustrates the advantage of using measurements through time, in order to grasp any subtle BBB disturbances (39). In addition, since the readout gives information on processes that affect paracellular and transcellular currents, we could potentially obtain a better understanding on how BBB works. However, our results are not in agreement with most of the studies that investigate how ZIKV is able to cross BBB system (36). This could be explained by the fact that they mainly rely on TEER measurements during the later stages of infection (e.g. 24h to 48h p.i.), and not on the first minutes, as we propose (21). In addition, our analysis was based on the first 2 days of infection. For that reason, we can not exclude the possibility of BBB disruption at later stages. This disruption could be associated with the secretion of proinflammatory cytokines and chemokines, which are produced during viral infections (40). To get more insight on what really happens in endothelial cells after EVs or virus entry and to understand what leads to these temporal disturbances, we focused on one of the most abundant adherent proteins of hcMEC/D3, VE-cadherin. This molecule is responsible for controlling the barrier function by regulating the passage of macromolecules in and out of the endothelium (41). Notably, we observed that addition of ZIKV and IEVs leads to reorganization of VE-cadherin (temporal changes in the architecture, which leads to gap formation) at 30 min p.i, without affecting its expression levels. However, these alterations were restored after 1h, possibly indicating that the rapid remodeling of VE- cadherin is one possible mechanism that allows both IEVs and ZIKV to pass through the endothelial cell layer. Although changes in VE- cadherin are mostly related with the paracellular pathway, the concept of interconnectedness between paracellular and transcellular routes leads into a more complicated picture on how VE-cadherin affects the barrier function (42). However, this needs to be further evaluated. Despite the fact that our findings propose that the observed transient changes of BBB might be correlated with the rearrangement of VE-cadherin, it is extremely important to note that other proteins could also be affected during ZIKV or IEVs entry, including filament actin or the tight junction protein ZO-1 (38).

Although the number of EV studies is rising over the last years, there are still many unresolved answers regarding their biogenesis and signaling

mechanisms. Specifically, it has been described that a number of proteins, such as the endosomal sorting complex required for transport (ESCRT) and tetraspanins, have been involved in these pathways (43), (44). However, new articles have proposed that lipid molecules can also interact with these proteins, and as a result they are likely to be involved in the biogenesis of EVs (45). In addition, different lipid species have been reported to play a vital role in intracellular signaling (46), (47). To shed more light on this interesting class of macromolecules, we conducted an extensive lipidomic analysis in EV preparations and hcMEC/D3 cells. The most abundant lipid species per class are shown in Figure 5.5 and Supplemental Figure. In general, our analysis demonstrated that EVs are highly enriched in SM and DG, as compared to the majority of phospholipids. These findings were in accordance with another study (26), indicating their pivotal role in signaling (48). The relative abundance of several lipid species per class in EVs (as compared to these found in their originating cells) might suggest a selective sorting mechanism during their biogenesis. Interestingly, our study also revealed five lipid species that appeared to be enriched in IEVs, as compared to the NIEVs. From these detected hits, only Cer(d18:0/18:3) was significantly upregulated in the infected condition. Ceramides have been implicated in the biogenesis of EVs, as well in apoptosis (49), (50). Among the other lipid species, PS(18:0/18:1) was found, an important phospholipid with multiple functions. Particularly, this phosphatidylserine has been shown to retain cholesterol (role in membrane structure) into the inner leaflet of the membrane, thereby protecting it from oxidation (51). Furthermore, PS(18:0/18:1) is known to interact and bind with cytoplasmic proteins (e.g. Rab family), thus leading to activation of various signaling cascades (52). Finally, exposure of PS to the outer leaflet of the membrane has been reported as a recognition marker for apoptosis, which is indicative for viral infections (53). By summarizing the mechanisms that PS is implicated in, we hypothesize that ZIKV-infected EVs might be able to trigger various signaling pathways via PS(18:0/18:1) upregulation. Regarding the other species, both LacCer and Cer have been involved in intracellular signaling, not only by mediating inflammatory events (secretion of cytokines) but also through production of nitric oxide (NO), during viral infections (54), (20). The fact that Cer(d18:0/18:3) has been found to be significantly upregulated in the IEVs, makes this lipid molecule a promising species for future investigation. Further evaluation can promote this ceramide as a potential biomarker during ZIKV infection.

Finally, we also evaluated the degree of saturation in the majority of lipid classes. Saturated, monounsaturated, diunsaturated and polyunsaturated acyl chains vary in their structural properties. Interestingly, we found that hcMEC/D3 cells and their secreted vesicles contained much more saturated and monounsaturated acyl chains in most of the detected lipid classes. A high percentage of (mono-un)saturated lipids provides two main advantages to EVs. Firstly, it increases membrane rigidity (55), leading to a more selective sorting mechanism of proteins and lipids into their interior. Secondly, it makes EVs less susceptible to oxidative stress conditions (56). The latter is of utmost importance during viral infections, since it allows the vesicles to transfer and deliver their content over short and long distances within the extracellular space, without being affected by the presence of reactive oxygen species (ROS).

To conclude, in this study, we aimed to characterize the potential role of ZIKV-infected EVs (IEVs) on the BBB system. Interestingly, our isolation method revealed the heterogeneity of secreted vesicles, regarding their protein and lipid composition. In addition, we confirmed that IEVs can be used as transport vehicles for viral material, enhancing ZIKV transmission to susceptible cells. For the first time, we showed that both ZIKV and IEVs are able to pass through the BBB and alter monolayer integrity during the early time points of their exposure, possibly by the rearrangement of VE- cadherin. Finally, further studies will be important in order to identify the "key" elements that ZIKV and IEVs use during their entry into BBB.

5.5 Materials and Methods

5.5.1 Cell culture and viral infection

Human brain microvascular endothelial cells (hcMEC/D3) were used in this study. Specifically, 75 cm^2 flasks were pre-coated with 0.1% gelatin for 1-2h, followed by washing steps with PBS. Then, low-passage hcMEC/D3 were cultured in EndoGRO-MV Basal Medium (5% serum, Merck Millipore, Belgium) supplemented with the essential growth factors (Supplement kit). The ZIKV clinical isolate PRVABC59 (ATCC), from the Asian lineage, was used to infect hcMEC/D3 cells at a multiplicity of infection (MOI) of 0.5 for 72h.

5.5.2 Isolation of extracellular vesicles (EVs)

HcMEC/D3 ($3*10^5$ cells/well) were cultured in 6-well plates (Corning, USA) in EndoGRO-MV culture medium for 24h. The next day, culture medium was replaced, cells were washed with PBS and further incubated with heat inactivated exosome-depleted serum (Exo-FBS, System Biosciences, USA) for an additional 3h. Cells were exposed to culture medium (non-infected) and ZIKV PRVABC59 at MOI 0.5 (virus-infected) for 72h. Subsequently, cell culture medium was collected in sterile 50 ml tubes (Greiner Bio-One, Belgium) and differential centrifugation steps (500 g for 10 min, followed by 2000 g for 15 min) were applied to remove dead cells and cellular debris. Then, the supernatant for each condition was placed into 15 ml Amicon filter units (10 kDa, Merck Millipore, Belgium) and centrifuged at 4000 g for 30 min. Next, the fraction that remained on the filter was further passed through a syringe (0.2 μm pore size, Corning, USA). Finally, 1 ml of the concentrated sample was placed at the top of a discontinuous Optiprep™ density gradient (from top to bottom iodixanol solution: 2.5 ml of 5% and 10%, 2 ml of 20% and 40%) in 10.2 ml reseal tubes (Thermo Fisher Scientific, USA), followed by ultracentrifugation (no brake) at 100,000 g for 18h (Th641 rotor, Beckman Coulter, USA). Six different fractions of EVs per each condition (1.5 ml each) were put into new tubes (diluted in PBS) and subsequently ultracentrifuged at 100,000 g for 3h. The pellet from each fraction was collected, diluted in 300 μl PBS and stored at -80° C for further analysis.

5.5.3 Protein isolation and western blot analysis

Proteins from non-infected EVs (NIEVs), infected EVs (IEVs), as well as cell lysates (virus and cell controls) were extracted using Radio Immuno Precipitation Assay (RIPA) buffer (89900, Thermo Fisher Scientific) with freshly added protease and phosphatase cocktail inhibitor (1861281, Thermo Fisher). Particularly, 20 μl of each EV fraction were mixed with an equal volume of RIPA buffer for 15 min on ice, where after the mixture was further diluted in 2X Laemmli buffer (33401-1VL, Sigma Aldrich, USA) and heated at 95°C for 15 min. Then, 30 μl of each sample were loaded into sodium dodecyl sulfate (SDS) polyacrylamide 4–12% ready gels (Bio-Rad, USA) and electrotransferred to a nitrocellulose membrane using a trans-blot transfer pack system (Biorad). Milk Tris-Buffered Saline with 0.05% Tween20 (TBS-T) was used to block the membranes for 1h. Blots were probed with the following primary antibodies overnight at 4°C: rabbit anti-CD63 (CD63A-1,

170

190523-001) anti-ALIX (ALIX-1, 180312-005), anti-TSG101 (TSG101-1, 180312- 006) (1/1,000, System Biosciences), anti-calnexin (PA5-34665) (1/1,000, Invitrogen) and mouse anti-NS1 (5123) (1/1000, Virostat, USA), diluted in 5% milk TBS-T. Finally, membrane blots were washed three times with 0.05% TBS-T and incubated with secondary anti-rabbit (P0399) and anti-mouse (P0447) antibodies (Dako, 1/4000) in 5% milk TBS-T for 1h at room temperature. Finally, the blots were visualized using the ChemiDoc MP imaging system (Bio-Rad).

5.5.4 Transmission Electron Microscopy (TEM)

Non-infected and infected EVs were fixed with 2% paraformaldehyde (PFA, Merck Millipore, USA) for 10 min at room temperature and 3 µl of the mixtures were placed on glow-discharged 300 mesh Cu-grids (Ted Pella, Redding, USA). In order to increase the number of vesicles, each sample was deposited multiple times on the same grid, each time followed by a brief blotting step. Then, samples were negatively stained by placing the grids on a drop of 1% uranyl acetate for 1 min, after which they were blotted and allowed to dry. Finally, grids were introduced in a transmission electron microscope (JEOL JEM1400, Japan) equipped with an EMSIS Quemesa 11Mpxl camera, and imaged at an acceleration voltage of 80 kV.

5.5.5 Nanoparticle tracking analysis (NTA)

The concentration and size distribution of EVs in different fractions were determined using the Nanosight model NS300 (Malvern Instruments Company, UK). The instrument was cleaned using PBS and the temperature was maintained at 25°C. In addition, the detection threshold was set at 4 and the screen gain at 10, in order to remove any background for the measurement. Nanoparticles of 100 nm were used to calibrate the system prior to examination of our samples. Then, 1 ml of each fraction (diluted in PBS) was put into the syringe and slowly pushed through the laser module. Six recording video measurements (30 seconds each) were obtained for each EV sample. The data were averaged and analyzed using Nanosight NTA 2.3 software.

5.5.6 Immunofluorescence staining and qPCR analysis

Susceptible HcMEC/D3 ($3*10^4$ cells/well) were seeded in gelatin pre-coated black 96-well plates (Falcon, Germany) for 96h to achieve a confluent monolayer. Next, the cells were exposed to ZIKV PRVABC59 (MOI 0.5) and different fractions of NIEVs/IEVs for 72h. The amount of EVs, added during the assay, was normalized based on the number of particles. EV-depleted supernatant (supernatant taken after the 2nd ultracentrifugation step) was used as negative control in the study. Cells were first fixed for 5 min with 2% paraformaldehyde (PFA) at room temperature and then permeabilized with 0.1% Triton X-100 (Sigma Aldrich) for 10 min. Later, 1% Bovine Serum Albumin (BSA, Cell Signaling Technology, The Netherlands) was used to block the fixed cells for 1h followed by two washing steps with PBS. Incubation of hcMEC/D3 cells with the primary 4G2 pan-flavivirus antibody (clone D1-4G2-4-15, Merck Millipore, Belgium) was performed overnight at 4^oC. Goat anti-mouse IgG Alexa Fluor 488 (Invitrogen) was used as a secondary antibody. The nucleus was stained with DAPI (Invitrogen). Fluorescence microscopy was performed on a Zeiss Axiovert 200M inverted microscope (Zeiss, Göttingen, Germany) using Long Distance (LD) Plan-Neofluar 20X/0.4 objective.

For the detection of viral RNA in the vesicles, uninfected hcMEC/D3 were cultured in 96-well plates (Corning, USA) as previously described. ZIKV PRVABC59, IEVs and NIEVs were added to the cells. Cell lysates were collected at 72h post infection (p.i.) and viral RNA was measured by the Cells Direct One- step qRT-PCR kit (Thermo Fisher), according to manufacturer's instructions. RT-PCR was performed using the ABI 7500 Fast Real-Time PCR System (Applied Biosystems, NJ, USA). The primer and probe sequences used for qRT- PCR were: 5'- TGA CTC CCC TCG TAG ACT G-3' (ZIKV forward), 5'- CAC CTT TAG TCA CCT TCC TCT C-3' (ZIKV reverse) and 5'- 6-FAM/AGA TCC CAC/ZEN/AAA TCC CCT CTT CCC/3IABkFQ-3' (ZIKV probe). The following amplification conditions were used for qRT-PCR: $50^°C$ for 15 min, $95^°C$ for 2 min, followed by 45 cycles of $95^°C$ for 15 sec and $60^°C$ for 1 min. The infection efficiency was calculated using a curve of serial dilutions of ZIKV standard sample. All data were analyzed in GraphPad Prism 7 software.

5.5.7 Transwell assay

HcMEC/D3 ($3*10^4$ cells) were seeded on 24-well transparent filter inserts (0.4 μm) (Greiner Bio-One) for 4 days. As soon as hcMEC/D3 cells formed a

confluent monolayer (microscopic and impedance-based biosensing evaluation), both ZIKV PRVABC59 (virus stock, MOI 0.5) and EVs ($1.5*10^7$ particles) were added to the upper chamber of the insert. Human primary glioblastoma U87-MG (10^4 cells) were also added to the bottom of the lower chamber. Cell lysates from U87- MG were collected 6 days post-infection and viral RNA levels were measured by qPCR, as previously described.

5.5.8 Label-free impedance based biosensor analysis

8-well 20idf-PET plates (Applied Biophysics, NY, USA) were coated with 0.1% gelatin for 1h and washed with ultrapure water (MilliQ, Millipore). Then, 100 µl of growth medium (EndoGRO-MV Basal Medium) were added to each well and the plate was placed in the 16-well module of the Electric Cell-substrate Impedance Sensing (ECIS) device (Applied Biophysics) that was located in an incubator (37^0C, 5% CO_2). The 8WCP array type was chosen in the setup and the plate was stabilized using the built-in stabilization function. After removing the plate from the device, 200 µl of hcMEC/D3 cells were added to achieve a density of $3*10^4$ cells per well. Plates were then left on the benchtop for 30 min to let the cells settle to the bottom. Next, the plate was placed in the ECIS device for 4 days to achieve confluency. The growth of the cells was continuously monitored using the multifrequency mode (MFT) thereby obtaining frequency measurements at 4, 16 and 64 kHz. Before addition of the samples, the measurement was paused. Then, 100 µl of either NIEVs, IEVs (same number of particles) or virus (MOI 0.5) were added to the cells and the MFT measurement was resumed for up to 50 h with a time interval of approximately 3.5 min. Data were exported as .abp files and further analyzed using the ECIS software. Both the resistance (obtained at low frequency current – 4,000 Hz) and capacitance (obtained at high frequency current – 64,000 Hz) were used to assess whether ZIKV and EVs could induce cellular changes. The data were normalized by dividing each data point of a well by the value of that well at the time point prior to sample addition.

5.5.9 Immunofluorescence staining and western blot analysis for VE-cadherin detection

HcMEC/D3 ($3*10^4$ cells/well) were seeded as previously described. ZIKV PRVABC59, IEVs, NIEVs and TNF-α (100 ng/ml) were added to the cells for 30 min, 1h and 24h. After fixation, permeabilization and blocking steps, cells were incubated with the primary CD144 (VE- cadherin) monoclonal antibody

(clone 14-1449-82, Invitrogen) overnight at 4°C. Goat anti-mouse IgG Alexa Fluor- 488 was used as a secondary antibody and the nucleus was stained with DAPI. Fluorescence microscopy was performed using LD Plan-Neofluer 40X/0.6 objective. For the western blot analysis, cell lysates were collected at 30 min, 1h and 24h p.i. and proteins were further extracted by a solution containing RIPA buffer along with the cocktail phosphatase/protease inhibitor. 15 μg/ml of lysate per condition (30 μl) was loaded into an SDS polyacrylamide gel and transferred to a membrane as mentioned above in detail. Mouse anti-CD144 (1/500) was used to probe the membranes (overnight), followed by incubation with the secondary anti-mouse antibody for 1h, before the visualization of the blots.

5.5.10 Statistical analysis

Two different statistical tests were implemented to evaluate the significance of our results. Particularly, unpaired t-test was performed for Figure panels 5.1B and 5.5B, while one-way ANOVA (Tukey's post-correction test) was used to perform multiple comparisons in Figure panels 2B, 3B and 4B. Significance was calculated based on p-values.

*ns: $p > 0.05$, * : $p < 0.05$, ** : $p < 0.005$, *** : $p < 0.0005$, **** : $p < 0.0001$*

5.5.11 Lipidomic analysis

Lipid extraction

Each sample (700 μl) was mixed with 800 μl 1 N HCl:CH$_3$OH 1:8 (v/v), 900 μl CHCl$_3$, 200 μg/ml of the antioxidant 2,6-di-tert-butyl-4-methylphenol (BHT; Sigma Aldrich) and 3 μl of SPLASH® LIPIDOMIX® Mass Spec Standard (#330707, Avanti Polar Lipids). After vortexing and centrifugation, the organic fraction was evaporated using a Savant Speedvac spd111v (Thermo Fisher Scientific) at room temperature and the remaining lipid pellet was stored at - 20°C under argon atmosphere.

Mass spectrometry

Just before mass spectrometry analysis, lipid pellets were reconstituted in 100% ethanol. Lipid species were analyzed using liquid chromatography

electrospray ionization tandem mass spectrometry (LC-ESI/MS/MS) on a Nexera X2 UHPLC system (Shimadzu) coupled with hybrid triple quadrupole/linear ion trap mass spectrometer (6500+ QTRAP system; AB SCIEX). Chromatographic separation was performed on a XBridge amide column (150 mm × 4.6 mm, 3.5 µm; Waters) maintained at 35°C using mobile phase A [1 mM ammonium acetate in water-acetonitrile 5:95 (v/v)] and mobile phase B [1 mM ammonium acetate in water-acetonitrile 50:50 (v/v)] in the following gradient: (0-6 min: 0% B → 6% B; 6-10 min: 6% B → 25% B; 10-11 min: 25% B → 98% B; 11-13 min: 98% B → 100% B; 13-19 min: 100% B; 19-24 min: 0% B) at a flow rate of 0.7 ml/min which was increased to 1.5 ml/min from 13 min onwards. SM, CE, CER, DCER, HexCER, LacCER were measured in positive ion mode with a precursor scan of 184.1, 369.4, 264.4, 266.4, 264.4 and 264.4 respectively. TG, DG and MG were measured in positive ion mode with a neutral loss scan for one of the fatty acyl moieties. PC, LPC, PE, LPE, PG, LPG, PI, LPI, PS and LPS were measured in negative ion mode with a neutral loss scan for the fatty acyl moieties. Lipid quantification was performed by scheduled multiple reactions monitoring (MRM), the transitions being based on the neutral losses or the typical product ions as described above. The instrument parameters were as follows: Curtain Gas = 35 psi; Collision Gas = 8 a.u. (medium); IonSpray Voltage = 5500 V and −4,500 V; Temperature = 550°C; Ion Source Gas 1 = 50 psi; Ion Source Gas 2 = 60 psi; Declustering Potential = 60 V and −80 V; Entrance Potential = 10 V and −10 V; Collision Cell Exit Potential = 15 V and −15 V. The following fatty acyl moieties were taken into account for the lipidomic analysis: 14:0, 14:1, 16:0, 16:1, 16:2, 18:0, 18:1, 18:2, 18:3, 20:0, 20:1, 20:2, 20:3, 20:4, 20:5, 22:0, 22:1, 22:2, 22:4, 22:5 and 22:6 except for TGs which considered: 16:0, 16:1, 18:0, 18:1, 18:2, 18:3, 20:3, 20:4, 20:5, 22:2, 22:3, 22:4, 22:5, 22:6.

Data Analysis

Peak integration was performed with the MultiQuant^{TM} software version 3.0.3. Lipid species signals were corrected for isotopic contributions (calculated with Python Molmass 2019.1.1) and were normalized to internal standard signals. Unpaired t-test p-values and False Discovery Rate corrected p-values (using the Benjamini/Hochberg procedure) were calculated in Python StatsModels version 0.10.1.
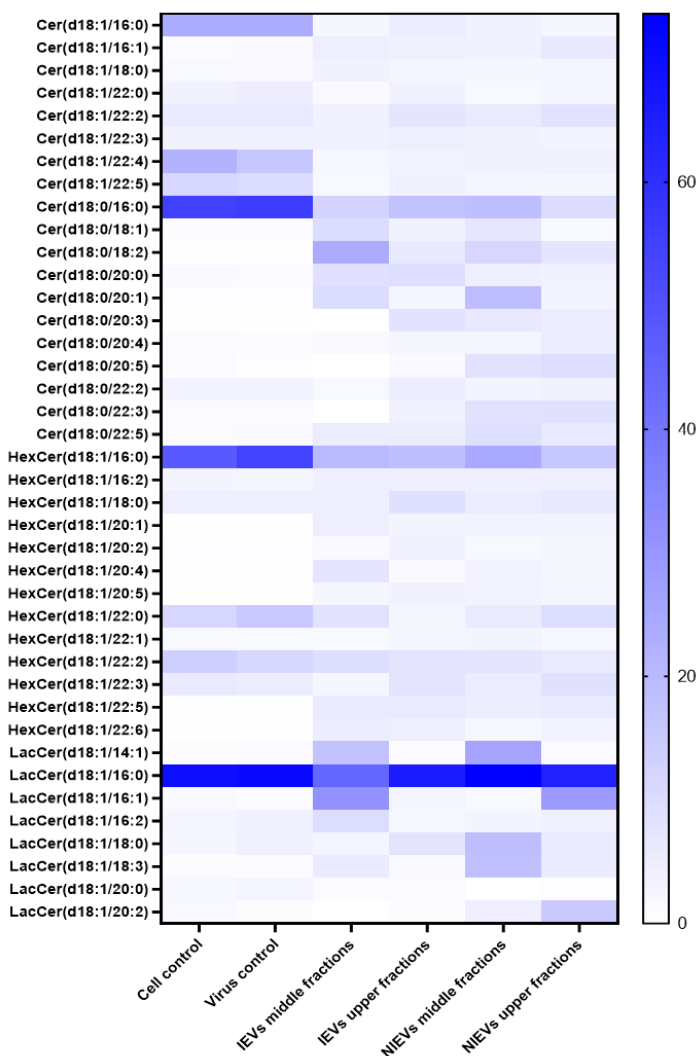
5.6 Supplemental Material
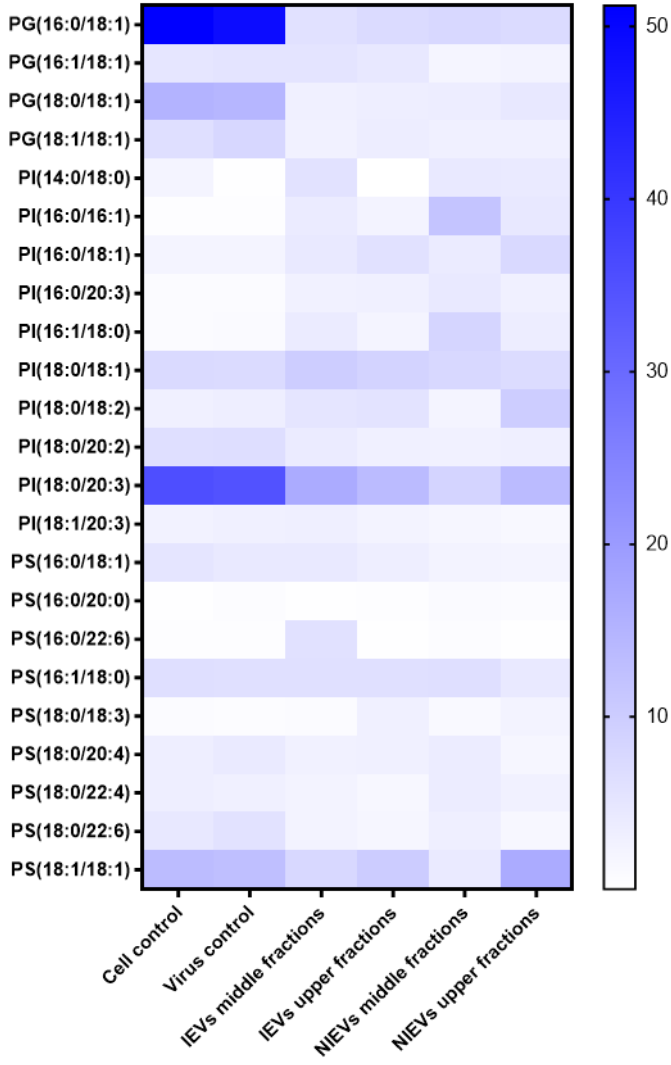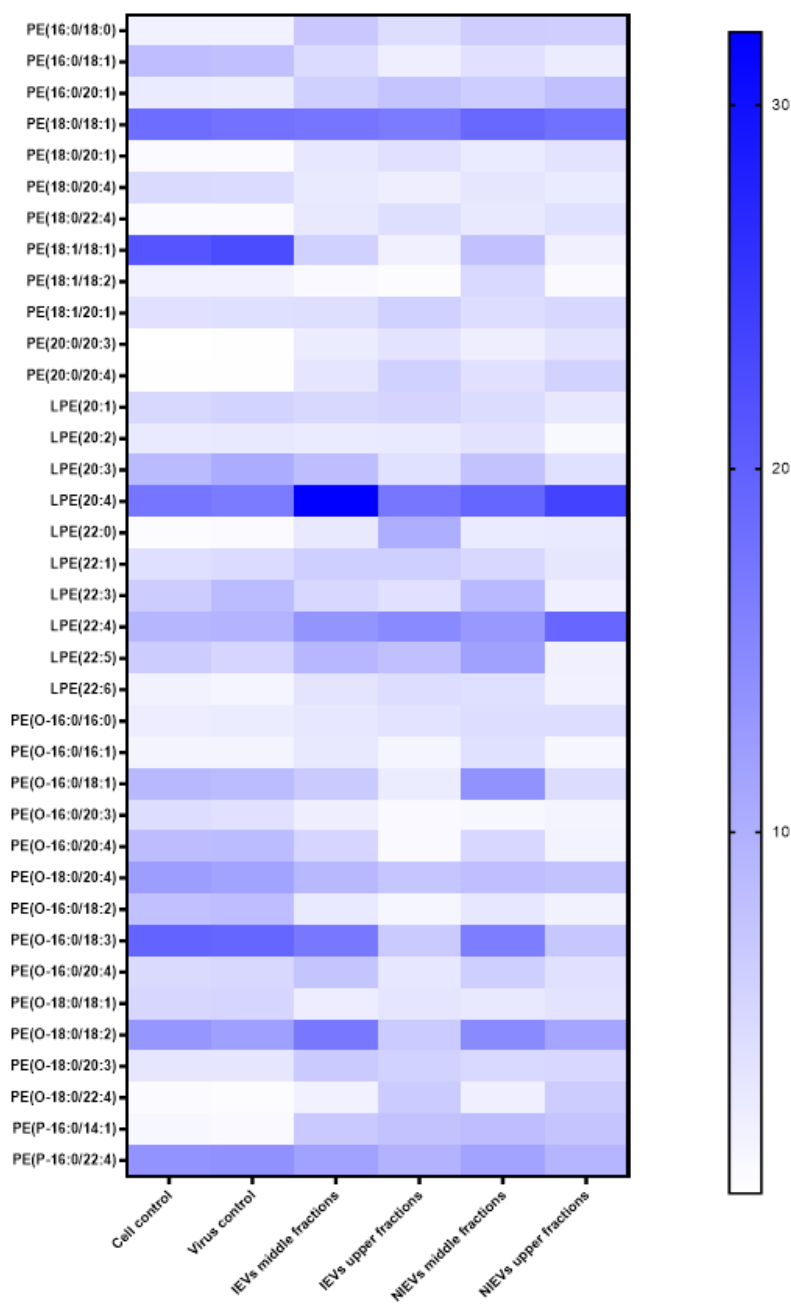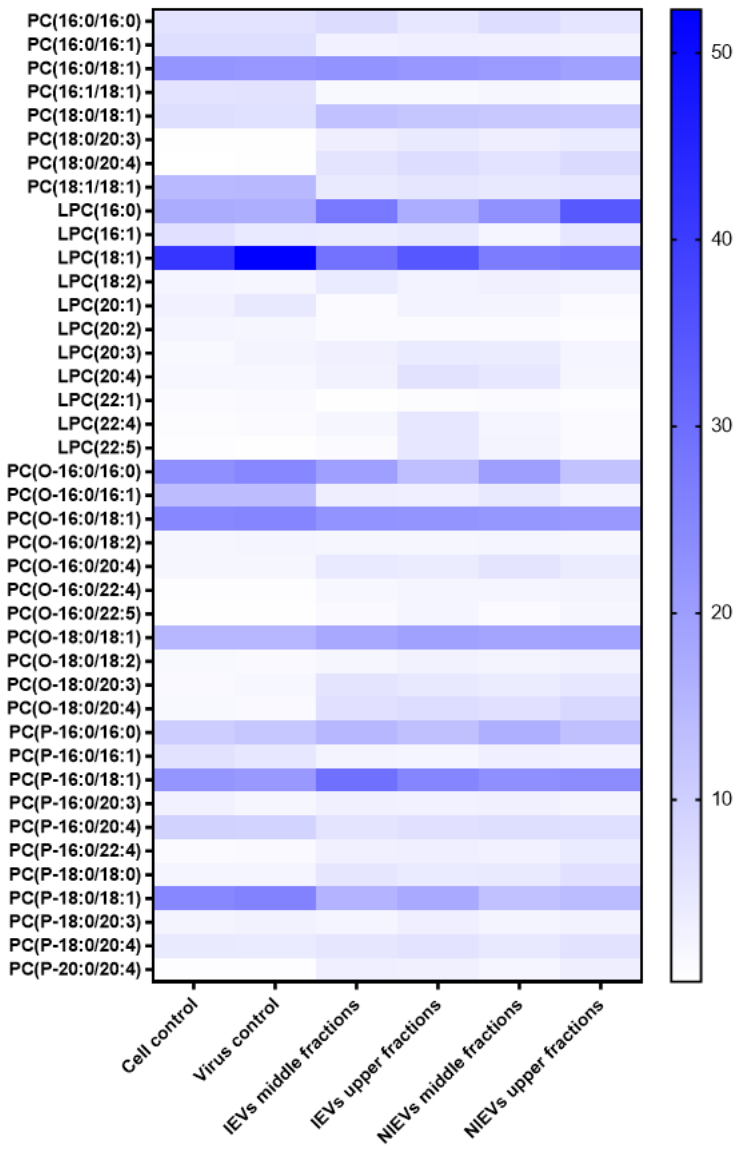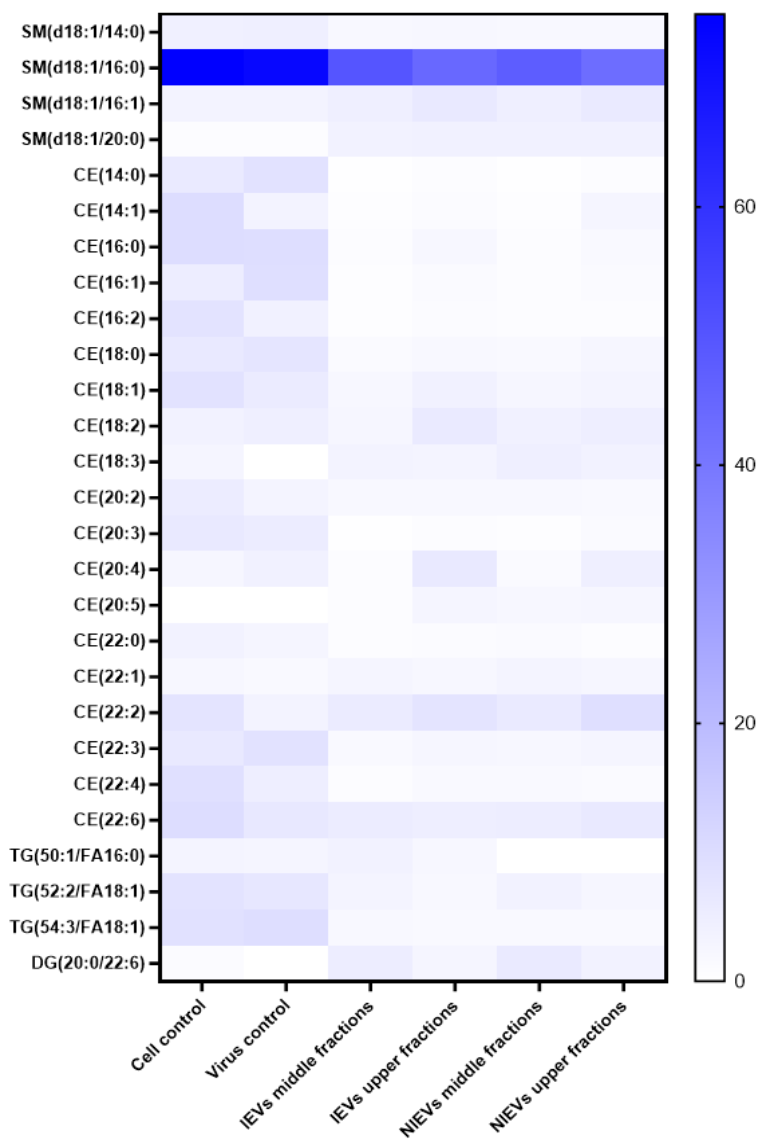
***Supplemental Figure*: Heatmaps representing the lipidomic profile of cell lysates, IEVs- and NIEVs- fractions.** Several lipid species within each class appear to be enriched in cell lysates, EV preparations or both. Lipid abundance ratios are colored according to their percentage. Higher and lower enrichment are indicated in blue and white, respectively. PE: phosphatidylethanolamine, LPE: lysophosphatidylethanolamine, PC: phosphatidylcholine, LPC: lysophosphatidylcholine, PG: phosphatidylglycerol,PI:phosphatidylinositol, PS: glycerophosphoserine, SM: sphingomyelin, CE: cholesteryl ester, TG: triacylglycerol, DG: diacylglycerol, Cer: ceramide, HexCer: hexosylceramide, LacCer: lactosylceramide. Data shown are from 3 independent experiments.

5.7 References

1.   Kazmi SS, Ali W, Bibi N, Nouroz F. A review on Zika virus outbreak, epidemiology, transmission and infection dynamics. J Biol Res. 2020;27(1):1–11.

2.   Hastings AK, Fikrig E. Zika virus and sexual transmission: A new route of transmission for mosquito-borne flaviviruses. Yale J Biol Med. 2017;90(2):325–30.

3.   Grischott F, Puhan M, Hatz C, Schlagenhauf P. Non-vector-borne transmission of Zika virus: A systematic review. Travel Med Infect Dis. 2016;14(4):313–30.

4.   Baud D, Gubler DJ, Schaub B, Lanteri MC, Musso D. An update on Zika virus infection. Lancet. 2017;390(10107):2099–109.

5.   Yun SI, Lee YM. Zika virus: An emerging flavivirus. J Microbiol. 2017;55(3):204–19.

6.   Faizan MI, Abdullah M, Ali S, Naqvi IH, Ahmed A, Parveen S. Zika Virus-Induced Microcephaly and Its Possible Molecular Mechanism. Intervirology. 2017;59(3):152–8.

7.   Merfeld E, Ben-Avi L, Kennon M, Cerveny KL. Potential mechanisms of Zika-linked microcephaly. Wiley Interdiscip Rev Dev Biol. 2017;6(4):1–14.

8.   Katz I, Gilburd B, Shovman O. Zika autoimmunity and Guillain-Barré syndrome. Curr Opin Rheumatol. 2019;31(5):484–7.

9.   Pegtel DM, van de Garde MDB, Middeldorp JM. Viral miRNAs exploiting the endosomal-exosomal pathway for intercellular cross-talk and immune evasion. Biochim Biophys Acta - Gene Regul Mech. 2011;1809(11–12):715–21.

10.   Bobrie A, Colombo M, Raposo G, Théry C. Exosome Secretion: Molecular Mechanisms and Roles in Immune Responses. Traffic. 2011;12(12):1659–68.

11.   Zhang G, Yang P. A novel cell-cell communication mechanism in the nervous system: exosomes. J Neurosci Res. 2018;96(1):45–52.

12. Corrado C, Raimondo S, Chiesi A, Ciccia F, De Leo G, Alessandro R. Exosomes as intercellular signaling organelles involved in health and disease: Basic science and clinical applications. Int J Mol Sci. 2013;14(3):5338–66.

13. Théry C, Witwer KW, Aikawa E, Alcaraz MJ, Anderson JD, Andriantsitohaina R, et al. Minimal information for studies of extracellular vesicles 2018 (MISEV2018): a position statement of the International Society for Extracellular Vesicles and update of the MISEV2014 guidelines. J Extracell Vesicles. 2018;7(1).

14. Urbanelli L, Buratta S, Tancini B, Sagini K, Delo F, Porcellati S, et al. The role of extracellular vesicles in viral infection and transmission. Vaccines. 2019;7(3):1–20.

15. Diosa-Toro M, Prasanth KR, Bradrick SS, Garcia Blanco MA. Role of RNA-binding proteins during the late stages of Flavivirus replication cycle. Virol J. 2020;17(1):1–14.

16. Cantin R, Méthot S, Tremblay MJ. Plunder and Stowaways: Incorporation of Cellular Proteins by Enveloped Viruses. J Virol. 2005;79(11):6577–87.

17. Kutchy NA, Peeples ES, Sil S, Liao K, Chivero ET, Hu G, et al. Extracellular vesicles in viral infections of the nervous system. Viruses. 2020;12(7):1–28.

18. Retallack H, Di Lullo E, Arias C, Knopp KA, Laurie MT, Sandoval-Espinosa C, et al. Zika virus cell tropism in the developing human brain and inhibition by azithromycin. Proc Natl Acad Sci U S A. 2016;113(50):14408–13.

19. Chen J, Yang YF, Yang Y, Zou P, Chen J, He Y, et al. AXL promotes Zika virus infection in astrocytes by antagonizing type i interferon signalling. Nat Microbiol. 2018;3(3):302–9.

20. Diop F, Vial T, Ferraris P, Wichit S, Bengue M, Hamel R, et al. Zika virus infection modulates the metabolomic profile of microglial cells. PLoS One. 2018;13(10):1–16.

21. Alimonti JB, Ribecco-Lutkiewicz M, Sodja C, Jezierski A, Stanimirovic DB, Liu Q, et al. Zika virus crosses an in vitro human blood brain barrier

model. Fluids Barriers CNS. 2018;15(1):1–9.

22.   Bukong TN, Momen-Heravi F, Kodys K, Bala S, Szabo G. Exosomes from Hepatitis C Infected Patients Transmit HCV Infection and Contain Replication Competent Viral RNA in Complex with Ago2-miR122-HSP90. PLoS Pathog. 2014;10(10).

23.   Ramis JM. Extracellular Vesicles in Cell Biology and Medicine. Sci Rep. 2020;10(1):3–4.

24.   Zhou W, Woodson M, Neupane B, Bai F, Sherman MB, Choi KH, et al. Exosomes serve as novel modes of tick-borne flavivirus transmission from arthropod to human cells and facilitates dissemination of viral RNA and proteins to the vertebrate neuronal cells. PLoS Pathogens. 2018;14:1–36.

25.   Stolwijk JA, Matrougui K, Renken CW, Trebak M. Impedance analysis of GPCR-mediated changes in endothelial barrier function: overview and fundamental considerations for stable and reproducible measurements. Pflugers Arch. 2015;467(10):2193-218

26.   Hessvik NP, Llorente A. Current knowledge on exosome biogenesis and release. Cell Mol Life Sci. 2018;75(2):193–208.

27.   Gurunathan S, Kang M, Jeyaraj M, Qasim M, Kim J. Function, and Multifarious Therapeutic Approaches of Exosomes. Cells. 2019;8(4):307.

28.   Ha D, Yang N, Nadithe V. Exosomes as therapeutic drug carriers and delivery vehicles across biological membranes: current perspectives and future challenges. Acta Pharm Sin B. 2016;6(4):287–96.

29.   Kumar A, Kodidela S, Tadrous E, Cory TJ, Walker CM, Smith AM, et al. Extracellular vesicles in viral replication and pathogenesis and their potential role in therapeutic intervention. Viruses. 2020;12(8).

30.   Barroso-González J, García-Expósito L, Puigdomènech I, de Armas-Rillo L, Machado JD, Blanco J, et al. Viral infection: Moving through complex and dynamic cell-membrane structures. Commun Integr Biol. 2011;4(4):398–408.

31.   Caobi A, Nair M, Raymond AD. Extracellular vesicles in the

pathogenesis of viral infections in humans. Viruses. 2020;12(10).

32. Vora A, Zhou W, Londono-Renteria B, Woodson M, Sherman MB, Colpitts TM, et al. Arthropod EVs mediate dengue virus transmission through interaction with a tetraspanin domain containing glycoprotein Tsp29Fb. Proc Natl Acad Sci U S A. 2018;115(28):E6604–13.

33. Sun Y, Saito K, Saito Y. Lipid profile characterization and lipoprotein comparison of extracellular vesicles from human plasma and serum. Metabolites. 2019;9(11):10–4.

34. Mladinich MC, Schwedes J, Mackow ER. Zika virus persistently infects and is basolaterally released from primary human brain microvascular endothelial cells. MBio. 2017;8(4):1–17.

35. Mustafá YM, Meuren LM, Coelho SVA, De Arruda LB. Pathways exploited by flaviviruses to counteract the blood-brain barrier and invade the central nervous system. Front Microbiol. 2019;10(MAR).

36. Papa MP, Meuren LM, Coelho SVA, de Oliveira Lucas CG, Mustafá YM, Matassoli FL, et al. Zika virus infects, activates, and crosses brain microvascular endothelial cells, without barrier disruption. Front Microbiol. 2017;8(DEC).

37. Xu Y, He Q, Wang M, Wang X, Gong F, Bai L, et al. Quantifying blood-brain-barrier leakage using a combination of evans blue and high molecular weight FITC-Dextran. J Neurosci Methods. 2019;325(April).

38. Leda AR, Bertrand L, Andras IE, El-Hage N, Nair M, Toborek M. Selective Disruption of the Blood–Brain Barrier by Zika Virus. Front Microbiol. 2019;10(September):1–14.

39. Tu K, Yu L, Sie Z, Hsu H, Al-jamal KT, Wang JT, et al. Development of Real-Time Transendothelial Electrical Resistance Monitoring for an In Vitro Blood-Brain Barrier System. Micromachines (Basel). 2020;12(1):37

40. Spindler KR, Hsu TH. Viral disruption of the blood-brain barrier. Trends Microbiol. 2012;20(6):282–90.

41. Winger RC, Koblinski JE, Kanda T, Ransohoff RM, Muller WA. Rapid

Remodeling of Tight Junctions during Paracellular Diapedesis in a Human Model of the Blood–Brain Barrier. J Immunol. 2014;193(5):2427–37.

42. Komarova Y, Malik AB. Regulation of endothelial permeability via paracellular and transcellular transport pathways. Annual Review of Physiology. 2009;72:463–493.

43. Colombo M, Moita C, Van Niel G, Kowal J, Vigneron J, Benaroch P, et al. Analysis of ESCRT functions in exosome biogenesis, composition and secretion highlights the heterogeneity of extracellular vesicles. J Cell Sci. 2013;126(24):5553–65.

44. Jankovičová J, Sečová P, Michalková K, Antalíková J. Tetraspanins, more than markers of extracellular vesicles in reproduction. Int J Mol Sci. 2020;21(20):1–30.

45. Hough KP, Wilson LS, Trevor JL, Strenkowski JG, Maina N, Kim Y Il, et al. Unique Lipid Signatures of Extracellular Vesicles from the Airways of Asthmatics. Sci Rep. 2018;8(1):1–16.

46. De Craene JO, Bertazzi DL, Bär S, Friant S. Phosphoinositides, major actors in membrane trafficking and lipid signaling pathways. Int J Mol Sci. 2017;18(3).

47. Skotland T, Sandvig K, Llorente A. Lipids in exosomes: Current knowledge and the way forward. Prog Lipid Res. 2017;66:30–41.

48. Green SM, Padula MP, Marks DC, Johnson L. The Lipid Composition of Platelets and the Impact of Storage: An Overview. Transfus Med Rev. 2020;34(2):108–16.

49. Haraszti RA, Didiot MC, Sapp E, Leszyk J, Shaffer SA, Rockwell HE, et al. High-resolution proteomic and lipidomic analysis of exosomes and microvesicles from different cell sources. J Extracell Vesicles. 2016;5(1):1–14.

50. Haimovitz-Friedman A, Kolesnick RN, Fuks Z. Ceramide signaling in apoptosis. Br Med Bull. 1997;53(3):539–53.

51. Maekawa M, Fairn GD. Complementary probes reveal that phosphatidylserine is required for the proper transbilayer distribution

of cholesterol. J Cell Sci. 2015;128(7):1422–33.

52. Fujimoto T, Parmryd I. Interleaflet coupling, pinning, and leaflet asymmetry-major players in plasma membrane nanodomain formation. Front Cell Dev Biol. 2017;4:1–12.

53. Mariño G, Kroemer G. Mechanisms of apoptotic phosphatidylserine exposure. Cell Res. 2013;23(11):1247–8.

54. Won JS, Singh AK, Singh I. Lactosylceramide: a lipid second messenger in neuroinflammatory disease. J Neurochem. 2007;103 (Suppl 1):180–91.

55. Press EB, Blitterswijk WJV an, Veer GDE, Krol JH, Emmelot P, Leeuwenhoekhuis A Van. Estimation of lipid fluidity by fluorescence polari- Isolation of plasma membranes and extracellular. 1982;688:495–504.

56. Rysman E, Brusselmans K, Scheys K, Timmermans L, Derua R, Munck S, et al. De novo lipogenesis protects cancer cells from free radicals and chemotherapeutics by promoting membrane lipid saturation. Cancer Res. 2010;70(20):8117–26.

Chapter 6: General Discussion

The recent outbreak of COVID-19 disease (caused by SARS-CoV-2 virus) clearly highlights the importance of developing novel antivirals. Prophylactic and treatment strategies are the main keepers against viral infections. Despite the extensive scientific efforts, no antiviral agents are commercially available against a number of viruses, including DENV and ZIKV. These members of the *Flaviviridae* family are mainly transmitted by arthropod vectors (*Aedes* mosquitoes) and target a large number of human cells/tissues.

DENV, a prevalent arbovirus is predominantly circulated in Southeast Asia, America and Africa. Besides the four known serotypes (DENV1- 4), a new DENV isolate was discovered from the outbreak in Malaysia in 2007 (1). The occurrence of this serotype further complicates the development of vaccines and antiviral drugs. On the other hand, ZIKV is mainly found in areas where DENV is endemic. Co-circulation of these members can contribute to increased phenomenon of ADE that leads to the enhancement of viral infection. In addition, the neurotropic nature of ZIKV has raised a number of questions, regarding its ability to reach into the central nervous system, as well as the development of antiviral candidates, able to pass through the semi-permeable BBB system. As already discussed in Chapter 1, there are two main types of antivirals: direct-acting (DAA) and host-directed (HDA) that interact with viral and cellular factors, respectively, in order to inhibit viral replication and spread (2)(3).

In this final chapter, we will address the major findings of our thesis and further discuss about limitations and future perspectives on the projects.

In the first two chapters (3 and 4), we determined the antiviral activity and mechanism of action of two different classes of molecules. Specifically, a novel series of tryptophan trimers and tetramers has shown to inhibit viral attachment and entry processes (**Chapter 3**), by interfering with the viral envelope (E) glycoprotein (domain III). This interaction is possibly mediated through the positively charged residues of viral E protein with the negatively charged tryptophan residues. The interesting class of compounds belong to the large family of polyanionic dendrimers (4). They are highly branched, star- shaped macromolecules, with a central core and external layers, which are crucial for their interaction with targeting moieties. In addition, these molecules present several advantages, as compared to small molecules, such as precise structure, stability and high efficiency, due to their capacity to bind on the target in a multivalent way (5). In contrast, one of the drawbacks

described in the literature is their poor absorption (e.g. dextran sulfate) that definitely hampers their use in the clinic (6). However, modifications on the synthetic process can result in changes on the structure that might increase the therapeutic properties of these agents.

Different classes of dendrimers have been developed so far for biomedical applications. Dendrimers are used as nanoparticles to transfer antiretroviral drugs to target organs. For example, Cardoba *et al*. have found that polyanionic-based dendrimers containing tenofovir are able to inhibit HIV-1 infection in different human cells (7). The formulation and use of dendrimers as efficient delivery system strategy overcome the limitations that might occur by the poor availability of the drug, as well as the development of resistance. In addition, the functional external groups of dendrimers are known to interact with viral proteins or cellular receptors, thus restricting virus attachment/entry to susceptible cells (8). However, several issues regarding target specificity have been raised. In **Chapter 3**, we interestingly observed that our leading compounds constitute specific inhibitors of DENV and ZIKV, since no antiviral activity was noticed against other viral strains (e.g. HIV). This observation led us to the conclusion that these dendrimers specifically interact with motifs of envelope protein, which are not present in HIV-1 and HIV-2 strains.

In **Chapter 4**, we have identified a class of intermediates in the synthesis of indole alkaloids with good potency against DENV and ZIKV. Additionally, we have determined their mechanism of action and we observed the anti-ZIKV cell-dependent inhibition profile of these molecules. Interaction of the compounds with cellular factor(s), possibly implicated in the formation of the viral replication complex, led to inhibition of viral replication and infection. Our metagenomics analysis on compounds-resistant mutants have shown that the leading molecules present the same single amino acid mutation on NS4B protein and more specifically in the pTMD1 domain (position 31). This particular site is highly conserved among different flavivirus members and constitutes a potential spot that could be effectively targeted by several antiviral strategies. In the literature, several reports have demonstrated the therapeutic potential of (indole) alkaloids in many biological activities, such as antiviral, anticancer, antiparasitic and anti-inflammatory (9)(10). These secondary metabolites are produced by a large variety of organisms, including plants, animals and bacteria and have shown to present pharmacological activities.

In **Chapters 3** and **4**, cellular-based approaches were implemented to identify new antiviral compounds against DENV/ZIKV infection. To further proceed with antiviral drug development strategy, numerous requirements have to be met. As shown, antiviral activity of molecules was evaluated in a number of non-human and human cell lines. The choice of cells is crucial in the development of antivirals, since cellular tropism of each virus should be taken into consideration (11). Different human primary cells (e.g. MDDC, hepatocytes, macrophages), as well as placental and brain endothelial cells constitute the natural targets of DENV and ZIKV infection (12)(13). In addition, newly developed organoid cultures, such as 3 dimensional organoids, may be helpful to evaluate antiviral activity in a more complex *in vitro* model (14). Besides these assays, great advances have been made in bioinformatics, by the use of open databases and x-ray structure determination of different viral proteins that allows in-depth research of virus-host cell interactions and structure-based design of inhibitors, respectively (15)(16).

To conclude, we identified and characterized two families of compounds, with distinct mode of actions (*Figure 1*) against DENV and ZIKV, in a number of susceptible cells (*Figure 6.1*). In the next step of our research, new analogues of these two classes of molecules have to be synthesized and tested in order to increase their potency against DENV and ZIKV (17), and further qualify them as potential antiviral agents against these two viruses. In addition, assessment of their activity against several flavivirus members (e.g. YFV, JEV) will be a "key factor" to even promote them as pan-flavivirus drugs.
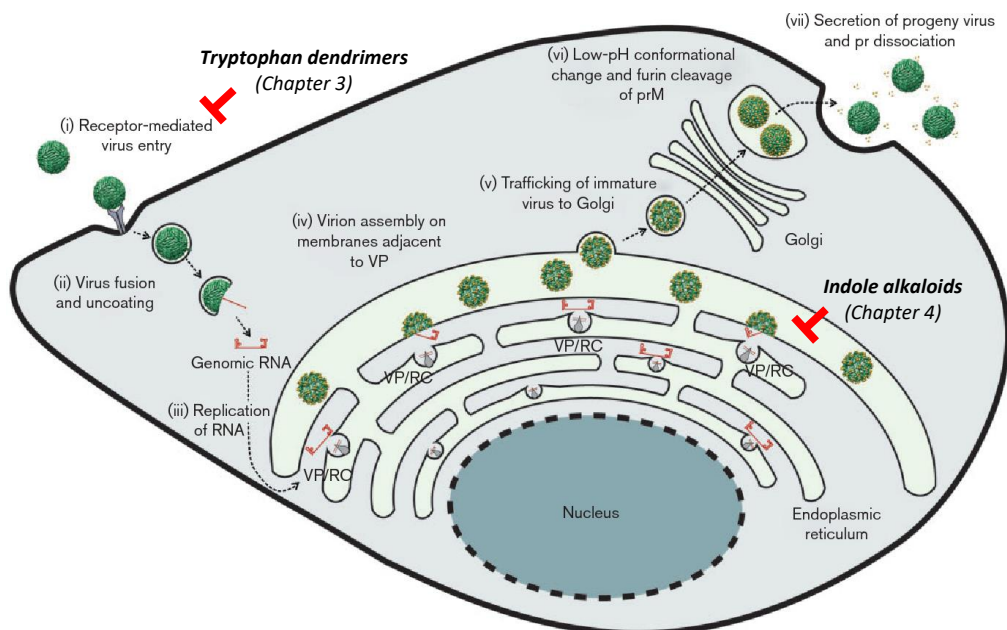
Figure 6.1: **Model of flavivirus replication cycle and mechanism of action of the molecules, studied in this thesis.** Tryptophan trimers and tetramers (polyanionic dendrimers) interfere with virus attachment process, by inhibiting viral envelope glycoprotein (first step of lifecycle). On the other hand, indole alkaloid derivatives prevent virus replication/assembly process that mainly takes place in the endoplasmic reticulum (replication complex (RC)). The exact mechanism of this family of compounds is still unknown, but there is an involvement of cellular factors that interact with the pTMD1 domain of NS4B protein (18).

In the last part of this research project (**Chapter 5**), we investigated the potential role of small membrane-enclosed particles (EVs) in ZIKV transmission on the BBB system. These vesicles are released from different cells/organs, in response to extracellular stimuli, such as cellular stress, cancer, inflammation and viral infections (19). Although EVs are originally believed to be a cellular waste mechanism to discard unwanted material, it is now established that these vesicles participate in broad cell-to-cell communication events both in normal and pathological conditions. In addition, the terminology of EVs refers to a diverse population of vesicles (e.g. ABs, MVs, exosomes), classified by their size, subcellular origin, as well as biogenesis mechanism (20). Despite the rapid ongoing work on EV biogenesis and sorting cargo process, there is still limited knowledge on the molecular mechanisms that lead to the formation of these tiny vesicles.

ESCRT- dependent and - independent pathways (e.g. tetraspanins and lipid rafts) have been demonstrated to play a key role in the biogenesis of EVs with a unique composition (21). Moreover, isolation of specific EV subpopulations constitutes a difficult task, since no protein markers exist to identify/discriminate exosomes from microvesicles and larger particles. Besides that, the presence of proteins and lipids, found in several biological fluids (e.g. plasma, urine, saliva) further complicates the isolation process, due to their co-precipitation with the vesicles (22).

In response to viral infections, cells secrete a number of heterogeneous population of EVs, which can lead to: (i) enhancement of viral infection by the transfer of viral proteins and nucleic acid molecules to recipient cells, (ii) activation of immune responses, through the recognition of viral material (present on the surface of EVs) by different immune cells (e.g. macrophages, dendritic cells), (iii) immune suppression and evasion from host responses (23). Until now, only few reports have been published on the role of arthropod- or vertebrate-EVs from ZIKV-infected cells. Particularly, ZIKV-infected C6/36 mosquito cells produce EVs that are able to incorporate and transfer viral RNA, phosphatidylserine and E protein to human peripheral blood monocytes and endothelial vascular cells, thus promoting viral spread. On the other hand, EVs from ZIKV-infected primary cortical neuron cells, have found to contain HSP70, E protein, as well as viral genome and further induce the expression of SMPD3. EV-mediated transmission of the content leads to severe neuronal death, which might result in severe neurological manifestations. However, treatment with GW4869 (inhibitor of nSMase) has led to reduced levels of ZIKV in both primary cells and their secreted vesicles. Regarding their immunomodulatory role, EVs derived from ZIKV-infected C6/36 mosquito cells promote the differentiation of susceptible monocytes, through the induction of TNF-α mRNA expression. Furthermore, these vesicles are involved in the increase of vascular permeability and endothelial damage, via the upregulation of tissue factor (TF) at the surface of endothelial cell membranes and the promotion of a pro-inflammatory antiviral state.

It has been described that ZIKV can be detected in the brain of fetuses and the cerebrospinal fluid of adults, indicating its neurotropic nature. Papa and colleagues indicated that endothelial cells of the BBB (major cell type of this system) are highly permissive to ZIKV infection, leading to release of viral particles that are able to further infect and replicate in other cells of the brain (24). However, the exact mechanisms associated with virus entry into the CNS

are still unclear. Several papers have described that ZIKV may reach the CNS by cell-free transcytosis, basolateral release or through the infiltration of infected leukocytes, resulting in increased infection of astrocytes and neurons (25)(26). Subsequently, infection of brain-related cells induces inflammatory responses (such as production and secretion of TNF- α, VEGF and RANTES) to the barrier that further trigger BBB disruption and leakage (27) at later time points.

In this study, we used hcMEC/D3 cells, a well-established cell line for the BBB system. After infection of cells with a ZIKV isolate (Asian lineage), a number of different lipid-bound vesicles was secreted and subsequently isolated by a combination of several isolation procedures. Using *in vitro* cellular assays, we observed that EVs-derived from ZIKV-infected cells are able to transfer viral components, including ZIKV RNA, as well as NS1 and E proteins to naïve cells. These elements are highly protected inside the vesicles (confirmed by RNase A treatment) and are able to be transferred into other cell types. The fact that viral RNA can be detected in the lower chamber of the transwell system, suggest that ZIKV might cross BBB through virus release, transcytosis or paracytosis. To answer this question, a label-free impedance-based biosensor was implemented to explore the potential mechanisms, used by both ZIKV and EVs to pass through the endothelial cells of the BBB. This technology offers great advantages, compared to the conventional transepithelial measurements (e.g. FITC-dextran), as we are able to detect short-time changes in the permeability of cells after virus incubation. In addition, no cytotoxicity issues occur, as observed in TEER measurements using the FITC-dextran substrate. Furthermore, by applying different electrical frequencies on the device, we can measure distinct routes of viral transmission. Specifically, low frequencies (4,000 Hz) account for cell-cell contacts (paracellular route), while higher frequencies (64,000 Hz) depict the confluency of cell monolayer (transcellular route). Our findings demonstrated that EVs-derived from ZIKV- infected cells, as well as virions follow transcytosis, during the first minutes of inoculation (*Figure 6.2*). To our knowledge, this is the first time that the EV-mediated virus transmission to the BBB system is described. In addition, we observed that virus/EVs entry result in temporal rearrangement of VE-cadherin, an adherent protein with vital role in the maintenance of endothelial structure and permeability. These results are in accordance with previous findings, where ZIKV was able to pass through BBB (hcMEC/D3 cells) via the transcellular route, but without any

disruption of cell monolayer (24). Additional reports in mouse models have also indicated the ability of ZIKV to reach the CNS, without disruption of the BBB, especially during the first days of infection. Since transcytosis is a critical pathway to transport macromolecules into the cells through the vesicular system, it is extremely difficult to target ZIKV via this mechanism (28).

At this point, we would like to emphasize the need for the development of a new protocol, in order to efficiently isolate pure EVs from ZIKV contamination. As noted above, this is a challenging task since both EVs and ZIKV share common pathways (e.g. exocytosis, during EV biogenesis and virus egress) and similar physiochemical characteristics (e.g. size). The current approach minimizes the presence of viral particles in EV preparations; however, we can not rule out the possibility of co-presence in some of these fractions, which might influence how we interpret our findings regarding the EV-specific effects on the recipient cells. A large proteomics study in each of these EV fractions and cell-free ZIKV virions would identify "protein signatures" that distinguish EVs from viruses. However, this study has to be conducted in several virus-susceptible cells, as well as in biofluids from ZIKV-infected patients. Although the isolation process is a crucial step, it is wise to consider whether EVs and viruses are two distinct entities or they might co- operate to sufficiently deliver their content to naïve cells.

Finally, a comprehensive lipidomics analysis on both cells and their secreted vesicles was performed using LC-ESI/MS/MS to identify potential biomarkers during ZIKV infection. Lipids possess great scientific value, not only as energy storage molecules and membrane building blocks, but also as important cell signaling inducers. Our analysis showed that specific lipid classes, such as SM, DG and cholesterol are highly enriched in EVs, suggesting a role in their biogenesis and signal transduction. Additionally, we found that different lipid species are relatively abundant in both cells and EVs, while others (e.g. Cer(18:1/14:0), DG(20:0/20:0)) are mainly detected in EV preparations. These data indicate a selective preference of specific lipids into EVs during sorting mechanism. However, the exact process is still unknown and further work needs to be conducted. Studies on the saturation degree of all detected lipids showed that most of these macro-biomolecules are (mono-) unsaturated, thus influencing the stability of the vesicles. Lastly, our analysis revealed that Cer(d18:0/18:3) is significantly upregulated in EVs-derived from ZIKV-infected cells, as compared to their non-infected counterpart, thus promoting this lipid molecule as a potential biomarker during ZIKV infection.
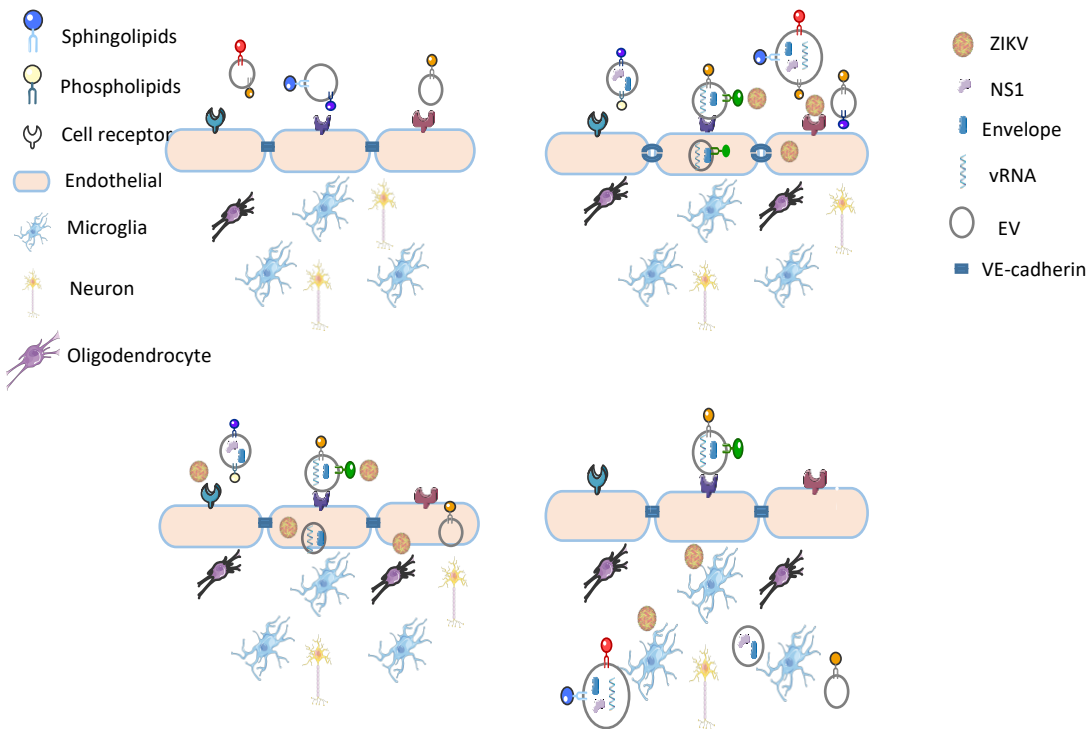
Figure 6.2: **Proposed model for ZIKV transmission through the BBB system.** (Left upper panel) In physiological conditions, lipid-bound vesicles are present in the blood circulation. (Right upper panel) Following virus infection, ZIKV virions and EVs-derived from ZIKV infected endothelial cells (carry NS1 and E proteins, as well as viral RNA) are recognized by cellular receptors and further transported by transcytosis. In addition, temporal rearrangement of VE-cadherin takes place during the first 30 minutes of incubation. (Left bottom panel) Transcytosis still occurs, but no sign of VE- cadherin reorganization takes place at 1 h post infection. (Right bottom panel) Both EVs and ZIKV pass through the BBB and transfer viral elements (proteins, nucleic acid and lipid molecules) to the brain-associated cells, such as microglial and neurons, thus contributing to enhanced virus transmission.

The ability of EVs to travel long distances within the body and successfully transfer cellular and viral elements into cells/tissues/organs has attracted the attention of many researchers to explore EVs as potential therapeutic agents. Although many observations testify the potential use of EVs in the clinic, main challenges hamper this process, including efficient isolation and large-scale

production. EVs can be used as safe drug delivery systems, since they present significant advantages, as compared to the already existing systems (e.g. liposomes and polymeric nanoparticles). Particularly, EVs can directly fuse with the targeted plasma membrane, allowing a more efficient internalization of the desired drug. In addition, they contain surface markers (anti-phagocytosis) that prevent their recognition from monocytes and macrophages, thus enhancing their presence in circulation. Finally, their small size and cell-derived nature allow them to efficiently pass through physical barriers (e.g. BBB, placenta), without the activation of immune system (as observed for the liposomal formulations) (29). Therefore, the limited induction of side effects along with the high specificity make EVs ideal vehicles for drug delivery to several tissues/organs. For example, it has been demonstrated that the administration of EVs-carrying chemotherapy drugs leads to a significant reduction of drug accumulation in off-target organs, thus preventing important side effects.

Regarding the therapeutic potential, several studies have demonstrated the role of mesenchymal stem cells (MSCs) in immune suppression (30). MSC-derived EVs are currently under investigation for their participation in inflammatory conditions. Particularly, these vesicles have the ability to induce the differentiation of anti-inflammatory macrophages, inactivate T cells and induce regulatory immune cells such as T/B lymphocytes and dendritic cells. Based on this context, Pocsfalvi *et al*. have described the ability of these EVs to treat acute inflammatory conditions such as those observed in severe cases of COVID-19 (31). Moreover, EVs isolated from MSCs have been loaded with chemotherapeutic drugs (e.g. doxorubicin), demonstrating an increased target specificity and biodistribution for the treatment of different tumor types. Besides MSCs, immature DCs constitute an interesting EV source, due to their low immunogenicity and immunosuppressive effects. For example, rabies viral glycoprotein (RVG) fused with Lamp2b on EVs results in specific delivery of the vesicles to neurons and glia cells (32). Similarly, immature dendritic cells have been modified to express Lamp2b fused with an integrin-specific peptide to target tumor cells (33). These findings show that the use of EVs as drug delivery vehicles could overcome the limitations that occur by the cell-free transfer of drugs/molecules, including limited bioavailability, poor absorption and rapid systemic clearance.

Another potential therapeutic use of EVs is vaccination against cancer and infectious diseases (34). Specifically, EVs can be engineered to display viral

antigens and induce strong immune responses and specific T cell and B cell reactions, without the need to inactivate pathogenic viruses. These characteristics highlight the importance of these antigen-carrying EVs as a novel vaccine strategy (35). The first EV-based treatment application was based on the use of DC-derived EVs as a surrogate for DC-based anticancer vaccination. Particularly, APC-derived EVs contain MHC type I and II as well as co-stimulatory factors, in order to trigger T cell responses. The use of DC-derived EVs has already been evaluated in clinical trials for melanoma (phase I) and non-small-cell lung carcinoma (phase II) (36)(37). Regarding viral infections, different groups have described the ability of EVs to trigger immune responses. For instance, EVs released from monocytes, loaded with viral-specific proteins (e.g. influenza and Epstein-Barr virus) are able to produce and secrete IFN-γ from CD8^{+} T cells. In addition, Anticoli *et al*. used a mutated form of HIV Nef protein as an EV-anchoring protein, and fused it with peptides from different viruses, including Ebola VP40, influenza NP, West Nile and HCV NS3. Administration of this vaccine platform to mice leads to induction of specific CD8^{+} T cellular responses for all tested viral proteins, while maintaining a high safety profile (38). Finally, EV-based vaccines against the new SARS-CoV-2 virus have been under development by several companies (39). Particularly, the first type is developed in the human HEK293 cells, transfected with expression vectors of the four structural virus proteins (spike, nucleocapsid, membrane and envelope). As a result, the produced vesicles carry all viral antigens, thus inducing immune responses. The second formula is an mRNA-type vaccine, which consisted of EVs loaded with five different mRNAs coding for modified spike, nucleocapsid, membrane, envelope and the full-length spike protein of the Wuhan isolate. This vaccine shows an increase in the number of CD4^{+} and CD8^{+} T-cells. Another vaccine developed against COVID- 19 disease is called CoVEVax. This formula is also based on HEK293T-derived EVs, which are engineered to display the full spike protein on their surface, due to its fusion with an EV-sorting peptide. Despite the advantages that EV-based vaccines offer as compared to the conventional technologies, there are some challenges that need to be considered for their robust clinical application. More specifically, the existing EV isolation methods are not able to efficiently distinguish EV subpopulations, due to the lack of specificity. Additionally, EVs derived from *in vitro* cellular systems

should only contain the desired antigens, in order to avoid any potential immunogenicity.

To conclude, EVs possess particular characteristics that promote them as attractive systems for drug delivery. Some of them are (i) stability in blood circulation, (ii) biocompatibility, (iii) efficient interaction with encapsulated drugs, (iv) slow immune clearance from the system and (iv) low immunogenicity, as compared to toxic nanoparticles and liposomes. Recently, their potential use is also evaluated in vaccine development, with encouraging results. However, additional studies should be performed to assess their pharmacokinetics and increased target specificity.

6.1 References

1. Normile D. Tropical medicine. Surprising new dengue virus throws a spanner in disease control efforts. Science. 2013;342(6157):415

2. Kanda T, Nakamoto S, Wu S, Nakamura M, Jiang X, Haga Y, et al. Direct-acting antivirals and host-targeting agents against the hepatitis a virus. J Clin Transl Hepatol. 2015;3(3):205–10

3. Chitalia VC, Munawar AH. A painful lesson from the COVID-19 pandemic: the need for broad-spectrum, host-directed antivirals. J Transl Med. 2020;18(1):1–6

4. Sepúlveda-Crespo D, Jiménez JL, Gómez R, De La Mata FJ, Majano PL, Muñoz-Fernández MÁ, et al. Polyanionic carbosilane dendrimers prevent hepatitis C virus infection in cell culture. Nanomedicine Nanotechnology, Biol Med [Internet]. 2017;13(1):49–58. Available from: http://dx.doi.org/10.1016/j.nano.2016.08.018

5. Urbinati C, Chiodelli P, Rusnati M. Polyanionic drugs and viral oncogenesis: A novel approach to control infection, tumor-associated inflammation and angiogenesis. Molecules. 2008;13(11):2758–85

6. Lorentsen KJ, Hendrix CW, Collins JM, Kornhauser DM, Petty BG, Klecker RW, et al. Dextran sulfate is poorly absorbed after oral administration. Ann Intern Med. 1989;111(7):561–6

7. Vacas-Córdoba E, Maly M, De la mata FJ, Gómez R, Pion M, Muñoz-Fernández MÁ. Antiviral mechanism of polyanionic carbosilane dendrimers against HIV-I. Int J Nanomedicine. 2016;11:1281–94

8. Sun L, Lee H, Thibaut HJ, Lanko K, Rivero-Buceta E, Bator C, et al. Viral engagement with host receptors blocked by a novel class of tryptophan dendrimers that targets the 5-fold-axis of the enterovirus - A 71 capsid. PLoS Pathog. 2019;15(5):1–20

9. Omar F, Tareq AM, Alqahtani AM, Dhama K, Sayeed MA, Emran T Bin, et al. Plant-Based Indole Alkaloids : A Comprehensive Overview from a Pharmacological Perspective. 2021. 26(8):2297

10. Li S, Liu X, Chen X, Bi L. Research Progress on Anti-Inflammatory Effects and Mechanisms of Alkaloids from Chinese Medical Herbs.

Evidence-based Complement Altern Med. 2020. 2020:1303524

11. Postnikova E, Cong Y, DeWald LE, Dyall J, Yu S, Hart BJ et al. Testing therapeutics in cell-based assays: Factors that influence the apparent potency of drugs. PLoS One. 2018;13(3):e0194880

12. Guabiraba R, Ryffel B. Dengue virus infection: Current concepts in immune mechanisms and lessons from murine models. Immunology. 2014;141(2):143–56

13. Lee JK, Shin OS. Advances in zika virus–host cell interaction: Current knowledge and future perspectives. Int J Mol Sci. 2019;20(5):1101

14. Tsang JOL, Zhou J, Zhao X, Li C, Zou Z, Yin F, et al. Development of three-dimensional human intestinal organoids as a physiologically relevant model for characterizing the viral replication kinetics and antiviral susceptibility of enteroviruses. Biomedicines. 2021;9(1):1–16

15. Navratil V, De chassey B, Meyniel L, Delmotte S, Gautier C, André P, et al. VirHostNet: A knowledge base for the management and the analysis of proteome-wide virus-host interaction networks. Nucleic Acids Res. 2009;37(SUPPL. 1):661–8

16. Dai W, Zhang B, Jiang XM, Su H, Li J, Zhao Y, et al. Structure-based design of antiviral drug candidates targeting the SARS-CoV-2 main protease. Science. 2020;368(6497):1331–5

17. Chen YL, Yokokawa F, Shi PY. The search for nucleoside/nucleotide analog inhibitors of dengue virus. Antiviral Res. 2015;122:12–9

18. Roby JA, Setoh YX, Hall RA, Khromykh AA. Post-translational regulation and modifications of flavivirus structural proteins. J Gen Virol. 2015;96(7):1551–69.

19. Yuana Y, Sturk A, Nieuwland R. Extracellular vesicles in physiological and pathological conditions. Blood Rev. 2013;27(1):31–9

20. Willms E, Cabañas C, Mäger I, Wood MJA, Vader P. Extracellular vesicle heterogeneity: Subpopulations, isolation techniques, and diverse functions in cancer progression. Front Immunol. 2018;9:738

21. Tschuschke M, Kocherova I, Bryja A, Mozdziak P, Angelova Volponi A,

Janowicz K, et al. Inclusion Biogenesis, Methods of Isolation and Clinical Application of Human Cellular Exosomes. J Clin Med. 2020;9(2):436

22. Pang S-W, Teow S-Y. Emerging therapeutic roles of exosomes in HIV-1 infection. Exosomes. 2020;126(4):147–78

23. Zhang L, Ju Y, Chen S, Ren L. Recent Progress on Exosomes in RNA Virus Infection. Viruses. 2021;13(2)

24. Papa MP, Meuren LM, Coelho SVA, de Oliveira Lucas CG, Mustafá YM, Matassoli FL, et al. Zika virus infects, activates, and crosses brain microvascular endothelial cells, without barrier disruption. Front Microbiol. 2017;8:

25. Chiu CF, Chu LW, Liao IC, Simanjuntak Y, Lin YL, Juan CC, et al. The Mechanism of the Zika Virus Crossing the Placental Barrier and the Blood-Brain Barrier. Front Microbiol. 2020;11:1–15

26. Jurado KA, Yockey LJ, Wong PW, Lee S, Huttner AJ. Iwasaki A. Antiviral CD8 T cells induce Zika-virus-associated paralysis in mice. Nat Microbiol. 2018;3(2):141–7

27. Naveca FG, Pontes GS, Chang AYH, da Silva GAV, do Nascimento VA, Monteiro DC da S, et al. Analysis of the immunological biomarker profile during acute zika virus infection reveals the overexpression of CXCL10, a chemokine linked to neuronal damage. Mem Inst Oswaldo Cruz. 2018;113(6):1–13

28. Tuma PL, Hubbard AL. Transcytosis: Crossing cellular barriers. Physiol Rev. 2003;83(3):871–932

29. Villa F, Quarto R, Tasso R. Extracellular vesicles as natural, safe and efficient drug delivery systems. Pharmaceutics. 2019;11(11):1–16

30. Stremersch S, De Smedt SC, Raemdonck K. Therapeutic and diagnostic applications of extracellular vesicles. J Control Release. 2016;244:167–83

31. Pocsfalvi G, Mammadova R, Ramos Juarez AP, Bokka R, Trepiccione F, Capasso G. COVID-19 and Extracellular Vesicles: An Intriguing Interplay. Kidney Blood Press Res. 2020;45(5):661–70

32. Alvarez-Erviti L, Seow Y, Yin H, Betts C, Lakhal S, Wood MJA. Delivery of siRNA to the mouse brain by systemic injection of targeted exosomes. Nat Biotechnol. 2011;29(4):341–5

33. Tian Y, Li S, Song J, Ji T, Zhu M, Anderson GJ, et al. A doxorubicin delivery platform using engineered natural membrane vesicle exosomes for targeted tumor therapy. Biomaterials. 2014;35(7):2383–90

34. Dogrammatzis C, Waisner H, Kalamvoki M. Cloaked Viruses and Viral Factors in Cutting Edge Exosome-Based Therapies. Front Cell Dev Biol. 2020;8:1–20

35. Keshavarz M, Mirzaei H, Salemi M, Momeni F, Mousavi MJ, Sadeghalvad M, et al. Influenza vaccine: Where are we and where do we go? Rev Med Virol. 2019;29(1):1–13

36. Escudier B, Dorval T, Chaput N, André F, Caby MP, Novault S, et al. Vaccination of metastatic melanoma patients with autologous dendritic cell (DC) derived-exosomes: Results of the first phase 1 clinical trial. J Transl Med. 2005;3:1–13

37. Morse MA, Garst J, Osada T, Khan S, Hobeika A, Clay TM, et al. A phase I study of dexosome immunotherapy in patients with advanced non-small cell lung cancer. J Transl Med. 2005;3:1–8

38. Anticoli S, Manfredi F, Chiozzini C, Arenaccio C, Olivetta E, Ferrantelli F, et al. An Exosome-Based Vaccine Platform Imparts Cytotoxic T Lymphocyte Immunity Against Viral Antigens. Biotechnol J. 2018;13(4):1–7.

39. Sabanovic B, Piva F, Cecati M, Giulietti M. Promising extracellular vesicle-based vaccines against viruses, including SARS-CoV-2. Biology (Basel). 2021;10(2):94

Acknowledgements

This PhD work could not be fulfilled without the help of different people, which I would definitely want to say a BIG THANK YOU. Coming to Belgium, I was full of dreams, having expectations and I was willing to meet new people and acquire experiences. I am so lucky that I had the chance to meet so important people in my life the last 5 years.

First of all, I would like to thank my promoter, Prof. Dominique Schols for his decision to make me a member of his group. Thanks for all the advice and the help where needed. And the good time in the Bahamas as well!!! Many many thanks to my co-promoter, Prof. Christophe Pannecouque, the person who I consider as my mentor. I will always keep in my mind all the advice, talks that we had in your office and what I learned from you. Thank you for your time and help in the entire period that I was present in the Rega. I really appreciate it that.

I would like to thank all my jury members, the internal: Prof. Proost and Prof. Maes, and the external: Prof. Munch and Prof. Arien for all the effort and time to evaluate my thesis manuscript and contribute to its improvement. In addition, many thanks to Prof. Economou, Prof. Vermeire and Prof. Daelemans. Moreover, I would like to mention the group of Prof. Philippe Lemey for giving me the chance to start my scientific journey in Belgium and KU Leuven, as an Erasmus intern. Moreover, I would like to thank Cathy De Meyer and Inge Aerts for their great and valuable help in all the administrative stuff that I was unable to do!!

In addition, I wouldn't be able to succeed and finish my thesis without my colleagues. Eef, Sam, Jordi and Eva, I consider all of you as friends, not only colleagues. Thank you for your help and every moment that I share with you in the lab and outside of this (drinks, food, laughs). I was so lucky working with you. You are great people. I am waiting you in Greece to have some more of these moments. Also, Peter, Mo, Libao, Maxine, Arnaud, Nathan, Marijke, Merel, Anneleen, Thomas, Steve, Emiel, Katrijn, Laurenne, Evelien, Tom, Cindy, Anita, Becky, Joren, thank you so much for the time spending and all the nice conversations having with you. Joni and Elisabetta, thanks for being

there when I needed that. All the chats, drinks, work out moments, I will have them in my mind. I wish you all the best from the bottom of my heart. Isiah, my gym buddy, thank you for all the funny moments bro. Take care of yourself.

Besides my colleagues, nothing would be the same without my second family, my Greek friends over here. Τι να πω για εσάς πραγματικά.... Χωρίς εσάς δεν θα κατάφερνα να φτάσω εδώ. Ποτέ δεν πίστεψα ότι θα συναντήσω άτομα εδώ που θα μπορούσα να κολλήσω τόσο καλά. Κώστα, Νίκο, Γιώργο, Τεό, Βασίλη, Τάκη, Σόφο, Ρία, Σταυρούλα, Καραγιάννη, Βίδια, Ζαφείρω, Din, Σοφία, Χρήστο, Αμαλία, Κωνσταντίνα, Κυριάκο, Βάσια, Παναγιώτη, Ζέφη σας ευχαριστώ που κάνατε την καθημερινότητά μου εδώ όμορφη και με ανεβάζατε ψυχολογικά. Σας νιώθω οικογένειά μου και σας εύχομαι να καταφέρετε τα πάντα στη ζωή σας. Μάγδα μου, έχεις ξεχωριστή θέση στην καρδιά μου. Ήσουν αυτή που με έδωσε την ευκαιρία να ανοίξω τα φτερά μου και σε ευχαριστώ για όλα, δεν θα το ξεχάσω ποτέ. Σε εύχομαι πραγματικά τα καλύτερα και είμαι σίγουρος ότι θα πετύχεις στο μέλλον. Ξέρεις πως ότι και αν θελήσεις, εγώ θα είμαι εδώ να βοηθήσω.

Χόντρα, Άδα, Ράφα, Βερουτάκο και ξαδερφάκο μου σας ευχαριστώ για όλη την υποστήριξη φιλαράκια μου...Είστε πάντα δίπλα μου και σας θεωρώ δικούς μου ανθρώπους, αδέρφια μου. Σας υποστηρίζω σε ότι και αν κάνετε. Συνεχίστε έτσι. Πολλά ευχαριστώ στα υπόλοιπα φιλαράκια μου στη Βέροια.

Coming to the end, I can not forget the person who "suffered" more during these years. My girlfriend, my partner, Zoe. Συγγνώμη για όσες φορές ζορίστηκες από την συμπεριφορά μου, για τα νεύρα μου την τελευταία περίοδο και τα ξεσπάσματά μου. Ήσουν πάντα εκεί και αυτό δεν το ξεχνώ ούτε στιγμή. Με ηρεμούσες και έδινες κουράγιο μέχρι το τέλος. Ελπίζω να καταφέρεις όλα όσα σκέφτεσαι και εγώ θα είμαι εδώ να σε καμαρώνω και να σε στηρίζω. Μην τα παρατήσεις ποτέ και να αποβάλλεις ότι άσχημο υπάρχει γύρω σου. Love you so much!!! Αυτό να το θυμάσαι πάντα και να χαμογελάς γιατί σου πάει.

Finally, I would like to thank my family back in Greece. Τις γιαγιάδες μου, Νίκη και Αγγελική, τη θεία μου Ρούλα, το θείο μου Μάνο και τα μικρά και

αγαπημένα μου ξαδέρφια, Νικολέτα και Αντώνη για την αγάπη και την έμπρακτη υποστήριξή τους. Σας αγαπώ πολύ και σας ευχαριστώ. At the end, the three people who I love the most in this crazy world. My mother (Μαρία), brother (Παύλος) and father (Πέτρος). Αν και αυτά τα τελευταία 5 χρόνια δεν σας είχα κοντά μου, ήσασταν πάντα δίπλα μου, χωρίς να ζητήσετε τίποτα. Το μόνο που θέλατε είναι να δείτε αν είμαι καλά. Πολλές φορές σας μιλούσα απότομα ή ελάχιστα, και το μετάνιωνα απευθείας. Με καταλαβαίνατε κατευθείαν και σεβόσασταν κάθε επιθυμία μου. Σας λατρεύω και χρωστάω τόσα πολλά σε εσάς. Είστε το στήριγμα και το πρότυπο ανθρώπου που θέλω να γίνω. Θα ήθελα να γνωρίζετε ότι δεν είχα σκοπό να φτάσω ως εδώ όταν τελείωσα το Λύκειο. Έβαλα ένα στοίχημα όμως να ξεπεράσω τον εαυτό μου και να πάω όσο το δυνατόν παραπέρα για να σας κάνω περήφανους. Παρά τις πολλές κακές στιγμές, δεν μετάνιωσα για αυτήν την απόφαση ούτε λεπτό και ελπίζω να είστε χαρούμενοι.

Παππού μου καλέ, αυτό το διδακτορικό στο αφιερώνω. Δυστυχώς δεν μπόρεσα να είμαι δίπλα σου στο τελευταίο σου ταξίδι. Πάντα σε κουβαλάω στο μυαλό και την καρδιά μου γιατί ήσουν ο αγαπημένος μου. Ξέρω ότι από εκεί πάνω θα είσαι χαρούμενος και περήφανος τώρα. Τελείωσα παππούκα, στο είχα πει ότι θα τα καταφέρω.

Finally, I know that trying to be a scientist is not easy at all. So many working hours, so much disappointment and sometimes disrespect by other people. But what I learned from these years can be concluded in a few sentences already stated by the great Charlie Chaplin: "*Live your life, smile and don't care about others' opinion. At the end, everything is a gag*".

Personal contributions and conflict of interest

Antonios Fikatas designed and executed most of the experiments under the guidance of Prof. Dominique Schols and Prof. Christophe Pannecouque.

Contributions to this work are listed below:

Cellular-based assays were performed by Antonios Fikatas, Eef Meyen and Dr. Peter Vervaeke. Isolation and handling of PBMCs were done by Eric Fonteyn. Antiviral screening and mechanism of action studies were operated by Antonios Fikatas, Eef Meyen and Dr. Peter Vervaeke. Screening experiments against other viruses were performed by Leentje Persoons, Bianca Stals, Nathalie Van Winkel, Daisy Ceusters, Romy-Anna Brouwer and Niels Willems. SPR and immunofluorescence staining experiments were performed and analyzed by Sam Noppen. Compounds were synthesized by Prof. San-Felix and Prof. Amat Tuson along with their research groups. Selection of compound-resistant mutants was done by Antonios Fikatas and the sequencing analysis was implemented by Ine Boonen, Dr. Magda Bletsa and Dr. Liana Kafetzopoulou. EV-based experiments were set up and mostly performed by Antonios Fikatas with the valuable input of Sam Noppen and Dr. Mohammed Benkheil. Nanoparticle tracking analysis was done by Frank Vanderhoydonc, while electron microscopy images were acquired by Antonios Fikatas and Dr. Pieter Baatsen. Lipidomic experiments were performed by Dr. Jonas Dehairs and the analysis was implemented by Antonios Fikatas. Finally, electrical-based biosensor experiments (ECIS) were done by Antonios Fikatas and Dr. Jordi Doijen.

Statistical analysis (GraphPad) and illustrations (Adobe illustrator CC 2018) were designed by Antonios Fikatas.

Antonios Fikatas wrote this thesis with valuable inputs from Prof. Christophe Pannecouque, Prof. Dominique Schols, Dr. Jordi Doijen and Sam Noppen.

The author declares no conflicts of interest of this thesis manuscript.

Curriculum vitae

Personal details

Name: Fikatas Antonios

Date of Birth: July 28, 1992

Place of Birth: Veria, Greece

Education

2017 – 2021   **Doctoral Training in Biomedical Sciences**
Laboratory of Virology and Chemotherapy
Rega Institute for Medical Research
KU Leuven, Leuven, Belgium

2016-2017   **Volunteer Collaborator in Department of Microbiology and Immunology**
Laboratory of Evolutionary and Computational Virology
Rega Institute for Medical Research
KU Leuven, Leuven, Belgium

2014 – 2016   **Master Degree of Biomedical Sciences**
"Application of Molecular Biology, Genetics,

Diagnostic Biomarkers"

Department of Biochemistry and Biotechnology,

University of Thessaly, Larissa, Greece

Master thesis:

"Detection of negative and positive RNA strand of Sabin 1 virus by a stem-loop reverse transcription PCR in Rd cells".

Promoter: Prof. Markoulatos Panayotis

2010 – 2014   Bachelor Degree in Biochemistry and

Biotechnology, Biomedical Sciences

Department of Biochemistry and

Biotechnology, University of Thessaly, Greece

Bachelor thesis:

"Serum neutralization assay for the determination of antibody levels against non-polio enterovirus strains in Central and Western Greece."

Promoter: Prof. Markoulatos Panayotis

Publications in peer reviewed journals

- **Fikatas A**, Dehairs J, Noppen S, Doijen J, Vanderhoydonc F, Meyen E, Swinnen J, Pannecouque C, Schols D. Deciphering the role of extracellular vesicles derived from ZIKV-infected hcMEC/D3 cells on the blood-brain barrier system. *Under Review,* **2021**

- **Fikatas A**, Vervaeke P, Meyen E. Llor N, Ordeix S. Boonen I, Bletsa M, Kafetzopoulou L, Lemey P, Amat M, Pannecouque C, Schols D. A novel series of indole alkaloid derivatives inhibit dengue and Zika virus infection by interference with the viral

replication complex. *Antimicrob Agents Chemother*. 65(8):e0234920 **2021**

- **Fikatas A**, Vervaeke P, Martínez-Gualda B, Martí-Marí O, Noppen S, Meyen E, Camarasa MJ, San-Félix A, Pannecouque C, Schols D. Tryptophan trimers and tetramers inhibit dengue and Zika virus replication by interfering with viral attachment processes. *Antimicrob Agents Chemother*. 64:e02130-19 **2020**

- Bletsa M, Vrancken B, Gryseels S, Boonen I, **Fikatas A**, Li Y, Laudisoit A, Lequime S, Bryja J, Makundi R, Meheretu Y, Akaibe B, Mbatilini S, Van de Perre F, Van Houtte N, Těšíková J, Wollants E, Van Ranst M, Pybus O, Drexler JF, Verheyen E, Leirs H, de Bellocq JG, Philippe L. Molecular detection and genomic characterization of diverse hepaciviruses in African rodents. *Virus Evolution*. 7(1):veab036 **2021**

- Eremeeva E, **Fikatas A**, Margamuljana L, Abramov M, Schols D, Groaz E, Herdewijn P. Highly stable hexitol based XNA aptamers targeting the vascular endothelial growth factor. *Nucleic Acids Research*. 47:4927-4939 **2019**

- **Fikatas A,** Dimitriou TG, Kyriakopoulou Z, Moschonas G, Amoutzias GD, Mossialos D, Gartzonika C, Levidiotou-Stefanou S, Markoulatos P. Detection of negative and positive RNA strand of poliovirus Sabin 1 and echovirus E19 by a stem-loop reverse transcription PCR. *Lett Appl Microbiol*. 65:324-340 **2017**

- **Fikatas A,** Dimitriou TG, Kyriakopoulou Z, Tsachouridou O, Gartzonika C, Levidiotou-Stefanou S, Amoutzias GD, Markoulatos P. Serum neutralisation assay for the determination of antibody levels against non-polio enterovirus strains in Central and Western Greece. *Viral immunology*. 29:444-50 **2016**

Conference abstracts

- <u>**Fikatas A**</u>, Dehairs J, Noppen S, Baatsen P, Doijen J, Vervaeke P, Benkheil M, Pannecouque C, Swinnen J, Schols D. Exploring the role of EVs on the blood brain barrier during ZIKV infection. Oral

Presentation. Fusion Conferences-Exosomes in Human Infectious Diseases. 5th-8th May 2020, Nassau, Bahamas

- **Fikatas A**, Noppen S, Vervaeke P, Doijen J, Benkheil M, Pannecouque C, Schols D. Role of extracellular vesicles on the blood-brain barrier during ZIKV infection. Poster Presentation. ISEV meeting. 24th-28th April 2019, Kyoto, Japan
- **Fikatas A**, Noppen S, Vervaeke P, Doijen J, Benkheil M, Pannecouque C, Schols D. Role of extracellular vesicles on the blood-brain barrier during ZIKV infection. Oral Presentation. ISEV meeting. 24th-28th April 2019, Kyoto, Japan
- **Fikatas A,** Vervaeke P, Llor N, Ordeix S, Meyen E, Noppen S, Tuson A, Pannecouque C, Schols D. Antiviral activity of a series of indole alkaloids against emerging flaviviruses. Poster Presentation. 31st ICAR meeting. 11st-15th June 2018, Porto, Portugal
- **Fikatas A,** Dimitriou TG, Kyriakopoulou Z, Zisi Z, Markoulatos P. Serum-neutralization assay for the determination of antibody levels against non-polio enterovirus strains in Central and Western Greece. Poster presentation. 10th Panhellenic Conference of Virology. 27th – 28th February 2015, Athens, Greece